



**HAL**  
open science

# Hybrid Electric Locomotives: contributions to modeling and type-2 fuzzy logic energy management strategy

Jérôme Baert

► **To cite this version:**

Jérôme Baert. Hybrid Electric Locomotives: contributions to modeling and type-2 fuzzy logic energy management strategy. Electric power. Université de Franche-Comté, 2013. English. NNT: 2013BESA2049 . tel-01312176

**HAL Id: tel-01312176**

**<https://theses.hal.science/tel-01312176>**

Submitted on 4 May 2016

**HAL** is a multi-disciplinary open access archive for the deposit and dissemination of scientific research documents, whether they are published or not. The documents may come from teaching and research institutions in France or abroad, or from public or private research centers.

L'archive ouverte pluridisciplinaire **HAL**, est destinée au dépôt et à la diffusion de documents scientifiques de niveau recherche, publiés ou non, émanant des établissements d'enseignement et de recherche français ou étrangers, des laboratoires publics ou privés.



SPIM

Thèse de Doctorat



UFC

école doctorale sciences pour l'ingénieur et microtechniques  
UNIVERSITÉ DE FRANCHE-COMTÉ

Locomotives Electriques Hybrides:  
contribution à leur modélisation et  
à leur gestion énergétique par  
logique floue de type 2.

■ Jérôme BAERT



# SPIM

## Thèse de Doctorat



école doctorale sciences pour l'ingénieur et microtechniques  
UNIVERSITÉ DE FRANCHE-COMTÉ

N° 2 0 1 3 0 7 5

THÈSE présentée par

**Jérôme BAERT**

pour obtenir le

Grade de Docteur de  
l'Université de Franche-Comté

Spécialité : Génie électrique

## Locomotives Electriques Hybrides: contribution à leur modélisation et à leur gestion énergétique par logique floue de type 2.

Hybrid Electric Locomotives: contributions to modelling and type-2 fuzzy logic energy management strategy

Soutenue le 01/10/2013 devant le Jury :

M. Alain BOUSCAYROL	Président du jury	Professeur, Université Lille 1
M. Xavier ROBOAM	Rapporteur	Directeur de Recherche CNRS, Toulouse
M. Rochdi TRIGUI	Rapporteur	Directeur de Recherche IFSTTAR, Bron
M. Robert JOHN	Examineur	Professeur, The University of Nottingham, Royaume-Uni
M. Didier CHAMAGNE	Co-directeur de thèse	Professeur, Université de Franche-Comté
M. Samuel HIBON	Encadrant de thèse	Responsable projets R&D, Alstom Transport
M. Daniel HISSEL	Directeur de thèse	Professeur, Université de Franche-Comté
M. Samir JEMEI	Encadrant de thèse	Maitre de Conférence, Université de Franche-Comté
M. Pierre CHANAL	Membre invité	Directeur Technique, Alstom Transport
M. Dominique HEGY	Membre invité	Ingénieur expert, Alstom Transport
M. Christophe MOREAU	Membre invité	Manager Train Systems, Alstom Transport



# Acknowledgements

Firstly, I would thank a lot all the members of the jury for participating my thesis defence and for intensely animating the discussions.

I want to express how humbled and honoured I am that Alain Bouscayrol chaired the doctorate committee. I am also very grateful with Rochdi Trigui and Xavier Roboam for bringing their expertise and suggesting recommendations on this work.

I would like to thank especially the viva's examiners for their pertinent remarks: Robert John, Dominique Hegy and Samuel Hibon.

Dominique and Samuel, by representing Alstom Transport, you also shew the high interest of the industry in this work and I am thankful for all the fruitful technical and scientific exchanges we had.

Finally, I must acknowledge Samir Jemeï, Daniel Hissel and Didier Chagnagne without whom this work would never have been possible. It was a real pleasure to work with you, to benefit your exceptional scientific expertise, to humanely involve yourselves in the project and to support me in my decisions.

Thanks a lot to Nathalie Devillers and her invaluable contribution in the test bench installation, Javier Solano-Martinez for inheriting its fuzzy logic experience which helped me a lot and Christophe Espanet for the varied even exotic conversations we had during conferences and seminars.

I am grateful with Aysenur, Bob, Summer, Dario, Syibrah, Ahmed, Javier, Pilar, Peter, Eduard, Georgia and Mikdam of the University of Essex. I really enjoyed working and passing three months with you in Colchester. This research at Colchester has been possible thanks to the financial supports granted by the SPIM doctoral school, the regional council of Franche-Comte and the ERASMUS program.

All of the Ph.D students played an important role in making a success this work. Charly, Vincent, Raïssa, Raffaele, Mona, Kun, Serge, Destiny,

Zhixue, Elodie, Zongliang, Daniel, Joseba, François and Simon, thank you for your kindness.

All the colleagues of the Energy Department, the University of Franche-Comte, the FC-LAB, engineers, researchers, experts, administrative staff also participated in a way in this successful development and especially Guillaume, Florence, Isabelle, Bruno, Laurence, Sabine, Xavier and Fabien.

I can't forget to immensely thank my friends Julien, Blaise, Aurélien, Bruno, Valérie, France, Xavier and Emilie for their unconditional friendship.

I dedicate this manuscript to my family for its unflinching support till the end of the doctorate and for the organization of the viva.





# Résumé

Dans le cadre du transport de marchandises par voie ferroviaire, un certain nombre de verrous limitent les efforts consentis pour un fret plus "propre". Des améliorations doivent être faites afin de limiter le nombre de locotracteurs assurant les charges/décharges de marchandises en bout de ligne. Dans cette perspective, FEMTO-ST et Alstom Transport ont pour objectif de concevoir et développer un système de gestion d'énergie pour locomotive électrique hybride. Composée d'un groupe électrogène couplé à des accumulateurs électrochimiques et des super-condensateurs, la locomotive électrique hybride permet d'accroître la souplesse et l'efficacité du transport ferroviaire électrique, tout en réduisant encore son impact environnemental.

Cette étude a consisté dans un premier temps à développer une modélisation macroscopique de la chaîne de traction électrique hybride et à proposer une structuration de la commande avec l'identification des capteurs matériels et logiciels nécessaires au contrôle optimal de la chaîne de traction. La caractérisation expérimentale des moyens de stockage a permis l'amélioration comportementale et dynamique des modèles correspondant.

Dans un second temps, le contrôle de la tension de sortie d'un hacheur dévolteur a permis d'étudier l'application de la logique floue de type-2 (intervalle et générale) dans le cas d'applications industrielles (relativement simples).

Enfin, une gestion innovante des flux d'énergie au sein d'un système plus complexe: locomotive électrique hybride, a été développée. Mettant en oeuvre la logique floue de type-2 et des algorithmes s'inspirant de la théorie de l'évolution, cette gestion d'énergie optimale opère en temps réel et sans connaissance à priori du cycle de conduite. La gestion fréquentielle ainsi que le contrôle des états de charge des sources secondaires du véhicule contribuent également à leur bon fonctionnement.

**Mots-clés:** Locomotives électriques hybrides, accumulateurs électrochimiques, super-condensateurs, caractérisation expérimentale, stratégie de gestion d'énergie, logique floue de type-2, algorithme génétique, représentation énergétique macroscopique, dimensionnement fréquentiel.



# Abstract

To achieve a "greener" freight transport, efforts are still needed to overcome some technological barriers. New improvements must be carried out to limit the shunting locomotives' use intended for the goods' load/unload. Considering this aim, FEMTO-ST and Alstom Transport decided to conceive and develop an energy management strategy system for hybrid electric locomotives. Such locomotives include a diesel driven generator set which is coupled with batteries and ultra-capacitors. The architecture aims at improving the flexibility, the effectiveness of the electrical railway transport and at reducing the environmental impact of these activities again.

Firstly, the study consists in implementing a macroscopic modelling of the hybrid electric powertrain. Then, the control is optimally designed by identifying the hardware and software sensors of the powertrain. The dynamics and the behaviour of the secondary sources' models are improved thanks to their experimental characterizations.

Secondly, the use of Type-2 Fuzzy Logic (interval and general) controllers permits to study their efficiency in the control of a very simple industrial system: the output voltage of a buck converter.

Lastly, based on the obtained results, an innovative management of the system's energy flows is developed in the case of the hybrid electrical locomotive. The use of the type-2 fuzzy logic and evolutionary algorithms permit to optimally perform a real time energy management strategy without a priori knowledge of the duty cycle. The frequency approach and the secondary sources' state of charge control contribute to their efficient use.

**Keywords:** Hybrid Electric Locomotives, batteries, ultra-capacitors, experimental characterization, energy management strategy, Type-2 fuzzy logic, genetic algorithm, Energetic Macroscopic Representation, frequency sizing.



# Contents

Résumé	ix
Abstract	xi
Contents	xv
List of Figures	xxiii
List of Tables	xxv
List of Acronyms	xxvii
Introduction	1
<b>1 Energy and Hybrid Electric Vehicles Challenges</b>	<b>11</b>
1.1 Hybrid Electric Vehicles	11
1.1.1 Background	12
1.1.2 Classification	13
1.1.3 Hybrid Electric Locomotives	14
1.2 Energy Management Strategies	21
1.2.1 Energy management problematic	22
1.2.2 Strategies based on off-line optimization algorithms	23
1.2.3 Strategies based on on-line optimization algorithms	26
1.2.4 Hybrid Electric Locomotives' EMSs	35
1.3 Chapter conclusion	41
<b>2 Locomotive topology and sizing of the secondary sources</b>	<b>45</b>
2.1 Locomotive topology	45
2.2 Sizing of the secondary sources	49
2.2.1 Determination of the most restricting mission	49
2.2.2 Batteries and ultra-capacitors sizing - [Akl08]	55
2.2.3 Volume and weight estimations	73

2.2.4	Arrangement of the elements . . . . .	73
2.3	Chapter conclusion . . . . .	75
<b>3</b>	<b>Modelling and control of the Hybrid Electric Locomotive</b>	<b>77</b>
3.1	The diesel driven generator set . . . . .	78
3.1.1	The naturally aspirated diesel engine . . . . .	78
3.1.2	The salient pole synchronous machine . . . . .	87
3.1.3	The diesel driven generator set . . . . .	90
3.2	The Ultra-Capacitors . . . . .	94
3.2.1	Physical model of a cell . . . . .	94
3.2.2	Energetic Macroscopic Representation . . . . .	95
3.2.3	Maximum and Practical Control Structures . . . . .	96
3.2.4	Simulation results . . . . .	97
3.3	The batteries . . . . .	97
3.3.1	Physical model of a cell . . . . .	99
3.3.2	Energetic Macroscopic Representation . . . . .	100
3.3.3	Maximum and Practical Control Structure . . . . .	100
3.3.4	Experimental characterization . . . . .	102
3.4	The rheostat . . . . .	109
3.5	The Direct Current bus . . . . .	110
3.6	Global architecture . . . . .	112
3.7	Chapter conclusion . . . . .	116
<b>4</b>	<b>Type-1 and Type-2 Fuzzy Logic Controllers and Energy Management Strategies</b>	<b>119</b>
4.1	Type-1 and Type-2 Fuzzy Logic Controllers for DC/DC buck converter application . . . . .	120
4.1.1	Converter modelling and structure of the fuzzy logic controller based Type-1 fuzzy logic . . . . .	120
4.1.2	Interval and General Type-2 Fuzzy Logic Controllers . . . . .	125
4.1.3	Experimental results . . . . .	132
4.2	Energy Management Strategies . . . . .	137
4.2.1	Frequency Energy Management Strategy . . . . .	137
4.2.2	Optimal Fuzzy Logic Energy Management Strategy . . . . .	140
4.3	Chapter conclusion . . . . .	164
	<b>Conclusion and outlooks</b>	<b>167</b>
<b>A</b>	<b>The Energetic Macroscopic Representation</b>	<b>173</b>
A.1	Energetic Macroscopic Representation . . . . .	173
A.2	Maximum Control Structure . . . . .	174

A.3	Practical Control Structure . . . . .	176
<b>B</b>	<b>The salient pole synchronous machine modelling</b>	<b>179</b>
B.1	The d-q synchronous reference frame . . . . .	179
B.2	The salient pole synchronous machine model . . . . .	180
B.2.1	Parks' equations of the machine . . . . .	181
B.2.2	dq currents decoupling . . . . .	182
B.2.3	Inductor current decoupling . . . . .	183
<b>C</b>	<b>PI and IP controllers synthesis</b>	<b>185</b>
C.1	Proportional Integral (PI) controller synthesis . . . . .	185
C.2	Integral Proportional (IP) controller synthesis . . . . .	186
<b>D</b>	<b>Experimental characterization of the NiCd cell at <math>C_3</math> rate</b>	<b>189</b>
<b>E</b>	<b>Batteries' characterization test bench specifications</b>	<b>193</b>
	<b>Bibliography</b>	<b>206</b>



# List of Figures

1	Repartition of the energy consumption by transport sector [Ocd11]. . . . .	1
2	$NO_x$ - (a), $PM_{10}$ - (b) and $CO_2$ - (c) emissions for different goods transport modes [Ocd11]. . . . .	2
1.1	First Hybrid Electric Vehicle [Bouc05]. . . . .	12
1.2	Hybrid Electric Vehicles' configurations [Toyo13]. . . . .	14
1.3	Conventional Dongfeng 7G locomotive. . . . .	16
1.4	Iranian Hybrid G12 locomotive. . . . .	16
1.5	The Railpower Green Goat locomotive. . . . .	17
1.6	Fuel cell-hybrid switcher platform vehicle. . . . .	18
1.7	SNCF Hybrid Electric Locomotive - Plathee project. . . . .	18
1.8	Freight Hybrid Electric locomotive . . . . .	19
1.9	Configuration of the Fuel Cell-battery powered hybrid system for the tram. . . . .	20
1.10	Bombardier Mitrac Energy Saver - Hybrid tram. . . . .	21
1.11	a) Divide and conquer and b) Dynamic Programming . . . . .	24
1.12	Structure of a Type-1 fuzzy system . . . . .	27
1.13	Type-1 Primary (left) and Secondary (right) Membership Functions . . . . .	28
1.14	Structure of a Type-2 fuzzy system . . . . .	28
1.15	Interval Type-2 Primary (left) and Secondary (right) Membership Functions . . . . .	28
1.16	Hybrid Electric Vehicle and its considered configuration [Sola12b].	30
1.17	Process steps for Neural Network controller training and verification [Prok08] . . . . .	32
1.18	Classification of control approaches, global evaluation of optimality assuming a priori known driving cycles [Kutt10]. . . . .	33
1.19	System configuration of the multi-source hybrid vehicle power system [Zhan08]. . . . .	34
1.20	A schematic diagram of the developed energy management strategy [Erdi09]. . . . .	35

1.21	Combined Neural Network-Wavelet Transform Based Energy Management Strategy [Ates10]. . . . .	36
1.22	Neural network inputs and outputs [Asae07]. . . . .	37
1.23	Energy management strategy principle [Akli07]. . . . .	37
1.24	Energy management principle diagram based on fuzzy logic [Jian10]. . . . .	39
1.25	The relationship curve of SOC, power demand and DC/DC output power [Jian10]. . . . .	39
1.26	Concept of the fuel cell powered hybrid drive train [Mogh03]. . . . .	40
2.1	A typical diesel-electric propulsion system . . . . .	46
2.2	Diesel driven generator set use for a typical freight driving cycle . . . . .	47
2.3	Ragone plot . . . . .	47
2.4	Electric structure of the considered system . . . . .	48
2.5	Freight diesel-electric locomotive . . . . .	48
2.6	Freight Hybrid Electric locomotive . . . . .	48
2.7	First example of the evolution of the power requested by a driving cycle according to time. . . . .	50
2.8	Second example of the evolution of the power requested by a driving cycle according to time. . . . .	50
2.9	First theoretical mission with the associated PHP ( $PHP = 50\%$ ) . . . . .	51
2.10	Second theoretical mission with the associated PHP ( $PHP = 20\%$ ) . . . . .	51
2.11	First theoretical mission with $PHP = 50\%$ . . . . .	51
2.12	Second theoretical mission with $PHP = 50\%$ . . . . .	51
2.13	First theoretical mission with $PHP = 50\%$ and its associated useful energy. . . . .	53
2.14	Second theoretical mission with $PHP = 50\%$ and its associated useful energy. . . . .	53
2.15	EHP and PHP calculation applied to the 30 missions . . . . .	53
2.16	Zoom around the most restricting mission (bullet) . . . . .	53
2.17	Power required by the driving cycle number 28. . . . .	54
2.18	Speed of the locomotive (mission number 28). . . . .	54
2.19	Power required by the driving cycle number 3. . . . .	54
2.20	Speed of the locomotive (mission number 3). . . . .	54
2.21	Frequency approach principle . . . . .	55
2.22	Frequency decomposition of the mission power signal into low and high frequencies power signals . . . . .	56
2.23	Electric model adopted for ultra-capacitors representation . . . . .	59
2.24	Batteries technological constraints graph . . . . .	60
2.25	Conventional energy calculation . . . . .	61

2.26	Saturated energy calculation . . . . .	62
2.27	Evolution of the power dedicated to the batteries. . . . .	64
2.28	Batteries technological constraints graph (case 1). . . . .	64
2.29	Batteries technological constraints graph (case 2). . . . .	65
2.30	Batteries technological constraints graph (case 3). . . . .	65
2.31	Batteries technological constraints graph (optimal point). . . . .	66
2.32	Dichotomy algorithm - Top of the border line. . . . .	67
2.33	Dichotomy algorithm - Bottom of the border line. . . . .	68
2.34	Sizing algorithm of the batteries . . . . .	69
2.35	Electric model adopted for batteries representation . . . . .	70
2.36	Evolution of the total number of batteries' cells according to the low pass filter frequencies. . . . .	71
2.37	Evolution of the number of ultra-capacitors' cells according to the low pass filter frequencies. . . . .	71
2.38	Evolution of the number of battery cells in series (top) and in parallel (bottom) according to the low pass filter frequencies. . . . .	72
2.39	Evolution of the number of ultra capacitors cells in series (top) and in parallel (bottom) according to the low pass filter fre- quencies. . . . .	72
2.40	Evolution of the total volume according to the power delivered by the diesel engine . . . . .	73
2.41	Evolution of the total weight according to the power delivered by the diesel engine . . . . .	73
2.42	Arrangement of the cells in the packs . . . . .	74
3.1	Four stroke compression ignition engine steps [ <a href="#">Heyw88</a> ]. . . . .	79
3.2	Energetic Macroscopic Representation (EMR) model of an Internal Combustion Engine (ICE) proposed in [ <a href="#">Lhom04</a> ] . . . . .	80
3.3	General structure of the naturally diesel aspirated engine [ <a href="#">Verd10</a> ] . . . . .	80
3.4	EMR of the ambient air . . . . .	81
3.5	EMR of the intake manifold . . . . .	82
3.6	EMR of the fuel . . . . .	83
3.7	EMR of the cylinders . . . . .	83
3.8	EMR of the exhaust part . . . . .	84
3.9	EMR of the mechanical shaft . . . . .	85
3.10	EMR of the ICE . . . . .	85
3.11	EMR and MCS of the ICE . . . . .	86
3.12	EMR of the salient pole synchronous machine . . . . .	87
3.13	EMR of the alternator . . . . .	88
3.14	Estimation of the load torque and the electromotive forces . . . . .	89
3.15	EMR and MCS of the alternator . . . . .	90

3.16	Modelling of the diesel driven generator set [Baer12a]	91
3.17	Evolution of the power mission reference (red full line) and the electric power (blue dotted line) versus time	92
3.18	Evolution of the fuel volume flow versus time	92
3.19	Evolution of the fuel consumption versus time	93
3.20	Evolution of the $CO_2$ mass product versus time	93
3.21	Control of the mechanical torque of the shaft	93
3.22	Control of the rotational speed of the shaft	93
3.23	Equivalent circuit model for an ultra-capacitor's cell.	94
3.24	EMR of the smoothing reactor.	95
3.25	EMR of the Direct Current (DC) chopper.	96
3.26	Maximum Control Structure (MCS) of the ultra-capacitors' pack [Alle10]	97
3.27	Practical Control Structure (PCS) of a pack of ultra-capacitors	98
3.28	Characteristic of the ultra-capacitors	98
3.29	EMR of the pack of batteries and its relating power electronics.	100
3.30	MCS of a pack of batteries and its relating power electronics	101
3.31	PCS of a pack of batteries and its power electronics.	103
3.32	Batteries' test bench	104
3.33	Batteries' test bench structure	104
3.34	Batteries' capacity test protocol [Devi12]	106
3.35	Evolution of the internal resistance value of the cell according to its State Of Charge and the temperature ( $C_5$ )	107
3.36	NiCd's cell model validation for $-50^\circ C$ ( $C_5$ )	107
3.37	NiCd's cell model validation for $-40^\circ C$ ( $C_5$ )	107
3.38	NiCd's cell model validation for $-20^\circ C$ ( $C_5$ )	108
3.39	NiCd's cell model validation for $0^\circ C$ ( $C_5$ )	108
3.40	NiCd's cell model validation for $20^\circ C$ ( $C_5$ )	108
3.41	NiCd's cell model validation for $40^\circ C$ ( $C_5$ )	108
3.42	EMR and MCS of the rheostat.	110
3.43	EMR of the central DC bus.	111
3.44	Electric structure of the whole system	113
3.45	EMR and MCS of the whole system	115
4.1	Direct Current buck converter test bench	120
4.2	Direct Current buck converter topology	121
4.3	Membership Functions of the first input $e$	123
4.4	Membership Functions of the second input $de$	123
4.5	Membership Functions of the output $s$	123
4.6	Direct Current buck converter controller structure	124
4.7	Inference engine	126

4.8	Fuzzy surface with a 21 points discretized grid . . . . .	128
4.9	Fuzzy surface with a 301 points discretized grid . . . . .	128
4.10	Definition of the uncertainty . . . . .	129
4.11	General Type-2 Primary (left) and Secondary (right) Mem- bership Functions . . . . .	130
4.12	Third dimension representation based on 3 zslices . . . . .	130
4.13	Side view of a general type-2 fuzzy set, indicating three zLevels on the third dimension - [Wagn10]. . . . .	131
4.14	Fuzzy surface with a 21 points discretized grid and 100 zslices	132
4.15	Fuzzy surface with a 301 points discretized grid and 100 zslices	132
4.16	Interval Type-2 and General Type-2 fuzzy surfaces differences with a 21 points discretized grid . . . . .	133
4.17	Interval Type-2 and General Type-2 fuzzy surfaces differences with a 301 points discretized grid . . . . .	133
4.18	Direct Current test bench structure . . . . .	134
4.19	T1 only . . . . .	134
4.20	Experimental T1 and IT2 control results . . . . .	136
4.21	T1 and IT2 control zoom . . . . .	137
4.22	Power of the mission according to time . . . . .	138
4.23	Power delivered by the diesel engine set according to time . . .	138
4.24	Power delivered by the batteries according to time . . . . .	138
4.25	Power delivered by the UCs according to time . . . . .	138
4.26	Power dissipated by the rheostat according to time . . . . .	139
4.27	Evolution of the bus voltage according to time . . . . .	139
4.28	Evolution of the batteries estimated SOC according to time . .	139
4.29	Evolution of the UCs estimated SOC according to time . . . .	139
4.30	Evolution of the cut-off frequency of the filter . . . . .	141
4.31	Evolution of the limitation factor according to the estimated UCs' SOC . . . . .	142
4.32	Sub-Energy Management Strategy of the diesel driven gener- ator set . . . . .	143
4.33	Global Energy Management Strategy . . . . .	145
4.34	Interval Type-2 MF definition . . . . .	146
4.35	Output MF definition . . . . .	146
4.36	Structure of the IT2 FLC chromosome used for optimization .	146
4.37	Implemented Genetic Algorithm . . . . .	150
4.38	Third dimension isoscele triangular Membership Functions . .	151
4.39	Modeling of the third dimension using a chromosome of 21 genes. . . . .	151
4.40	dP Membership Functions implemented in [Sola12b] . . . . .	152
4.41	$e_{SOC_{batt}}^*$ Membership Functions implemented in [Sola12b] . . .	152

4.42	$dP_{ICE}$ Membership Functions implemented in [Sola12b]	153
4.43	Fuzzy map controller implemented in [Sola12b]	153
4.44	dP Membership Functions implemented for optimized T1-Fuzzy Logic Controller	153
4.45	$e_{SOC_{batt}}^*$ Membership Functions implemented for optimized T1-Fuzzy Logic Controller	153
4.46	$dP_{ICE}$ Membership Functions implemented for optimized T1-Fuzzy Logic Controller	153
4.47	Fuzzy map controller implemented for optimized T1-Fuzzy Logic Controller	154
4.48	dP Membership Functions implemented for optimized IT2-Fuzzy Logic Controller	154
4.49	$e_{SOC_{batt}}^*$ Membership Functions implemented for optimized IT2-Fuzzy Logic Controller	154
4.50	$dP_{ICE}$ Membership Functions implemented for optimized IT2-Fuzzy Logic Controller	155
4.51	Fuzzy map controller implemented for optimized IT2-Fuzzy Logic Controller	155
4.52	Differences between the optimized T1 (figure 4.47) and optimized IT2 (figure 4.51) fuzzy map controllers	156
4.53	dP Membership Functions implemented for optimized GT2-Fuzzy Logic Controller	156
4.54	$e_{SOC_{batt}}^*$ Membership Functions implemented for optimized GT2-Fuzzy Logic Controller	156
4.55	$dP_{ICE}$ Membership Functions implemented for optimized GT2-Fuzzy Logic Controller	157
4.56	Fuzzy map controller implemented for optimized GT2-Fuzzy Logic Controller	157
4.57	Differences between the optimized IT2 (figure 4.51) and optimized GT2 (figure 4.56) fuzzy map controllers	158
4.58	Evolution of the different powers (driving cycle, batteries, Internal Combustion Engine, UCs and rheostat) according to time	159
4.59	Zoom on the evolution of the different powers (driving cycle, batteries, Internal Combustion Engine, UCs and rheostat) according to time	160
4.60	Evolution of the estimated batteries' SOC (a) and evolution of the acceleration of the vehicle (b) according to time	160
4.61	Evolution of the estimated UCs' SOC (a) and evolution of the speed of the vehicle (b) according to time	161
4.62	Evolution of the bus voltage according to time	161

4.63	Evolution of the energy delivered by the diesel driven generator set according to the implemented controllers and the considered power mission . . . . .	163
A.1	Maximum Control Structure of an element of accumulation . . .	175
A.2	Maximum Control Structure of an element of conversion . . .	176
A.3	Maximum Control Structure of a coupling element (upstream - left and downstream - right) . . . . .	176
B.1	Model of the synchronous machine in the three phase frame .	180
B.2	Model of the synchronous machine in the three phase frame .	181
C.1	PI controller structure . . . . .	185
C.2	IP controller structure . . . . .	186
D.1	Evolution of the internal resistance value of the cell according to its State Of Charge and the temperature ( $C_3$ ) . . . . .	189
D.2	NiCd's cell model validation for $-50^{\circ}C$ ( $C_3$ ) . . . . .	190
D.3	NiCd's cell model validation for $-40^{\circ}C$ ( $C_3$ ) . . . . .	190
D.4	NiCd's cell model validation for $-20^{\circ}C$ ( $C_3$ ) . . . . .	190
D.5	NiCd's cell model validation for $0^{\circ}C$ ( $C_3$ ) . . . . .	190
D.6	NiCd's cell model validation for $20^{\circ}C$ ( $C_3$ ) . . . . .	191
D.7	NiCd's cell model validation for $40^{\circ}C$ ( $C_3$ ) . . . . .	191



# List of Tables

3.1	NiCd cell characteristics . . . . .	103
3.2	Theoretical time to fully charge one element depending on applied currents . . . . .	105
3.3	Maximum and average errors between the experimental data and the Simulink model at $C_5$ rate. . . . .	109
4.1	Considered rule base for controlling the output voltage of the buck converter . . . . .	122
4.2	T1 and IT2 comparison for two different grids . . . . .	135
4.3	IT2 and GT2 comparison for a 50% uncertainty . . . . .	135
4.4	IT2 and GT2 comparison for a 100% uncertainty . . . . .	136
4.5	Rule base used in the Fuzzy Energy Management Strategy . .	144
4.6	Energy provided by the diesel driven generator set according to the 4 implemented FLCs . . . . .	162
A.1	Energetic Macroscopic Representation blocks [Boul10b] . . . .	174
A.2	Kinetic and potential variables [Lhom06] . . . . .	175
D.1	Maximum and average errors between the experimental data and the Simulink model at $C_3$ rate. . . . .	190



# List of Acronyms

<b>DC</b>	Direct Current
<b>DOD</b>	Depth Of Discharge
<b>DP</b>	Dynamic Programming
<b>EHP</b>	Energetic Hybridization Potential
<b>EMR</b>	Energetic Macroscopic Representation
<b>EMS</b>	Energy Management Strategy
<b>FLC</b>	Fuzzy Logic Controller
<b>FOU</b>	Footprint Of Uncertainty
<b>GA</b>	Genetic Algorithm
<b>GT2</b>	General Type-2
<b>HEL</b>	Hybrid Electric Locomotive
<b>HEV</b>	Hybrid Electric Vehicle
<b>IAE</b>	Integral Absolute Error
<b>ICE</b>	Internal Combustion Engine
<b>IP</b>	Integral Proportional
<b>IPCC</b>	Intergovernmental Panel on Climate Change
<b>IT2</b>	Interval Type-2
<b>MCS</b>	Maximum Control Structure
<b>MF</b>	Membership Function

**NiCd** Nickel Cadmium  
**NNs** Neural Networks  
**OCV** Open Circuit Voltage  
**PCH** Port-Controlled Hamiltonian  
**PCS** Practical Control Structure  
**PHP** Power Hybridization Potential  
**PI** Proportional Integral  
**PMP** Pontryagin Minimum Principle  
**RFF** Réseau Ferré de France  
**SOC** State Of Charge  
**SNCF** Société Nationale des Chemins de Fer Français  
**UCs** Ultra-Capacitors





# Introduction

## Project Context

Energetically and environmentally speaking, the railway transportation is known to be one of the most efficient mean of transport. From the seventies till today, the repartition of the energy consumption by transport sector is represented on figure 1 - [Ocd11].

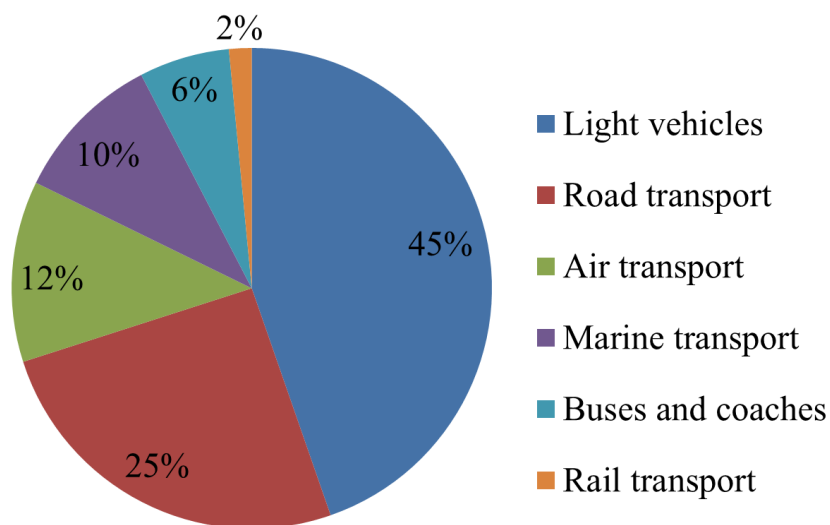


Figure 1: Repartition of the energy consumption by transport sector [Ocd11].

The evolution of the  $CO_2$  emissions chargeable to the different transport forms is also comparable to the transports energy consumption repartition. For instance, figure 2 represents the  $NO_x$  - (a),  $PM_{10}$ <sup>1</sup> - (b) and  $CO_2$  - (c)

---

<sup>1</sup>The  $PM_{10}$  (Particulate Matter 10) concern the particles which diameter is less than 10 micrometers.

emissions (g/t.km) for the different goods transport modes.

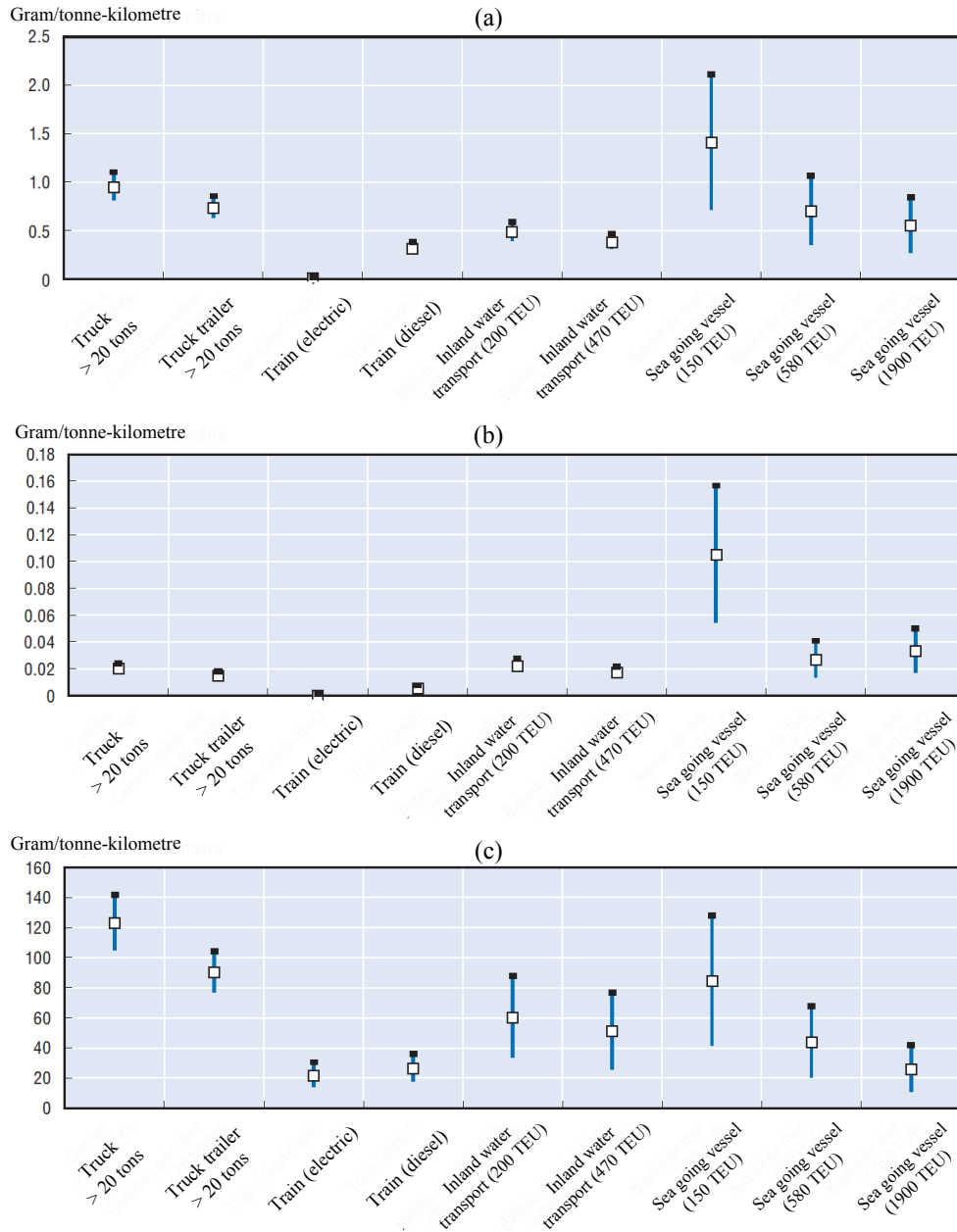


Figure 2:  $NO_x$  - (a),  $PM_{10}$  - (b) and  $CO_2$  - (c) emissions for different goods transport modes [Ocd11].

However, the freight activities <sup>2</sup> are confronted to technical issues preventing their cleaner evolution. Different technological bolts are identified. The European freight activities are mainly performed on electrified junctions. However, the charging/discharging phases of a freight mission often occurs on non-electrified junctions such as in ports or factories. Thus, operators must use shunting locomotives to get back and dispatch a train transporting goods. The use of different machines (locomotive and shunting locomotive) induces time wasting, unproductive logistics and exploitation spending... Moreover, shunting locomotives are powered by diesel-electric propulsions. From environmental, economical and energetics points of view, diesel-electric propulsions are not the optimal solution. The use of a fossil energy and the fact that shunting locomotives are not stopped during idling time drives to an additional pollution and fuel waste. Indeed, engine low loads correspond to their worst efficiency. The noise pollution is also increased. The project aims at proposing solutions in order to:

- reduce the environmental impact of this kind of activities (atmospheric and noise pollutions),
- develop the efficiency of freight activities,
- propose solutions adapted to the tunnel maintenance operations,
- provide independent autonomy to the locomotive for the mission duration.

Thus, a hybrid electric powertrain architecture is proposed in this project. The modelling of the on-board sources, the control architecture implementation and the identification of the required sensors are realised using the Energetic Macroscopic Representation (EMR) (appendix A). Moreover, a new real-time Energy Management Strategy (EMS) based on fuzzy logic is considered.

The best way to bring solutions, fitting with the railway market specifications, is to merge international industrial and laboratory/academic skills together. Thus, the research developed in this project is in direct line with preliminary researches realised at the Energy department of FEMTO-ST lab during the last years. Indeed, this study comes within the scope of FEMTO-ST research works relative to:

- the energy sources such as batteries ([Narj08, Mulo10, Boul10a]), Ultra-Capacitors (UCs) ([Bont05, Gual05, Louk10]) and fuel cells ([Jeme04, Teki04]),

---

<sup>2</sup>Transportation of goods using a locomotive

- Hybrid Electric Vehicle (HEV) design and EMS & control such as hybrid helicopters ([[Bien11](#), [Devi11](#)]), military heavy-duty vehicles ([[Wu10](#), [Sola09](#)]) or urban vehicles ([[Mai10](#)]).

## Partners and contributors of the project

The Franche-Comte region holds exceptional research teams specialized in the railway market and also world recognised in the development of innovative solutions for HEVs and renewable energy sources. The two partners of the project (Alstom Transport Group and FEMTO-ST Laboratory) are presented. This work is also the subject of an European collaboration (University of Essex).

### Alstom Transport Group

This partner provides the project specifications, the freight locomotives' characteristics, the shunting activities attributes and the railway market background. Alstom Transport is the world leader in urban rail transport systems (trams, undergrounds) and holds the number 2 position in very high-speed trains. The company has an 19% share of the full accessible rail transport equipment and service market. Alstom Transport's range of offerings includes rolling stock products, rail infrastructure equipment, signalling systems and maintenance services. In partnership with Réseau Ferré de France (RFF) and the Société Nationale des Chemins de Fer Français (SNCF), Alstom Transport set a new world rail speed record of 574.8 km/h on the 3<sup>rd</sup> of April 2007. The previous world record was 515.3 km/h.

### FEMTO-ST Laboratory

FEMTO-ST is a joint research unit which is affiliated with the French National Centre of Scientific Research (CNRS), the University of Franche-Comte (UFC), the National School of Mechanical Engineering (ENSMM) and Microtechnology, and the Belfort-Montbéliard University of Technology (UTBM). It was founded in January 2004 from the merging of 5 different laboratories active in different fields of engineering science: mechanics, optics and telecommunications, electronics, time-frequency, energetics and fluidics. FEMTO-ST is organized according to the seven following research departments: AS2M, Energy department, Mechanics, Optics, Time and Frequency, MN2S and DISC.

- **Energy research department** The Energy research department is part of the FEMTO-ST Laboratory. It is composed of researchers specialized in Energetics and Electrical Energy. This specificity permits major scientific advances in different themes such as:  $\mu$ -cogeneration, electric and thermal machines, hybrid vehicles, fuel cells, Energy Storage Systems,...
- **Hybrid & Fuel Cell Systems Research Team** The team is part of the Energy research department. It proposes and provides the technological solutions in terms of modelling of the on-board sources, control of the system and implementation of the intelligent EMS. The Hybrid & Fuel Cell Systems Research Team is highly specialized in a systemic approach of multiphysics systems such as fuel cell systems or hybrid electrical vehicles. The group looks forward to develop original modelling approaches, real-time and less-expensive diagnostics, prognostics and control systems.

## Computational Intelligence Center

This European collaboration aims at bringing the expertise of the foreign laboratory on a precise point of the project during three months (development of Type-1 and Type-2 Fuzzy Logic Controllers using a genetic algorithm). The Centre for Computational Intelligence is based at the University of Essex, United Kingdom. The Centre field of interests are in theory, design, application, and development of biologically, socially and linguistically motivated computational paradigms emphasising genetic algorithms, evolutionary programming, fuzzy systems, neural networks and hybrid intelligent systems in which these paradigms are contained. The centre includes experts from biological sciences, social sciences, mathematical sciences, entrepreneurship and business as well as experts from computer sciences and engineering.

## MEGEVH research group

This work is also part of the research group MEGEVH (Energy Modelling and Energy Management of Hybrid and Electric Vehicles) which is a thematic group of the inter-regional network RT3 (Technological Research for Land Transport) of the Ministry of Research. It aims at fostering collaboration between academic and industrial partners on the subject of modelling and power management of hybrid vehicles through various actions:

- the diffusion of information to review the responsibilities of each partner within the group, as well as the collaborations,

- the coordination of the projects to define the priority goals and themes,
- the labelling of the projects to ensure consistency of the various work projects and to assist the funding requests.

The MEGEVH policy consists in defining generic methods for the modelling, the energy management and optimisation of the hybrid electrical vehicles. The scientific activities of this work take over from previous research works:

- modelling methodologies of different HEVs [Boul09, Chen10],
- control methodologies of different HEVs [Walt07, Letr12],
- optimisation methodologies of different HEVs [Kerm11],
- modelling and control of Fuel Cell subsystems [Chre08],
- modelling and control of storage subsystems [Alle13],
- new powertrain topology for different hybrid trucks [Syed11],
- new powertrain topology using electric variable Transmission [Chen11],
- multi-phase starter-alternator for mild HEVs.

## Structure of the manuscript

The first chapter introduces the main energy and HEVs challenges. It includes a background on the evolution and improvements of the HEVs in our society. The main existing architectures are also presented and a literature review informs about the different projects dealing with the development of Hybrid Electric Locomotives. Then, the literature overview focuses on the considered techniques and methodologies to design an EMS. The overview is a chance to expose the fuzzy logic principles and existing applications. Thus, basic concepts of the fuzzy logic are given. The motivations, to consider type-2 fuzzy logic instead of type-1 fuzzy logic and their application in engineering applications and particularly EMSs works, are explained. Finally, the chapter presents the former EMSs' applications dedicated to the hybrid railway powertrains.

The second chapter deals with the evolution of the conventional shunting locomotive architecture towards the series hybrid electric architecture. It specifies the choice and the benefits of the secondary sources which are used

in the project according to its specifications. Then, the sizing problematic of these on-board secondary sources is discussed. Thus, the second part of the chapter aims at presenting the indicators to detect the most representative mission profile among all available ones. Next, it focuses on the development of a mathematical tool to have an estimation of the number of secondary sources' elements to be loaded into the locomotive. The method also includes the series-parallel sizing with weight and volume estimations.

The third chapter details the characteristics, the modelling, the Energetic Macroscopic Representations and the Maximum Control Structures (MCS)s of each available sources. The knowledge of the benefits, the drawbacks and the behaviour of each source is very important for the future design of the EMS. This work pays a special attention to the implementation of a new dynamical Energetic Macroscopic Representation for the Internal Combustion Engine (ICE). The Energetic Macroscopic Representation is very useful to model the entire structure, to couple the different sources, to identify sensors/estimators and to deduce the Practical Control Structure (PCS). Moreover, the development of a test bench leads to the experimental characterization of the considered batteries. Experimental results are presented and used to improve the models. They mainly focus on the thermal behaviour of the batteries. Then, the modelling emphasizes the coupling of all these elements into a unified structure. The series architecture modelling of the Hybrid Electric Locomotive (HEL) also includes the power electronics and the central Direct Current (DC) bus.

The fourth chapter is fully dedicated to the fuzzy logic control. The first study is dedicated to the control of the output voltage of a DC/DC buck converter already used in previous studies [Sola12a]. It aims at evaluating the performances of the fuzzy logic control in real time conditions and at performing preliminary tests. Thus, the study focuses on the design of the controller and the discussion of the experimental results. They lead to the comparison of the performances of the different fuzzy logic controllers and the experimental validation of the controllers. The second application presents the intelligent EMS of the studied HEL. It is also partially based on a Fuzzy Logic Controller (FLC) which parameters are optimized using a Genetic Algorithm (GA). The GA consists in minimizing the use of the primary source. Thus, the research proposes a comparison of the efficiency of the different synthesized FLCs and the validation by simulation of the controllers. Both applications are tested with Type-1, Interval Type-2 and General Type-2 based on zSlices FLCs.

Finally, conclusions and possible outlooks for the continuation of the study are presented.





# Chapter 1

## Energy and Hybrid Electric Vehicles Challenges

The research presented in the dissertation focuses on the study of the EMS based on Type-2 Fuzzy Logic for HEL. First, this chapter states the main challenges to be faced by human societies in energy and transportation. Thus, a background aims at describing the reasons of the HEVs' evolutions and their sudden improvements in our society since their birth up until now. Secondly, the chapter presents the available techniques and methodologies used in HEVs' EMSs' design.

Section 1.1 deals with the HEVs' challenges, benefits and drawbacks of the existing architectures and also summarizes the existing research works about HELs. Then, section 1.2 highlights the different methods that can be considered to implement EMSs. Finally, section 1.3 presents concluding remarks.

### 1.1 Hybrid Electric Vehicles

In addition to have a primary source, a HEV is also made up of reversible storage sources. Those secondary sources can be chemical (electrochemical accumulators) or electrostatic (UCs) or kinetic (flywheel) sources... The powertrain of a HEV presents a primary source (ICE for instance) coupled with secondary sources. HEVs are a bridge between conventional vehicles and electric vehicles. In this section, the background and the classification of the HEVs are firstly tackled. Then, a subsection deals with a background of the HELs' studies. Finally, important and available existing EMSs are depicted.

### 1.1.1 Background

The first HEV was developed in 1899 by the Pieper family (father and son) [Gutf11]. Indeed, at these early days, no one cared about petroleum reserves and no more about the environment. However, two points of interests were pointed out: easy driving and a more powerful vehicle. From March 1899, Pieper family developed a system including a gasoline engine, a generator and a pack of batteries (figure 1.1).

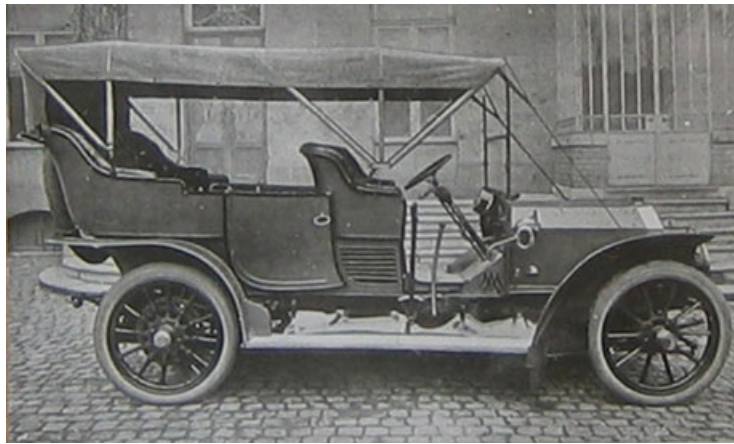


Figure 1.1: First Hybrid Electric Vehicle [Bouc05].

However, this study was rapidly left due to the following improvements of the ICEs. The Seventies and Eighties were marked by a revival interest for this kind of technology. This interest, aroused by the increasing pollution in the cities, was limited again by the improvement of the fuels and ICEs (introduction of the catalytic convertors, turbochargers or High Pressure Direct Injection systems for instance) till today. Now, the air pollution, the greenhouse gas emissions, the deterioration of the air quality, the rarefaction of the petroleum reserves are factors renewing the interest in HEVs. Above all, the cost to access and to use this resource mainly impacts the transportation market. Those new vehicles reconcile autonomy and flexibility of ICEs with the electric engines cleanness.

Environmental and Transportation energetic challenges are linked to:

- the pollution and the greenhouse gas emissions,
- the resources' rarefaction plus the cost to access and exploit them,
- the congestion of the urban areas.

A strong consensus, dealing with the global warming and the greenhouse gas emissions, rapidly appeared. For instance, the Intergovernmental Panel on Climate Change (IPCC) <sup>1</sup> recommends a stabilization of the atmosphere CO<sub>2</sub> rates at 440 ppm (Part Per Million) if the stabilization is performed between 2010 and 2015. The convergence of the scientific community and industry confirms the urgency and the reality of the problem. Even if the hydrogen is presented like the ultimate solution, intermediary possibilities must be developed previously. HEVs are intermediary solutions and are classified according to three main architectures presented in the next subsection.

### 1.1.2 Classification

Conventional vehicles are equipped with classical powertrains (thermal engine, gearbox, transmission). These systems are not optimal in case of transportation requiring frequent starts and stops or traffic jams. Nevertheless, such systems are very flexible because of their large power panel (slow speed moving, hill starts or overtaking). The low loads correspond for thermal engines to their worst efficiency. Thus, cars and buses running in high density urban areas or shunting locomotives are concerned. HEVs appear like a good compromise between pure electric vehicles and conventional vehicles. Three main architecture families stand out:

- Series HEV: All traction power is converted from electricity. A DC bus ensures the electrical energy balance of the system. The primary source (ICE or fuel cell) is not mechanically coupled to the powertrain but is coupled to an electrical generator to supply energy to the DC bus. The architecture presents some benefits for the engine use. It never idles (thus leads to reduction of the vehicle emissions) and it can continuously operate in its most efficient region. The architecture is presented on figure 1.2.a). However, series HEVs require large and heavy batteries packs which charge level is maintained by the engine.
- Parallel HEV: A parallel configuration presents a direct mechanical connection between the power unit and the wheels, as in conventional vehicles, but also has an electric motor that drives the wheels. Both the engine and the motor supply power simultaneously. Most parallel vehicles do not need a separate generator because the motor regenerates the batteries. The architecture is presented on figure figure 1.2.b).

---

<sup>1</sup>The IPCC is a scientific body under the auspices of the United Nations. It reviews and assesses the most recent scientific, technical and socio-economic information produced worldwide relevant to the understanding of climate change.

- Series-Parallel HEV: The architecture is a combination between series and parallel architectures. The ICE drives the powertrain or supplies energy to the DC bus. This architecture also called power split configuration is presented on figure 1.2.c).

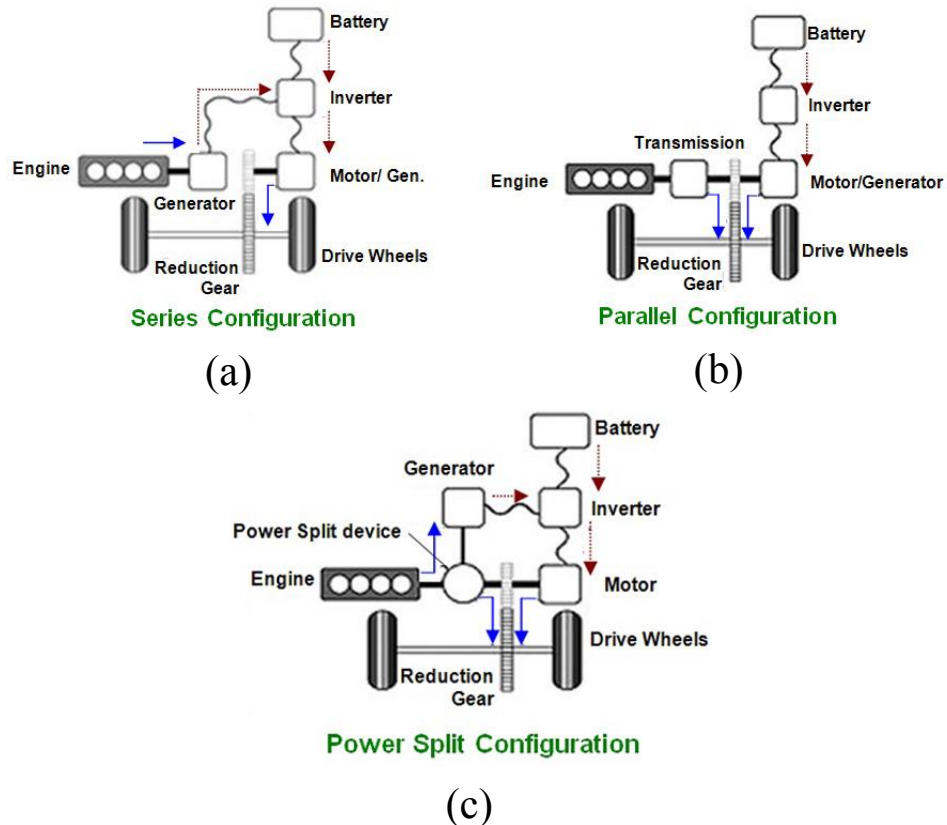


Figure 1.2: Hybrid Electric Vehicles' configurations [Toyo13].

Generally, HEVs' architecture (cars, trucks, locomotives, helicopters...) are based on one of these configurations. Their respective benefits and drawbacks clearly lead to different control structures and EMSs' design. The next subsection presents the main research works and projects dealing with the particular case of the HELs.

ba

### 1.1.3 Hybrid Electric Locomotives

The met energy and environmental problems are the two major themes in the world. Thus, focused on the freight market, HEL is becoming a new

development in many countries. In the following descriptions, some of the existing HELs' research projects and developments are presented. They are focused on the hybridisation problematic of switcher locomotives. As explained previously, these conventional locomotives are mainly used for the disintegration of the train, organization, pull-out and changing railway lanes. Most of the time, the primary source (diesel engine) runs at idle state. HELs could effectively adjust the engine's operating range, reduce locomotive fuel consumption and emissions. Moreover, two tram studies (out of the switcher locomotives' scope) are also presented in this subsection.

### **The Chinese Dongfeng 7G HEL**

Electric locomotives have usually two braking modes: air-braking and resistor-braking. In traditional locomotives, a part of the braking energy from the generator is dissipated through a heat resistance. Using on hybrid technology, the regenerative braking energy from the motor could be stored with batteries, which could save energy effectively. Thus, according to the locomotive's performance requirements of Ministry of Railways in China and the requirements of manufacturers, the hybrid locomotive in [Xin11] (figure 1.3) is equipped with a 1324 kW engine, a synchronous traction generator, six DC traction motors and lithium iron phosphate ( $LiFePO_4$ ) batteries. The series mode is used. In traction conditions, the generator creates a three-phase alternating current, and after rectification, supply the six DC traction motors.

### **The Iranian G12 HEL**

A four axles G12 locomotive is converted to a HEL. Two induction motors are used and the 750 kVA diesel generator is replaced by a 80 kW diesel engine and a 50 kVA generator. The 1200 V, 300 A inverters are supplied by 480 V traction lead acid batteries [Asae07].

According to [Asae07], the system advantageous are:

- up to 80% reduction in the fuel consumption,
- up to 80% reduction in the pollution and emission gases,
- recovering energy brake by regenerative braking,
- noise reduction,
- diesel generator downsizing,



Figure 1.3: Conventional Dongfeng 7G locomotive.



Figure 1.4: Iranian Hybrid G12 locomotive.

- better maneuver,
- cost saving up to 300,000 US\$,
- possibly of using the old system chassis and converting it.

## The American Railpower Green Goat

The Railpower Green Goat locomotive is a low-emissions diesel hybrid switcher locomotive built by Railpower Technologies Corporation [Cous06] (figure 1.5).



Figure 1.5: The Railpower Green Goat locomotive.

It is powered by a single Caterpillar six cylinder inline engine developing 300 horsepower (224 kW), which is also connected to a large battery bank where both sources combine for a total power output of 2,000 horsepower (1,490 kW). For an energy storage device, a valve-regulated lead-acid (VRLA) battery is used. Their lower specific energy is not as much a concern given that locomotives are not as constrained by weight considerations as other vehicles as they need a certain amount of weight to maintain traction.

This Green Goat platform has also been used in [Mill07] - figure 1.6.

This fuel cell-battery hybrid switcher locomotive is used for urban and military-base rail applications leading to commercial locomotives purposes. The diesel fuel tank is removed in preparation for retrofitting the fuel cell power plant and hydrogen storage. Fuel cell power for locomotives combines the environmental benefits of a catenary-electric locomotive with the higher overall energy efficiency and lower infrastructure costs of a diesel-electric locomotive [Mogh03].

## The French PLATHEE Project

The SNCF developed a demonstrator of a new HEL (figure 1.7). Firstly, a 600 kW diesel engine used for "BB63000" locomotives was replaced by a smaller one associated with batteries and UCs and four electric engines [Akli07].



Figure 1.6: Fuel cell-hybrid switcher platform vehicle.

The use of a mechanical energy buffer such as a flywheel [Jaaf09], instead of accumulators, has also been tested. Now, the locomotive is composed of an ICE, an UCs' bank, an electrochemical battery bank and a fuel cell system [Baer11b] for the generation subsystem. The traction subsystem is composed of two driven-bogies associated with two series DC machines. An interleaved chopper supplies the machines [Maye12].



Figure 1.7: SNCF Hybrid Electric Locomotive - Plathee project.

## The German Alstom Hybrid Loco

An electrical propulsion system, consisting of a battery, a diesel driven generator, power electronics, electrical motors and a mechanical gearbox have been integrated into an existing shunting locomotive. The new vehicle is powered by batteries (figure 1.8).



Figure 1.8: Freight Hybrid Electric locomotive

The generator charges the battery-set when needed, and can provide additional energy to the propulsion in peak times, as a booster of the batteries. Thus, electrical propulsion is not consuming energy during idle time, which save until 40% of fuel consumption in an operation cycle with 75% idle time. The generator recharging the batteries is smaller than diesel engines powering conventional shunters, thus generating 60% less particles and 40% less  $NO_x$ . Between the recharging cycles of the generator, the hybrid locomotive could be operated in hall or tunnels with no pollution. The noise is 15 dB less than in a conventional solution. The maintenance costs are 15% less, thus the life cycle cost is 30% less. The traction force at zero/low speed is 195 kN and the "wake-up time" is 2 s.

## The Spanish hybrid tram

A 540 kW hybrid tram based on fuel cell and battery is developed for a real surface tram in the centre of Seville in Spain [Fern11]. Lead by a Spanish

consortium and supported by the Spanish Ministry of Science and Technology, the goal is to eliminate the infrastructure associated to catenary instead of operating requiring overhead line and pantograph. The hybrid tram is composed of two 127 kW Proton Exchange Membrane Fuel Cells (PEMFCs) and a 34 Ah Nickel Metal Hydride (Ni-MH) directly connected to the traction DC bus.

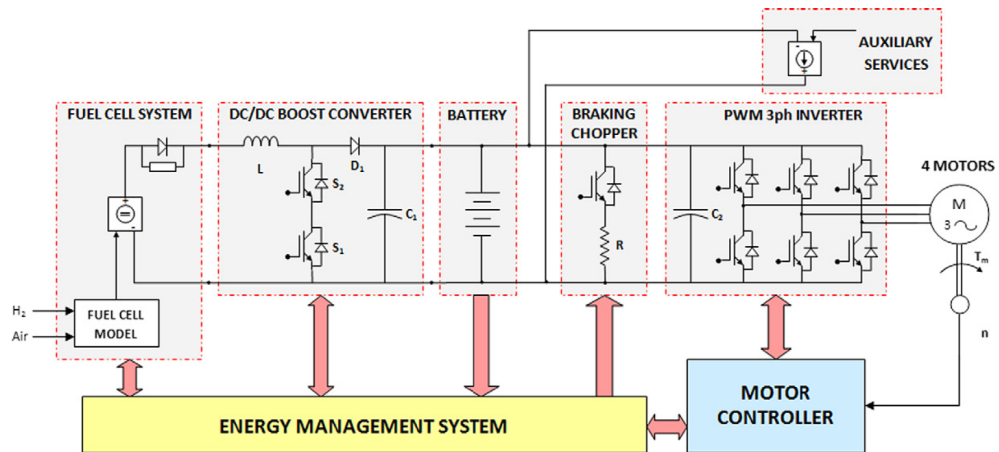


Figure 1.9: Configuration of the Fuel Cell-battery powered hybrid system for the tram.

The figure 1.9 shows the configuration of the system and includes a fuel cell, a battery, a converter, auxiliaries, traction motors, a braking chopper, controllers and an EMS module. The rechargeable battery supplies the fuel cell during the tram acceleration and recovers energy during braking phases.

### Mitrac Energy Saver

Jointly with MVV Energy (Mannheim - Germany) and Bombardier, a hybrid tram, called "Mitrac Energy Saver", was developed. The system is based on UCs which allow frequent starting and braking. 600 UCs' cells are placed on the roof of the tram and help to reduce the energy consumption up to 30%. Moreover, lower peak current demand means that fewer substations are needed which reduces infrastructure investment. The additional power can be used to boost the tram's speed when the line current is limited. This extra power results in additional tractive effort and allows significantly higher acceleration. Then, it is also a solution if sections without a catenary are desired. It enables catenary free operation for short distances and makes possible to continue operation in case of maintenance work or power failures [Bomb13].

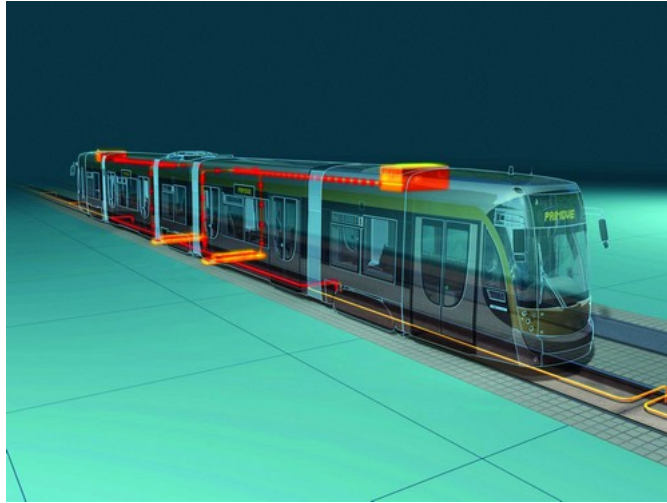


Figure 1.10: Bombardier Mitrac Energy Saver - Hybrid tram.

This non-exhaustive list could be completed quoting other examples and hybridisation railway projects such as:

- the ULEV-TAP2 (Ultra Low Emission Vehicle - Transport using Advanced Propulsion 2) project co-ordinate by Siemens Transportation Systems [Jeff04],
- Siemens Avanto Light Rail Vehicle (flywheel, ICE).

Some of these examples and other projects are also used in the subsection 1.2.4 dealing with the existing EMSs dedicated to the HELs.

## 1.2 Energy Management Strategies

A correct energy management is a critical problem for HEVs. The EMS determines which power source must be used according to the power requests defined by the driver, driving situations and mission profiles. In other words, an EMS is a mathematical algorithm managing the produced, used and saved on-board energy. This subsection aims at presenting the most used methods to develop an EMS respecting the imposed specifications of a HEV design project. Indeed, it looks like more interesting to emphasize the benefits and the drawbacks of the two methods' categories (on-line and off-line methods) dealing with the most common ones. The subsections 1.2.1 to 1.2.3 are

relating to the global HEVs' literature. Then, the subsection 1.2.4 describes the different existing EMSs in the HELs' literature.

### 1.2.1 Energy management problematic

The torque reference supplied from an ICE depends on the injected fuel quantity. For HEVs, the torque reference applied to the wheel depends on the number of electric engines in the vehicle, on the driver's power demand and on the on-board energy availability. The two different torque reference uses permit to carry out some goals:

- the minimization of fuel consumption and CO<sub>2</sub> emissions,
- the decrease of the pollutant emissions (CO, NO<sub>x</sub>, HC),
- by stopping the ICE and by using an electric engine there is no pollutant emission, noise pollution is reduced and the fuel consumption is improved. However, this electric mode is time limited because of energy sources capacity (batteries, UCs...).

Among these possibilities, noise reduction does not give rise to the resolution of a control problem because the electric mode is directly activated by the driver. This mode is also a consequence of the EMS. Consumption reduction is a difficulty because it depends on the electric engine functioning, its time working and the considered secondary sources specifications (their State Of Charge (SOC) for instance). Thus, to reduce pollutant emissions of a vehicle, two main solutions are available:

- the reduction of the losses due to aerodynamic resistance and inertia of the vehicle,
- the improvement of the energetic conversion efficiency.

Considering HEVs, the improvement of the energetic conversion efficiency is performed by controlling the power flows between the different sources. This kind of global control is the EMS. Two optimization categories of methods, to perform the minimization of the fuel consumption of an HEV, must be distinguished:

- off-line optimization methods with a priori knowledge of the input duty cycle [Kess07],
- on-line optimization methods without a priori knowledge of the driving cycle [Rous08].

## 1.2.2 Strategies based on off-line optimization algorithms

Off-line optimization techniques appear like effective methods for EMSs of HEVs [Fang12]. Those algorithms aim at optimally defining the power split between the ICE and electric motors to minimize the fuel consumption and/or gas emissions. This category of optimization processes take into account the system's physical constraints such as the UCs voltage limitation or the batteries' currents' limitation. Off-line optimal algorithms use a priori knowledge of the driving cycle to establish the optimal parameters of the EMS. They are referred to as non causal approaches. However, the results obtained should be considered as useful benchmarks for analysing, evaluating and deriving real-time control strategies. The off-line optimization algorithms presented in this manuscript are the Dynamic Programming, the Pontryagin minimum principle, the Lagrange multiplier and the Port-Controlled Hamiltonian. Even if the list remains to be non-exhaustive, they are the most implemented techniques in the research works.

### Dynamic programming

Dynamic Programming (DP) is an approach employing the principle of optimality introduced by Richard Bellman [Si09]. Instead of enumerating all possible control sequences, dynamic programming only searches admissible state and/or action values that satisfy the principle of optimality. All optimal solution relies itself on sub-problems solved locally [Gong08]. In other words, the optimal solution of a problem is deduced in combining optimal solutions of a serie of sub-problems. Problem solutions are studied from bottom to top. The smaller sub-problems' solutions are solved and the global optimal solution is obtained gradually [Liu08, Joha07]. This method is opposed to the recursive methods which solutions are studied from top to bottom (divide and conquer - figure 1.11).

Some considerations must be done in order to have an accurate solution. The complexity increases when constraints are added to the optimization problem and in consequence, the time computation also increases [Caux10a, Lesc10]. For instance, in [Vino07], the fuel consumption is the only one operating variable of the DP problem to minimize the CO<sub>2</sub> emissions with a priori knowledge of the driving cycle. For instance, in [Lin03], the minimization of the fuel consumption/gas emissions is also solved using an EMS based on a DP resolution. A cost function, introducing fuel consumption and gas emissions variables, is minimized (equation 1.1).

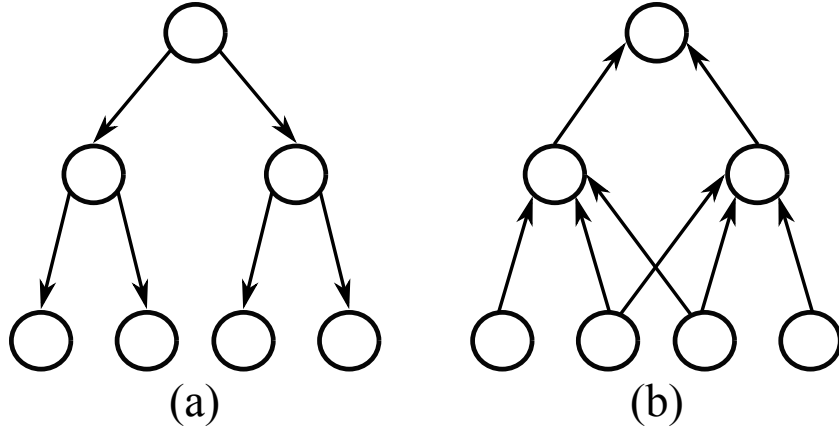


Figure 1.11: a) Divide and conquer and b) Dynamic Programming

$$\left\{ \begin{array}{l} J = \sum_{k=0}^{N-1} L(x(k), u(k)) \\ J = \sum_{k=0}^{N-1} fuel(k) + \mu NOx(k) + \nu PM(k) \end{array} \right. \quad (1.1)$$

with:

- $u(k)$ , the control variables vector,
- $x(k)$ , the state vector of the system,
- $N$ , the duration of the driving cycle,
- $L$ , the instantaneous cost including fuel use or consumption ( $fuel(k)$ ) and engine-out NOx and Particulate Matters (PM) emissions,
- $\mu$  and  $\nu$ , weighting factors.

### Pontryagin Minimum Principle

The Pontryagin Minimum Principle (PMP) is also an optimal control algorithm. It brings a dynamical system from a precise state to another one state with constraints [Lesc10]. Moreover, the PMP permits to replay a control sequence optimally realized [Caux10b]. It provides good results when the criteria can be linearly expressed and derived. The main drawback resides in the constraints and parameters definition of the optimization problem to reach a global optimal solution.

## Lagrange multiplier

The Lagrange multiplier is a method permitting to find stationary points of a single or multi-variable derivable function, with no constraints [Ayad07]. For instance, the implementation of this multiplier applied to one operating mode of a vehicle gives in [Kerm09b] an optimal solution for fuel consumption minimization. Even if this principle seems to be attractive from a time computation point of view, models must be derivable and the control must be an open loop one [Kerm09a].

## Port-Controlled Hamiltonian

Port-Controlled Hamiltonian (PCH) systems were introduced by Van Der Schaft and Maschke in the early nineties [Orte02]. Some of the advantages of expressing systems in the PCH form are that they cover a large set of physical systems and capture important structural properties. They exhibit some system characteristics (the total system energy, the damping and the states interconnections [Ayad10]) and they simplify the stability proof of the systems [Bech07]. From the PCH form, control laws are deduced using passivity theory. Contrary to PI controllers or hysteresis controls, no sensor device intervenes in the control. For instance, in [Hadd03], it is shown that under certain conditions for the studied system, the Hamiltonian function is the difference between the physical energy of the hybrid system and the energy supplied by the controller. In [Hank08], the study focuses on the power distribution management between a fuel cell stack and an ultra-capacitor pack in order to ensure the power demand in a hybrid vehicle. To minimize the hydrogen consumption on a given driving cycle, a global optimization problem under constraints is formulated. First, the system is represented by a discretized dynamic equation and a dynamic programming algorithm is implemented. Then, after approaching the cost criterion by a polynomial function, the Hamiltonian function is minimized.

In theory, strategies based on off-line optimization algorithms give an optimal solution. Even if a combination of the Lagrange multiplier with predictive control looks like an alternative solution to respect the real time constraints, such algorithms are complex, time consuming and are off-line methods (necessity to have a priori knowledge of the driving cycle). Moreover, these approaches only perform optimization for a particular vehicle in particular conditions which will probably never be repeated in real use. The on-line optimization algorithms are a possible alternative to these methods.

### 1.2.3 Strategies based on on-line optimization algorithms

Strategies based on on-line optimization algorithms perform a global optimization taking into account the whole system. These methods are real time computing ones. They only consider available real-time information of the system like the speed, the acceleration, the required power, voltages, currents and SOC for instance [Haji06]. Moreover, the project focuses on a railway application which driving conditions are highly uncertain and without priori knowledge of the driving cycle. The conditions depend on the traffic, the weather, the driver, the road profile, the state of the locomotive... Thus, on-line techniques, without previous knowledge of future drive conditions, appear to be more adequate to perform vehicles' energy management and easier to implement [Salm07]. The rule based on-line techniques, like fuzzy logic, enable on-line optimization without priori knowledge of the road profile. Even if the final solution is not necessarily optimal [Kerm09a] (some constraints can be neglected to lighten the optimization process), it provides a realistic solution. Among on-line optimization algorithms, fuzzy logic, Neural Networks (NNs), predictive control and wavelet transform are now presented.

#### Fuzzy logic

This paragraph introduces the basic concepts, notation, and basic operations for the type-1 and type-2 fuzzy sets. Because of 35 years of research on fuzzy set theory, it is practically impossible to cover all aspects of current developments in this area. Thus, after an introduction to the basic concepts and operations of type-1 and type-2 fuzzy sets, HEVs EMSs using fuzzy logic are listed.

**Basic concepts** Over recent years, fuzzy logic has found extensive use in a variety of applications. It has rapidly become one of the most successful of today's technologies for developing sophisticated control systems. The rise in interest in fuzzy logic can be explained by the fact that it provides a way to compute human knowledge easily [Jamm09]. It fills an important gap in engineering design methods left vacant by purely mathematical approaches, and purely logic-based approaches in system design. While other approaches require accurate equations to model real-world behaviours, fuzzy design can accommodate the real-world human knowledge and logic [Liao08]. It provides both an intuitive method for describing systems in human terms and automates the conversion of those system specifications into effective models [Stew04]. Fuzzy logic has also proven its ability to model uncertainties in-

herent in real-world systems. It has found successful applications in a wide variety of fields such as control [Jama09], decision analysis [Sola11, Bezi02], expert systems and navigation [Schm12, Vena09, Kara03]... A fuzzy logic system is described by a certain number of fuzzy if-then rules, each one describing a behaviour. Introduced by Zadeh in 1965, Type-1 Fuzzy Logic (T1-FL) is the most conventional one. It was first used to control steam engines [Mamd99]. However, the use of type-1 fuzzy sets with crisp degrees of membership remains unsuitable for the modelling of some uncertain concepts [Karn01]. Research has shown that the ability of T1 fuzzy sets to model and minimize the effect of uncertainties is limited [Wu12, Caza12]. A reason may be that a T1 fuzzy set is certain in the sense that for each input, there is a crisp membership grade [Suge95, Hans99]. The structure of a T1 fuzzy system is depicted figure 1.12.

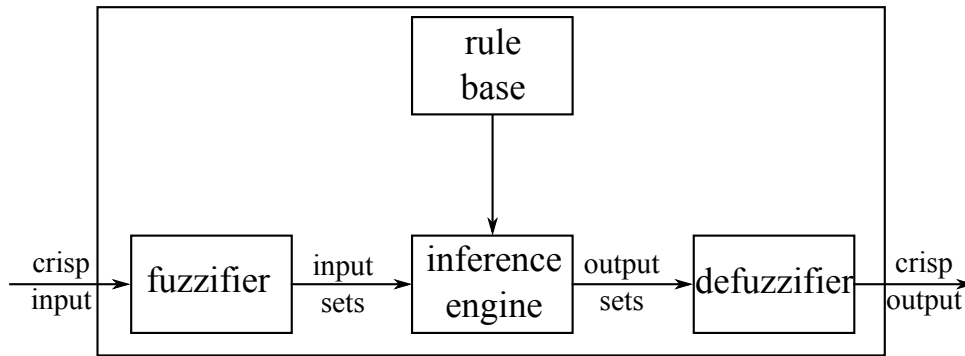


Figure 1.12: Structure of a Type-1 fuzzy system

The secondary Membership Function (MF), also called the Footprint Of Uncertainty (FOU) (figure 1.13), is a singleton when considering Sugeno-type fuzzy systems.

The concept of Type-2 (T2) fuzzy sets was proposed by Zadeh in 1975 to overcome T1 limitations. The T2 fuzzy structure is presented on figure 1.14.

Type-2 fuzzy systems use an additional degree of freedom in the definition of membership functions. Type-2 fuzzy approach gives better performance in the face of highly uncertain conditions. It has been successfully applied in different applications such as vehicles' control [Suge84], helicopters' stability [Phil96], hybrid electric vehicles energy management strategies [Sola12b], control of active systems [Li12, Lin05]... As shown on figure 1.15, the secondary MF is a crisp value.

The proposed studies of the chapter 4 of this manuscript will lead to the comparison of the general type-2 based on zSlices against interval type-2 and type-1 fuzzy logic controllers in the control of the output voltage of a buck

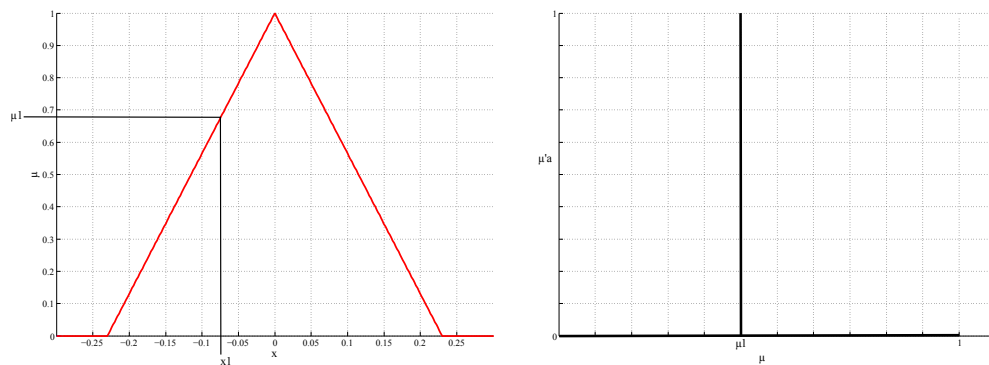


Figure 1.13: Type-1 Primary (left) and Secondary (right) Membership Functions

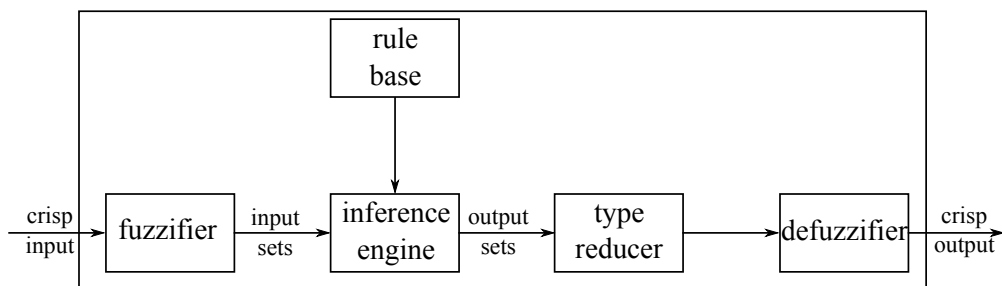


Figure 1.14: Structure of a Type-2 fuzzy system

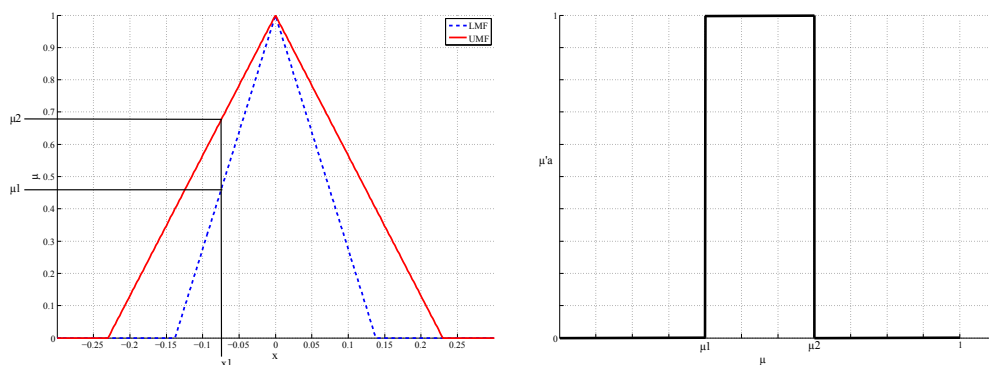


Figure 1.15: Interval Type-2 Primary (left) and Secondary (right) Membership Functions

converter and the implementation of the EMS of the studied HEL.

**Fuzzy Logic Controllers design** To design a Fuzzy Logic Controller (or determine its parameters), two methods are available:

- the survey based one using human experience or data from the system: this technique was successfully implemented and experimentally validated in [Sola12b]. Survey-based fuzzy logic systems permit to combine the knowledge from different experts to design a MF [Mend09]. To handle the uncertainties associated with the meaning of the words and the different rules and MFs, Type-2 Fuzzy Logic is used.
- the optimization one using a genetic algorithm [Wagn07]: this technique is going to be implemented in this project. Generally, the FLC is optimally designed in order to minimize the fuel consumption of the studied HEV. This kind of optimisation is performed for specific driving cycles in specific vehicles. However, nothing guarantees that the calculated set of parameters is still appropriate in different vehicles or in variable driving conditions. Thus, Type-2 Fuzzy Logic is also used to handle uncertainties conditions. Additionally, accurate models to represent the vehicle and to calculate the fuzzy system parameters are required.

**Application to HEVs** Fuzzy logic can be described as a decision making method rather than a controller [Farr93]. To sum up, some researches dealing with hybrid vehicles recommend a formulation using fuzzy rules [Baum00, Salm00, Cerr94]. The main idea of these strategies is based on the concept of charge level trying to operate the ICE in an efficient region and to use the electric engine like a device of charge level. Fuzzy controllers' structure and parameters are built according to the knowledge of the problem of the user solving it. This method permits to have a better comprehension of the energy management and improves the driving comfort thanks to more flexible changes of working modes. For instance, according to [Lee90], the fuzzy controller of the studied vehicle is divided in two blocks. The first one called "Power Balance Controller" aims at controlling batteries' SOC and gas emissions. The second one called "Driver's Intention Predictor" aims at determining the power demand of the driver. A drawback of this approach comes from the fact that defined rules do not depend of membership functions and in consequence there is no guarantee that the fuzzy controller will provide a good performance in the case of complex systems [Wang06a]. Due to the complexity of hybrid vehicles, this kind of controller built on intuitions, frequently fails. To deal with this difficulty, optimization algorithms can be used to obtain an optimal fuzzy controller. For instance, genetic algorithms are used to define the membership functions parameters [Wang06b], [Cord01]. Systems based type 1 fuzzy logic do not have the ability to treat uncertainties linked to past events and fuzzy rules consequences. So, there is a need to

use type 2 fuzzy logic as explained previously. Indeed, instead of assigning a single value to the membership functions, a scale of values is assigned. An EMS based Type-2 Fuzzy Logic Control has already been successfully implemented only once in [Sola12b]. This is the first industrial application of type-2 fuzzy logic in France and the first experimental validation of an energy management system on a HEV using type-2 fuzzy logic designed on the experience of multiple experts. It concerns a military application (figure 1.16) using a fuel cell, batteries and UCs.

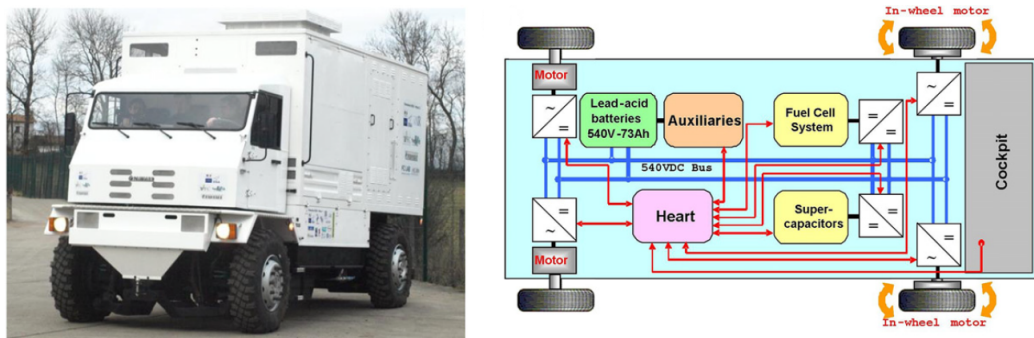


Figure 1.16: Hybrid Electric Vehicle and its considered configuration [Sola12b].

The implemented EMS considers the vehicle speed to define the dynamic reference for the UCs' SOC reference and permits an easy operation in degraded mode. For this application, the Type-2 FLC is used to perform the local management of the fuel cell system. The design of the fuzzy logic controller is done by using knowledge engineering technique. This technique allows extracting knowledge from experts using surveys. The consideration of type-2 fuzzy logic membership functions enables modelling the uncertainty in the answers of the experts.

## Neural networks

**Basic concepts** NNs are information processing models inspired by the brain biology [Jeme04, Dush63]. It aims at imitating, acquiring human knowledge and taking "intelligent" decisions. The NNs are made up of artificial neural connected together to treat information and provide results. For instance,

$$n = f(\sum_{i=1}^R w_i p_i + b_i)$$

with  $n$  the output,  $f$  a sigmoid, linear or sinusoidal function.  $w_i$  are the corresponding weight to the inputs,  $p_i$ ,  $R$ , the number of inputs and  $b$ , a

bias. When such neurons are stored together and provided with the same inputs, they form neuron layers. By connecting these layers, a network called multi-layer NN is obtained. NNs have an input layer and an output layer. Between the layers, some hidden layers exist too. The number of layers and neurons is determined when the treated network becomes sufficiently non linear regarding the application. NNs must be trained to evaluate inputs' weights. Generally speaking, the weights are determined thanks to a back-propagation algorithm. Thus, the neurons' weights are calculated in order to minimize the difference between the obtained output and a desired output reference.

**Application to hybrid vehicles** The proposed hybrid architecture in [Rous08] is managed using a NN controller. It takes into account several informations such as batteries SOC, the ICE speed and the torque demand to calculate and define the powers to be delivered by the sources. The NNs permit to design light structures controllers. Their implementation and modelling only rest on additions and multiplications which make them an attractive solution. However, their use necessitates a previous training based on a large scale of different operating cycles. Thus, it requires high computer resources and time computing. Moreover, the training step remains to be limited to only one operating conditions (figure 1.17).

If particular operating conditions occur, the obtained solution will not necessarily be optimal. In [Scor04], the obtained results show that even if results seem to be good, the system is placed in particular conditions and it becomes impossible to identify the real contribution of this module. In [Feld09], a NN controller is developed to manage the energy flows in a parallel HEV which is made up of an UC coupled with an ICE. Their charge/discharge cycles must be optimal in order to reduce the fuel consumption and avoid a deterioration of the vehicle behaviour. The problem is tackled using a trained NN controller. The results prove that the training step permits to nearly optimize all the possible behaviours met by the system.

## **Predictive control**

Today, three main competing approaches classes exist (figure 1.18). They are themselves gathered into categories classified according to three criterion: optimality, control horizon and optimization objective. The majority of control strategies are controllers based on heuristic. The heuristic approach has a medium complexity and needs few computation resources. However, its adaptability is limited and it gives sub-optimal results [Kutt10]. From an optimality point of view, predictive control based models using dynamic

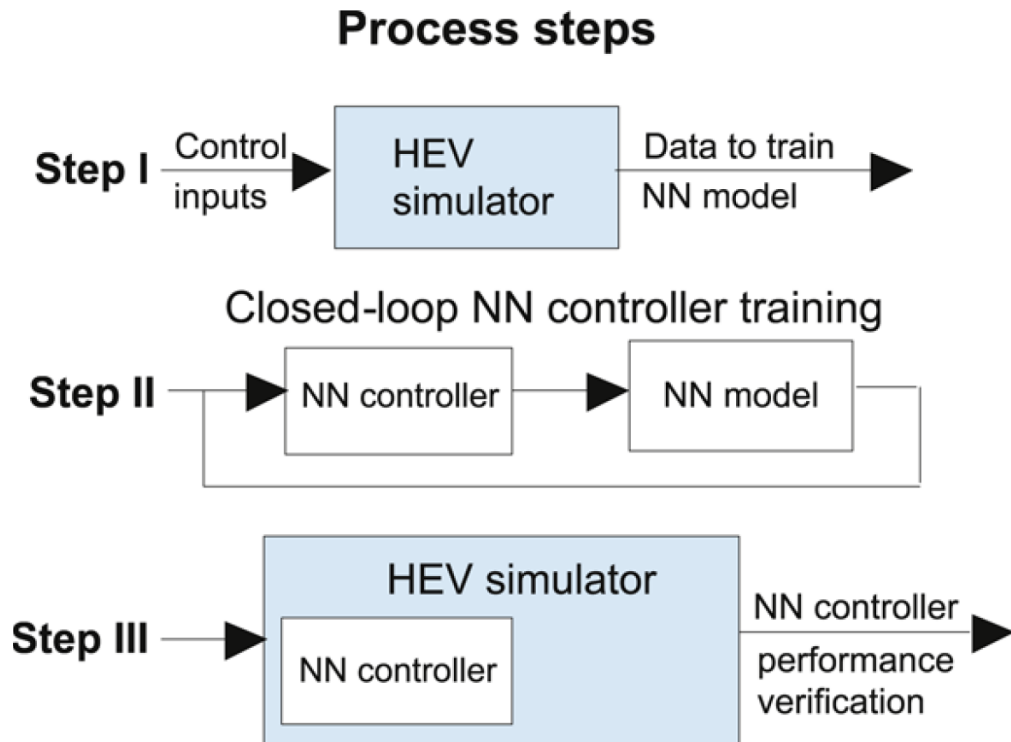


Figure 1.17: Process steps for Neural Network controller training and verification [Prok08]

programming techniques are considered as the best category of algorithms for optimization and search problems. The main drawbacks are:

- the important computing effort to provide which is opposed to a real time control implementation of a vehicle EMS,
- the need to have a compulsory control horizon.

A certain number of predictive control models were studied and have proven their effectiveness to be an alternative and practical method to build an EMS for hybrid vehicles [Prei07, Beck05]. In [Arce09], a hybrid vehicle (fuel cell and batteries) is studied. The objective of the project is to minimize the fuel cell consumption according to driving constraints and the components characteristics. The EMS and the minimization goal are based on predictive control. The same kind of study is performed in [Bord10] and [Bubn10]. The implemented controllers based on prediction aims at predicting the required energy to optimally use batteries and make work the fuel cell in its most efficient region for hydrogen reduction purpose.

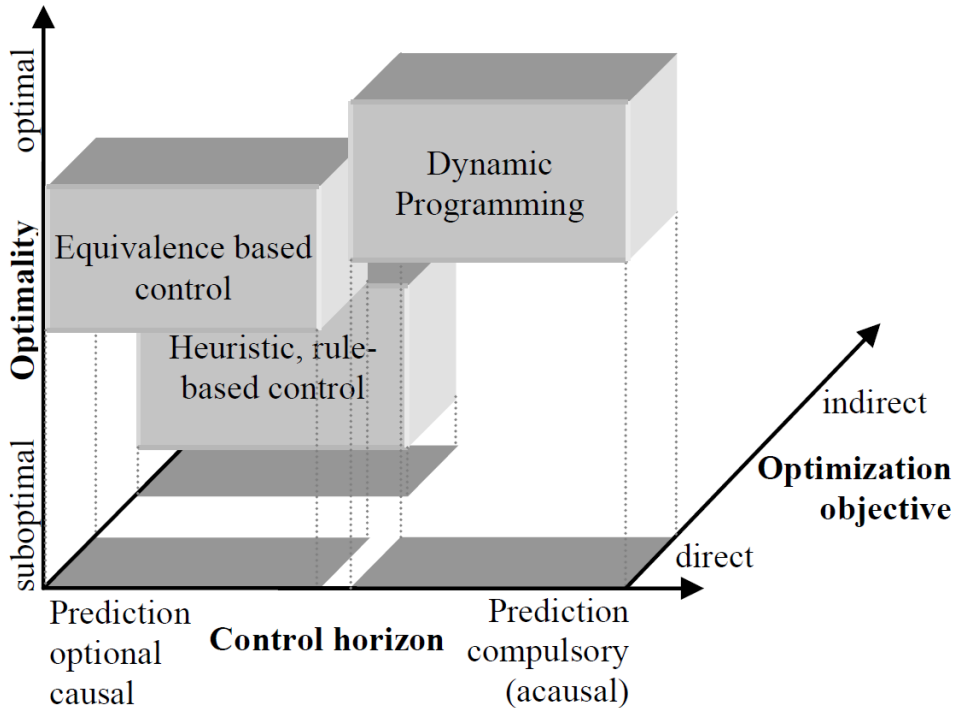


Figure 1.18: Classification of control approaches, global evaluation of optimality assuming a priori known driving cycles [Kutt10].

### Equivalence based control

As shown figure 1.18 and explained previously, heuristic, rule-based controls present a limited complexity, need low computational resources, don't need an important control horizon but they achieve to suboptimal results. DP is the most suitable technique to reach global solutions but it requires an important horizon. A compromise between these two approaches are the equivalence based control algorithms. They aim at partially solving the conflict between the global optimality and real time capability (prediction optional causal on figure 1.18). In [Kutt10] the adaptation towards changing driving conditions is realized by an independent calculation and adjustment of the main decision criterion of the EMS towards the predicted operational profile using a calculation time optimized dynamic programming approach. Thus, the combination of the predictive DP with the considered EMS provide respectively the global optimality of the solution and the real-time capability.

## Wavelet transform

To illustrate the usefulness of the wavelet transform in the EMS implementation application field, let's consider a hybrid vehicle powered by a fuel cell, batteries and UCs. Fuel cells are alternative power sources. They are less polluting and more efficient than ICEs [Iwan98, Aso07]. However, the cost and performance are obstacles for their use on a large scale in vehicle applications. Moreover, energy braking recovery is impossible with this kind of technology. In HEVs, life time and fuel cell sizing are directly impacted by fast dynamic and disrupted power demands of the system [Erdi09]. The use of batteries and UCs and the development of an appropriated EMS is the considered solution in [Mark03]. The EMS aims at splitting the power in the system, maximizing its performances, saving fuel and guaranteeing elements durability. A wavelet transform approach permits to identify high transient frequencies [Ates10] and real time power demand of the HEV. This algorithm allocates powers to the components with different frequencies according to the considered source to ensure optimality (figure 1.19).

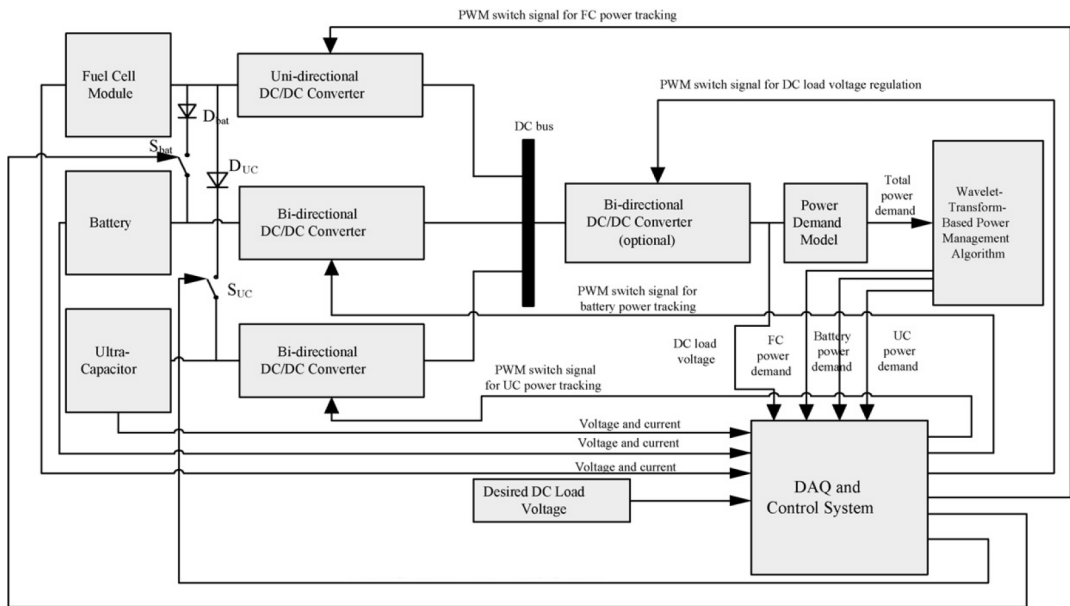


Figure 1.19: System configuration of the multi-source hybrid vehicle power system [Zhan08].

In sharing the high frequencies (respectively the low and medium frequencies) of the power demand between the UCs (respectively the batteries and the fuel cell) using a wavelet transform of the driving cycle signal, the

efficiency and life duration of the system can be greatly improved [Zhan08]. Despite the fact that wavelet transform has the same efficiency as a load share algorithm, an EMS only based on wavelets is inadequate to regulate system's power flow [Uzun08]. According to the batteries and UCs SOC, the power delivered by the fuel cell should be reduced when they are enough loaded. Besides, the fuel cell should provide more power if they have a low SOC. Thus, fuel economy is increased as system performances and the EMS must guarantee good hybrid system performances. As proposed in [Erdi09], the wavelet transform is coupled to a FLC. Indeed, the proposed EMS uses the wavelet transform to study instantaneous changes like the power demand of the HEV and the FLC to define the powers to be delivered by the fuel cell system and the batteries according to the secondary sources SOC (figure 1.20).

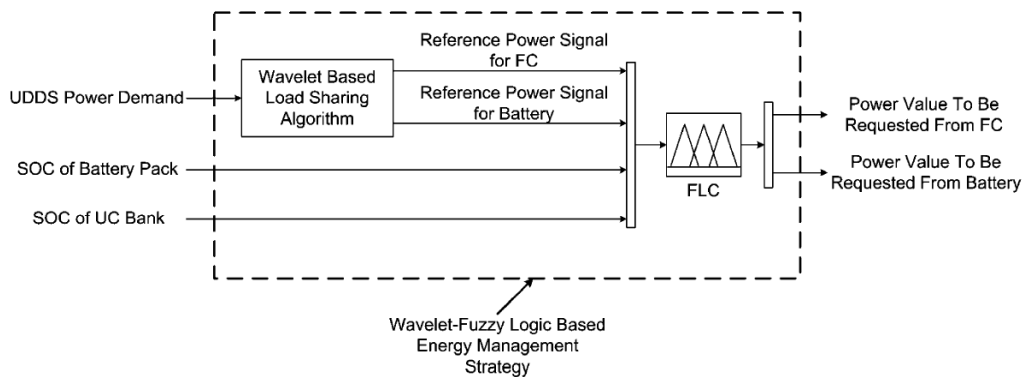


Figure 1.20: A schematic diagram of the developed energy management strategy [Erdi09].

The wavelet transform has also been coupled with NNs in [Ates10]. The method combines the capability of wavelet transform to treat transient signals with the ability of auto-associative neural network supervisory mode control. Wavelet transform intentionally reduce primary source dynamics in transient conditions and secondary source supplies instantaneous load variations. The neural network controller ensures an improvement of the fuel consumption according to the UC bank SOC - figure 1.21.

## 1.2.4 Hybrid Electric Locomotives' EMSs

This subsection proposes a description of the different existing EMSs dedicated to the HELs.

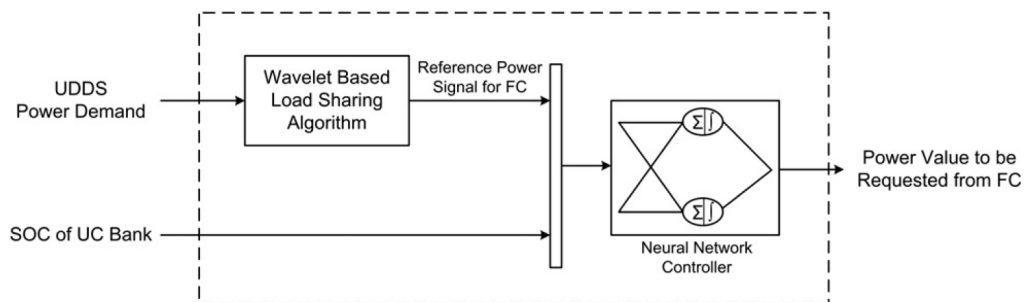


Figure 1.21: Combined Neural Network-Wavelet Transform Based Energy Management Strategy [Ates10].

### The Chinese Dongfeng 7G HEL

The implemented EMS in [Xin11] aims at defining the power delivered by the engine according to the batteries' SOC:

- if the SOC is lower than a define minimum value, the diesel engine works at the maximum output power,
- if the SOC is higher than a define maximum value, the diesel engine stops working.

Thus the batteries' SOC is maintained within a reasonable range and the engine is used in its "optimal economic region".

### The Iranian G12 HEL

The locomotive motors are controlled by an EMS to maintain maximum efficiency in all working conditions. Firstly, according to the command torque, the motor temperature, and the locomotive or motor speed, a neural network system (figure 1.22) controls the motor for optimum efficiency performance. It calculates the best set of voltage and frequency to maintain and drive the motors at maximum efficiency [Aae07]. Then, based on thermostatic method like in [Xin11], the EMS takes into account the acceleration and brake commands, the SOC, the speed, the temperature, and the engine status (on or off) to turn on or off the engine and maintain the battery SOC between two levels.

The project heralds 80% reduction in the fuel consumption of the locomotive and emission gases.

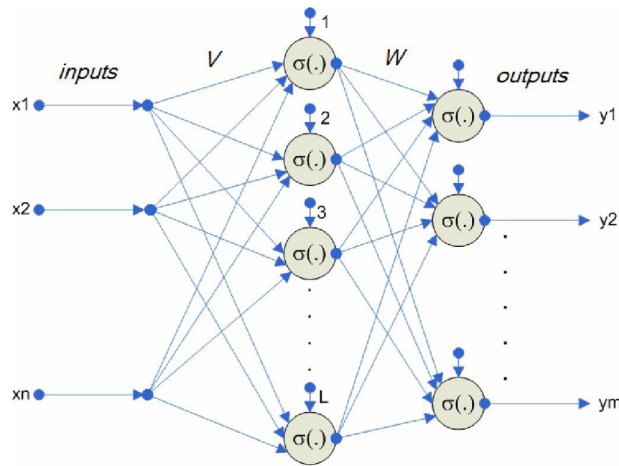


Figure 1.22: Neural network inputs and outputs [Aae07].

### The frequency filtering approach

The SNCF HEL (Plathee project - [Aki07]) aims at downsizing the diesel engine and accumulating/storing energy thanks to the secondary sources when the power demand is higher than diesel engine capacities. The use of mechanical energy buffer (a flywheel), instead of accumulators, is also a solution tested in [Jaaf09]. Both of the projects are building the EMS on a frequency approach (figure 1.23).

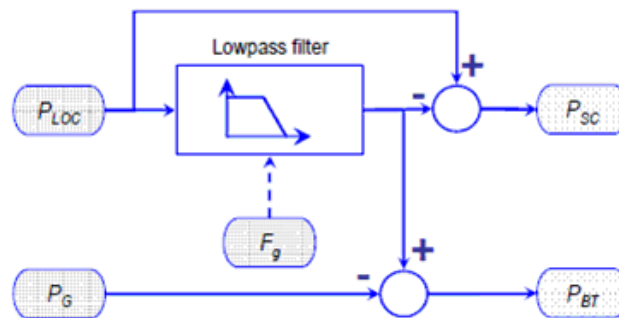


Figure 1.23: Energy management strategy principle [Aki07].

This kind of EMS is based on the frequency characteristics of the on-board sources. UCs contribute to reduce batteries' stress in absorbing micro-cycles and fast dynamic harmonics of the power profile [Aki07]. The configuration presented in [Jaaf09] permits to share a part of the power demand at low frequencies dedicated to the batteries with the flywheel leaving mission's

high frequencies, a priority.

The diesel-electric shunting locomotive powertrains produced in the former Soviet Union ([Hoim10]) are also confronted to the same diesel electric propulsion problematic:

- the existing diesel generator units are poorly utilised and mostly operate below the optimal specific fuel consumption region,
- the diesel generator unit can be downsized several times if an hybridised powertrain is used,
- the limits are set only by the cost and space constraints.

The research concentrates on their upgrades and their hybridisation. The developed EMS is also based on a low pass filter.

### **The fuzzy logic approach**

Even though a frequency approach is a possibility, the use of fuzzy logic is also a solution [Jian10]. A fuzzy logic EMS of a hybrid locomotive composed of two sources (fuel cell and batteries) is presented in this study. The EMS satisfies the following requirements:

- the fuel cell system is used at its optimal efficiency,
- the regenerative energy is effectively stored,
- the output power of the motor always meets the power demand of the vehicle. If the required motor input power is greater than the rated power of the fuel cell stack, the latter operates with its rated power and the battery provides the peak power demand.
- battery is used for improving the lower dynamic transient response of the fuel cell,
- when a locomotive is running slowly inside a station or making a stop, battery output should be mainly used, and the fuel cell should not be operated unless necessary.

Fuzzy Logic EMS adapts the behaviour of the system according to the real physical state of the vehicle in order to control the power flows of the system. The FLC (figure 1.24) has two inputs (Batteries' SOC and power demand) and one output (the fuel cell power reference to be delivered). The control aims at maintaining the batteries' SOC to a defined level and using the considered primary source as optimal as possible.

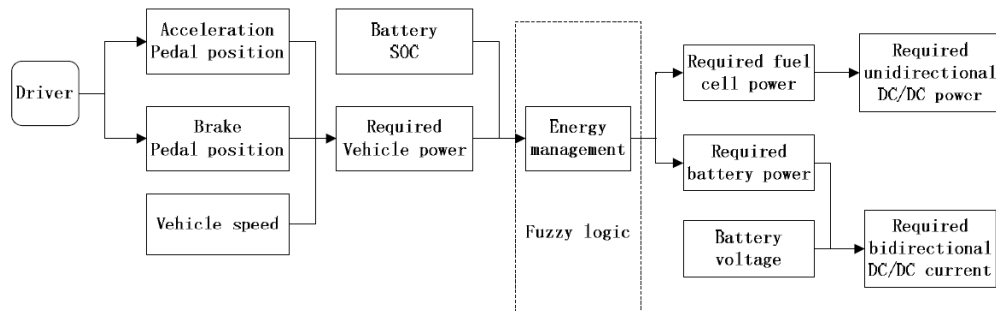


Figure 1.24: Energy management principle diagram based on fuzzy logic [Jian10].

For instance:

- IF the power requirement is low or the locomotive is braking AND IF the battery's SOC is low THEN the most part of the fuel cell power is used to charge the battery.
- IF the required power is high AND IF the battery SOC is high THEN the fuel cell and the battery jointly provide the required power.

The obtained fuzzy map (figure 1.25) represents the evolution of the FLC's output according to its two inputs.

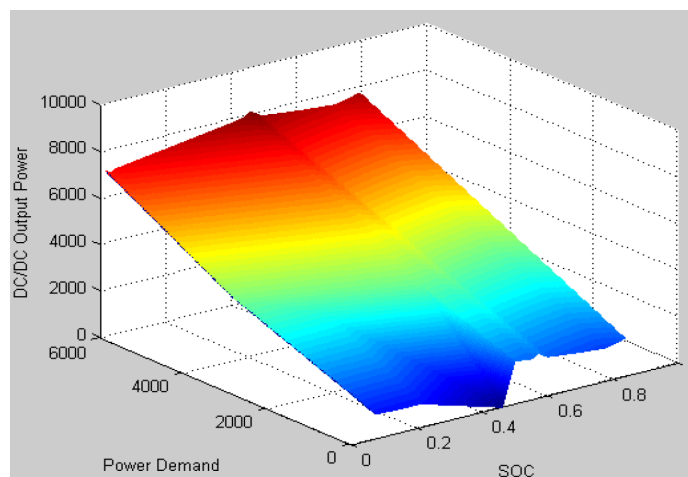


Figure 1.25: The relationship curve of SOC, power demand and DC/DC output power [Jian10].

In [Mogh03], the global control of a combined fuel cell with battery/UCs or flywheel/UCs locomotive architecture is also tackled. Conceptually, the

fuel cells supplies the power for constant speed driving. The secondary sources (batteries/UCs or flywheel/UCs) supplies the peaking power (acceleration, grade climbing) and recovers the braking energy instead of dissipating it in brakes. In other words, the secondary sources supply whatever the traction motors require and the fuel cells recharges them when needed (figure 1.26).

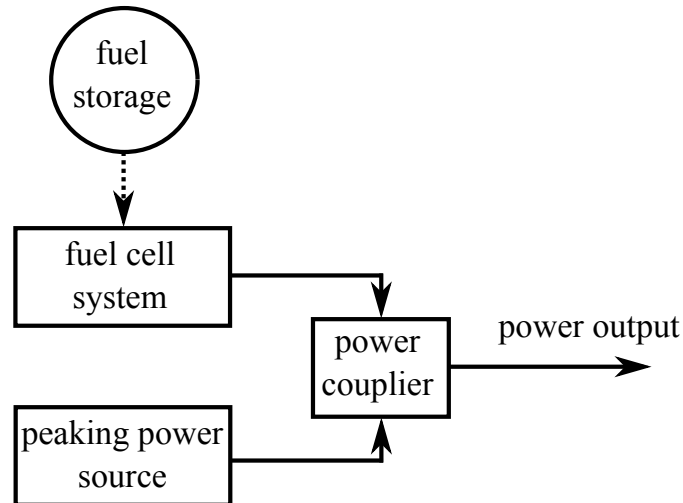


Figure 1.26: Concept of the fuel cell powered hybrid drive train [Mogh03].

However, apart from the EMS purpose, in [Mill07], another fuel cell and battery hybrid switcher locomotive prototype is presented. Even if it combines the environmental benefits of a catenary-electric locomotive with the higher overall energy efficiency and lower infrastructure costs of a diesel-electric, it also underlines the technical challenges not found in the development of smaller HEVs arise when designing and developing such a large and heavy vehicle (weight, center of gravity, packaging, safety...). Indeed, a fuel cell provides a limited power which does not meet the energy storage requirements with compressed hydrogen ([Guo11]). Therefore, Solid Oxide Fuel Cells (SOFCs) compared to the PEMFCs allow more flexible fuels, such as bio-diesel, presenting higher energy density than hydrogen. In such a case, the fuel cell is still supplied with hydrogen produced from the hydrocarbon reforming.

To open up this overview, it is interesting to note that some research works try to solve the environment pollution problem (exhaust gases, noise...) focusing on the improvement of the performances of the diesel engine of a railway traction system ([Bont06]). A control strategy based on a model of the diesel engine and the injection control and monitoring are developed.

The HELs' architectures and configurations solutions usually propose the coupling of a primary source (ICE or fuel cell) with secondary sources (UCs, batteries, flywheel). Today, even if these solutions aim at solving the met diesel electric propulsion efficiency issues, this efficiency greatly depends on the designed EMS. Indeed, for a common configuration, there are as much possible EMSs' solutions as designers.

### 1.3 Chapter conclusion

Even if ICEs have proven their efficiency for over a century and a half, environmental and transportation energetic challenges are now essential. The pollution and the greenhouse gas emissions, the resources' rarefaction plus the cost to access and exploit them, the congestion of the urban areas lead societies to bring new solutions. HEVs combine at least two sources. One or several electric machines and an energy storage system are associated to a conventional primary source (fuel cell or ICE). Series, Parallel and Series-Parallel are the most famous architectures. Thus, to split the power into the system, an EMS must be implemented to provide:

- required functioning of the system,
- pollutant emissions and fuel consumption reductions,
- power and energy sources increased life time.

Even if off-line optimization algorithms provide an optimal solution, they don't meet the project demand. In relation to the specifications and the constraints of the railway application, on-line optimization techniques and especially fuzzy logic appears to be the best approach. It considers:

- real-time information,
- the driving conditions uncertainties,
- the ignorance of the road profile,
- the reach of a realistic solution.

However, the definition of the FLC's rules directly impact the global efficiency of the EMS. These rules must be precisely and optimally defined using a GA. Thus, the method suffers from an increasing implementation complexity. The optimization of a Type-2 FLC using a GA to perform the HEL's EMS is the new research direction of the partners. The next chapter presents

the improvements from a conventional locomotive toward a hybrid electric architecture. Then, the determination of the most difficult road profile and a tool to observe the tendency of the sizing evolution of the secondary sources are developed.





## Chapter 2

# Locomotive topology and sizing of the secondary sources

As described in chapter 1, in a series architecture, all traction power is supplied from electricity and a DC bus ensures the electrical energy balance of the system. Thus, the ICE can continuously operate in its most efficient region but it requires large and heavy secondary sources banks.

First, section 2.1 presents the topology of a conventional electric locomotive and the expected improvements toward a series hybrid electric architecture. It also justifies the choice to couple the diesel driven generator set with batteries and UCs contrary to other studies (the German Hybrid loco - page 19) coupling it with batteries only.

Section 2.2 is dedicated to the estimation and the evaluation of the sizing of the batteries and the UCs' banks. The determination of the most difficult driving cycle, which is by definition the worst case in terms of power and energy requirements, constitutes the first step. Then, a method is proposed to perform the sizing calculation. This algorithm takes into account the driving cycles requirements (power, energy) and the secondary sources' characteristics (nominal voltage, power, lifespan...). The study starts with the determination of the total number of cells to be used and then, the elaboration of a series-parallel configuration is presented. Finally, section 2.3 presents the conclusions of the chapter.

### 2.1 Locomotive topology

In diesel-electric transmission systems, the mechanical energy produced by the diesel engine is converted into electricity. The conversion is performed

thanks to a generator and the electrical power is transferred to an electric traction drive and also to auxiliaries (lighting, heating...). In a diesel-electric propulsion, the ICE is optimally used in a limited speed range. Diesel-electric locomotives do not need a catenary. A conventional diesel-electric propulsion system layout is depicted in figure 2.1. The driver controls the power flow from the diesel driven generator set to the wheels by selecting the position of the throttle handle.

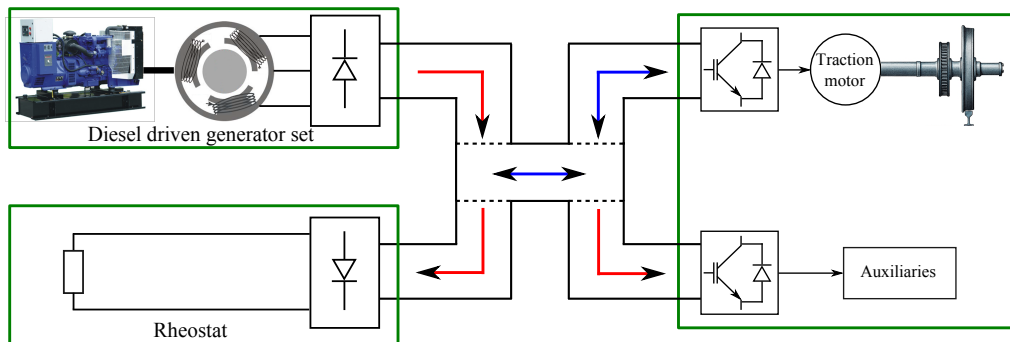


Figure 2.1: A typical diesel-electric propulsion system

As explained in the previous chapter, the local French freight activities are performed by diesel electric/shunting locomotives. The on-board ICE mainly operates on low loads as depicted on figure 2.2. Low loads correspond to the worst efficiencies of the engines.

The hybridization of a shunting locomotive consists in deporting a part of the power required by the freight activity on other energy sources. Here, the developed HEL is a series HEV. The architecture and its benefits have already been presented in the chapter 1. The on-board primary source (an ICE) is coupled with batteries and UCs. Even if the first chapter states about HEVs using fuel cells like a primary source, in our case they can't provide the power range requirements of the studied shunting activities contrary to an ICE. The Ragone plot depicted on figure 2.3 shows that the coupling of an ICE (according to the fuel tank dimensions which is used) with batteries and UCs permits to cover large specific energy and specific power ranges.

This study aims at evaluating the hybridization benefits by considering only the ICE, batteries and UCs. The use of UCs in the locomotive is motivated by the need to protect the batteries from premature deterioration. Indeed, UCs present:

- high charging and discharging currents (hundreds of Amperes),
- quick charging and discharging times (1 to 10 s),

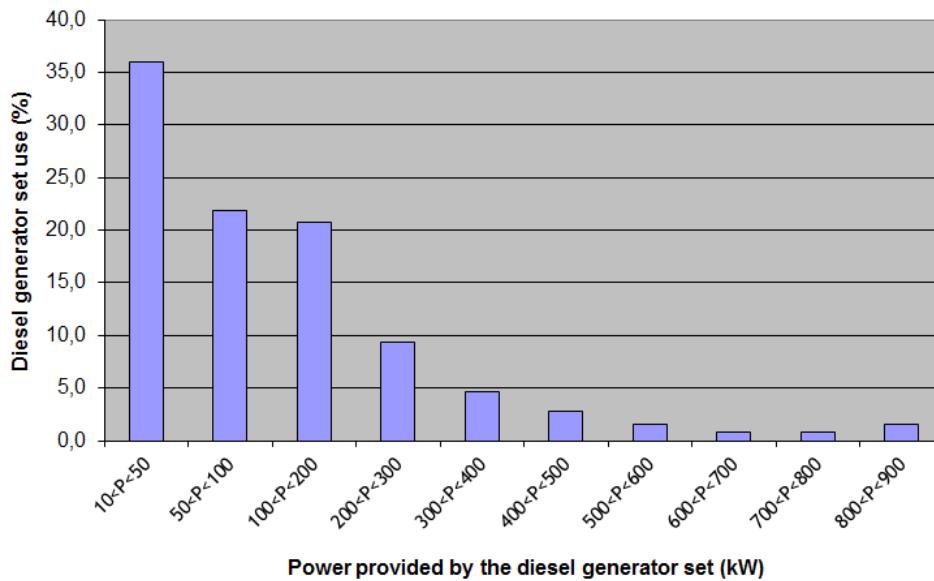


Figure 2.2: Diesel driven generator set use for a typical freight driving cycle

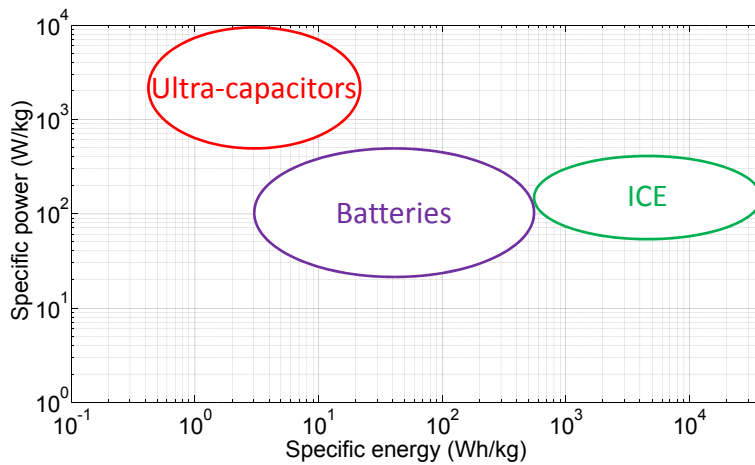


Figure 2.3: Ragone plot

- a high lifespan and a high number of charging/discharging cycles (more than 100 000 cycles).

UCs have much higher power density than batteries which are based on the movement of charge carriers in a liquid electrolyte and present relatively slow charge and discharge times. Thus, UCs are mainly used to provide fast and important power demands and limit the stress applied to the batteries. The latter typically presents about 1000 charging/discharging electrical cycles.

The studied hybrid electric propulsion system layout is depicted on figure 2.4. The driver still controls the power flow that comes from the diesel driven generator set, the batteries and the UCs and is provided to the traction motors.

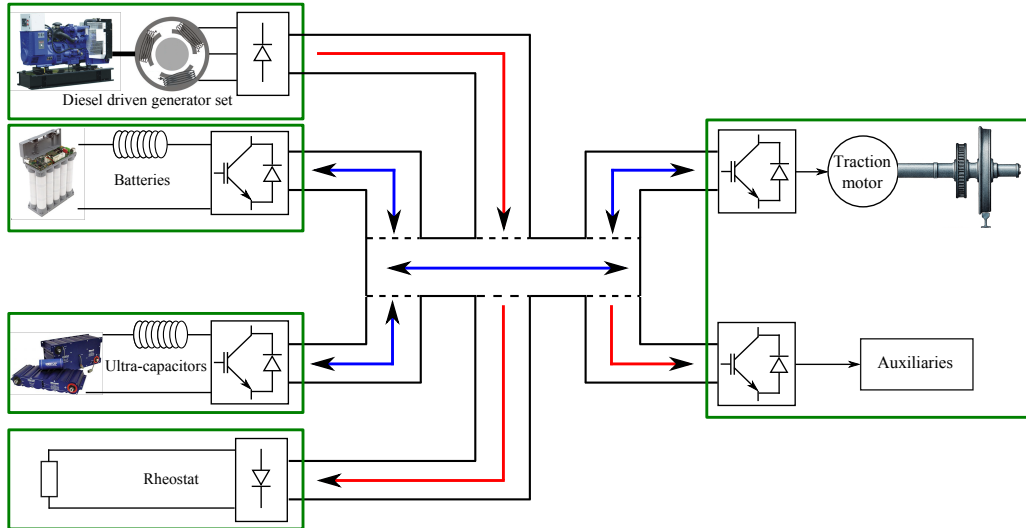


Figure 2.4: Electric structure of the considered system

Figures 2.5 and 2.6 represent the conventional diesel electric and new hybrid electric locomotives.



Figure 2.5: Freight diesel-electric locomotive



Figure 2.6: Freight Hybrid Electric locomotive

## 2.2 Sizing of the secondary sources

Considering a sizing problem, it clearly appears that the number of cells to be used depends on:

- their own physical characteristics (capacity, voltage, resistance...),
- the driving cycle characteristics (average and maximum powers, energy, speed of the locomotive...)

Thus, the proposed method, which is based on the approach developed in [Akl08], must take into account these parameters. It consists in two main steps:

- The determination of the most restricting driving cycle. Indeed, the future HEL will perform shunting activities. Figures 2.7 and 2.8 represent the evolution of the power requested by a diesel locomotive to perform a freight activity. Data are provided by Alstom Transport and are based on real measurements of the power delivered by the diesel engine to supply traction and auxiliaries powers of a conventional locomotive for 30 different shunting missions. However, it is certainly easier to focus the work on only one driving cycle to size the secondary sources. The most difficult driving cycle, in terms of power and energy for instance, among the 30 different ones must be considered. To determine it, two indicators are used (Power Hybridization Potential and Energetic Hybridization Potential). They respectively aim at evaluating the "difficulty" of the driving cycle in terms of power and energy. These indicators are developed in details in the subsection 2.2.1.
- The calculation of the number of batteries and UCs' cells to be set up in series and in parallel into the system. First, the method consists in using a low pass filter to dedicate the high (respectively low) frequencies of the power mission to the UCs (respectively batteries and diesel engine) [Jaaf09, Jaaf10]. Based on these two signals, the different algorithms which are presented in this chapter permit to calculate the number of cells to be set in series and in parallel into the system according to the power and the energy requested by the driving cycle, the energy stored by the sources and the power they can provide.

### 2.2.1 Determination of the most restricting mission

To find the most restricting driving cycle among the 30 available ones, two indicators are considered. They provide information on the need to hybridize

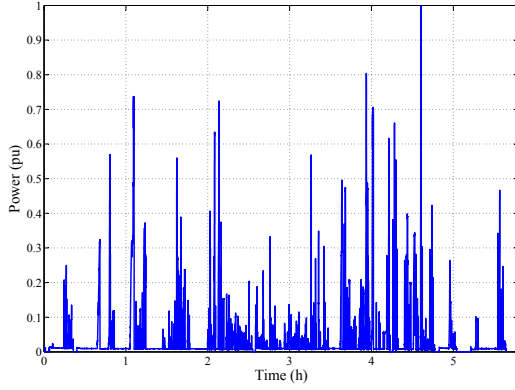


Figure 2.7: First example of the evolution of the power requested by a driving cycle according to time.

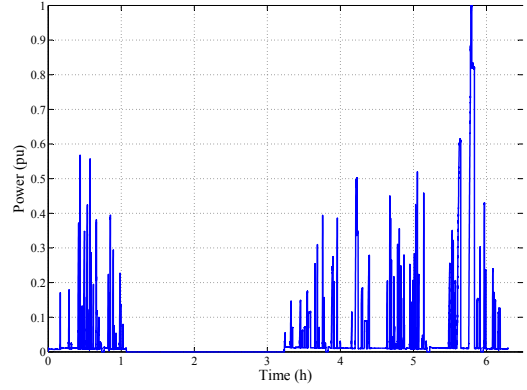


Figure 2.8: Second example of the evolution of the power requested by a driving cycle according to time.

or not the system. They are defined and presented in details on the next pages below.

### Power Hybridization Potential - [Akl08]

The first indicator to be considered is the Power Hybridization Potential (PHP). It informs about the possible reduction of the primary source (ICE) and about the need to hybridize the system thanks to secondary or storage sources. Using the average power ( $P_{average}$ ) and the maximum power ( $P_{max}$ ) of a driving cycle, the PHP is defined equation 2.1. Restrictions were applied to avoid some particular cases such as negative average and maximum powers.

$$PHP = \begin{cases} 1 - \frac{P_{average}}{P_{max}} & \text{if } P_{average} \geq 0 \text{ and } P_{max} > 0 \\ 1 & \text{otherwise} \end{cases} \quad (2.1)$$

Figures 2.9 and 2.10 illustrate theoretical examples for evaluating the indicator contribution. Higher is the indicator (almost equal to 1) and better will be the results obtained with an hybridized system for the considered driving cycle. Indeed, a high PHP value implies that average and maximum powers have very different values (figure 2.9) whereas a low PHP value implies a near equality between them (figure 2.10). In the second case, there is no need to hybridize because the power source will work at maximum level.

Figure 2.9 presents a theoretical mission which PHP value is higher than the PHP value of the theoretical mission depicted figure 2.10. The maximum power of the mission "b" is very close to the average power (PHP almost equals to 0). In such a case, the considered primary source would always

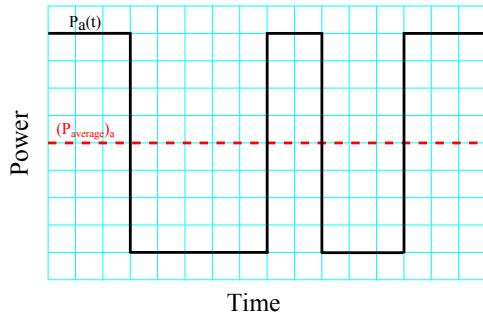


Figure 2.9: First theoretical mission with the associated PHP ( $PHP = 50\%$ )

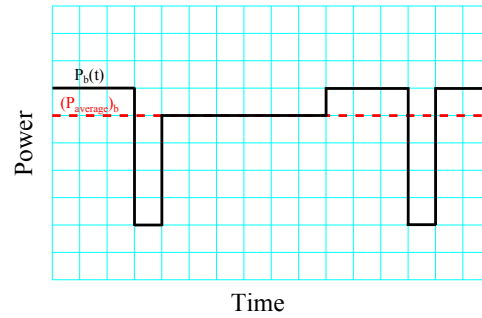


Figure 2.10: Second theoretical mission with the associated PHP ( $PHP = 20\%$ )

work on high loads. However, the maximum power of the mission "a" is very different from its average power (PHP almost equals 1). Thus, the hybridization is really obvious.

However, the PHP indicator presents some limits. Considering two power missions having the same PHP values (figures 2.11 and 2.12), it appears that energetically speaking, the two missions present some differences. These differences are due to the frequency and the regularity of the driving cycle. Thus, the PHP indicator limits and a second indicator principle are described afterwards.

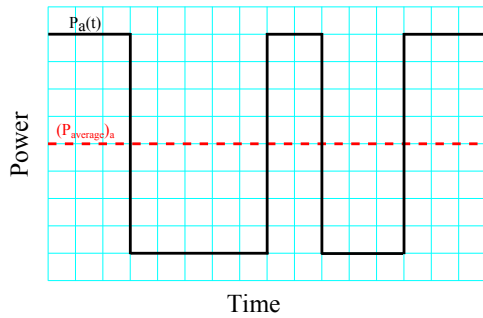


Figure 2.11: First theoretical mission with  $PHP = 50\%$

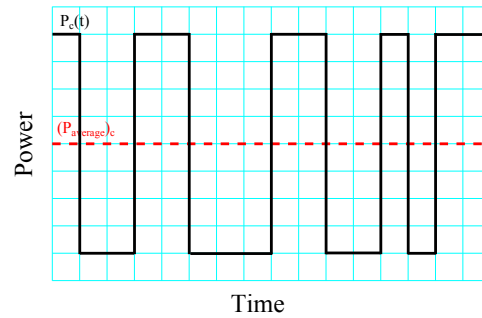


Figure 2.12: Second theoretical mission with  $PHP = 50\%$

## Energetic Hybridization Potential - [Akli08]

The second indicator is the Energetic Hybridization Potential (EHP) which is comparable to the PHP indicator in terms of energy. It corresponds to the characterization of the frequency and the regularity of a mission. For instance, figures 2.13 and 2.14 give the evolution of the energy for missions

"a" and "c" (same PHP values) and the determination of the useful energy. The useful energy corresponds to the energy to be stored into the secondary sources to ensure the considered driving cycle. The energy evolution into the storage devices ( $E_s$ ) is defined by equation 2.2. The used convention considers a negative (respectively positive) power for a charging (respectively discharging) power. Thus, the equations dealing with the calculation of the energy to be stored into the elements present a negative sign. Indeed, a negative (charging) power corresponds to an energy accumulation into the elements and a positive (discharging) power corresponds to an energy released from the storage system.

$$E_s(t) = - \int_0^t (P(t) - P_{average}) dt \quad (2.2)$$

$P_{average}$  represents the average power of the considered driving cycle and  $P(t)$  is the power required by the driving cycle. The average power is subtracted from the total power because we focus on the energy relative to the secondary sources. Then, equation 2.3 calculates the useful energy (difference between the maximum and the minimum energy throughout the driving cycle).

$$E_u = \max(E_s(t)) - \min(E_s(t)) \quad (2.3)$$

Mathematically speaking, the EHP indicator is homogeneous to a frequency. It corresponds to the ratio between the maximum power ( $P_{max}$ ) of the mission and the useful energy ( $E_u$ ) - equation 2.4.

$$EHP = \begin{cases} \frac{P_{max}}{E_u} & \text{if } E_u \neq 0 \text{ and } P_{max} \geq 0 \\ +\infty & \text{otherwise} \end{cases} \quad (2.4)$$

From an energetic point of view, the PHP is an indicator informing about the average power required by a mission and the EHP informs about the useful energy. For instance, the mission "a" (figure 2.13) requires more useful energy than the mission "c" (figure 2.14). However, they have the same maximum power. The EHP value of the mission "a" is lower than the EHP value of the mission "c". Thus, the lowest EHP value corresponds to the most difficult driving cycle because it requires more useful energy.

The association of the two indicators informs about the difficulty of the studied driving cycle in terms of power and energy.

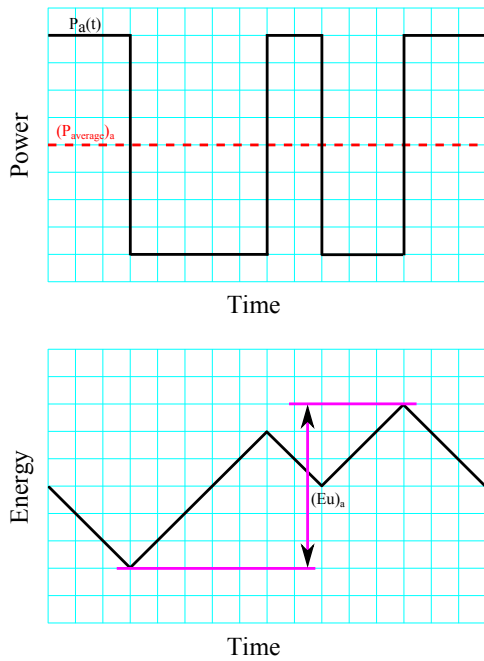


Figure 2.13: First theoretical mission with  $PHP = 50\%$  and its associated useful energy.

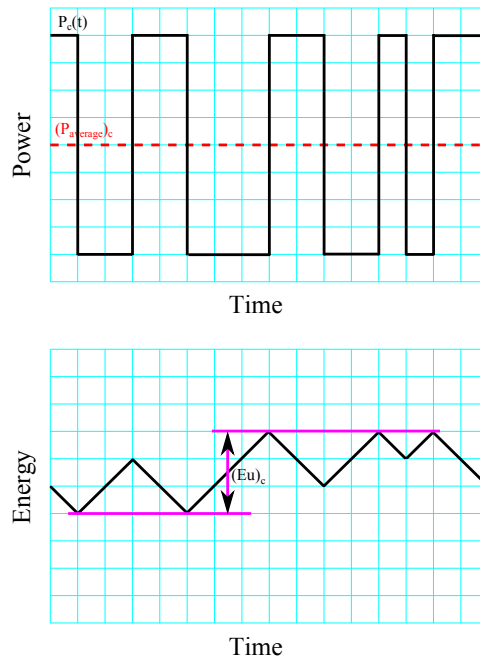


Figure 2.14: Second theoretical mission with  $PHP = 50\%$  and its associated useful energy.

## Results

The calculation of the two indicators is performed for the 30 different driving cycles provided by Alstom Transport. Results are depicted on figures 2.15 and 2.16.

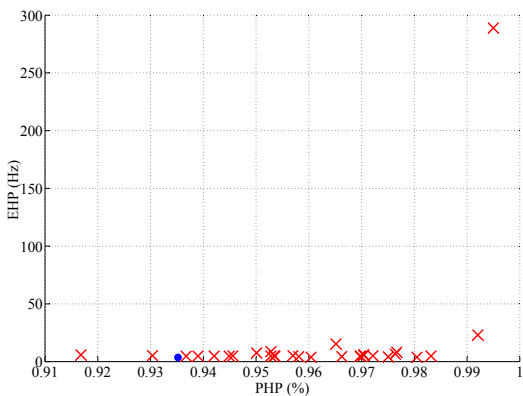


Figure 2.15: EHP and PHP calculation applied to the 30 missions

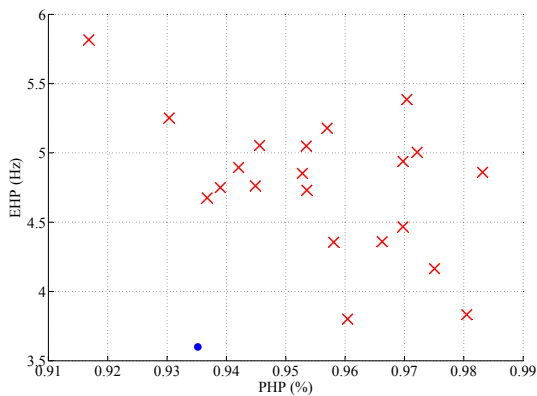


Figure 2.16: Zoom around the most restricting mission (bullet)

They represent 30 different markers in the EHP-PHP plane. The marker at the bottom of the figures (the bullet) corresponds to the lowest obtained EHP value and deals with the mission number 28. This driving cycle is the one presenting the highest power peak value, the highest speed of the locomotive and the longest distance among all the available driving cycles. Figures 2.17 and 2.18 represent the power mission and the speed of the locomotive for the mission number 28.

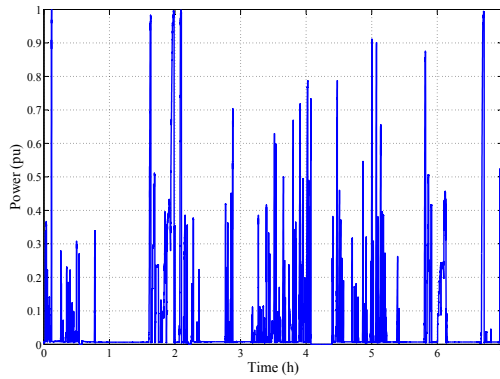


Figure 2.17: Power required by the driving cycle number 28.

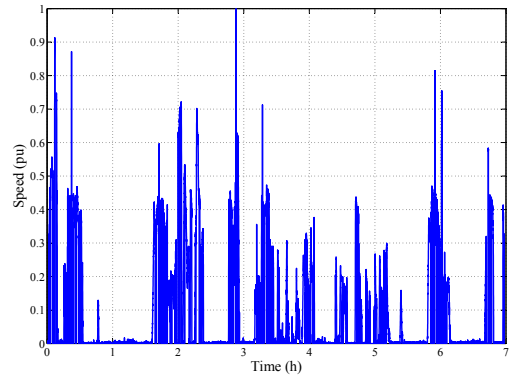


Figure 2.18: Speed of the locomotive (mission number 28).

Contrary to this marker, on the figure 2.15, the higher cross marker corresponds to the mission number 3. The locomotive is here parked in a shed. Figures 2.19 and 2.20 represent the power mission and the speed of the locomotive for the mission number 3.

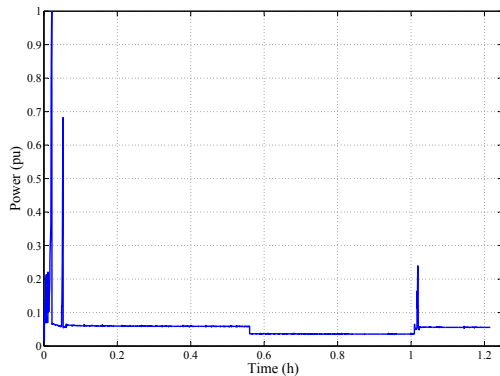


Figure 2.19: Power required by the driving cycle number 3.

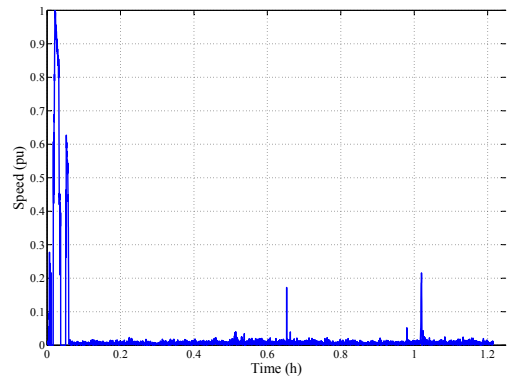


Figure 2.20: Speed of the locomotive (mission number 3).

Thus, our knowledge confirms the theoretical indicators. The lowest EHP value corresponds to the most restricting driving cycle and the highest value

to the less restricting one. Now, considering the PHP indicator, it appears that all missions are favourable to hybridization. Indeed, all the PHP results are nearly equal to one. Moreover, it confirms that the shunting activities targeted by Alstom Transport in this study are effectively chosen to be performed by a HEL.

## 2.2.2 Batteries and ultra-capacitors sizing - [Akli08]

The considered sizing methodology is based on a frequency approach of the driving cycle and of the constraints of the on-board power sources. Figure 2.21 presents the principle of this methodology.

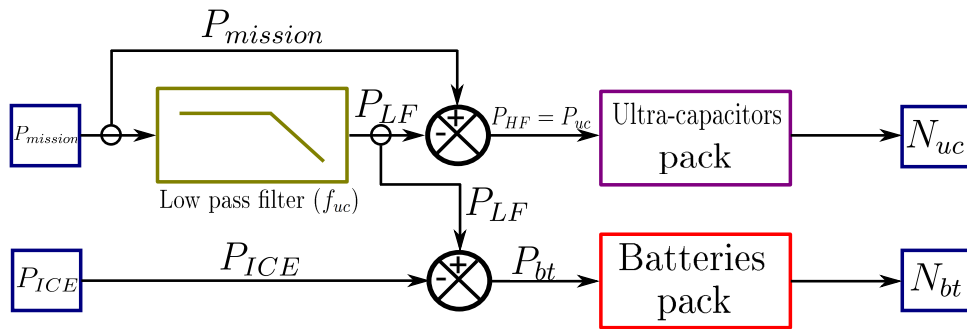


Figure 2.21: Frequency approach principle

The power mission <sup>1</sup> ( $P_{mission}$ ) is filtered thanks to a low pass filter characterized by its cutoff frequency ( $f_{uc}$ ). Low and high frequencies of the driving cycle signal  $P_{mission}$  are obtained from this filter (figure 2.22). The negative values of the high frequencies signal are due to the dynamics of the low pass filter. Indeed, the low frequencies signal variations have a lower dynamic than those of the original signal. Thus, the high frequencies signal variations correspond to the difference between the original and the low pass filtered signals.

High frequencies are dedicated to the UCs' bank and low ones are subtracted from the power delivered by the ICE to be dedicated to the batteries' bank. In the next parts, the algorithms implemented in the blocks named "Ultra-capacitors pack" and "Batteries pack" of the figure 2.21 which aim at performing the calculation of the total number of UCs' and batteries' cells ( $N_{uc}$  and  $N_{bt}$ ), are developed. The algorithms take into account the efficiency of the elements and permit to:

<sup>1</sup>Power required over the driving cycle

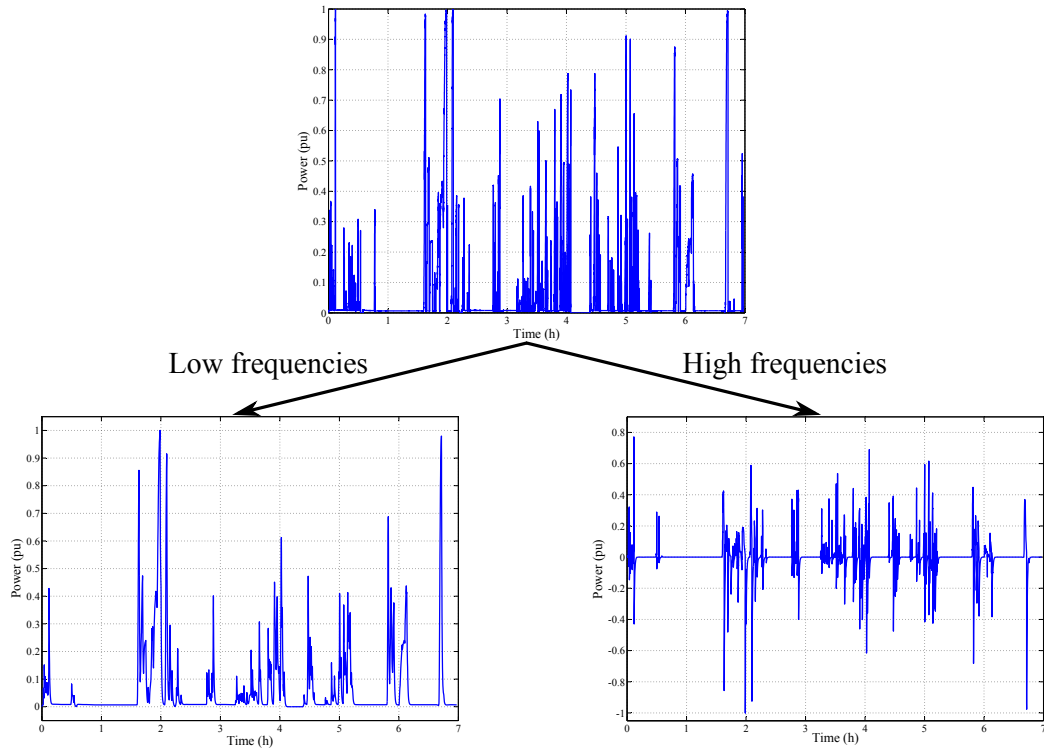


Figure 2.22: Frequency decomposition of the mission power signal into low and high frequencies power signals

- calculate the total number of cells (batteries and UCs to be set up into the system),
- perform the series-parallel organization of the cells.

For the first point, algorithms are applied to all the driving cycles. It aims at confirming the previous results obtained with the PHP and EHP indicators. Then, the series-parallel configuration is performed only based on the mission number 28. The results are presented like an evolution of the number of cells according to the working cutoff frequency of the low pass filter and the considered driving cycle. As a reminder the used convention considers a negative (respectively positive) power like a charging (respectively discharging) power for the storage devices. Thus, the equations dealing with the calculation of the energy to be stored into the elements present a negative sign. Indeed, a negative (charging) power corresponds to an energy accumulation into the elements and a positive (discharging) power corresponds to an energy release out of the elements.

## Sizing of the ultra-capacitors' bank - [Akli08]

**Determination of the total number of cells** UCs present the same behaviour and power limitations for charging and discharging phases. Thus, their sizing only depends on the operating cutoff frequency ( $f_{uc}$ ). To calculate the total number of UCs' cells -  $N_{uc}$ , the first step consists in calculating the energy to be stored by UCs thanks to the equation 2.5.

$$E_{uc}(t) = - \int_0^t P'_{uc}(\tau) d\tau \quad (2.5)$$

with  $P'_{uc}$  the high frequencies of the power mission signal. To calculate the useful energy to be stored into the UCs, equation 2.6 is used. The principle is exactly the same as explained previously with the equation 2.3 and figures 2.13 and 2.14.

$$E_{u_{uc}} = \max(E_{uc}(t)) - \min(E_{uc}(t)) \quad (2.6)$$

Their Depth Of Discharge ( $DOD_{uc}$ ) is included in the calculation [Uno11]. Thus, the real capacity of the pack is given by equation 2.7.

$$E_{real_{uc}} = \frac{E_{u_{uc}}}{DOD_{uc}} \quad (2.7)$$

The total number of UCs' cells depends on:

- energy ( $N_{ucE}$  - equation 2.8),
- power ( $N_{ucP}$  - equation 2.9).

$$N_{ucE} = \frac{E_{real_{uc}}}{E_{0_{uc}}} \quad (2.8)$$

$$N_{ucP} = \frac{\max(P'_{uc})}{P_{0_{uc}}} \quad (2.9)$$

where  $E_{0_{uc}}$  and  $P_{0_{uc}}$  are respectively the nominal energy and power of a single UC cell.

Finally,  $N_{uc}$  is determined with equation 2.10.

$$N_{uc} = \max(N_{ucE}, N_{ucP}) \quad (2.10)$$

**Series-Parallel configuration** The series/parallel sizing is reduced to a single (battery/UC) cell study. The same method is indifferently applied to batteries and UCs. Thus, it is only going to be detailed for the UCs' case. In theory, the total number of UCs' cells ( $N_{uc}$ ) corresponds to the number of cells in series ( $N_{suc}$ ) multiplied by the number of cells in parallel ( $N_{puc}$ ) (equation 2.11).

$$N_{uc} = N_{suc} \times N_{puc} \quad (2.11)$$

Thus, UCs' bank current ( $I_{uc}$ ) and voltage ( $V_{uc}$ ) are defined by equation 2.12.

$$\begin{cases} I_{uc} = N_{puc} \times i_{uc} \\ V_{uc} = N_{suc} \times v_{uc} \end{cases} \quad (2.12)$$

with ( $v_{uc}$ ) and ( $i_{uc}$ ) UCs' cells' voltage and current. UCs' bank is linked to the central DC bus thanks to a chopper. Its minimum and maximum duty cycles are defined by ( $\alpha_{min}$ ) and ( $\alpha_{max}$ ) - equations 2.13 and 2.14.

$$\alpha_{min} V_{bus} \leq V_{uc} \leq \alpha_{max} V_{bus} \quad (2.13)$$

$$\alpha_{min} \frac{V_{bus}}{v_{uc_{min}}} \leq N_{suc} \leq \alpha_{max} \frac{V_{bus}}{v_{uc_{max}}} \quad (2.14)$$

From equation 2.11, minimum and maximum of UCs' cells' in series and in parallel are deduced (equation 2.15).

$$\begin{cases} N_{suc_{min}} = \alpha_{min} \frac{V_{bus}}{v_{uc_{min}}} \\ N_{suc_{max}} = \alpha_{max} \frac{V_{bus}}{v_{uc_{max}}} \end{cases} \quad (2.15)$$

Minimum ( $v_{uc_{min}}$ ) and maximum ( $v_{uc_{max}}$ ) voltages that can be applied to a cell are determined using the electrical model represented on figure 2.23.

An equivalent circuit as shown in figure 2.23 may be used to represent the operating characteristics of an UC's cell.  $C_R$  is an ideal capacitor, which is connected to the resistor  $r_{uc}$  for emulating the series resistance. It would have been possible to emulate the self discharging of the element thanks to another resistance in parallel with the capacitor. However, since this parallel resistance is very large, this parallel branch may be ignored in modelling and simulation without much influence on the results [Chen09]. However, it will be used to predict the self discharge behaviour of the element when developing the EMS of the vehicle.

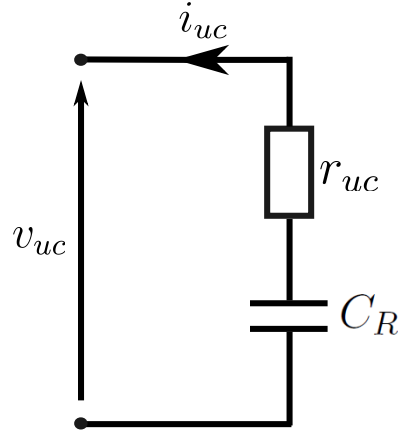


Figure 2.23: Electric model adopted for ultra-capacitors representation

The filtered power dedicated to the whole bank of UCs ( $P_{uc}$ ) is reduced to a single battery cell power ( $p_{uc}$  - equation 2.16)

$$p_{uc} = \frac{P_{uc}}{N_{uc}} \quad (2.16)$$

Thus, the current applied to a single cell is the ratio between this power ( $p_{uc}$ ) and the voltage of the same considered cell ( $v_{uc}$ ) (equation 2.17).

$$i_{uc} = \frac{p_{uc}}{v_{uc}} \quad (2.17)$$

Minimum and maximum currents ( $i_{uc_{min}}$  and  $i_{uc_{max}}$ ) are then extracted (equation 2.18).

$$\begin{cases} i_{uc_{min}} = \min(i_{uc}) \\ i_{uc_{max}} = \max(i_{uc}) \end{cases} \quad (2.18)$$

The voltage  $v_{uc}$  is deduced from equations 2.19 and 2.20.

$$v_c(t) = v_0 - \frac{1}{C_R} \int_0^t i_{uc}(\tau) d\tau \quad (2.19)$$

$$v_{uc} = v_c(t) - r_{uc} i_{uc} \quad (2.20)$$

$Ns_{uc_{min}}$  and  $Ns_{uc_{max}}$  are deduced using equation 2.15 and  $Np_{uc_{min}}$  -  $Np_{uc_{max}}$  thanks to equation 2.11.

## Sizing of the bank of batteries - [Akli08]

**Determination of the total number of cells** Contrary to UCs, batteries do not have the same power limitation for charging and discharging phases. The sizing method is based on three algorithms. In this study, we will consider a positive (respectively negative) power like a discharging (respectively charging) power for all the three on-board sources and the power mission. The rheostat only dissipates power which corresponds to a negative power. Considering discharging/charging powers ( $P_{dch}$ ;  $P_{ch}$ ) and constant discharging/charging times ( $t_{dch}$ ;  $t_{ch}$ ), the batteries' energy  $E_{batt}$  must cover the considered discharging and charging requirements (equation 2.21). The constant times correspond to the time necessary to fully charge/discharge the batteries.

$$\begin{cases} E_{batt} \geq t_{dch} \times P_{dch} \\ E_{batt} \geq -t_{ch} \times P_{ch} \end{cases} \quad (2.21)$$

These inequalities define the area limits of the energy - power plan which represents the batteries sizing domain (figure 2.24). These technological constraints graphs constitute the common basis of the study to explain the met problems and the developed solutions.

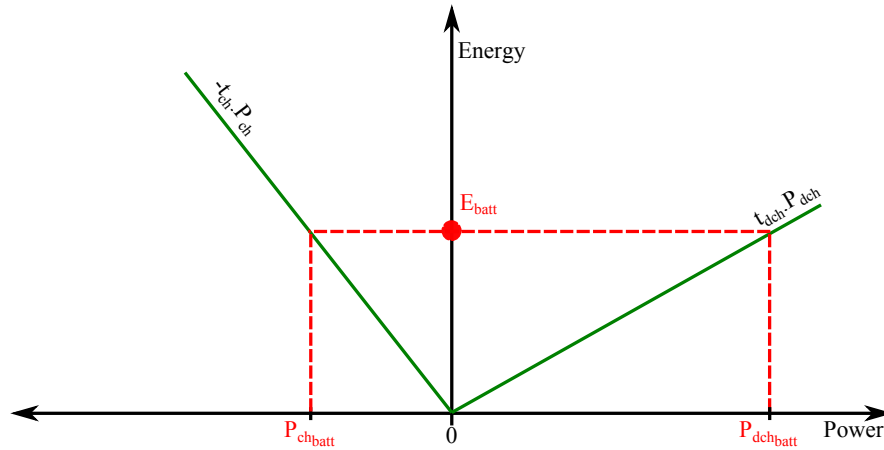


Figure 2.24: Batteries technological constraints graph

Considering maximum batteries' discharging/charging powers  $P_{dch_{batt}}$  and  $P_{ch_{batt}}$ , the figure 2.24 shows the necessary batteries' energy  $E_{batt}$  to respect the equation 2.21.

Like for the UCs' sizing method (equations 2.5 and 2.6), the useful energy is also used to perform the batteries' sizing. However, a simple integration is not adequate in this new problem.

### Calculation of the useful energy based on a saturated integration

Lets consider a theoretical power mission ( $P_{th}$ ) applied to the batteries (figure 2.25) and the corresponding evolution of the energy (equation 2.22).

$$E(t) = - \int_0^t P_{th}(\tau) d\tau \quad (2.22)$$

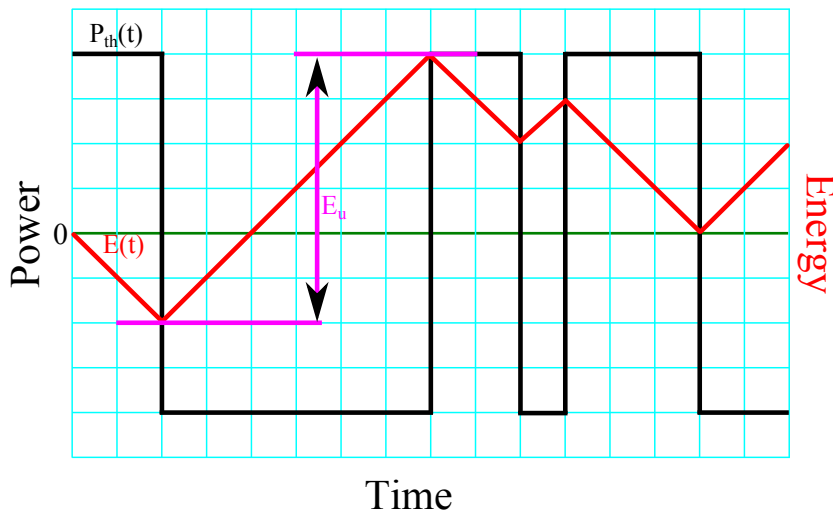


Figure 2.25: Conventional energy calculation

Considering this theoretical power, the energy level is higher at the end of the mission than at its beginning. In other words, the energy balance is positive and the batteries are more charged at the end of the mission than at its beginning. This energy drives to an over-sizing. Indeed, the most important thing is the determination of the energy to be stored in the batteries in regard to the discharging phases requirements (positive powers). Then, it is not necessary to cover all the charging phases of the mission. If the point 0 of the figure 2.25 corresponds to the maximum batteries' SOC level, the energy can not exceed this maximum. In practice, batteries would be over-charged which is not recommended. This is the reason why all the batteries' energy is not used and this energy calculation (equation 2.22) drives to an over-sizing. The solution consists in calculating the energy differently. The batteries are considered to be fully charged at the beginning. Then, the calculated energy can not exceed this value when recharging (figure 2.26). That kind of integration aims at ignoring charging phases if energy level reaches a defined maximum. According to the UCs' SOC and the implemented EMS, this energy is stored into UCs or dissipated thanks to the rheostat.

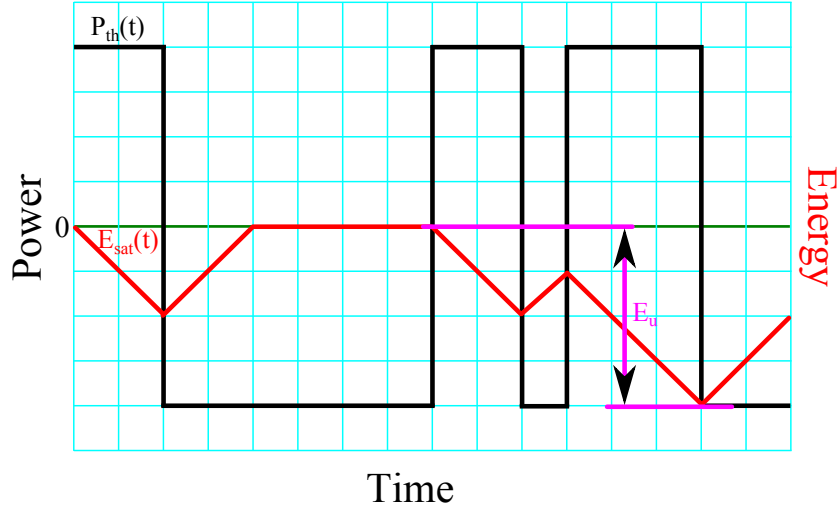


Figure 2.26: Saturated energy calculation

Thus, the new useful energy is lower than the previous calculated one. The equation 2.23 deals with the new saturated integration.

$$E_{sat}(t) = - \left( \int_0^t P_{th}(\tau) d\tau \right)_{sat} \quad (2.23)$$

with  $E_{sat}(t)$ , the saturated energy of the signal  $P_{th}(t)$ . To perform this saturated integration, the power mission is sampled.  $d_{mission}$ , the mission duration is sampled such as  $d_{mission} = NT_e$  thanks to the sampling period  $T_e$  ( $T_e = 1s$ ) - equation 2.24.

$$\forall n \in [0, \dots, N], \begin{cases} P_{th}(n) = P_{th}(nT_e) \\ E(n) = E(nT_e) \end{cases} \quad (2.24)$$

Lets consider  $\delta e(n)$ , the exchanged quantity of energy between  $(n-1)T_e$  and  $(n)T_e$  instants (equation 2.25).

$$\begin{cases} e(0) = 0 \\ \forall n \in [1, \dots, N], \delta e(n) = -\frac{1}{2}T_e [P_{th}(n-1) + P_{th}(n)] \end{cases} \quad (2.25)$$

Thus, the integrated saturation  $E_{sat}(t)$  of the power mission  $P_{th}(t)$  is given by equation 2.26.

$$\left\{ \begin{array}{l} E_{sat}(0) = 0 \\ \forall n \in [1, \dots, N], \quad E_{sat}(n) = \begin{cases} 0 & \text{if } E_{sat}(n-1) + \delta e(n) \geq 0 \\ E_{sat}(n-1) + \delta e(n) & \text{otherwise} \end{cases} \end{array} \right. \quad (2.26)$$

The saturated energy ( $E_{sat}(n)$ ) is lower than the initial saturated energy ( $E_{sat}(0) = 0$ ) which corresponds to the maximum acceptable saturated energy. Thus,  $E_{sat}(n) \leq 0$ .

If the exchanged energy decreases ( $\delta e(n) < 0$ ) then the saturated energy also decreases ( $E_{sat}(n) = E_{sat}(n-1) + \delta e(n) \leq 0$ ) and the batteries deliver power.

If the exchanged energy increases ( $\delta e(n) > 0$ ) then the saturated energy ( $E_{sat}(n)$ ) also increases until it reaches its maximum acceptable value ( $E_{sat}(0)$ ). The batteries recover power until they reach the saturation.

Finally, useful energy corresponds to the difference between the minimum and the maximum of the previous calculated energy (equation 2.27).

$$\forall n \in [1, \dots, N], \quad E_u = \max(E_{sat}(n)) - \min(E_{sat}(n)) \quad (2.27)$$

Now, it is necessary to check that the calculated useful energy is enough to cover the charging and discharging powers required by the mission. These powers ( $P_{ch_{mission}}$  and  $P_{dch_{mission}}$ ) are represented on figure 2.27.

Both evolutions of the batteries power missions (ideal power mission and power mission taking into account batteries efficiency) are depicted. The figure aims at determining which is the most suitable power mission to define the extreme charging and discharging powers values ( $P_{ch_{mission}}$  and  $P_{dch_{mission}}$ ). It appears that the ideal power mission is a penalty for the charging phase and the "real" power mission is a penalty for the discharging phase. Thus,  $P_{ch_{mission}}$  and  $P_{dch_{mission}}$  are defined by equation 2.28.

$$\left\{ \begin{array}{l} P_{dch_{mission}} = \max(P_{batt}^{th}(t)) \\ P_{ch_{mission}} = \min(P_{batt}^{real}(t)) \end{array} \right. \quad (2.28)$$

When the useful energy is calculated, three cases are possible.

**Case 1:** The calculated useful energy (calculation of the useful energy using the saturated integration -  $E_{u(batt)_{sat}}$ ) is enough to cover the charging and discharging powers requirements of the mission. This case is depicted on figure 2.28 and  $|P_{ch_{batt}}| > |P_{ch_{mission}}|$ ;  $P_{dch_{batt}} > P_{dch_{mission}}$ .

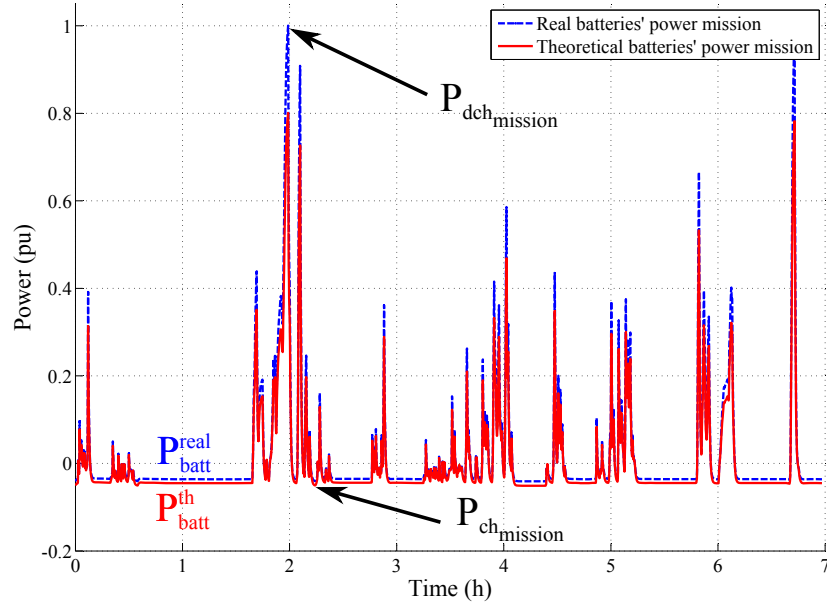


Figure 2.27: Evolution of the power dedicated to the batteries.

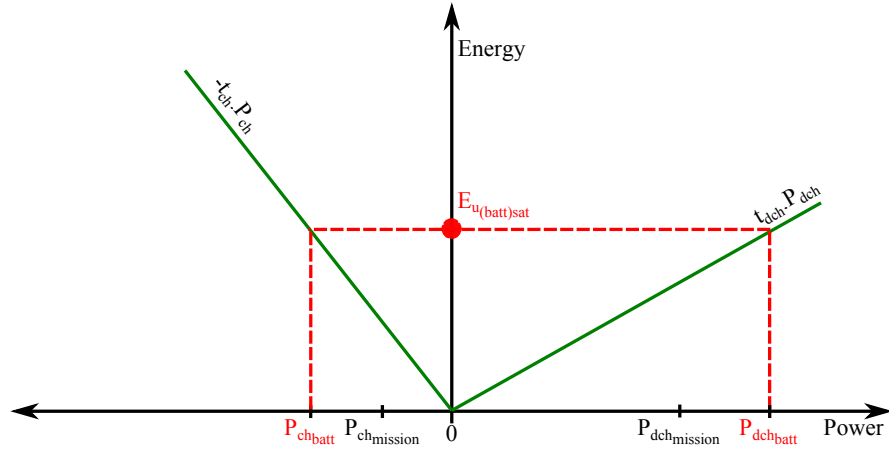


Figure 2.28: Batteries technological constraints graph (case 1).

**Case 2:** The calculated useful energy is not enough to cover the charging and discharging powers requirements of the mission. This case is depicted on figure 2.29 and  $|P_{ch_{batt}}| < |P_{ch_{mission}}|$ ;  $P_{dch_{batt}} < P_{dch_{mission}}$ .

In such a case, it is essential to ensure the discharging power mission. Thus, to cover the discharging mission power peaks, the useful energy is increased till obtaining a new useful energy  $E_{u(batt)sat}'$  in such a way that  $P_{dch_{batt}} = P_{dch_{mission}}$  on the figure 2.29. However, the charging power requirement of the mission is not necessarily solved ( $|P_{ch_{batt}}| < |P_{ch_{mission}}|$ ).

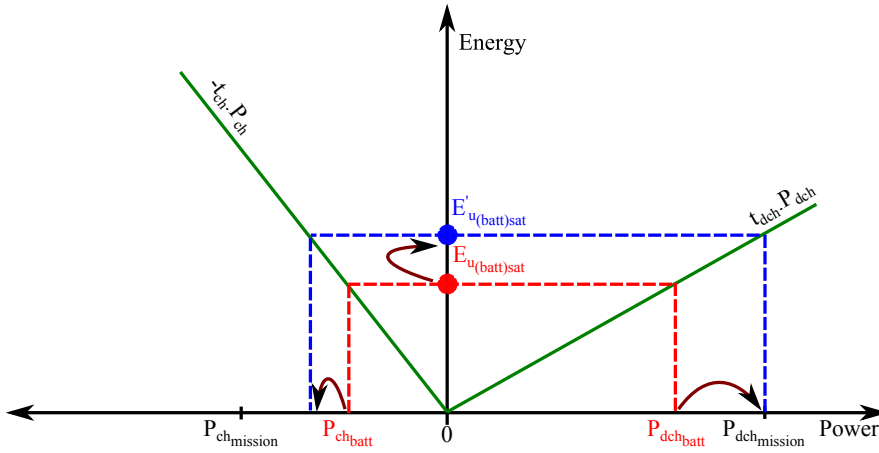


Figure 2.29: Batteries technological constraints graph (case 2).

**Case 3:** This case is an extension of the second case. The calculated useful energy is enough to cover the discharging power requirement of the mission but it is not enough to cover the charging power requirement of the mission. It would also be possible to increase the useful energy  $E_{u(batt)sat}$  in such a way that  $P_{chbatt} = P_{chmission}$ . However, this increase is estimated too important (around 150% in [Akli08]) for the sizing problem (figure 2.30).

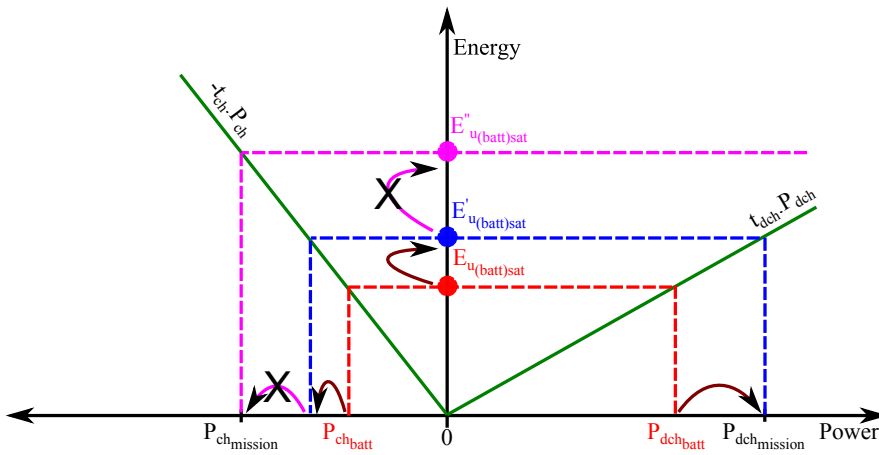


Figure 2.30: Batteries technological constraints graph (case 3).

Moreover, the charging power is a lower requirement than the discharging one. If the batteries' pack is downsized in regard to the charging phase, it only means that the charging possibilities won't be totally used to recharge the pack. In other words, charging power is available to recharge the batteries but it can not be used because they are not sized to recover so much power.

This case is less important than a pack of batteries which is not able to deliver the necessary power to perform the driving cycle (discharging power).

**Correction of the charging power mission requirement** The solution consists in directly changing the batteries power profile in reducing the charging mission power. In other words, this power profile is corrected in increasing the mission charging power minimum value of the figure 2.27 ( $P'_{ch_{mission}} > P_{ch_{mission}}$ ) and in consequence the useful energy to be stored in the batteries' pack increases to compensate the lost energy. This lost energy was used to recharge the pack. To change this power, it is taking back to the border line ( $-t_{ch} \cdot P_{ch}$  - figure 2.30) by the equation 2.29.

$$P_{ch_{corrected}} = -\frac{E_{u(batt)_{sat}}}{t_{ch}} \quad (2.29)$$

A subtle issue persists and is presented on figure 2.31.

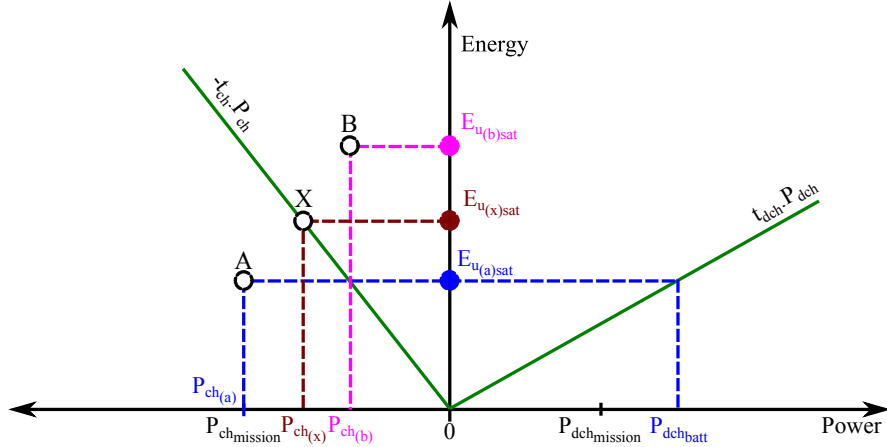


Figure 2.31: Batteries technological constraints graph (optimal point).

- The point "B" corresponds to the obtained useful energy ( $E_{u(b)_{sat}}$ ) after limiting the charging power of the mission  $P_{ch_{mission}}$  to  $P_{ch(b)}$ . However, it corresponds to a non-optimal energy. The useful energy  $E_{u(b)_{sat}}$  is sufficient to cover the charging phases but it is also over-sized.
- The point "A" corresponds to the obtained useful energy ( $E_{u(a)_{sat}}$ ) when respecting the charging power of the mission such as  $P_{ch_{mission}} = P_{ch(a)}$ . However, it corresponds to a point which is out of the sizing domain. The useful energy ( $E_{u(a)_{sat}}$ ) is not sufficient to cover the charging power mission requirement.

- The point "X" corresponds to the obtained useful energy ( $Eu_{(x)sat}$ ) after limiting the charging power of the mission such as  $P_{ch_{mission}} = P_{ch_{(x)}}$  and belonging to the sizing domain. This point is the optimal point in terms of power and useful energy.  $Eu_{(a)sat} < Eu_{(x)sat} < Eu_{(b)sat}$ , the point "X" belongs to the sizing domain and it is the closer point to the border line ( $-t_{ch} \cdot P_{ch}$ ).

**Dichotomy algorithm** To find the optimal point "X", a dichotomy algorithm is implemented. Each iteration of the algorithm calculates  $P_{center}$  defined by equation 2.30 and the corresponding useful energy  $E_{center}$  using the saturated integration (equation 2.23).

$$P_{center} = \frac{1}{2} \left( P_{ch_{(a)}} + P_{ch_{(b)}} \right) \quad (2.30)$$

Then, the stopping criterion of the algorithm is checked. The "distance" between the center point and the border line ( $-t_{ch} \cdot P_{ch}$ ) is calculated and compared to the error  $\epsilon$  (equation 2.31).

$$|E_{center} - t_{ch} \cdot P_{center}| \leq \epsilon \quad (2.31)$$

If the the criterion is confirmed, the algorithm stops else it checks if the center point is on top (figure 2.32) or below (figure 2.33) the border line.

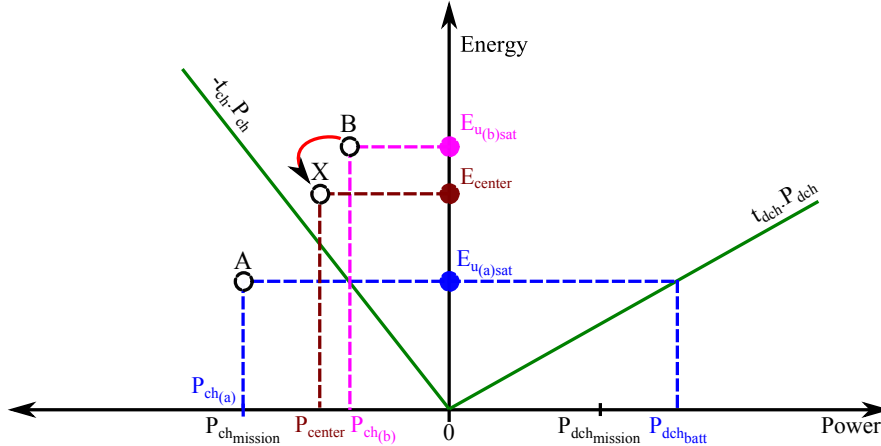


Figure 2.32: Dichotomy algorithm - Top of the border line.

The next iteration of the dichotomy algorithm reallocates the new "B" point (respectively the new "A" point) like the calculated center point if the latter is located on top (respectively below) the border line.

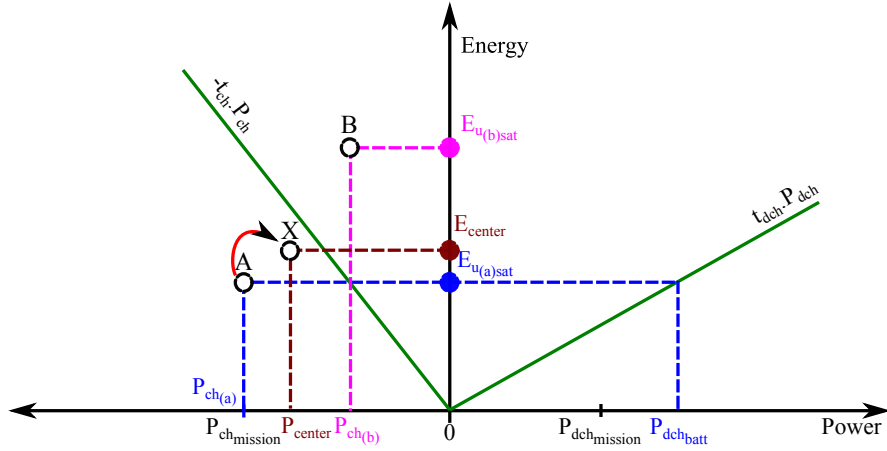


Figure 2.33: Dichotomy algorithm - Bottom of the border line.

**The global sizing method of the batteries** The figure 2.34 presents the global batteries' sizing method including the described algorithms.

From the considered mission  $k$ , the cutoff frequency of the low pass filter ( $f_{uc}$ ) and the power delivered by the ICE ( $P_{ICE}$ ), the batteries theoretical and real power missions ( $P_{batt}^{th}$  and  $P_{batt}^{real}$ ) are calculated. From these two powers, a first useful energy is calculated using the saturated integration ( $E_{u(batt)sat}$ ). Then, from the mission charging/discharging powers ( $P_{ch_{mission}}/P_{dch_{mission}}$  - equation 2.28) and the time constants ( $t_{dch}$  and  $t_{ch}$ ) either the useful energy covers the discharging power requirements of the mission:

- *and* covers the charging power requirements of the mission (case 1 - figure 2.28). Then, the algorithm stops.
- *but* does not cover the charging power requirements of the mission (case 3 - figures 2.30 and 2.31). The calculation of a corrected charging power (equation 2.29) permits to define a new useful energy ( $E'_{u(batt)sat}$ ) which is then optimised thanks to the dichotomy algorithm. Then, the algorithm stops.

Or the useful energy does not cover the discharging power requirements of the mission (it is increased till covering them (case 2 - figure 2.29)):

- *and* covers the discharging power requirements of the mission. Then, the algorithm stops.
- *but* does not cover the charging power requirements of the mission. As previously, the charging power is corrected and the dichotomy algorithm is also applied. Then, the algorithm stops.

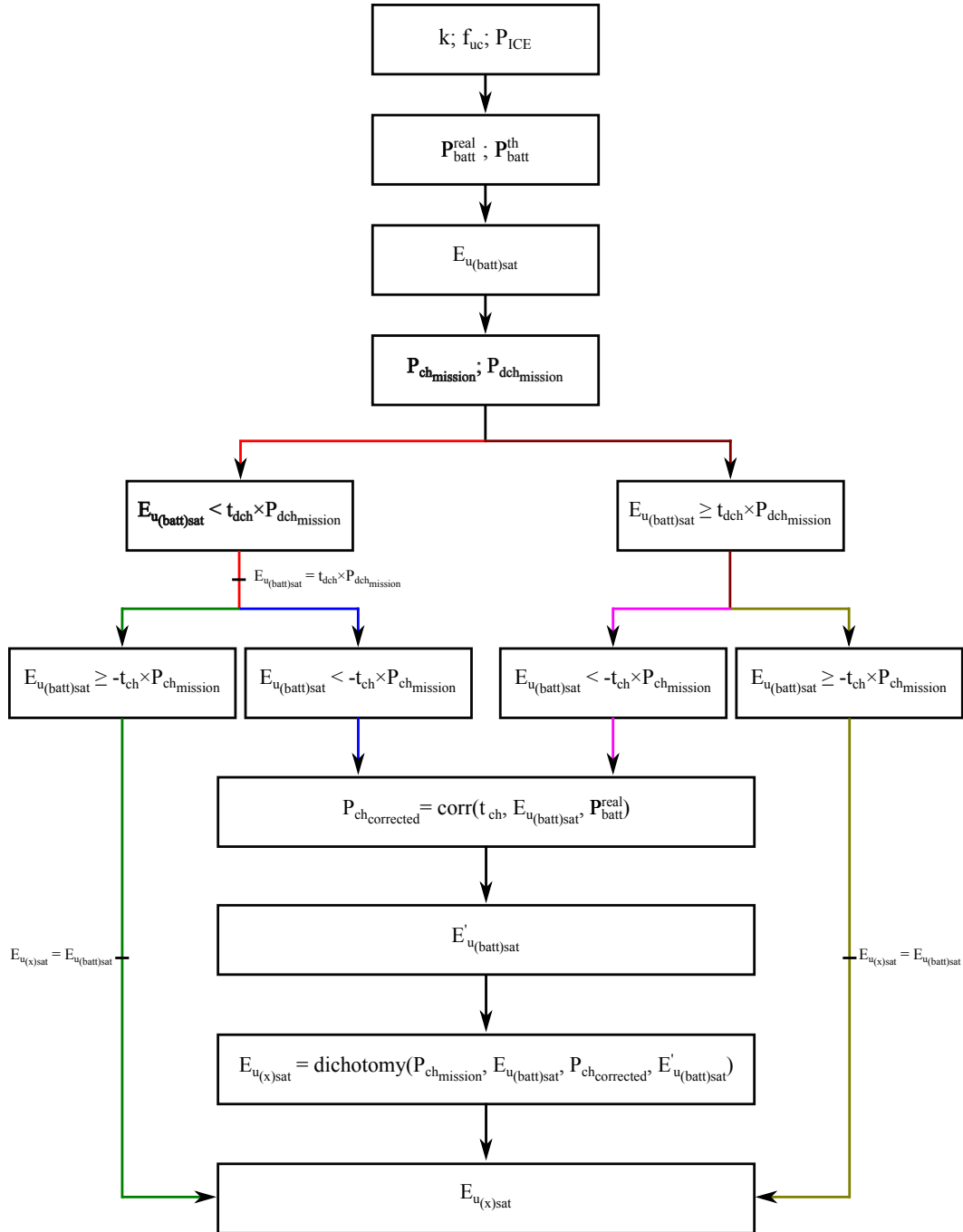


Figure 2.34: Sizing algorithm of the batteries

Finally, the total number of cells is the ratio of the calculated energy ( $E_{u(x)sat}$ ) with the nominal energy of a single battery cell ( $E_{batt}^0$ ).

**Series-Parallel configuration** The method developed for the UCs is also applied for the batteries (equations 2.32 to 2.35). In the same way, minimum ( $v_{bt_{min}}$ ) and maximum ( $v_{bt_{max}}$ ) voltages are determined using the electrical model represented on figure 2.35.

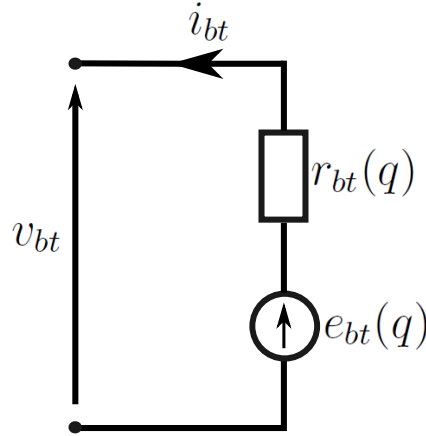


Figure 2.35: Electric model adopted for batteries representation

It is made up of an internal resistance ( $r_{bt}$ ) and a nominal voltage ( $e_{bt}$ ).

$$p_{bt} = \frac{P_{bt}}{N_{bt}} \quad (2.32)$$

$$i_{bt} = \frac{p_{bt}}{v_{bt}} \quad (2.33)$$

$$\begin{cases} i_{bt_{min}} = \min(i_{bt}) \\ i_{bt_{max}} = \max(i_{bt}) \end{cases} \quad (2.34)$$

$$v_{bt} = e_{bt} - r_{bt}i_{bt} \quad (2.35)$$

## Results

**Determination of the total number of cells** Figures 2.36 and 2.37 present the evolution of the total number of batteries' and UCs' cells according to the low pass filter frequencies. The algorithm is applied to all the available missions with a constant 200 kW power delivered by the ICE.

The results corresponding to the mission number 28 are represented with lozenges (highest curve - figure 2.36) and appear to be the driving cycle requiring the highest number of batteries' and UCs' cells. It confirms the results obtained with the PHP and EHP indicators.

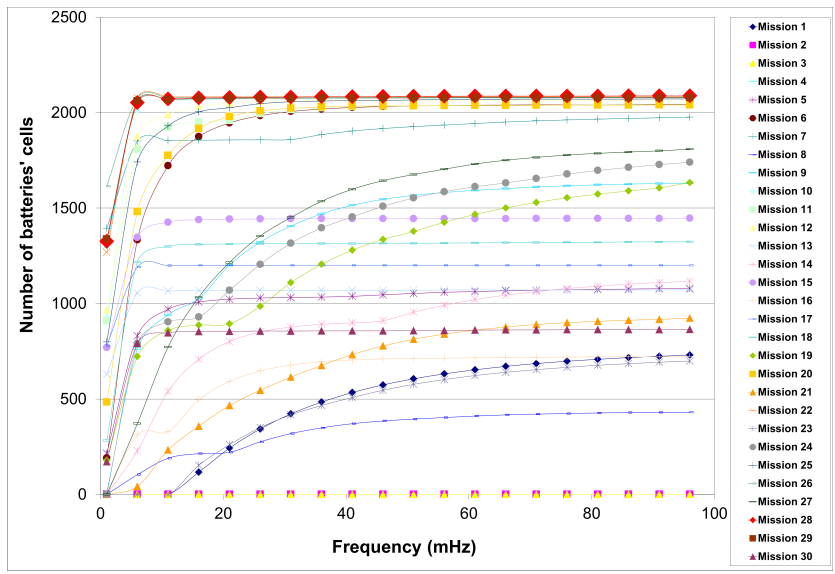


Figure 2.36: Evolution of the total number of batteries' cells according to the low pass filter frequencies.

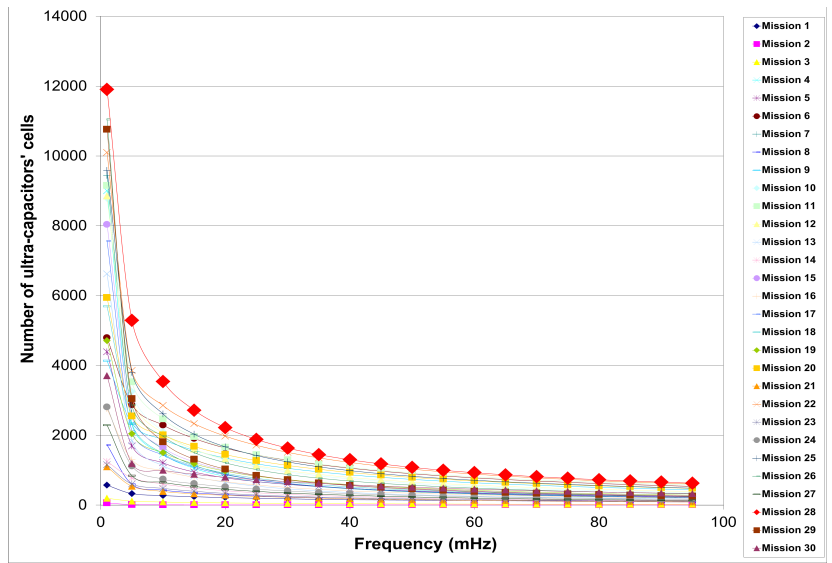


Figure 2.37: Evolution of the number of ultra-capacitors' cells according to the low pass filter frequencies.

**Series-Parallel results** The results are depicted on figures 2.38 and 2.39. They also represent the evolution of the number of batteries and UCs' cells in series and in parallel according to the low pass filter frequencies. The real number of cells must be rounded to have an integer.

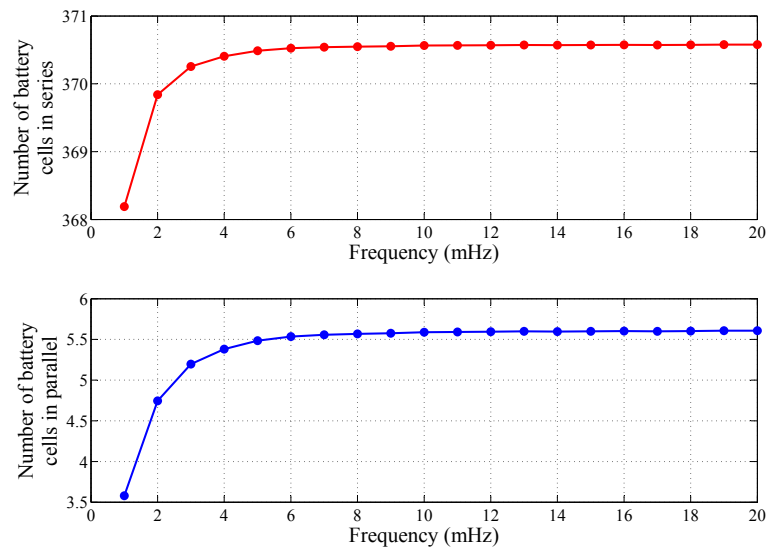


Figure 2.38: Evolution of the number of battery cells in series (top) and in parallel (bottom) according to the low pass filter frequencies.

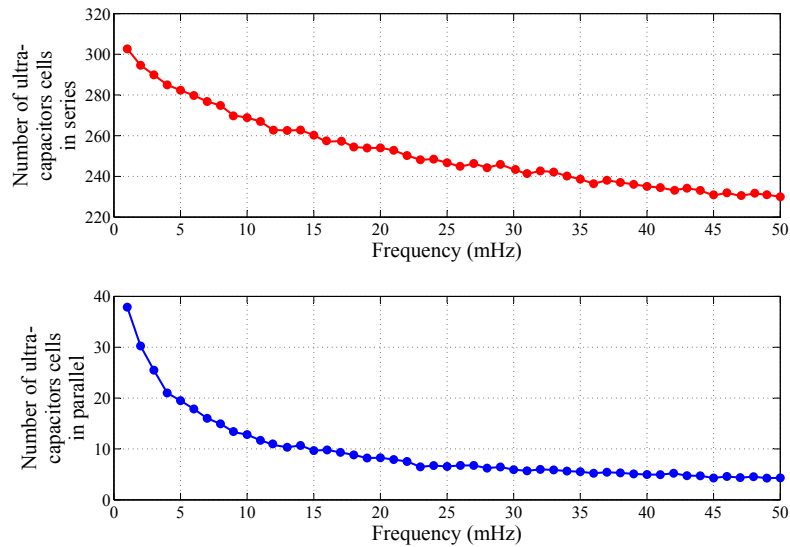


Figure 2.39: Evolution of the number of ultra capacitors cells in series (top) and in parallel (bottom) according to the low pass filter frequencies.

Results are in accordance with figures 2.36 and 2.37. Indeed, curves have the same characteristic and the product of the parallel sizing and series sizing values is equal to the total number of batteries and UCs elements.

### 2.2.3 Volume and weight estimations

The obtained results are used to estimate the weight and the volume of the secondary sources of the system. The characteristics (volume and weight) of a single cell are:

- 7.05 kg and 4.34 l for battery - [Akli08],
- 0.26 kg and 0.21 l for UC - [Devi12].

They do not take into account the power electronics volume and weight characteristics. Based on these parameters, the figures 2.40 and 2.41 present the evolution of the total (batteries plus UCs) volume and weight for increasing constant powers delivered by the ICE. The used frequency range is from 1 mHz up to 100 mHz.

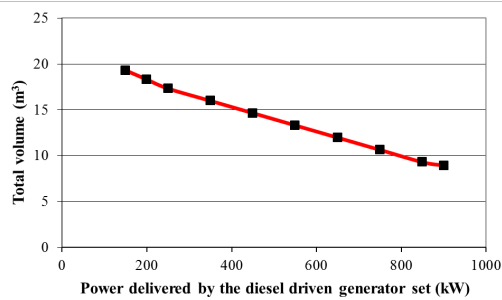


Figure 2.40: Evolution of the total volume according to the power delivered by the diesel engine

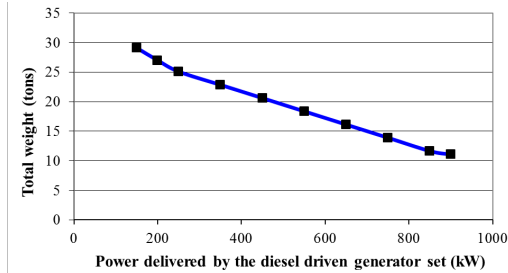


Figure 2.41: Evolution of the total weight according to the power delivered by the diesel engine

### 2.2.4 Arrangement of the elements

Configuration of the packs of batteries and UCs is described on figure 2.42. This configuration associates a chopper per parallel pack. Indeed, in order to avoid imbalances problems, the assembly of the parallel packs under a common chopper is not recommended. According to [Hija06], the assembly in series of an important number of UCs' cells causes voltage imbalances between them. Indeed, their SOC depends on their voltage. Thus, UCs' voltage have a fast and important band variation when using them during a mission. Voltage imbalances accelerate their ageing and reduce their lifespan. This problem is partially solved in associating power electronics in parallel to control voltages individually. Even if this configuration improves the individual control of the sources according to their physical state (SOC, degradation,

failure...) and reduces imbalances, it remains more complex and the system is heavier and larger. This choice is not optimal. A high bus voltage is a solution to limit the number of parallel packs, to minimise the choppers' losses and to reduce their weight/size. However, a high bus voltage presents some drawbacks:

- security problems due to high voltages,
- maintenance specific precautions relating to the electric class protection.

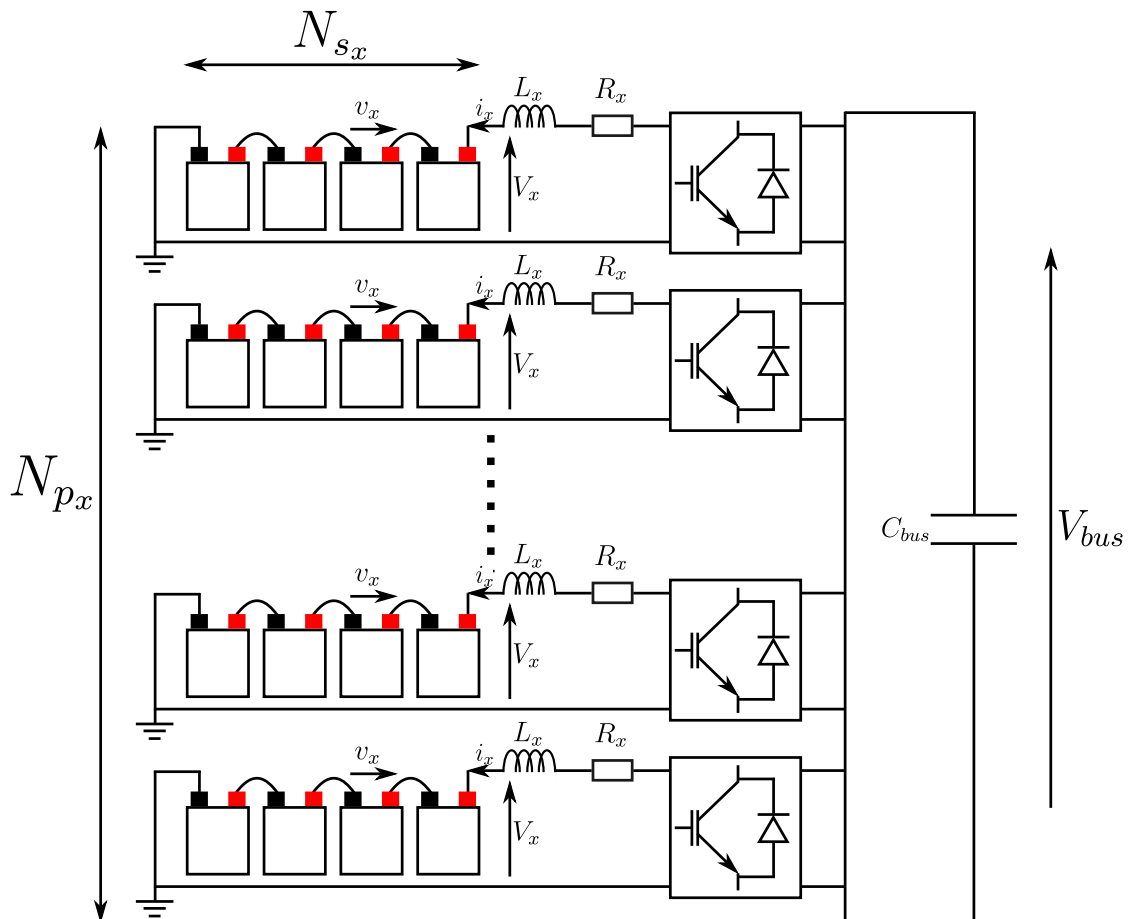


Figure 2.42: Arrangement of the cells in the packs

## 2.3 Chapter conclusion

The locomotive architecture is improved from a conventional diesel electric propulsion to a Hybrid Electric one. An ICE is still set up on-board and coupled with batteries' and UCs. The new configuration (series HEV) aims at deporting a part of the power required by the freight activity on other sources and avoid operating the ICE on low loads. Moreover, this solution permits to cover a large range of specific energy and power (Ragone plot - figure 2.3).

The new configuration raises the sizing problem of the batteries and UCs' banks. The use of the PHP and EHP indicators permits determining the most constraining driving cycles among the thirty different available in terms of power and energy [Baer11a]. Then, according to the considered architecture and the frequency approach of the on-board sources, algorithms aim at proposing estimations of the requested number of batteries and UCs' cells to assemble in series and in parallel in the locomotive. The obtained results obviously depend on the working cutoff frequency of the low pass filter, the considered driving cycle and the elements' characteristics/specifications. Moreover, the method takes into account the efficiency of the secondary sources and their different behaviours during charging and discharging phases.



## Chapter 3

# Modelling and control of the Hybrid Electric Locomotive

Before developing an Energy Management Strategy, it is necessary to model the available sources. A good modelling necessitates a precise knowledge and understanding of the different sources functioning and behaviour. This simulation step is necessary to represent the benefits and drawbacks of the considered sources as accurate as possible. To reach a good precision of the control structures and EMSs of the sources, dynamical and experimentally validated models must be developed. The appendix A sums up the theoretical basis of the EMR, the MCS and PCS design. The considered models are mainly based on existing ones which are presented using the EMR. From a laboratory expertise point of view, the use of the EMR also aims at capitalising the research developments.

The chapter is structured in seven sections. The first three sections present the implemented models and control structures of the ICE, the UCs and the batteries. Experimental characterisations of the batteries are also described in this section. Sections 3.4 and 3.5 deal with the rheostat uses in the HEL and the modeling of the DC bus. Section 3.6 depicts the global energetic architecture of the HEL with the merging of all presented models. Finally, section 3.7 presents the conclusions of the chapter.

## 3.1 The diesel driven generator set

### 3.1.1 The naturally aspirated diesel engine

A diesel engine (also known as a compression-ignition engine) is an ICE that uses the heat of compression to initiate ignition to burn the fuel, which is injected into the combustion chamber. In compression stroke, when both inlet and outlet valves are closed, the air is compressed. The compression provokes the rising of the air temperature and before the piston reaches Top Dead Centre <sup>1</sup> of the chamber, diesel oil is injected in it. When this atomized spray comes in contact with hot compressed air, the ignition takes place. Thus, in these engines, spark plugs for igniting the fuel are not provided. The fuel which is in atomized form gets ignited due to the high temperature of compressed air. The figure 3.1 presents the steps of the process.

1. **Induction Stroke:** The induction stroke in a Diesel engine is used to draw in a new volume of charge air into the cylinder.
2. **Compression Stroke:** The compression stroke begins as the inlet valve closes and the piston is driven upwards in the cylinder bore.
3. **Compression Ignition:** Compression ignition takes place when fuel directly injected into the cylinder with a high pressure fuel injector spontaneously ignites.
4. **Power Stroke:** The power stroke begins as the injected fuel spontaneously ignites with the air in the cylinder and the pressure generated by the combustion process forces the piston downwards in the cylinder.
5. **Exhaust Stroke:** During the exhaust stroke, the gases formed during combustion are ejected from the cylinder.
6. **Exhaust and inlet valve overlap:** Exhaust and inlet valve overlap is the transition between the exhaust and inlet strokes and is a practical necessity for the efficient running of any ICE. Given the constraints imposed by the operation of mechanical valves and the inertia of the air in the inlet manifold, it is necessary to begin opening the inlet valve before the piston reaches top dead centre on the exhaust stroke. Likewise, in order to effectively remove all of the combustion gases, the exhaust valve remains open until after top dead centre.

---

<sup>1</sup>In a reciprocating engine, the top dead centre is the position of a piston in which it is farthest from the crankshaft.

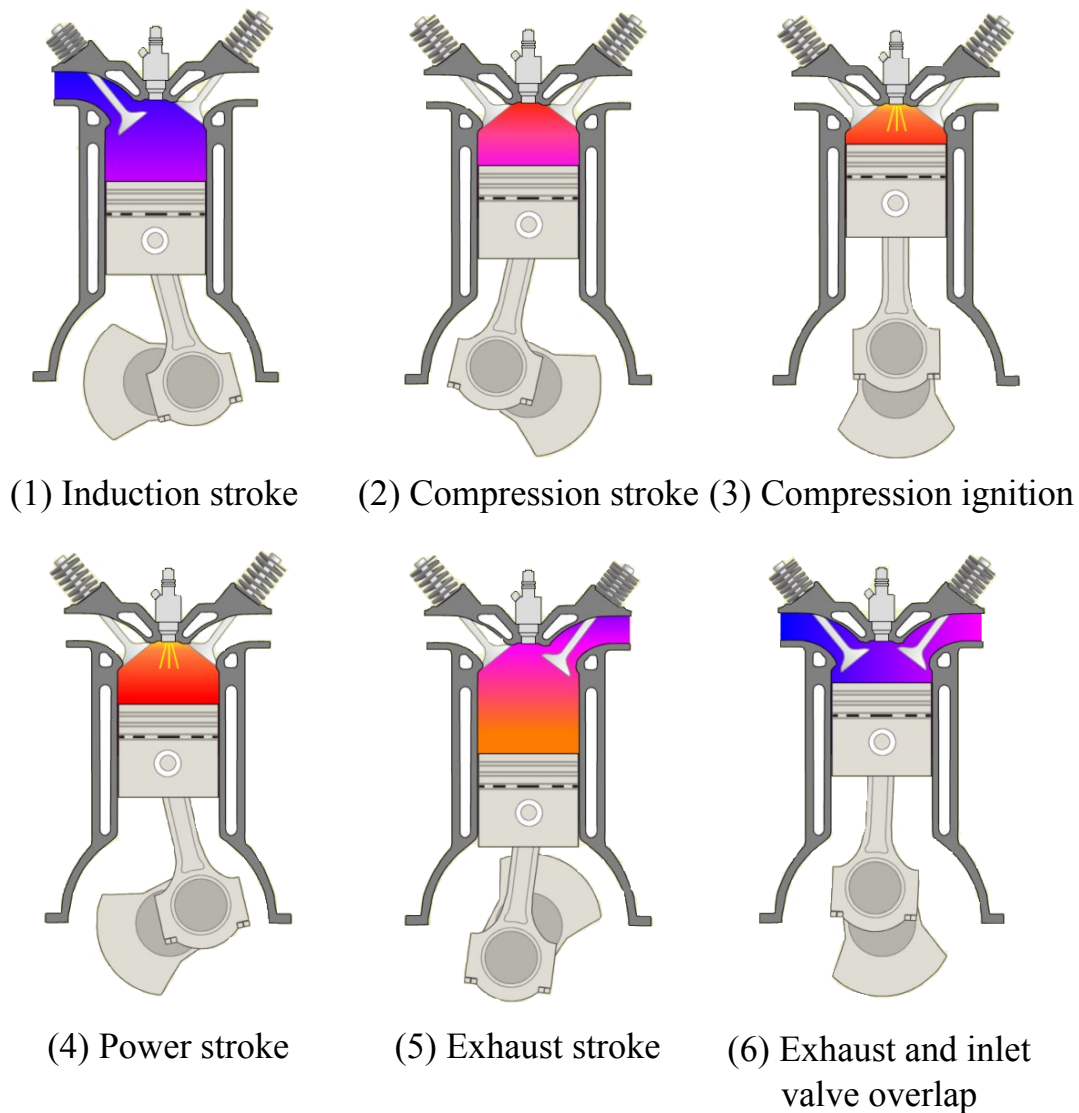


Figure 3.1: Four stroke compression ignition engine steps [Heyw88].

In accordance with EMR literature, most of the ICE models are static ones and do not provide information about the type of fuel injected in. For instance, [Sola09] discusses about the difficulty to develop an EMR of such a complete multi-physics system. The use of an engine map involves the assumption that the dynamic behaviour of the engine is similar to a succession of static points [Boul08]. [Lhom04] also proposes a static ICE model - figure 3.2. This EMR pictogram is no more used today and it should be replaced by a circle.

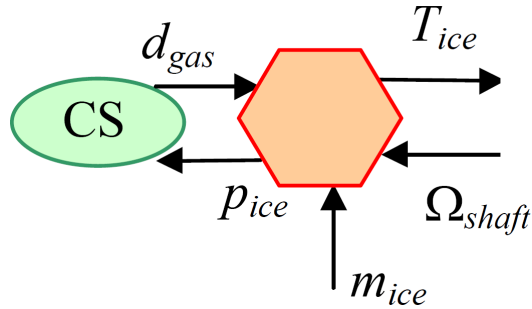


Figure 3.2: EMR model of an ICE proposed in [Lhom04]

In other words, to implement the mechanical behaviour of an ICE (mechanical torque depending on velocity of the shaft), cartographies are used. Thus, dynamics are neglected and this kind of model is generally associated with dynamic components such as electric filters. A new EMR of an ICE is here proposed. It aims at including fluidic, mechanical dynamics, introducing the fuel characterization and proposing a speed control of the engine. The naturally aspirated diesel engine (figure 3.3) proposed in [Verd10] is the considered structure for the study.

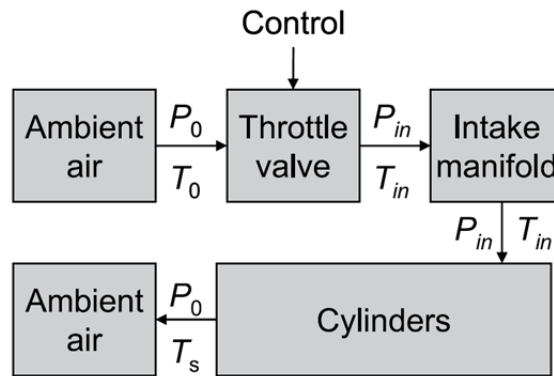


Figure 3.3: General structure of the naturally diesel aspirated engine [Verd10]

The models of the systems of a naturally diesel aspirated engine (figure 3.3) are now presented one by one. They deal with:

- the ambient air,
- the intake manifold,
- the fuel tank,

- the cylinders,
- the mechanical shaft.

### Ambient air (intake part)

Ambient air is considered as a hydraulic source and characterised by a volume flow rate ( $\dot{m}_{air}$ ) and a pressure ( $P_{im}$ ).

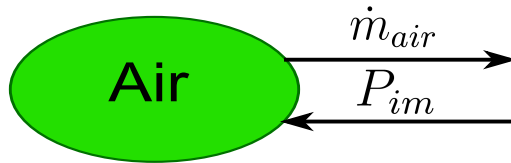


Figure 3.4: EMR of the ambient air

### Throttle valve

A throttle valve is a mechanism which manages the fluid flow by constriction or obstruction. The engine's power can be increased or decreased by the restriction of inlet gases using a throttle valve. In a fuel-injected engine, the throttle valve is placed at the entrance of the intake manifold. The throttle valve is not directly represented in the EMR. This element is indirectly taken into account into the MCS of the system when controlling the air and fuel flows.

### Intake manifold

The simulation models the intake manifold as a differential equation on the pressure. The difference in the incoming and outgoing mass flow rates represents the net rate of change of air mass with respect to time. This quantity, according to the ideal gas law, is proportional to the time derivative of the manifold pressure. Thus, it corresponds to an accumulation element using the EMR formalism. With this approach the differential equation for the pressure  $P_{im}$  in the volume  $V_{im}$  is:

$$\frac{dP_{im}}{dt} = \frac{RT_{im}}{V_{im}} (\dot{m}_{air} - \dot{m}_{cyl}) \quad (3.1)$$

where  $R$  is the ideal gas constant,  $\dot{m}_{air}$  and  $\dot{m}_{cyl}$  represent the in- and out- mass flows respectively. In this model, the temperature of the air flowing into the intake manifold  $T_{im}$  is assumed to be constant.

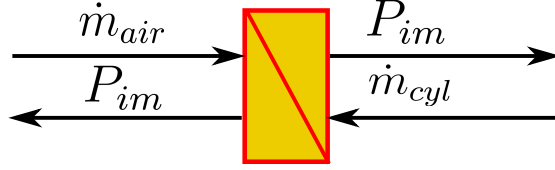


Figure 3.5: EMR of the intake manifold

As explained in [Erik07], even if this model gives good agreement with measured pressures, it would be possible to consider the intake manifold air temperature ( $T_{im}$ ) as a state variable thanks to the mass and the energy balances - equation 3.2.

$$\left\{ \begin{array}{l} m = \frac{P_{im} V_{im}}{RT_{im}} \\ \frac{dT_{im}}{dt} = \frac{1}{mc_v} \left[ \dot{m}_{air} c_v (T_{air} - T_{im}) + R(T_{air} \dot{m}_{air} - T_{im} \dot{m}_{cyl}) + \dot{Q} \right] \\ \frac{dP}{dt} = \frac{RT_{im}}{V_{im}} (\dot{m}_{air} - \dot{m}_{cyl}) + \frac{mR}{V} \frac{dT_{im}}{dt} \end{array} \right. \quad (3.2)$$

where  $c_v$  is the specific heat at constant volume,  $T_{air}$  is the ambient air temperature and  $\dot{Q}$  is the heat transfer between the intake manifold inlet-outlet. The temperature of the out-flow from this component is the same as the temperature in the control volume ( $T_{im} = T_{cyl}$ ). However, the EMR use in such a case remains difficult. Indeed, state variables are interdependent and inseparable. As described in [Chre08], a gas flow presents at the same time a thermal energy and a pneumatic energy. A separation between the thermal and pneumatic domains can not be done. Indeed a change in the gas composition due to a chemical reaction changes the internal energy. This internal energy evolution also has an impact on the temperature variation. If the choice of the variables does not comply to the general EMR approach using two variables, its application on EMR might be called pseudo-EMR and it would bring more than two variables. This topic is part of another study fully dedicated to the modelling of such a system.

### Fuel tank

The fuel is considered as a hydraulic source too - figure 3.6. In order to characterise the nature of the fuel which is injected in cylinders, its heating value<sup>2</sup> and more specifically its exergy rate in J/kg is coupled with a mass

<sup>2</sup>The heating value or energy value of a substance, usually a fuel, is the amount of heat released during the combustion of a specified amount of it. The energy value is

flow rate ( $\dot{m}_{fuel}$ ).

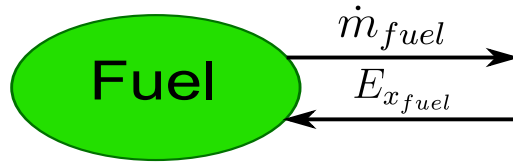


Figure 3.6: EMR of the fuel

### Cylinders

Cylinders mix the intake manifold air ( $P_{im}$  and  $\dot{m}_{cyl}$  variables) and the fuel ( $\dot{m}_{fuel}$  and  $E_{x_{fuel}}$  variables) provided by the fuel tank. The reaction of combustion produces exhaust gases ( $\dot{m}_{exh}$  and  $P_{air}$  variables) and a mechanical power ( $\Gamma_{cyl}$  and  $\Omega_{shaft}$  variables). As a hydraulic power is converted into a mechanical power, the cylinders are represented by a multi-physics conversion element - figure 3.7.

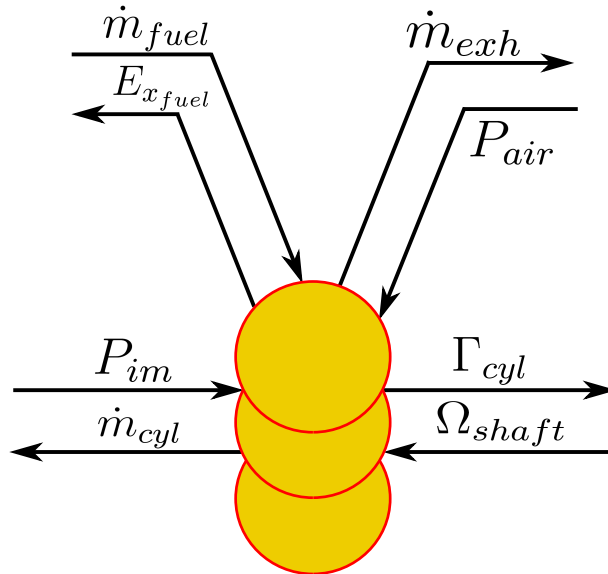


Figure 3.7: EMR of the cylinders

Equations 3.3 and 3.4 give respectively the mathematical expressions of the mechanical torque and the intake volume flow rate.

---

a characteristic for each substance. It is measured in units of energy per unit of the substance.

$$\Gamma_{cyl} = \frac{1}{\Omega_{shaft}} \left( \eta_{ind} \dot{m}_{fuel} E_{x_{fuel}} - \frac{\Omega_{shaft}}{4\pi} V_{ed} (P_{air} - P_{im}) \right) \quad (3.3)$$

$$\dot{m}_{cyl} = \frac{P_{im}}{RT_{im}} \eta_v \frac{\Omega_{shaft}}{4\pi} V_{ed} \quad (3.4)$$

with:

- $V_{ed}$  the engine displacement,
- $\eta_{ind}$  the global (fuel-torque) efficiency,
- $\eta_v$  the volumetric efficiency.

The volume flow rate of exhaust gases ( $\dot{m}_{exh}$ ) is considered as the sum of the intake volume flow rate ( $\dot{m}_{cyl}$ ) with the fuel volume flow rate (initial fuel mass flow rate  $\dot{m}_{fuel}$  converted in volume flow rate using the density of the considered fuel).

### Ambient air (exhaust part)

Ambient air is also considered as a hydraulic source and is represented on figure 3.8.

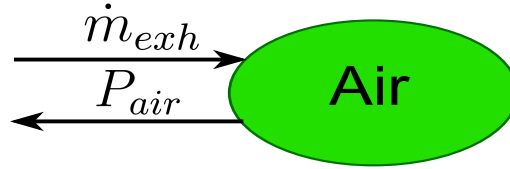


Figure 3.8: EMR of the exhaust part

### Mechanical Shaft

To finish, a mechanical shaft is required for transmitting the mechanical power to the synchronous salient pole machine on our application. Its EMR modelling is represented by an accumulation element (figure 3.9 and equation 3.5).

$$J \frac{d\Omega_{shaft}}{dt} = \Gamma_{cyl} - \Gamma_{load} - f_{shaft} \Omega_{shaft} \quad (3.5)$$

with:

- $J$  the inertia of the shaft,
- $f_{shaft}$  the friction forces.

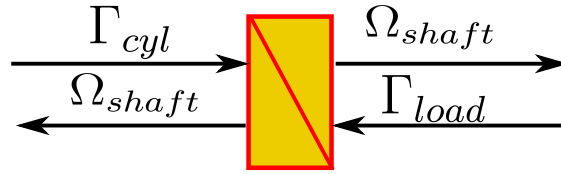


Figure 3.9: EMR of the mechanical shaft

### Energetic Macroscopic Representation of the naturally aspirated diesel engine

The figure 3.10 regroups all the EMR elements of the naturally aspirated diesel engine which were presented previously (the ambient air, the intake manifold, the fuel tank, the cylinders and the mechanical shaft).

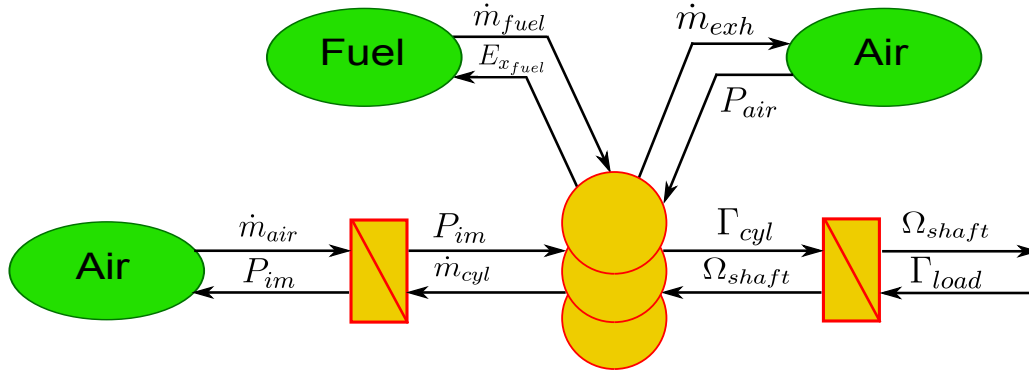


Figure 3.10: EMR of the ICE

Now, the MCS and PCS of the ICE must be developed to perform the control of the system.

### Maximum Control Structure of the naturally aspirated diesel engine

The MCS of the naturally aspirated diesel engine aims at controlling the rotational speed of the mechanical shaft. Thus, the use of a first controller permits to control the torque produced by the cylinders giving a reference of the shaft speed. The difficulty of this tuning chain lies in the mathematical inversion of the cylinders' equations. This kind of block combines at least two inputs in a single output. In terms of control, a single reference has to induce two output references. In such a case, a repartition factor  $k_{rep}$  shares out the input reference ( $\Gamma_{cyl_{ref}}$ ) between the two output references ( $P_{im_{ref}}$  and  $\dot{m}_{fuel_{ref}}$ ).



### 3.1.2 The salient pole synchronous machine

The equations of the salient pole synchronous machine are fully detailed in the appendix B. This part presents the EMR, the MCS and the PCS of this machine.

#### Energetic Macroscopic Representation of the machine

The salient pole synchronous machine EMR is made up of two parts. The main branch is composed of a circle (electromechanical conversion of the machine) and of an accumulation element (windings of the machine - equation B.18). The second branch in parallel, which also includes an accumulation element, models the separated excitation of the machine. Figure 3.12 gives the EMR of this part.

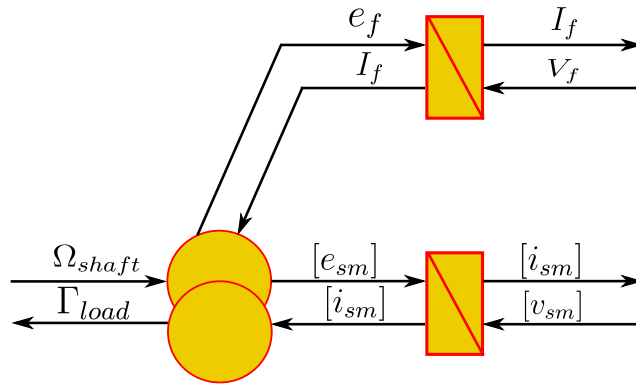


Figure 3.12: EMR of the salient pole synchronous machine

*Remark: Variables in brackets represent a vector.*

To complete the EMR of the synchronous machine, an inverter and a chopper are added to the model of the figure 3.12. The chopper of the separated excitation chain permits to link the machine to an external DC source. Working only on scalar variables, its transformation ratio is a scalar too ( $\beta_{ref}$ ). However, the principal chain inverter admits a vector transformation ratio ( $[\alpha_{ref}]$ ) and realises the link between the system and the DC bus. Figure 3.13 represents the EMR of the complete system.

#### Maximum and Practical Control Structures of the machine

The implemented MCS aims at controlling the torque ( $T_{load}$ ) using the two available degrees of freedom ( $\beta_{ref}$  and  $[\alpha_{ref}]$ ). Thus, MCS presents a repartition element to share currents' references. The problem of this block is

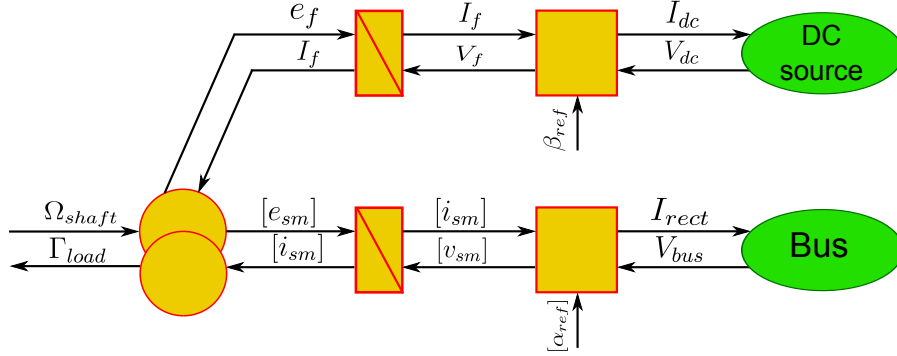


Figure 3.13: EMR of the alternator

to obtain three references (currents) from one reference (torque). In reality, the torque is not the only reference to be controlled. The magnetic flux ( $\phi_d$  and  $\phi_q$ ) are also imposed and coupled with the torque to deduce the three currents' references. The principle is to consider the defluxing characteristic of the machine and to work on its maximum flux ( $\phi_{ref}$ , equation 3.9).

$$I_{ref} = \frac{T_{load_{ref}}}{p\phi_{ref}} \quad (3.9)$$

The real flux ( $\phi$ , equation 3.10) is a combination of the magnetic flux along dq axis (equations B.7, B.8):

$$\phi = \sqrt{\phi_d^2 + \phi_q^2} \quad (3.10)$$

$\delta$ , the load angle, is also calculated:

$$\begin{cases} \cos \delta = \frac{\phi_d}{\phi} \\ \sin \delta = \frac{\phi_q}{\phi} \end{cases} \quad (3.11)$$

Windings' currents along d and q axis and inductor's current references are deduced thanks to equations 3.12 to 3.14.

$$I_{d_{ref}} = -I_{ref} \sin \delta \quad (3.12)$$

$$I_{q_{ref}} = I_{ref} \cos \delta \quad (3.13)$$

$$I_{f_{ref}} = \frac{\sqrt{\phi_{ref}^2 - (L_q I_{q_{ref}})^2} - L_q I_{d_{ref}}}{M} \quad (3.14)$$

Then, three controllers permit controlling the three voltages ( $V_d$ ,  $V_q$  and  $V_f$ ) from the currents ( $I_d$ ,  $I_q$  and  $I_f$ ). Finally, the inversion of inverters results in the control of transformation ratios.

The estimation of the mechanical torque and of the electromotive forces is performed (figure 3.14 and equations 3.15, 3.16). Indeed, electromotive forces are not directly measurable and a torque sensor is expensive.

$$\begin{cases} e_{dest} = -\omega_{r_{meas}} L_q I_{q_{meas}} + M \frac{dI_{f_{meas}}}{dt} \\ e_{q_{est}} = \omega_{r_{meas}} (L_d I_{d_{meas}} + M I_{f_{meas}}) \end{cases} \quad (3.15)$$

$$\Gamma_{load_{est}} = p((L_d I_{d_{meas}} + M I_{f_{meas}}) I_{q_{meas}} - L_q I_{q_{meas}} I_{d_{meas}}) \quad (3.16)$$

Equations deal with the measurement of currents and voltages expressed in the dq frame. They are expressed in such a way for simplification reasons. In the estimation block, the Park transform is used to work with outputs expressed in the three phase frame.

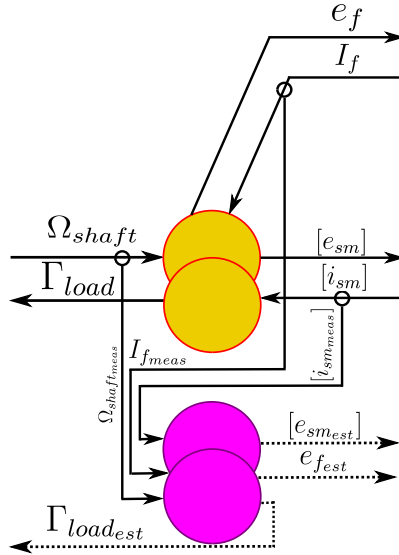


Figure 3.14: Estimation of the load torque and the electromotive forces

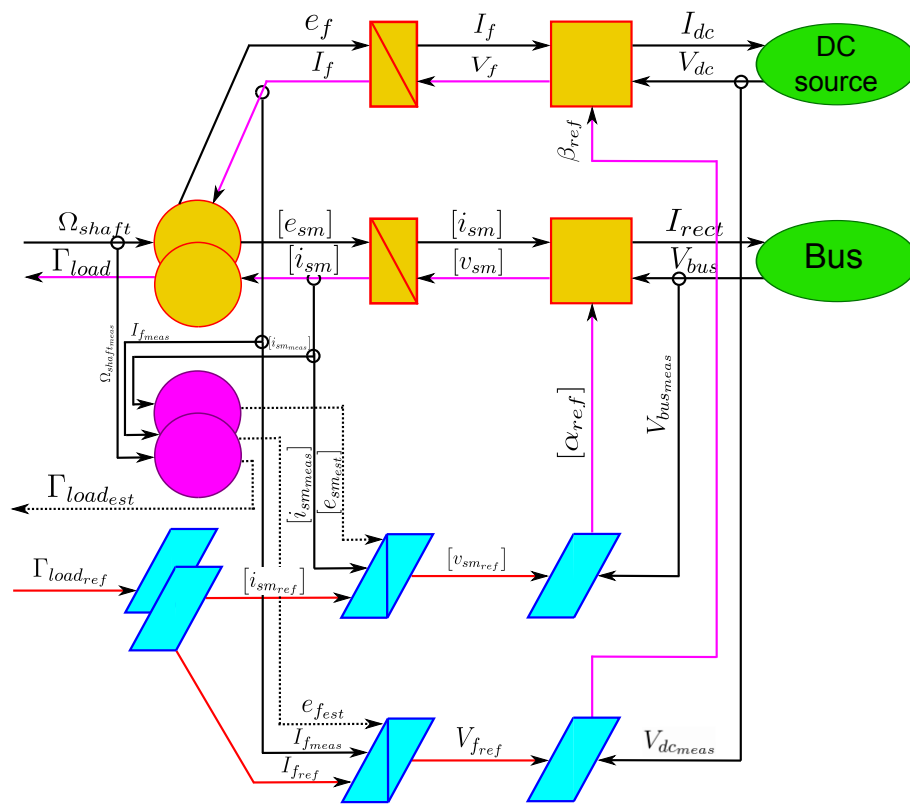


Figure 3.15: EMR and MCS of the alternator

### 3.1.3 The diesel driven generator set

#### Merging of the naturally aspirated diesel engine and the salient pole synchronous machine models

The diesel driven generator set EMR is made up of the two previous presented models developed on figures 3.11 and 3.15. The control of the mechanical power at the output of the crank shaft permits to control the electrical power at the output of the machine, depending on its losses.

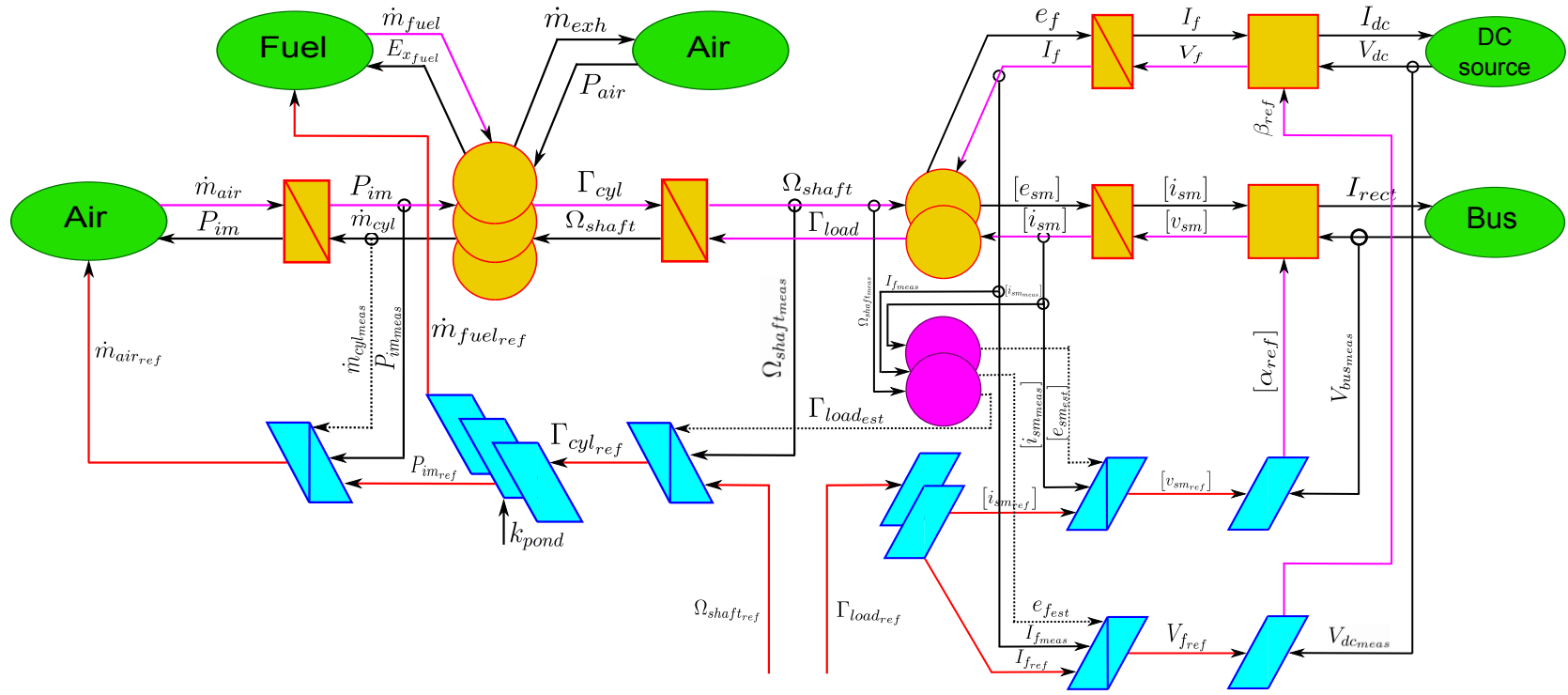


Figure 3.16: Modelling of the diesel driven generator set [Baer12a]

## Simulation results

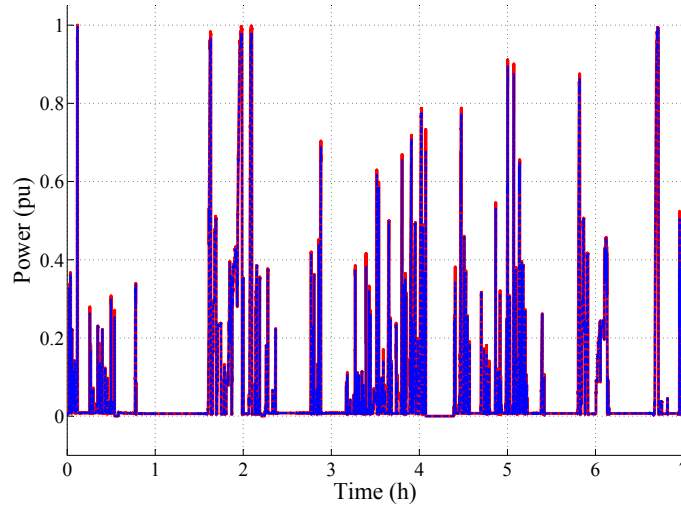


Figure 3.17: Evolution of the power mission reference (red full line) and the electric power (blue dotted line) versus time

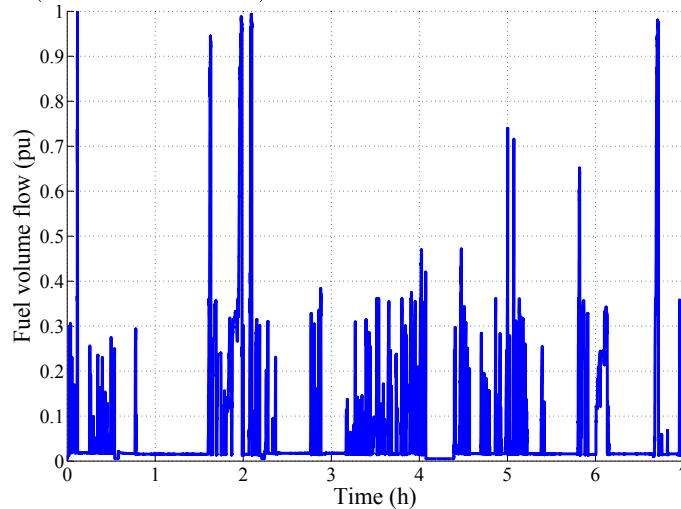


Figure 3.18: Evolution of the fuel volume flow versus time

Presented results on figures 3.17, 3.18, 3.19 and 3.20 were obtained using the most restricting mission as an input. Figure 3.17 underlines that the mechanical power reference is well converted into electrical power thanks to the salient pole synchronous machine according to its efficiency. Moreover, figures 3.18, 3.19 and 3.20 give an approximation of:

- the volume flow of the fuel at the intake,

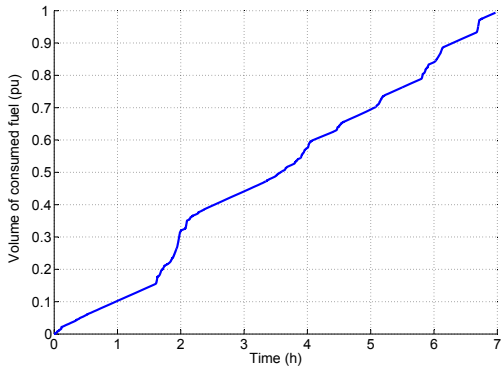


Figure 3.19: Evolution of the fuel consumption versus time

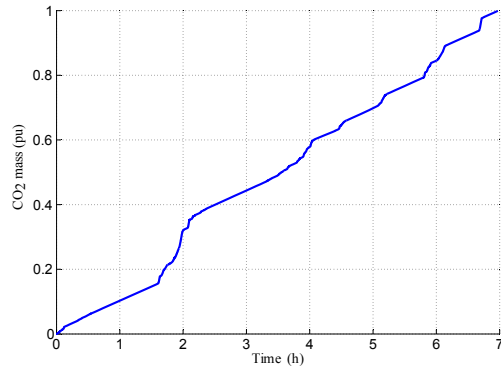


Figure 3.20: Evolution of the  $CO_2$  mass product versus time

- the corresponding volume of fuel used,
- the mass <sup>3</sup> of exhaust carbon dioxide gas during the mission.

The simulation results have also confirmed the good control of the intake manifold air pressure around the atmospheric pressure (1 bar). Finally, to check the good efficiency of the ICE control, mechanical torque and rotational speed references are applied to the shaft. On figures 3.21 and 3.22, references and the model responses are represented. Further data about the ICE are necessary to better model its mechanical dynamics.

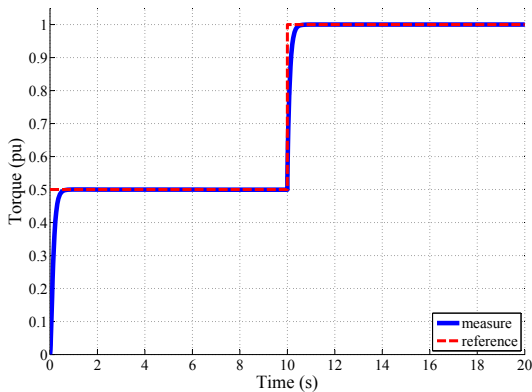


Figure 3.21: Control of the mechanical torque of the shaft

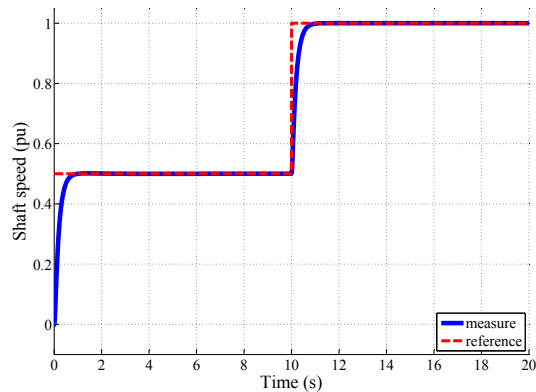


Figure 3.22: Control of the rotational speed of the shaft

<sup>3</sup>One litre of fuel produces around 2.662 kg of  $CO_2$

## 3.2 The Ultra-Capacitors

An electric double-layer capacitor or ultra capacitor is an electrochemical capacitor with relatively high energy density. The energy density is typically hundreds of times higher than conventional electrolytic capacitors. An ultra capacitor has much higher power density than batteries. The modelling of the UCs is now tackled. At first, an improved and easy-to-use ultra-capacitor single cell dynamic model is presented. The idea is then to develop a generic dynamic model based on a single cell. Then, the EMR and the MCS of a bank of UCs with its relating power electronics are depicted.

### 3.2.1 Physical model of a cell

The adopted ultra-capacitor's cell model is based on [Zubi00]. The use of a simple resistive capacitive equivalent circuit is insufficient to characterize the terminal behaviour of a double-layer capacitor for power applications. Indeed, it does not take into account the non-linear rise and fall of the voltage and the change in voltage after the charging and discharging stops. These phenomena are due to the internal charge redistribution between different equivalent internal capacitors. Thus, an equivalent circuit is used (figure 3.23 - equation 3.17).

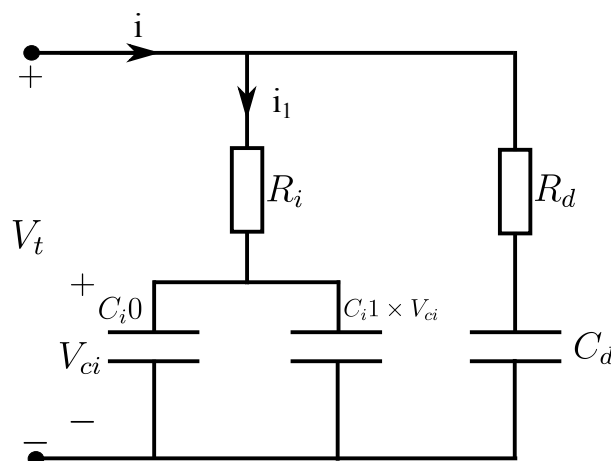


Figure 3.23: Equivalent circuit model for an ultra-capacitor's cell.

Each of the two branches has a distinct time constant. The first branch, with the elements  $(R_i, C_{i0})$  and the voltage-dependent capacitor  $C_{i1}$  (in F/V), dominates the behaviour of the element in the time range of seconds. The second or delayed branch, with parameters  $R_d$  and  $C_d$  dominates the

terminal behaviour in the range of minutes. To reflect the voltage dependence of the capacitance, the first branch is modelled as a voltage-dependent differential capacitor. The differential capacitor consists of a fixed capacitance  $C_{i0}$  and a voltage-dependent capacitor. A leakage resistor, parallel to the terminals, is added to represent the self discharge property. The third branch is the long term one which determines the behaviour for times longer than 10 minutes. This branch is neglected because its equivalent parameters were not determined by the experimental characterization and its resistance value is usually seven times higher than the resistance values of the first two branches. Thus, the corresponding current is negligible when compared to the two other branches' currents.

$$\begin{cases} i_1(s) = i(s) - \frac{V_t(s)}{R_d + \frac{1}{C_d s}} \\ V_t(s) = R_i i_1(s) + \frac{i_1(s)}{(C_{i0} + C_{i1} V_{ci}(s)) s} \end{cases} \quad (3.17)$$

### 3.2.2 Energetic Macroscopic Representation

The EMR of the UCs' bank takes into account the previous presented model of an UC's single cell and the power electronics. The power electronics are made up of a smoothing reactor and a DC chopper. The smoothing reactor is composed of a RL circuit and performs a smoothing of the direct current wave shape to reduce losses and improve the system performances (3.18). The EMR corresponds to an element of accumulation (figure 3.24).

$$V_{uc}(t) - V_{h-uc}(t) = R_{uc} I_{h-uc}(t) + L_{uc} \frac{dI_{h-uc}(t)}{dt} \quad (3.18)$$

$R_{uc}$  and  $L_{uc}$  are respectively the resistance and the inductance of the smoothing reactor.

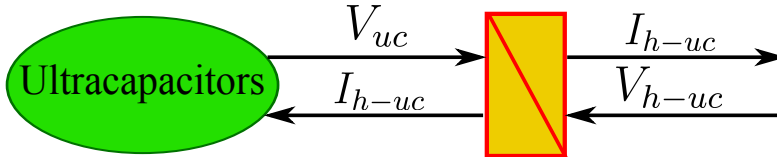


Figure 3.24: EMR of the smoothing reactor.

The DC chopper controls the power flow between the bank and the central DC bus of the system (figure 3.25 and equation 3.19).

$$\begin{cases} I_{uc} = \alpha_{uc} I_{h-uc} \\ V_{h-uc} = \alpha_{uc} V_{bus} \end{cases} \quad (3.19)$$

with  $\alpha_{uc}$ , the duty cycle of the chopper and  $V_{bus}$ , the bus voltage.

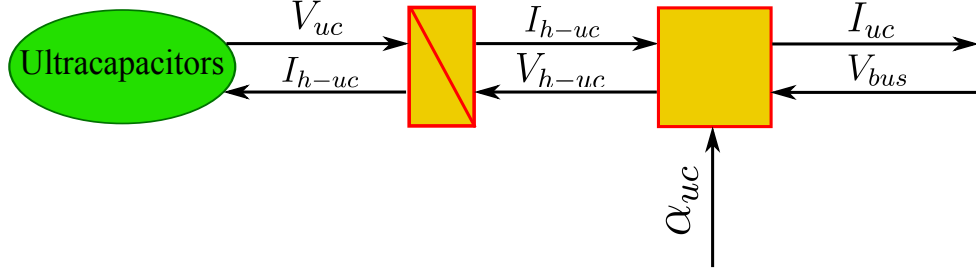


Figure 3.25: EMR of the DC chopper.

### 3.2.3 Maximum and Practical Control Structures

#### Maximum Control Structure

To determine the MCS, the setting chain is inverted to obtain the control chain. The MCS is made up of two mono-physical inverters and a controller. The idea is to control the current applied to the bank of UCs ( $I_{uc\_ref}$ ). This current is a bus current intended for UCs' bank. Thus, the first control block aims at converting this bus current into a bank current reference ( $I_{h-uc\_ref}$ ).

In other words, this block realises the adequacy of the power from the DC bus to the bank (equation 3.20).

$$I_{h-uc\_ref} = I_{uc\_ref} \frac{V_{bus\_meas}}{V_{h-uc\_meas}} \quad (3.20)$$

A controller is used to control the current  $I_{h-uc}$ . The PI and IP controllers' synthesis are detailed in appendix C.

The second mono-physical inverter block controls the duty cycle of the DC chopper.

$$\alpha_{uc\_ref} = \frac{V_{h-uc\_ref}}{V_{bus\_meas}} \quad (3.21)$$

The figure 3.26 presents the considered MCS.

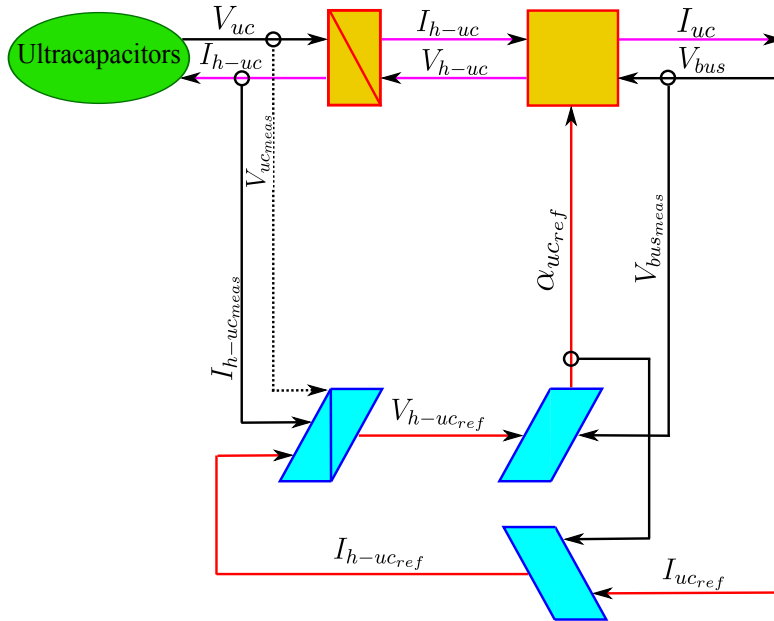


Figure 3.26: MCS of the ultra-capacitors' pack [Alle10]

### Practical Control Structure

Contrary to the UCs' voltage, the SOC is not physically measurable. The SOC is estimated (equation 3.22) thanks to the measure of the voltage of the bank of UCs ( $V_{uc_{meas}}$ ) and the nominal voltage ( $V_0$ ).

$$SOC_{uc_{est}} = \frac{V_{uc_{meas}}}{V_0} \quad (3.22)$$

An estimation block is used to calculate the SOC (figure 3.27).

### 3.2.4 Simulation results

Figure 3.28 presents the evolution of the voltage of an UC (top blue curve) according to a typical current profile (bottom red curve). A negative (respectively positive) current is a charging (respectively discharging) one.

## 3.3 The batteries

An electrochemical cell is a device which is able to either deriving electrical energy from chemical reactions, or facilitating chemical reactions through the introduction of electrical energy. The Nickel Cadmium (NiCd) battery

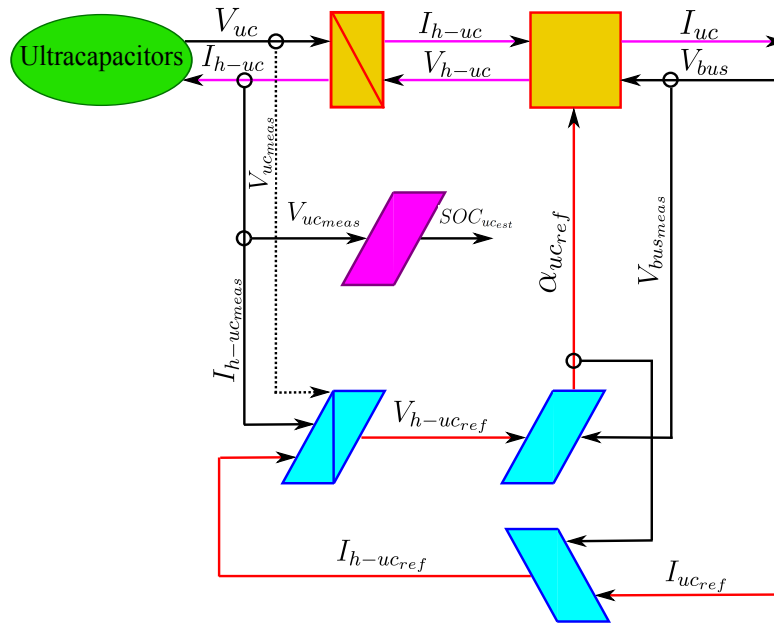


Figure 3.27: PCS of a pack of ultra-capacitors

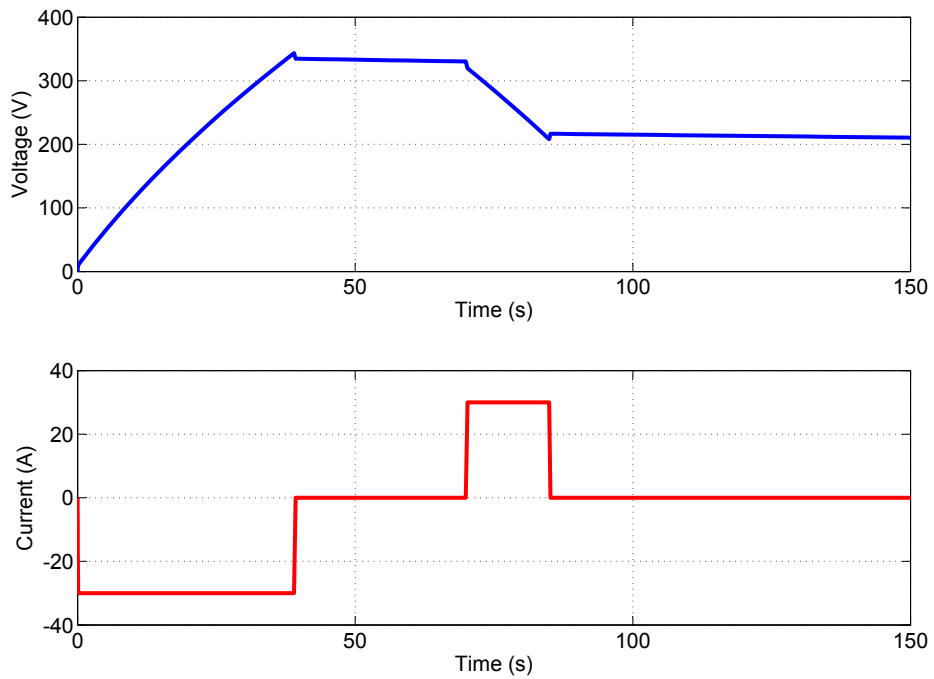


Figure 3.28: Characteristic of the ultra-capacitors

is a type of rechargeable battery using nickel oxide hydroxide and metallic

cadmium as electrodes. The development of a batteries' bank model is at first based on the implementation of the model of a single cell. This model is based on [Trem07, Trem09] which is an improved and easy-to-use battery cell dynamic model. The power electronics configuration is the same as the UCs' one (smoothing circuit and DC chopper).

### 3.3.1 Physical model of a cell

#### The discharge model

The proposed discharge model is similar to the Shepherd model [Shep65]. It accurately represents the voltage dynamics when the current varies and takes into account the Open Circuit Voltage (OCV)<sup>4</sup> as a function of SOC. A term dealing with the polarisation voltage is added to better represent the OCV behaviour. The obtained discharge model is given by equation 3.23.

$$V_{batt} = E_0 - Ri - K_1 \frac{Q}{Q - it} i^* - K_2 \frac{Q}{Q - it} it + f(t) \quad (3.23)$$

where:

- $V_{batt}$  is the battery voltage (V),
- $E_0$  is the battery constant voltage (V),
- $K_1$  is the polarisation resistance (V/A),
- $K_2$  is the polarisation constant (V/Ah),
- $Q$  is the battery capacity (Ah),
- $it = \int idt$  is the actual battery charge (Ah),
- $R$  is the internal resistance ( $\Omega$ ),
- $i$  is the battery current (A),
- $i^* = \frac{1}{T_{r_{batt}} \cdot s + 1} i$  is the filtered current flowing through the polarisation resistance (A).
- $T_{r_{batt}}$  is the battery response time (s).

---

<sup>4</sup>OCV is the difference of electrical potential between the two terminals of a battery when there is no external load connected.

The  $K_1 \frac{Q}{Q-it}$  term represents the polarisation resistance and  $K_2 \frac{Q}{Q-it} it$ , the polarisation voltage. The polarisation voltage term models the non linear variations of the OCV with the SOC. The NiCd batteries hysteresis phenomenon only occurs in the exponential area. This phenomenon is modelled using the exponential term  $f(t)$  (equation 3.24). The term depends on A, the exponential zone amplitude (V) and B, the exponential zone time constant inverse ( $Ah^{-1}$ ). A and B are determined using the discharge characteristic of the battery.

$$f(t) = Ae^{-Bit} \quad (3.24)$$

### The charge model

The charge model is represented for a NiCd battery using equation 3.25. Theoretically, when  $it = 0$  (fully charged), the polarisation resistance is infinite. This is not exactly the case in practice. Indeed, experimental results show that the contribution of the polarisation resistance is shifted by about 10% of the capacity of the battery ( $0.1Q$ ).

$$V_{batt} = E_0 - Ri - K_1 \frac{Q}{|it| - 0.1Q} i^* - K_2 \frac{Q}{it - 0.1Q} it + f(t) \quad (3.25)$$

### 3.3.2 Energetic Macroscopic Representation

The architecture, equations and the EMR of the bank of batteries with its relating power electronics are the same as the bank of UCs (figure 3.29).

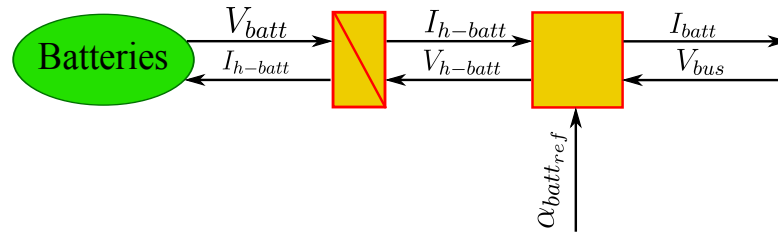


Figure 3.29: EMR of the pack of batteries and its relating power electronics.

### 3.3.3 Maximum and Practical Control Structure

#### Maximum Control Structure

The MCS of the bank of batteries is also the same as the MCS of the bank of UCs (figure 3.29).



such as current, voltage, internal resistance or impedance. These methods are non-invasive because they are based on mathematical models describing the relationship between the quoted measurable quantities and the SOC. However, their efficiency greatly depends on the mathematical models and the quality of the electric parameters measurements.

The selected method belongs to the electric methods category and is based on the mathematical integration of the current applied to the battery as explained in [Pei06] and [Pill01]. Thus, the problem of the determination of the actual battery SOC is based on the Coulomb counter which is extremely dependent of the initial SOC ( $SOC_0$ ) value. If the initial SOC is known, the evolution of the SOC according to time can be estimated (equation 3.26).

$$SOC(t) = SOC_0 - \frac{\int I_{h-batt}(t)dt}{Q} \quad (3.26)$$

To determine the initial SOC, a real time characterization of the impedance of the battery can be performed [Bech12a]. A non-linear formula for the determination of the initial SOC based on the measurement of the instantaneous battery impedance is proposed [Bech12b]. The other solution remains in fully recharging the battery before using it [Xion13].

Estimation based on no-load voltage [Chia03] is also available. Kalman filters are widely used for SOC estimation [Urba07] but they require a Gaussian distribution of the noise in the studied system. Other SOC estimation techniques include the fuzzy logic [Zena10] and the neural network [Affa03] based methods which necessitate a training phase of the system [Gao11]. Figure 3.31 presents the PCS of the bank of batteries.

### 3.3.4 Experimental characterization

#### NiCd cells characteristics

The tested batteries' cells are NiCd ones. Even if a European directive forbids the use of this kind of technology for portable applications (apart from emergency, alarm systems and medical equipments), the NiCd batteries intended for industrial and professional uses are not concerned by this directive. The NiCd technology is able to stand extreme temperatures that is why Alstom Transport proposes it like a solution for the applications intended to the continental climate countries. Indeed, the temperatures can vary between  $-50^{\circ}C$  and  $+50^{\circ}C$ . The known parameters and characteristics of the considered cell are summarized in the table 3.1.

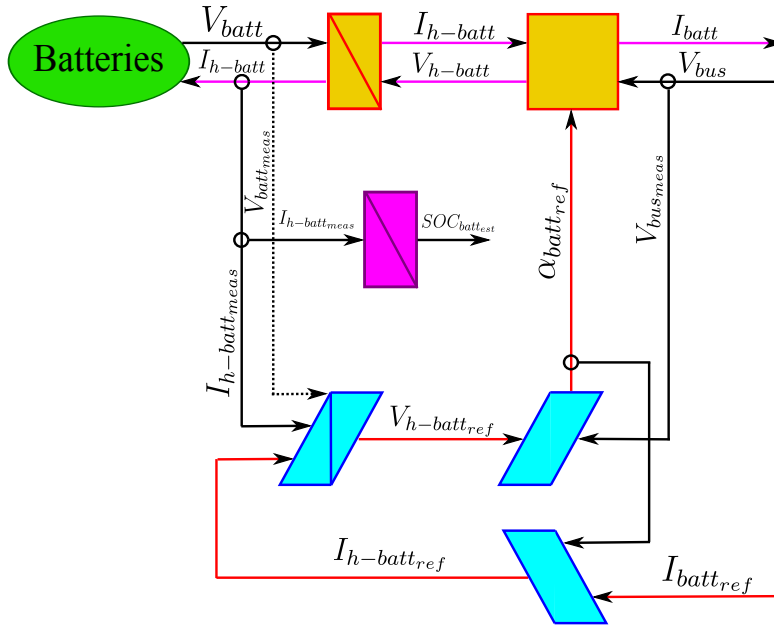


Figure 3.31: PCS of a pack of batteries and its power electronics.

<b>Hoppecke FNC-A 170 XR2 – NiCd Accumulator</b>	
Nominal voltage (V)	1.2
Nominal current (A)	34
Capacity (Ah)	170
Electrolyte	Potassium hydroxide (KOH)

Table 3.1: NiCd cell characteristics

### The experimental test bench - [Devi12]

The developed test bench (figure 3.32) is made up of a power source to charge the accumulator, an electronic load to discharge it (power source and electronic load characteristics are presented in appendix E), a thermal chamber to control the operating temperature and a Human Interface Machine (HIM) to record voltages, currents, temperature measures and define references (figure 3.33). Contactors are used to electrically isolate the power source circuit of the bench from the electronic load one.

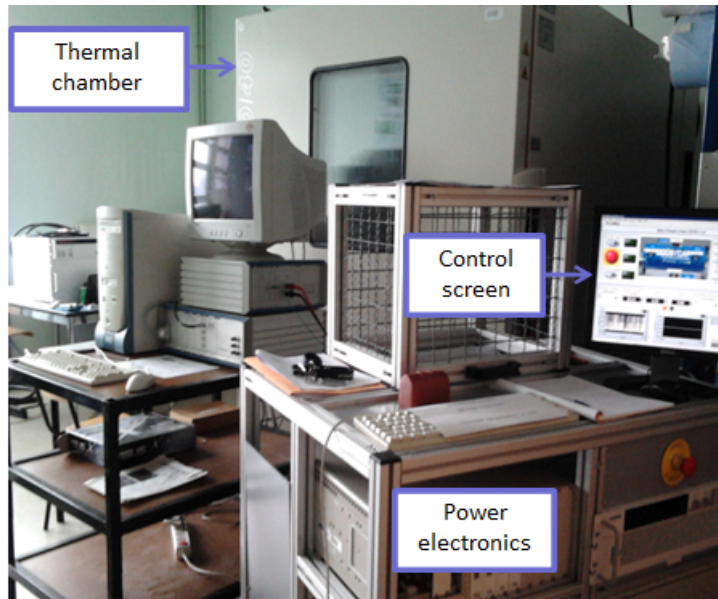


Figure 3.32: Batteries' test bench

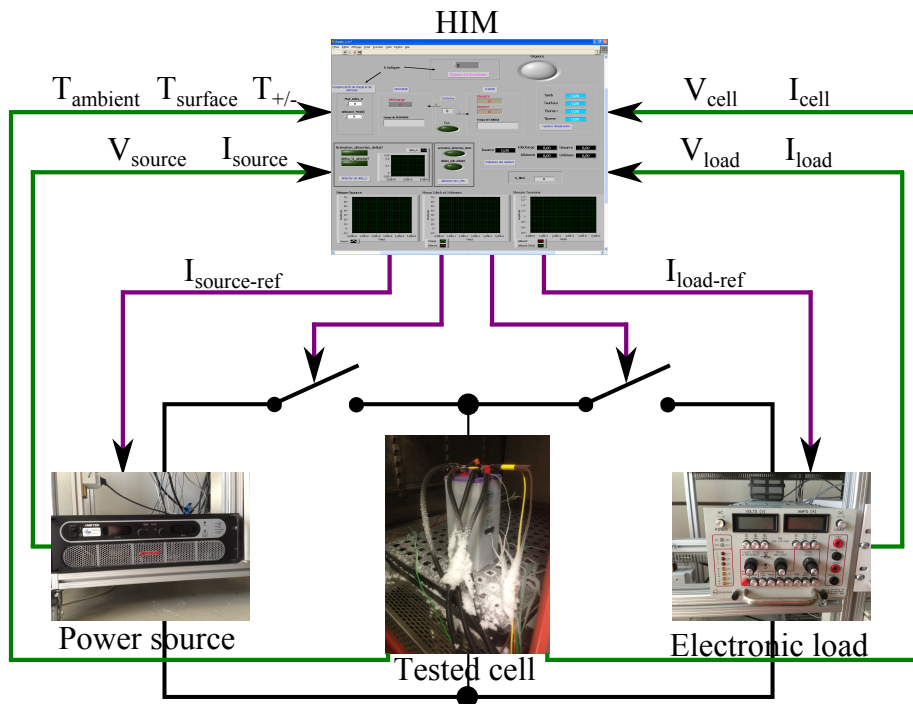


Figure 3.33: Batteries' test bench structure

### Charging/discharging protocol at ambient temperature and capacity test

The accumulator is charged with a constant current. To measure the capacity at ambient temperature, the maximum limit charge voltage must be respected and three cycles are necessary to obtain a reliable indication of the nominal capacity. The nominal capacity is determined during the discharging phase. Firstly, the accumulator is charged till its maximum voltage value applying a current equals to  $C_5$ . The table 3.2 gives the necessary time to fully charge an element according to the applied charging current.

Current (A)	Time (h)
$0.1 \times C = C/10 = C_{10} = 17$	10
$0.2 \times C = C/5 = C_5 = 34$	5
$0.5 \times C = C/2 = C_2 = 85$	2
$1.0 \times C = C/1 = C_1 = 170$	1
$2.0 \times C = C/0.5 = C_{0.5} = 340$	0.5
$3.0 \times C = C/0.33 = C_{0.33} = 510$	0.33
$4.0 \times C = C/0.25 = C_{0.25} = 680$	0.25
$5.0 \times C = C/0.2 = C_{0.2} = 850$	0.2

Table 3.2: Theoretical time to fully charge one element depending on applied currents

Once the maximum voltage value is reached, the voltage is controlled around the maximum value and the current is decreased until 0A. Then, a discharging current also equals to  $C_5$  is applied to the accumulator (figure 3.34) until obtaining the minimum voltage value. Experiments prove that the element is fully discharged after four hours and a half with a 34A solicitation. Compared to the manufacturer theoretical capacity of 170 Ah, it experimentally corresponds to a 153 Ah one.

### Internal resistance determination

The internal resistance of the cell is determined for a range of operating temperatures and SOCs of the element. Indeed, the proposed Matlab/Simulink dynamical model of a NiCd cell does not take into account the internal resistance behaviour of the source with the temperature variations and the SOCs. At first, the protocol consists in maintaining the stability of the cell's temperature. The cell is tested between  $[-50^\circ C; +40^\circ C]$  with a step of  $20^\circ C$ . The evaluation of the internal resistance value is performed every 10% of the SOC at constant temperature with the equation 3.27.

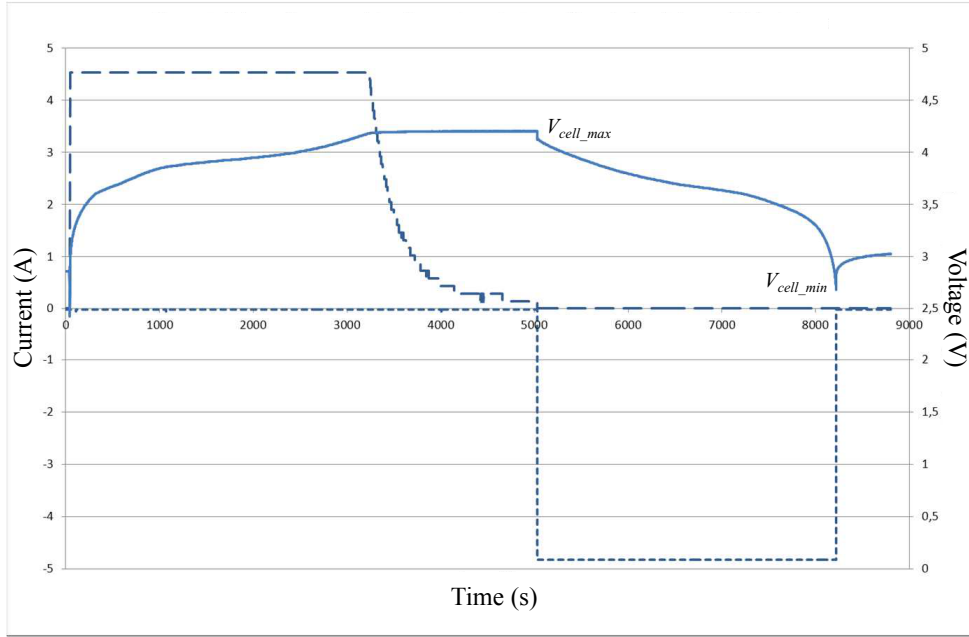


Figure 3.34: Batteries' capacity test protocol [Devi12]

$$R_{cell} = \frac{\Delta V}{\Delta i} = \frac{V_{cell-max} - V_{cell-min}}{\Delta i} \quad (3.27)$$

$\Delta i$  is the applied discharging current and  $\Delta V$  is the drop voltage of the element.

The figure 3.35 represents the evolution of the value of a single cell internal resistance according to its SOC and the working temperature at  $C_5$ . The internal resistance clearly increases for the lowest temperatures and the lowest SOC. The non linearities of the last experimental points (about  $25 \text{ m}\Omega$  at 50% SOC and  $-50^\circ\text{C}$  or  $22 \text{ m}\Omega$  at 10% SOC and  $+40^\circ\text{C}$ ) are due to the important drop voltage of the NiCd cell when fully discharging it. Indeed, the previous points are calculated for small voltage variations and drops (between 0.25h and 2.25h instants for instance - figure 3.36). However, around 2.5h, the voltage of the cell is dropping importantly (from 1V to 0.45V). Thus, the numerator value of the equation 3.27 is higher than before, its denominator remains constant ( $C_5$ ) and the internal resistance value is also higher.

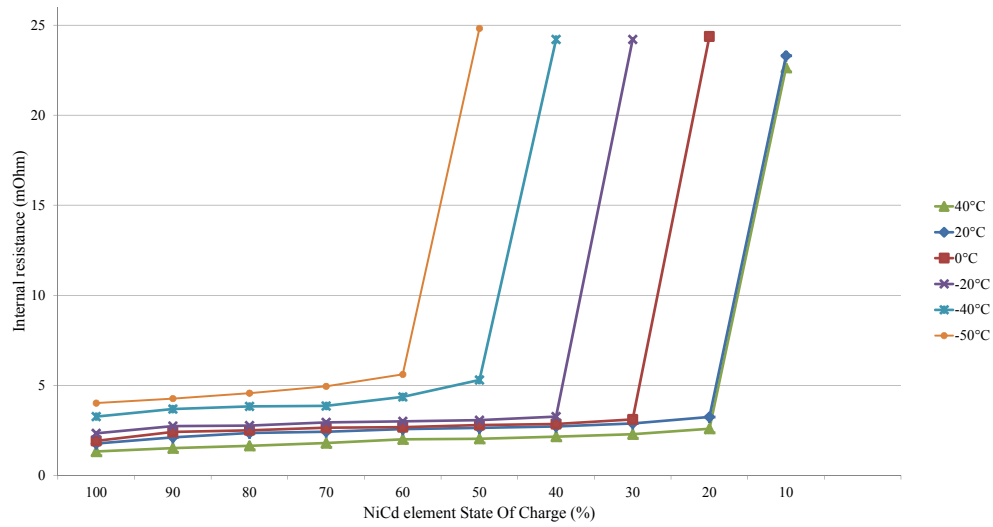


Figure 3.35: Evolution of the internal resistance value of the cell according to its State Of Charge and the temperature ( $C_5$ )

### Model validation

The following figures (3.36 to 3.41) aims at validating the implemented and improved Matlab/Simulink model of a NiCd cell. Instead of using a single resistance value, the improved model proposes a dependency of the internal resistance of the cell according to its working temperature and its SOC. The curves represent the numerical model behaviour and the recorded experimental data. For these results, a discharging nominal current ( $C_5 = 34A$ ) was applied.

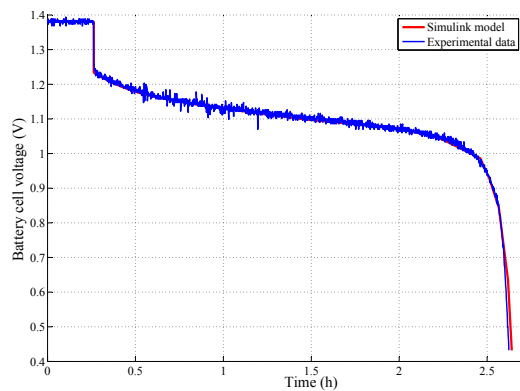


Figure 3.36: NiCd's cell model validation for  $-50^{\circ}C$  ( $C_5$ )

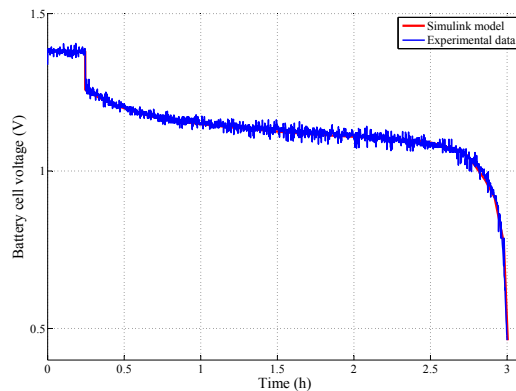


Figure 3.37: NiCd's cell model validation for  $-40^{\circ}C$  ( $C_5$ )

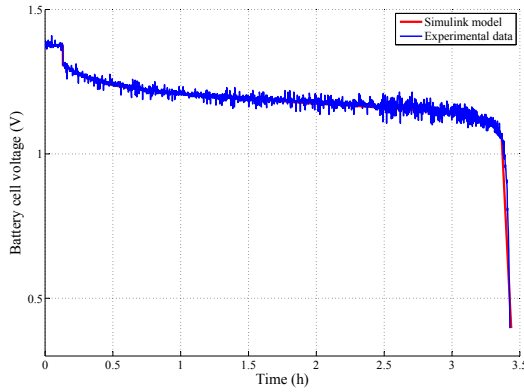


Figure 3.38: NiCd's cell model validation for  $-20^{\circ}C$  ( $C_5$ )

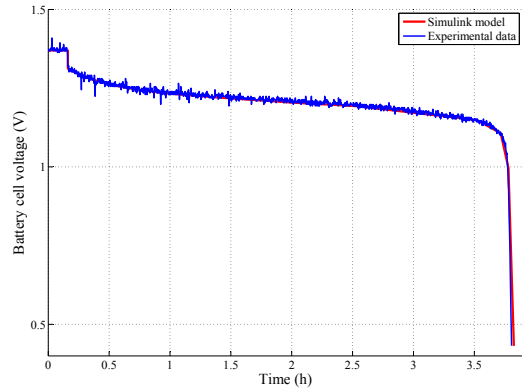


Figure 3.39: NiCd's cell model validation for  $0^{\circ}C$  ( $C_5$ )

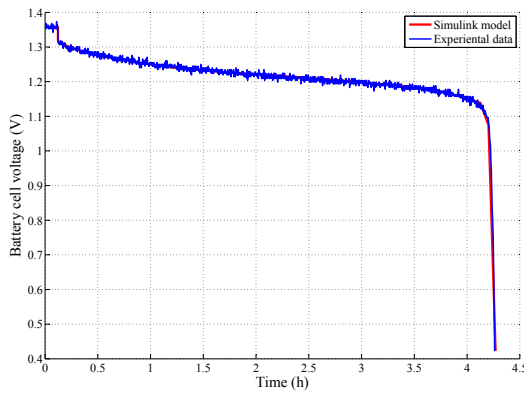


Figure 3.40: NiCd's cell model validation for  $20^{\circ}C$  ( $C_5$ )

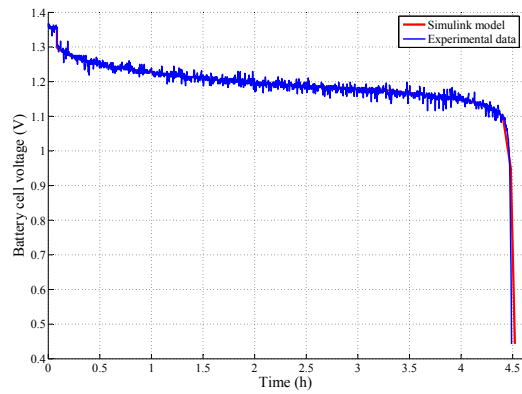


Figure 3.41: NiCd's cell model validation for  $40^{\circ}C$  ( $C_5$ )

Considering the results obtained for a temperature of  $-50^{\circ}C$ , the element only provides 50% of its global capacity. Indeed, instead of providing power during four hours and a half (figure 3.41), the cell only works during two hours and a half (figure 3.36). Once, the element is warmed up to the ambient temperature ( $20^{\circ}C$ ), the unfroze electrolyte is available again. Thus, a part of the electrolyte is frozen during the experiment. Also, rather than freezing solid, the electrolyte tends to become slushy at extremely low temperatures and the battery is still able to work.

The table 3.3 presents the maximum (maximum of the equation 3.28 results) and the average (average of the equation 3.28 results) errors of the Simulink model with the experimental data for the six temperatures.

$$error(\%) = 100 \times \frac{|V_{batt_{model}}(t) - V_{batt_{experimental}}(t)|}{V_{batt_{model}}(t)} \quad (3.28)$$

The differences between the maximum and the average errors is due to the final drop voltage phenomenon. Indeed, it is necessary to measure more resistances' values in this area (low SOC values) in order to improve the model accuracy.

Temperature	Maximum error (%)	Average error (%)
-50°C	19,3399	3,2851
-40°C	9,1647	3,3113
-20°C	15,2485	3,7581
0°C	13,3742	2,3548
20°C	11,6714	2,7363
40°C	6,2758	2,3841

Table 3.3: Maximum and average errors between the experimental data and the Simulink model at  $C_5$  rate.

The tests' results performed using a  $C_3$  current are presented in the appendix D.

### 3.4 The rheostat

A rheostat is considered when the DC bus is not able to recover braking energy like in the case of an autonomous powertrain. Its characteristic is its ohmic value which determines the dissipated power. Two kinds of rheostat exist:

- natural convection rheostats. Their working temperature is set between  $400^\circ C$  and  $600^\circ C$ . Suburban transports are the main application.
- Forced ventilation rheostats. They are set in caissons.

The rheostat is only composed of a DC chopper to link the DC bus to an electric resistance. The chopper is governed by equation 3.29 and the electric resistance by equation 3.30.

$$\begin{cases} V_{rh} = \alpha_{rh} V_{bus} \\ I_{rh} = \alpha_{rh} I_{h-rh} \end{cases} \quad (3.29)$$

$$I_{h-rh} = \frac{V_{rh}}{R_{rh}} \quad (3.30)$$

The MCS permits to control the current requested from the DC bus ( $I_{rh}$ ) using equation 3.31.

$$\alpha_{rh_{ref}} = \frac{I_{rh_{ref}}}{I_{h-rh_{meas}}} \quad (3.31)$$

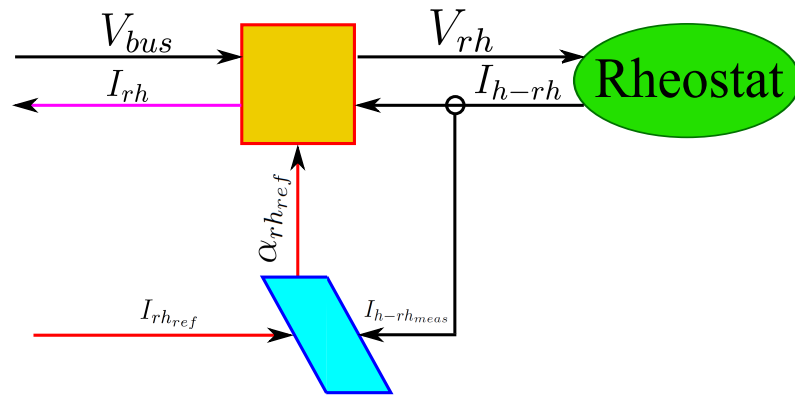


Figure 3.42: EMR and MCS of the rheostat.

### 3.5 The Direct Current bus

The DC bus permits to link all the elements (batteries, ultra-capacitors, diesel driven generator set, rheostat and load) together. The DC bus imposes a voltage ( $V_{bus}$ ) to the sources.

Figure 3.43 presents the EMR of the DC bus connected to the load. The bus imposes a voltage which is controlled using a controller which is also represented on figure 3.43.

The Kirchhoff's current and voltage laws defined by the equations 3.32 are implemented in the coupling block and equation 3.33 models the bus capacitance represented by the accumulation block.

$$\begin{cases} V_{bus} = V_{bus_{rh}} = V_{bus_{ICE}} = V_{bus_{batt}} = V_{bus_{uc}} \\ I_{bus} = I_{rh} + I_{batt} + I_{uc} + I_{ICE} \end{cases} \quad (3.32)$$

$$I_{bus}(t) - I_{load}(t) = C_{bus} \frac{dV_{bus}(t)}{dt} \quad (3.33)$$

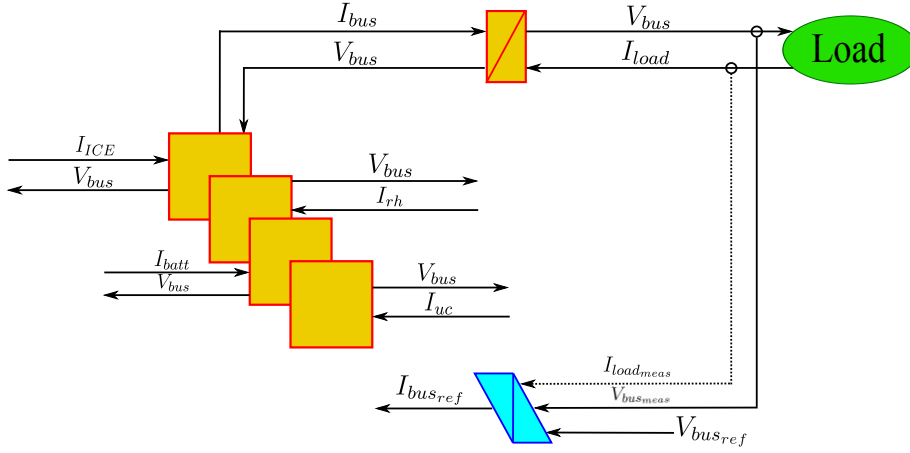


Figure 3.43: EMR of the central DC bus.

A PI controller is used to control the bus voltage (equations 3.34 to 3.38 and appendix C).

$$RegV_{bus}(s) = kp_{bus} + \frac{ki_{bus}}{s} \quad (3.34)$$

$$\frac{V_{bus}(s)}{V_{bus_{ref}}(s)} = \frac{(kp_{bus} + \frac{ki_{bus}}{s}) \left(\frac{1}{C_{bus}s}\right)}{1 + (kp_{bus} + \frac{ki_{bus}}{s}) \left(\frac{1}{C_{bus}s}\right)} \quad (3.35)$$

or

$$\frac{V_{bus}(s)}{V_{bus_{ref}}(s)} = \frac{1 + \frac{kp_{bus}}{ki_{bus}}s}{1 + \frac{kp_{bus}}{ki_{bus}}s + \frac{C_{bus}}{ki_{bus}}s^2} \quad (3.36)$$

Identification with a second order transfer function,

$$\begin{cases} \frac{1}{\omega_{n_{bus}}^2} = \frac{C_{bus}}{ki_{bus}} \\ \frac{2\zeta_{bus}}{\omega_{n_{bus}}} = \frac{kp_{bus}}{ki_{bus}} \end{cases} \quad (3.37)$$

Thus,

$$\begin{cases} ki_{bus} = C_{bus}\omega_{n_{bus}}^2 \\ kp_{bus} = 2\zeta_{bus}C_{bus}\omega_{n_{bus}} \end{cases} \quad (3.38)$$

## 3.6 Global architecture

Figure 3.44 represents the whole electrical structure of the system [Baer12b]. It takes into account:

- the sources,
- the load,
- the rheostat,
- the local controls,
- the energy management strategy.

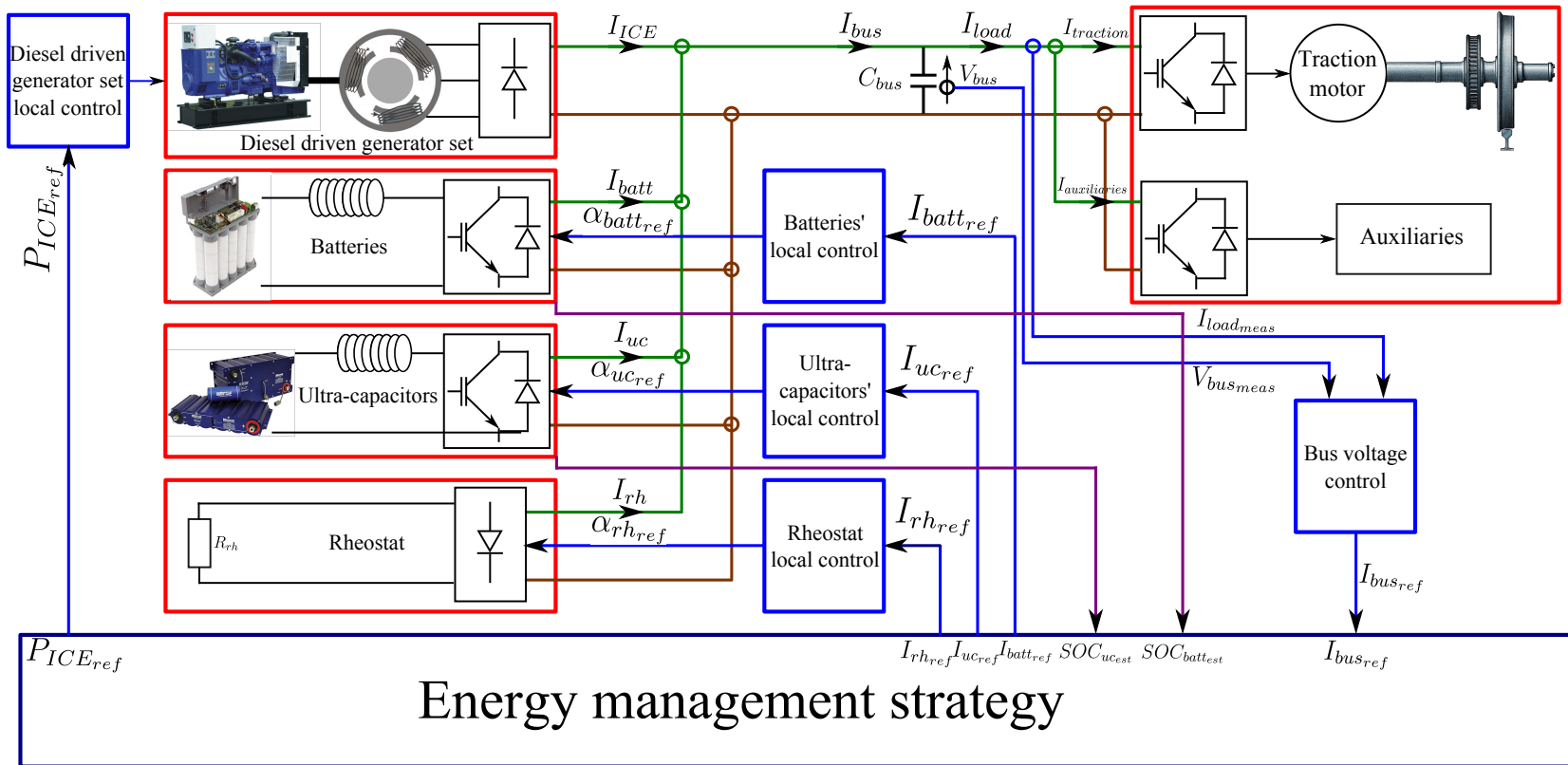


Figure 3.44: Electric structure of the whole system

The equivalent EMR architecture of the system is represented on figure 3.45. It gathers all the previous described sources and elements (batteries, ultra-capacitors, ICE, central DC bus, rheostat and load) with their EMR and their local control. The strategy block has three inputs:

- the bus current reference ( $I_{bus_{ref}}$ ),
- the estimated batteries' SOC ( $SOC_{batt_{est}}$ ),
- the estimated ultra-capacitors' SOC ( $SOC_{uc_{est}}$ ),

and five outputs:

- the power reference to be delivered by the diesel driven generator set ( $\Gamma_{load_{ref}}$  and  $\Omega_{shaft_{ref}} - P_{ICE_{ref}}$  on the figure 3.44),
- the ultra-capacitors' current reference ( $I_{uc_{ref}}$ ),
- the batteries' current reference ( $I_{batt_{ref}}$ ),
- the rheostat's current reference ( $I_{rh_{ref}}$ ).

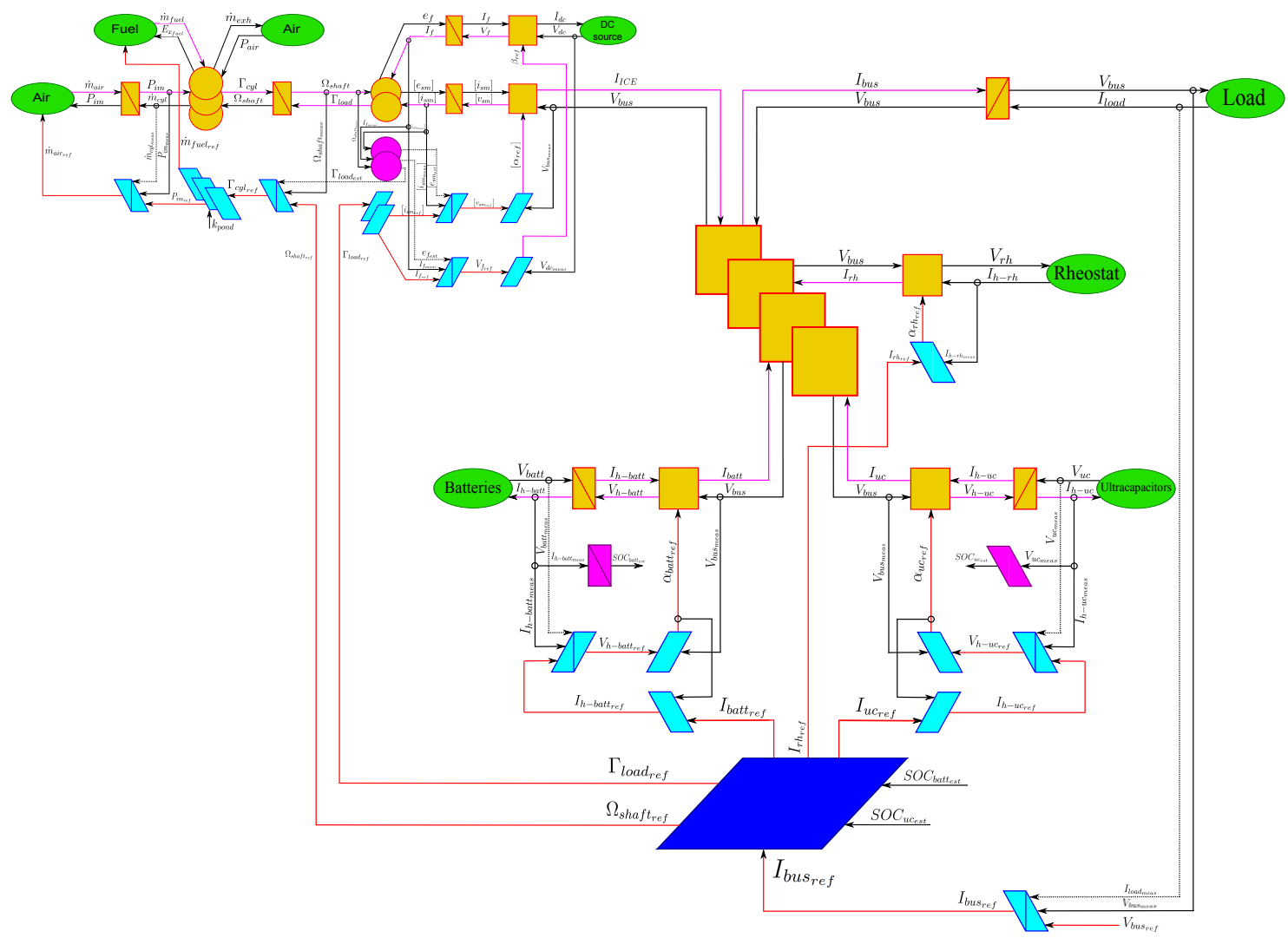


Figure 3.45: EMR and MCS of the whole system

### 3.7 Chapter conclusion

The EMRs of the different on-board sources were developed. Batteries, UCs and more particularly the ICE models are dynamical ones. The multi-physical representation is important regarding the design of the different MCSs. Indeed, its simplification leads to the estimation of some variables like the electromotive forces and the crank shaft torque for the salient pole synchronous machine, the batteries and UCs' SOCs too. Thanks to its modular approach, the EMR also enables using existing models performed in the laboratory.

- The diesel driven generator set is made up of a naturally aspirated diesel engine and a salient pole synchronous machine. Their respective EMRs and MCSs were developed. The exergy rate of the fuel is used to characterize the type of fuel injected into the cylinders of the ICE. The dynamics of the intake manifold are also taken into account. The implemented MCSs permit to control the power delivered to the rest of the system.
- The UCs model is based on a two RC branches equivalent circuit [Zubi00]. The parameters were experimentally identified.
- The NiCd battery cell physical model is based on [Trem07] and [Trem09]. The charging and discharging equations take into account the OCV as a function of the SOC, the polarisation voltage and the hysteresis phenomenon. The parameters were experimentally identified. The internal resistance variation of a cell according to its SOC and its working temperature was also added to the existing models.

All the sources, the rheostat and the load are linked together using a DC bus capacity.

Considering the EMS of the HEL, each source has its own specificity and function. The batteries and the ICE supply the low dynamics of the power in order to increase the lifespan of the batteries and to limit the transient uses of the ICE. UCs are the most interesting power source to supply the high dynamics of the power regarding their cyclability, efficiency and dynamical response. They nevertheless present a limited energy storage capacity.





## Chapter 4

# Type-1 and Type-2 Fuzzy Logic Controllers and Energy Management Strategies

The chapter 1 of the manuscript stated about the basic concepts and the benefits of the fuzzy logic in various applications. In this chapter, two applications of type-2 fuzzy logic control are presented. The first application is the output voltage control of a DC/DC buck converter. It aims at evaluating the performances of such a controller in real time conditions and at performing preliminary tests. The second application of the fuzzy logic control is dedicated to the energy management of a multi-sources system. Thus, the EMS of the HEL is presented. It also describes the first implemented EMS which aims at checking the good development of the sources' models and their control structures (chapter 3). Thus, the two applications address the comparison issue of the Type-1 and Type-2 Fuzzy Logic Controls. The three available Fuzzy Logic Controller categories are compared: the Type-1, the Interval Type-2 and the General type-2 based on zSlices. Their efficiencies are experimentally (first application) and numerically (second application) evaluated and compared. In the case of the HEL's EMS, the fuzzy logic controller performs the management of the ICE. Its design is optimized considering a genetic algorithm.

The section 4.1 is devoted to the design of the DC/DC buck converter voltage controller and discusses the experimental results. The first implemented fuzzy logic based EMS of the HEL is depicted in section 4.2. This section also proposes a genetic algorithm approach to determine the parameters of the Fuzzy logic Controllers. Finally, section 4.3 presents the conclusions of the study.

## 4.1 Type-1 and Type-2 Fuzzy Logic Controllers for DC/DC buck converter application

The DC/DC buck converter test bench represented on figure 4.1 is used. The proposed study will lead to the comparison of the general type-2 based on zSlices against interval type-2 and type-1 fuzzy logic controllers in the control of the output voltage of a buck converter.

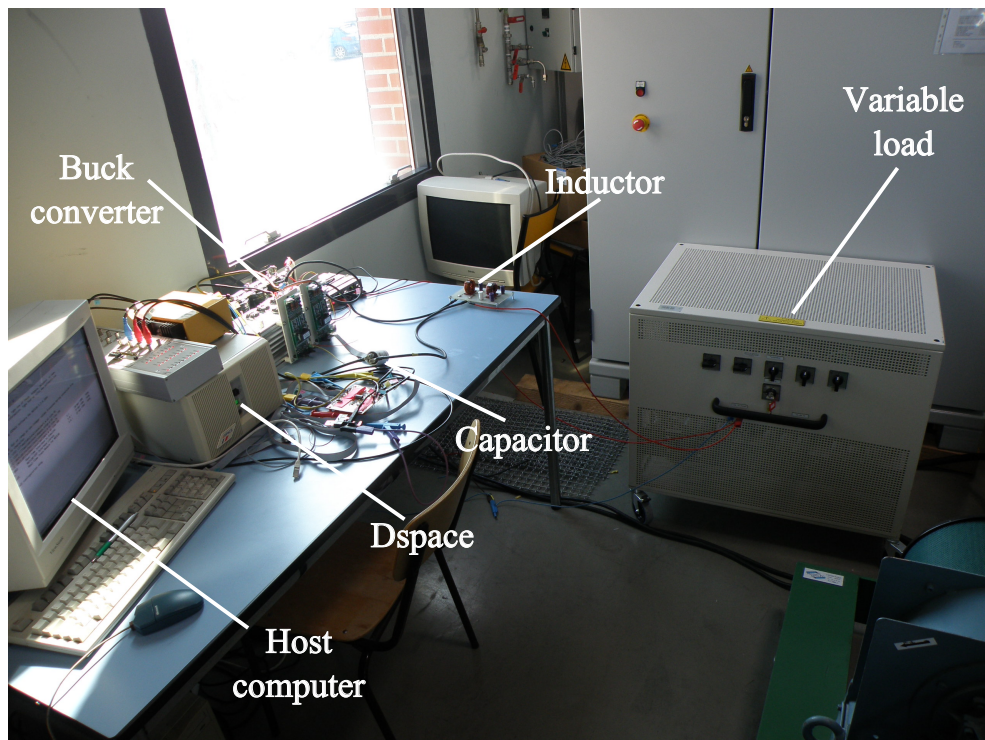


Figure 4.1: Direct Current buck converter test bench

### 4.1.1 Converter modelling and structure of the fuzzy logic controller based Type-1 fuzzy logic

#### Converter modelling

A buck converter is a switched-mode power supply that uses a transistor and a diode like switches, an inductor and a capacitor. The operation of the buck converter is based on connecting/disconnecting alternatively the inductor to the source voltage to store energy in the inductor and discharging the inductor into the load. The circuit of the DC/DC buck converter is shown

on figure 4.2.  $C$  represents the capacitor,  $L$  is the inductor,  $R$  is the variable load resistor,  $V_{in}$  is the input voltage and  $V_{out}$ , the output voltage to be controlled.

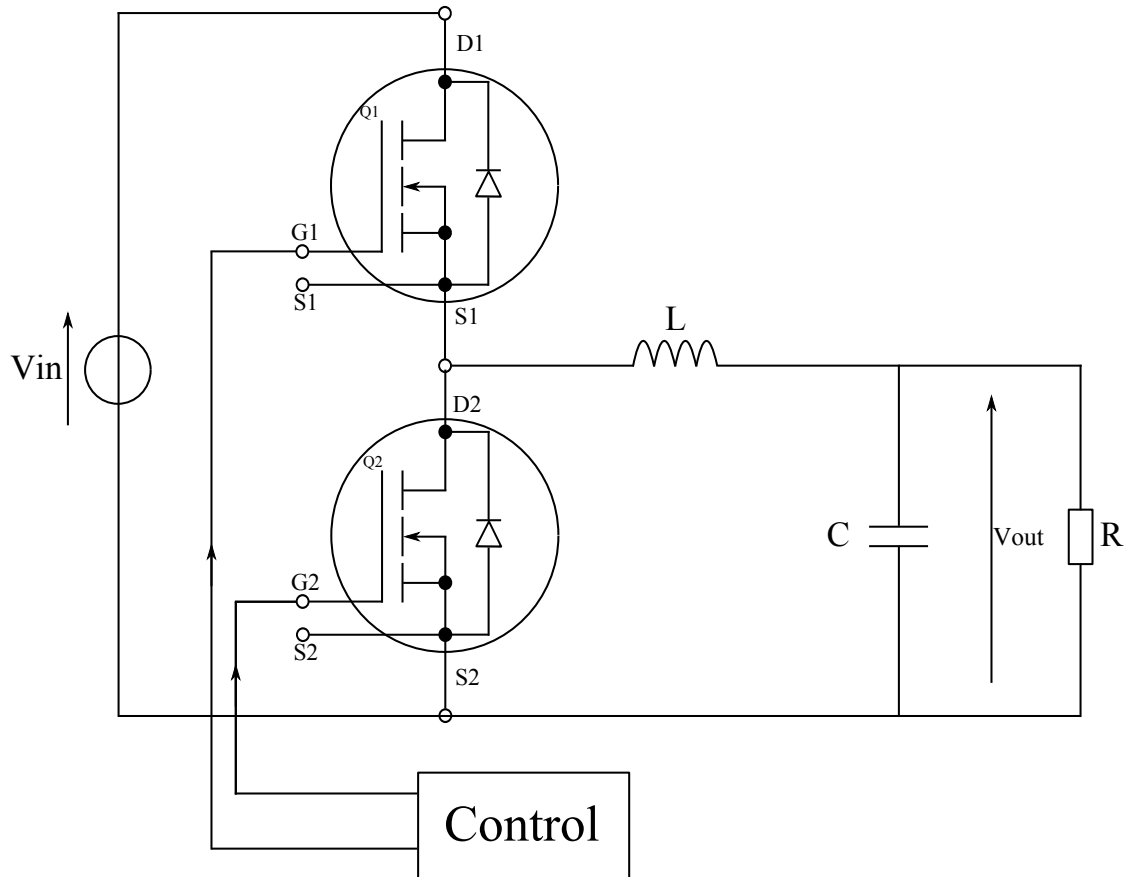


Figure 4.2: Direct Current buck converter topology

### Structure of the Type-1 Fuzzy Logic Controller

The considered fuzzy controller has two inputs ( $e(k)$ ,  $de(k)$ ) and one output ( $s(k)$ ) (equation 4.1), where  $k$  is the sampling time:

- the error  $e(k)$ : difference between the load voltage reference ( $V_{out_{ref}}(k)$ ) and the measured load voltage ( $V_{out_{meas}}(k)$ ),
- the variation of the error  $de(k)$ : difference of error  $e(k)$  between two sampling instants,
- the relative change in the duty cycle  $s(k)$ .

$$\begin{cases} e(k) = V_{out_{ref}}(k) - V_{out_{meas}}(k) \\ de(k) = e(k) - e(k-1) \end{cases} \quad (4.1)$$

with  $T_{samp}$ , the value of the sampling period.

Inputs and outputs are normalised between  $[-1, +1]$ . The control surface which represents the evolution of the output variables according to the inputs variables is represented by a surface in the three dimensional space ( $e$ ,  $de$ ,  $s$ ). The rule base is represented on table 4.1, is anti-diagonal and takes into account 7 different Membership Functions (MFs):

- $NH$  for Negative High,
- $NM$  for Negative Medium,
- $NL$  for Negative Low,
- $Z$  for Zero,
- $PL$  for Positive Low,
- $PM$  for Positive Medium,
- $PH$  for Positive High.

		$de$						
		<b>NH</b>	<b>NM</b>	<b>NL</b>	<b>Z</b>	<b>PL</b>	<b>PM</b>	<b>PH</b>
$e$	<b>NH</b>	NH	NH	NH	NH	NM	NL	Z
	<b>NM</b>	NH	NH	NH	NM	NL	Z	PL
	<b>NL</b>	NH	NH	NM	NL	Z	PL	PM
	<b>Z</b>	NH	NM	NL	Z	PL	PM	PH
	<b>PL</b>	NM	NL	Z	PL	PM	PH	PH
	<b>PM</b>	NL	Z	PL	PM	PH	PH	PH
	<b>PH</b>	Z	PL	PM	PH	PH	PH	PH

Table 4.1: Considered rule base for controlling the output voltage of the buck converter

Example to use the table: IF ( $e$  is  $NL$ ) AND ( $de$  is  $Z$ ) THEN ( $s$  is  $NL$ ).

Numerous MFs forms exist (triangle, trapezium, sigmoid, Gaussian, singleton...). The most used are triangle, trapezium and Gaussian.

Triangular MFs are used for the two inputs ( $e$  and  $de$ ) and singletons are used for the output ( $s$ ) as in [Hiss01] fir real time implementation purposes. MFs for inputs and outputs are considered as symmetrical (figures 4.3, 4.4 and 4.5). The positions of these different membership functions are obtained

(here for a T1-FL Controller - T1-FLC) based on an optimization procedure presented in [Hiss01]. Interval T2 (IT2) and General T2 (GT2) Fuzzy Logic Controllers (GT2-FLCs) will be described in the next section.

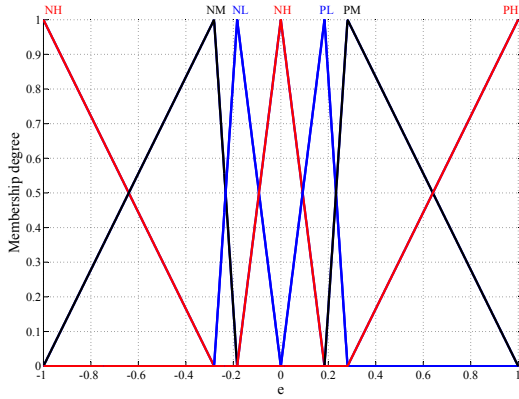


Figure 4.3: Membership Functions of the first input  $e$

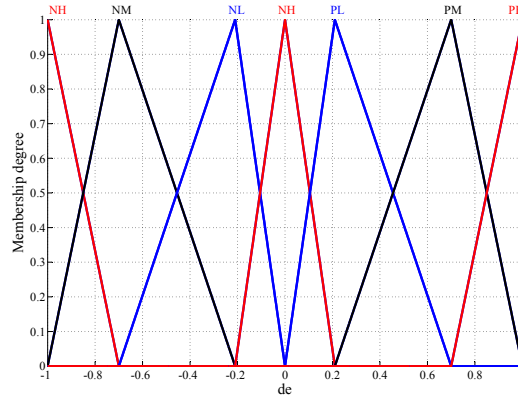


Figure 4.4: Membership Functions of the second input  $de$

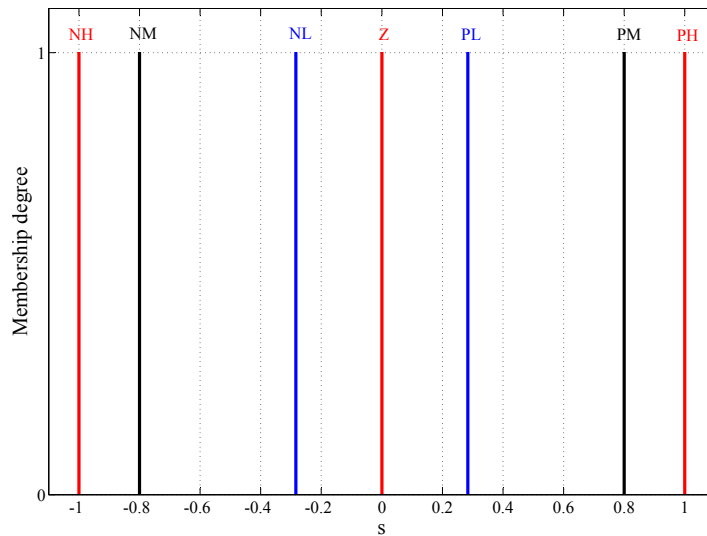


Figure 4.5: Membership Functions of the output  $s$

The controller structure is represented on figure 4.6.

The fuzzy logic part of the controller can be assimilated to a non linear Proportional Derivative (PD) controller which output  $S_{pd}$  is expressed thanks to equation 4.2.

$$S_{pd}(k) = k_p(e(k), de(k)).e(k) + k_d(e(k), de(k)).de(k) \quad (4.2)$$

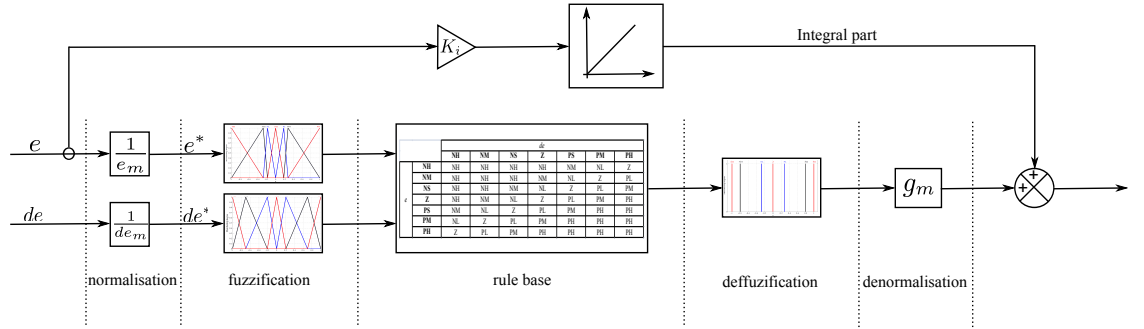


Figure 4.6: Direct Current buck converter controller structure

The addition of the parallel branch equipped with an integrator and a gain ( $K_i$ ) permits to realize a complete Proportional-Integral-Derivative (PID) controller. This structure presents the advantage to avoid the calculation of the variation of the variation of the error ( $de^2$ ), to obtain a PID-type nonlinear controller.

Normalisation, denormalisation coefficients ( $e_m$ ,  $de_m$  and  $g_m$ ) and the integral gain ( $K_i$ ) must be tuned according to the considered application. In electrical engineering, many actual systems can be approached in the form of an open loop first order with a pure delay transfer function (equation 4.3).

$$TF(s) = \frac{K.e^{-T.s}}{1 + \tau.s} \quad (4.3)$$

Numerous works have defined pre-established settings for conventional controllers (P, PI, PID) [Zieg93]. These settings are directly applicable and deductible thanks to a single open loop identification test. Optimized coefficients' expressions for T1-FLC are given using equation 4.4 [Hiss98].

$$\left\{ \begin{array}{l} e_m = c \\ de_m = \frac{1}{T\tau} (\tau + 0.4T) . T_{s\text{amp}} . c \\ g_m = \frac{2.26}{KT} (\tau + 0.4T) . c \\ K_i = \frac{1.78}{KT} \end{array} \right. \quad (4.4)$$

with  $c$ , the output voltage reference ( $V_{out_{ref}}$ ).

## 4.1.2 Interval and General Type-2 Fuzzy Logic Controllers

In this section, the design of IT2 and GT2 maps are detailed. The different steps of the methodology have already been represented on the figure 1.14.

### Interval Type-2 Fuzzy Logic Controller design

The fuzzy map is a plot corresponding to the evolution of the output ( $s$ ) according to the inputs ( $e$  and  $de$ ). To obtain the output from the inputs, four steps are necessary:

- fuzzification,
- inference,
- reduction,
- defuzzification.

The fuzzifier converts an input into T2 fuzzy sets. The same fuzzifier as in T1 fuzzy MFs is used in interval T2 fuzzy MFs. Thus, fuzzification is performed twice (one for the Upper MF (UMF) and one for the Lower MF (LMF)).

$$\mu'_a = \begin{cases} 0 \\ 1 \end{cases} \quad (4.5)$$

$\mu'_a$  has already been defined in the chapter 1 - figure 1.15 and represents the secondary MF in the case of the Type-2 fuzzy logic.

Figure 4.7 illustrates the inference engine. It uses the product method (equation 4.6).

$$\begin{cases} \mu_2 \times \mu'_2 = \bar{\omega} \\ \mu_1 \times \mu'_1 = \underline{\omega} \end{cases} \quad (4.6)$$

Contrary to the Type-1 fuzzy logic, this inference engine performs intervals with  $\omega \in [\underline{\omega}, \bar{\omega}]$  and  $z \in [\underline{z}, \bar{z}]$ . To come back to a crisp output  $z$ , a type reducer is necessary. It type-reducer combines T2 fuzzy sets into a T1 fuzzy MF called the type-reduced set. The type-reduced set is computed using the Karnik-Mendel algorithm [Wu07]. Inputs of the algorithm are the sets  $\omega_i$  and  $z_i$ . The problem is the following one:

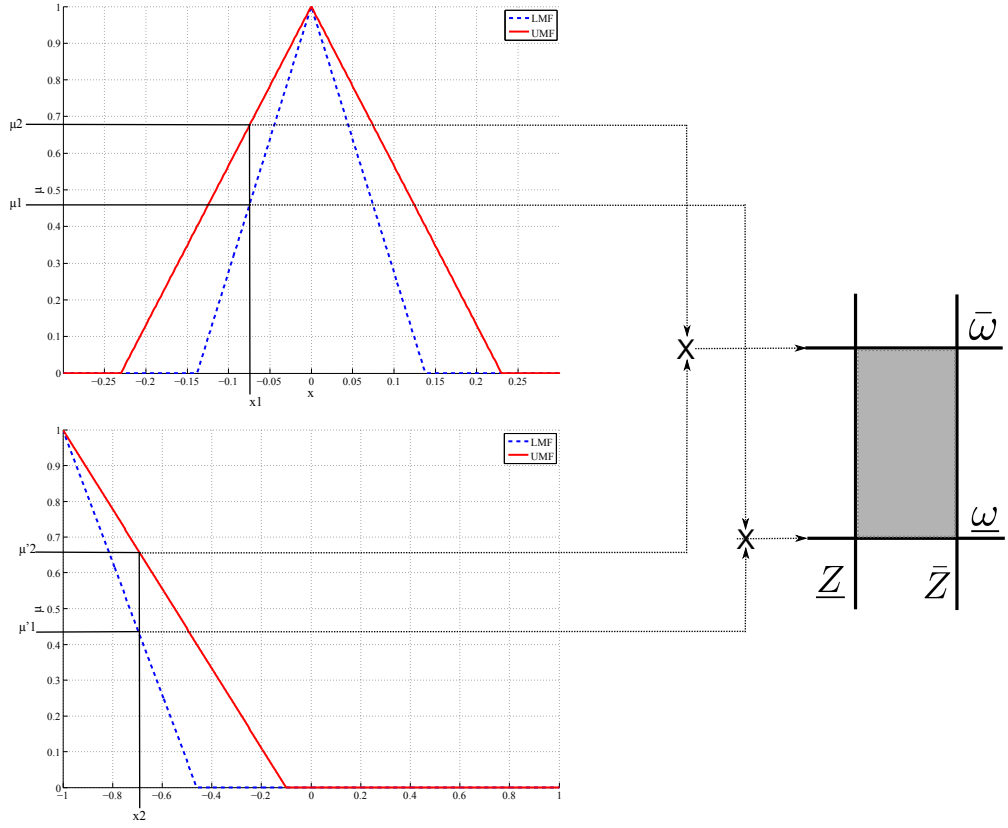


Figure 4.7: Inference engine

$$\begin{cases} z_i \in Z_i \equiv [z_i, \bar{z}_i], i = 1, 2, \dots, N \text{ with } z_i \leq \bar{z}_i \\ \omega_i \in W_i \equiv [\underline{\omega}_i, \bar{\omega}_i], i = 1, 2, \dots, N \text{ with } \underline{\omega}_i \leq \bar{\omega}_i \end{cases} \quad (4.7)$$

Compute:

$$Y = \frac{\sum_{i=1}^N Z_i W_i}{\sum_{i=1}^N W_i} \equiv [y_l, y_r] \quad (4.8)$$

with

$$\begin{cases} y_l = \min_{\substack{\forall z_i \in [z_i, \bar{z}_i] \\ \forall \omega_i \in [\underline{\omega}_i, \bar{\omega}_i]}} \frac{\sum_{i=1}^N z_i \omega_i}{\sum_{i=1}^N \omega_i} \\ y_r = \max_{\substack{\forall z_i \in [z_i, \bar{z}_i] \\ \forall \omega_i \in [\underline{\omega}_i, \bar{\omega}_i]}} \frac{\sum_{i=1}^N z_i \omega_i}{\sum_{i=1}^N \omega_i} \end{cases} \quad (4.9)$$

To compute  $y_l$ , first  $\underline{z}_i (i = 1, 2, \dots, N)$  must be sorted in increasing order. Thus,  $\underline{z}_1 \leq \underline{z}_2 \leq \dots \leq \underline{z}_N$  and weights  $\omega_i$  are matched and renumbered to correspond to their  $\underline{z}_i$ .

$\omega_i$  is then initialized by setting:

$$\omega_i = \frac{\omega_i + \bar{\omega}_i}{2} \quad (4.10)$$

and  $y$  is computed such as

$$y = \frac{\sum_{i=1}^N \underline{z}_i \omega_i}{\sum_{i=1}^N \omega_i} \quad (4.11)$$

The switched point  $k$  corresponds to  $\underline{z}_k \leq y \leq \underline{z}_{k+1}$ .

Thus,

$$\omega_i = \begin{cases} \bar{\omega}_i, & i \leq k \\ \omega_i, & i > k \end{cases} \quad (4.12)$$

and

$$y' = \frac{\sum_{i=1}^N \underline{z}_i \omega_i}{\sum_{i=1}^N \omega_i} \quad (4.13)$$

If  $y' = y$ , the algorithm stops and  $y_l = y$ . If not,  $y' \neq y$  and the switching point  $k$  is calculated again.

To compute  $y_r$ , the algorithm uses  $\bar{\omega}_i$  and  $\bar{z}_{i,k}$  instead of  $\omega_i$  and  $\underline{z}_{i,k}$  in equations 4.11 to 4.13.

The defuzzification aims at obtaining a crisp output value  $y$  from the two inputs  $y_l$  and  $y_r$  (equation 4.14).

$$y = \frac{y_l + y_r}{2} \quad (4.14)$$

Figure 4.8 (respectively 4.9) represents the evolution of  $s$  according to  $e$  and  $de$  with:

- a discretization of the mesh grid set to 21 points (respectively 301 points): two mesh grids are used in order to evaluate the influence of this parameter in the control performances.
- an uncertainty ( $U$  - figure 4.10) equal to 100% to define the Lower and Upper Membership Functions (LMF and UMF) from the Type-1 Membership Function.

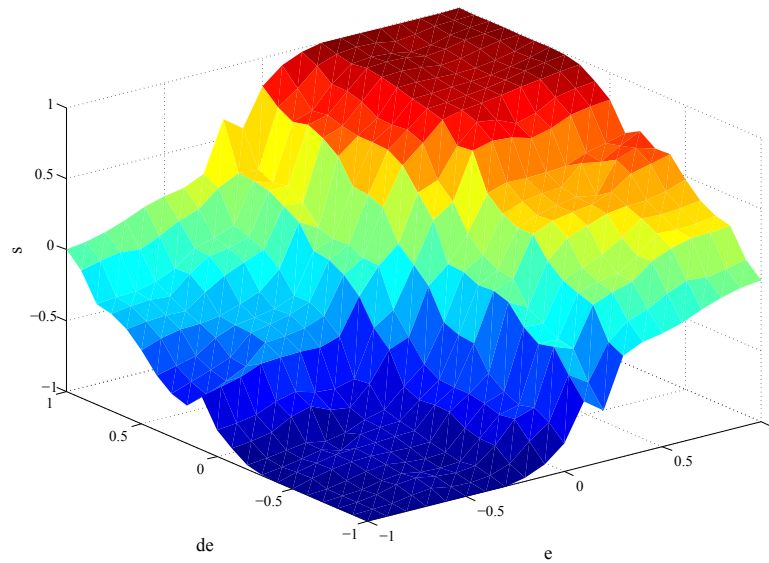


Figure 4.8: Fuzzy surface with a 21 points discretized grid

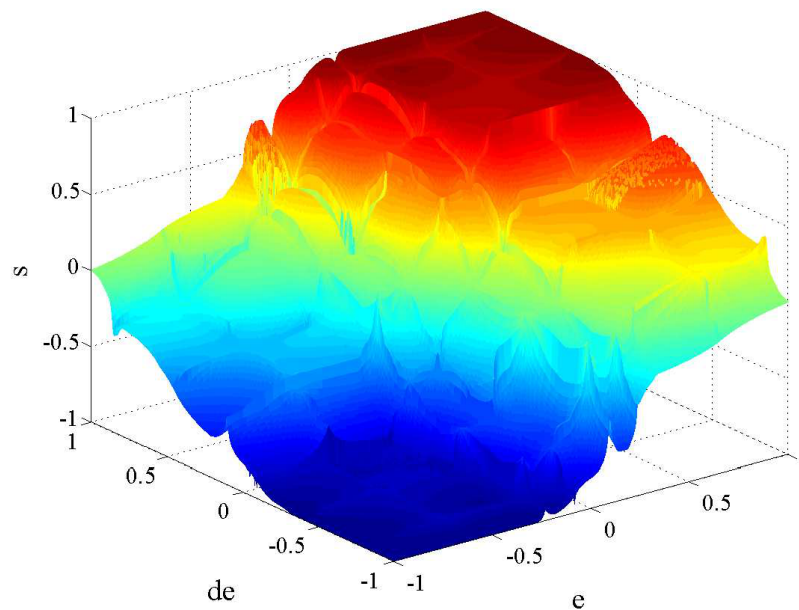


Figure 4.9: Fuzzy surface with a 301 points discretized grid

### General Type-2 Fuzzy Logic Controller design

The GT2 provides a new degree of freedom for the uncertainty [Mend09, Lou12]. The uncertainty of the IT2 in the plane primary MF according to the input values is kept. The uncertainty linked to the third space dimension

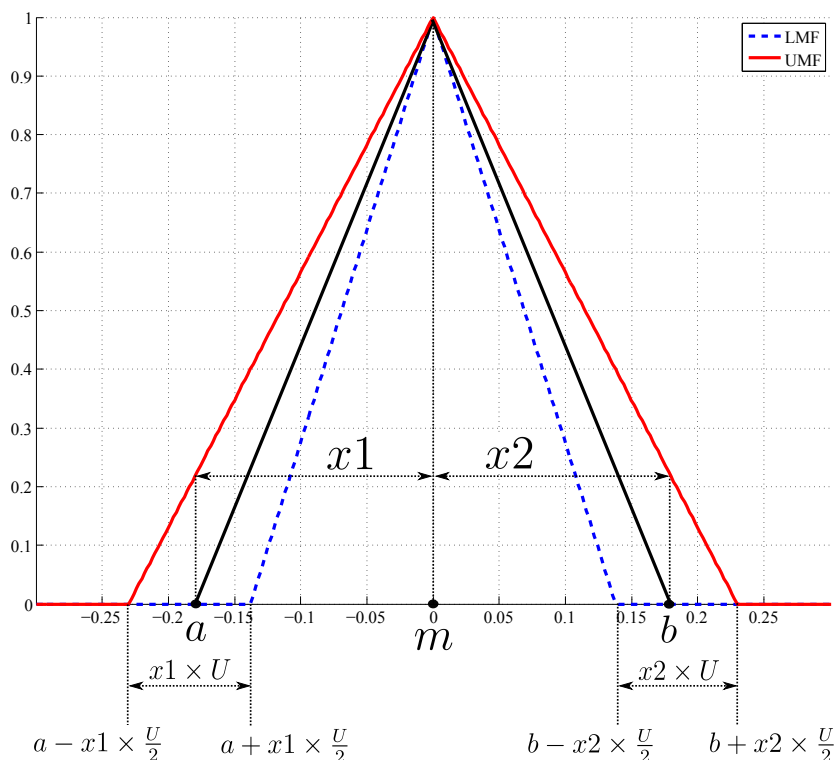


Figure 4.10: Definition of the uncertainty

(the plane represented by the secondary MF according to the primary MF) is represented in this case by a triangle (figure 4.11). GT2 MFs are here based on triangles. Nevertheless, lots of methods exist for determining the type and the parameters of MFs according to the studied system. [Wagn09] proposes a method to design the General Type-2 fuzzy Sets based on the studied device characteristics. Also according to [Wagn09], even if triangular MFs do not represent the best GT2 fuzzy sets, they remain to be a good first approximation to start a study. The selection and the determination of a more appropriate MF is discussed in the second application of this chapter. Steps to implement GT2-FLC are the same as IT2-FLC (figure 1.14). The difference is that all these steps are repeated as many times as the number of zslices [Wagn10].

The fuzzifier converts an input into T2 fuzzy sets. An input value ( $e$  or  $de$ ) will not only correspond to one LMF value and one UMF value but zslices LMF and zslices UMF values. The strength of the zslice approach is to divide the third dimension into zslice parts associated with a zlevel  $z_i$  with their own triangle MFs. The calculation of the LMFs and UMFs values is realised implementing an arithmetic sequence based on figure 4.12.

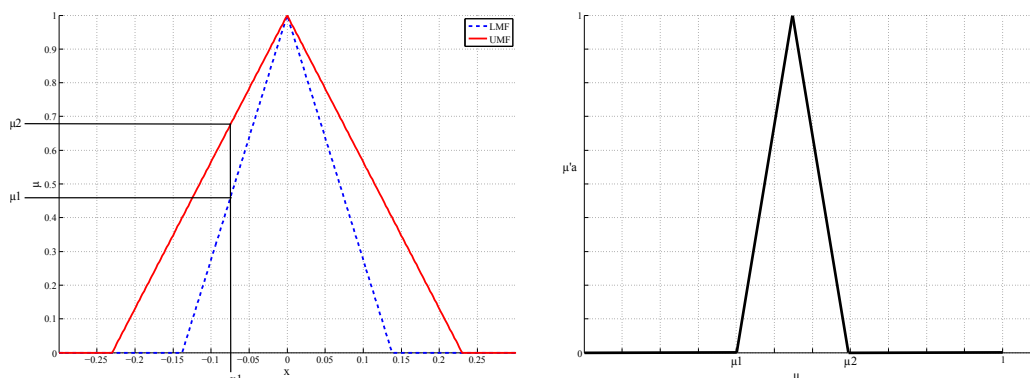


Figure 4.11: General Type-2 Primary (left) and Secondary (right) Membership Functions

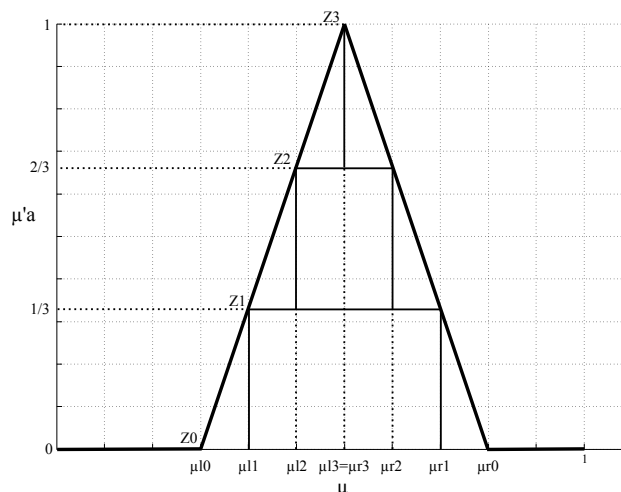


Figure 4.12: Third dimension representation based on 3 z-slices

The figure 4.13 gives a better representation of a triangular General Type-2 Membership Function in the three dimensions. The third dimension is discretized in three parts or three "zslices", three slices along the z-axis.

The inference engine is exactly the same as the IT2 one. Instead of applying it only on the z0-slice (figure 4.12) which corresponds to the triangular MF of the x-y plane, it is applied on z1, z2, z3, ..., zn-slices too in the case of "n-zslices". In other words, the inference engine computes "n"  $(y_l; y_r)$  pairs, one per discretization. Then, the defuzzifier calculates the average of the considered type-reduced set  $(y_c$  - equation 4.15 in the case of 3-zSlices and equation 4.16 in the case of n-zSlices).

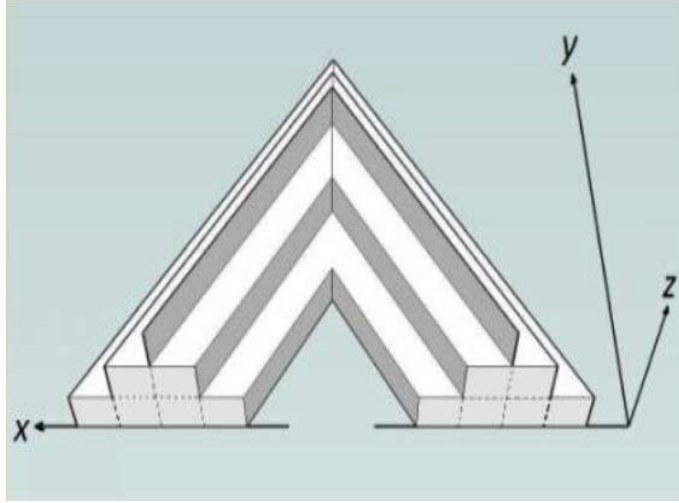


Figure 4.13: Side view of a general type-2 fuzzy set, indicating three zLevels on the third dimension - [Wagn10].

$$y_c = \frac{\left(\frac{1}{3}\left(\frac{y_{l1}+y_{r1}}{2}\right)\right) + \left(\frac{2}{3}\left(\frac{y_{l2}+y_{r2}}{2}\right)\right) + \left(\frac{3}{3}\left(\frac{y_{l3}+y_{r3}}{2}\right)\right)}{\frac{1}{3} + \frac{2}{3} + \frac{3}{3}} \quad (4.15)$$

$$y_c = \frac{\left(\frac{1}{n}\left(\frac{y_{l1}+y_{r1}}{2}\right)\right) + \left(\frac{2}{n}\left(\frac{y_{l2}+y_{r2}}{2}\right)\right) + \dots + \left(\frac{n}{n}\left(\frac{y_{ln}+y_{rn}}{2}\right)\right)}{\frac{1}{n} + \frac{2}{n} + \dots + \frac{n}{n}} \quad (4.16)$$

Figure 4.14 (respectively 4.15) represents the evolution of  $s$  according to  $e$ ,  $de$  with:

- a discretization of the mesh grid set to 21 points (respectively 301 points),
- an uncertainty equal to 100%,
- a discretization of the third dimension set to 100 zlices.

Figure 4.16 (respectively figure 4.17) represents the differences between IT2 and GT2 fuzzy maps of figures 4.8 and 4.14 (respectively figures 4.9 and 4.15). According to these figures, the GT2 fuzzy logic tends to reduce the IT2 fuzzy logic irregularities of the surface. Indeed, as explained with the equation 4.16, the GT2 fuzzy logic systems is a kind of combination of IT2 fuzzy logic systems.

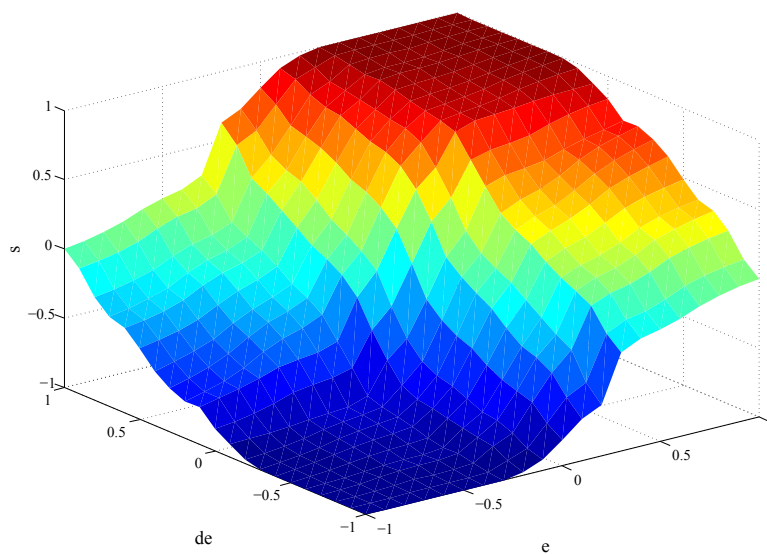


Figure 4.14: Fuzzy surface with a 21 points discretized grid and 100 zslices

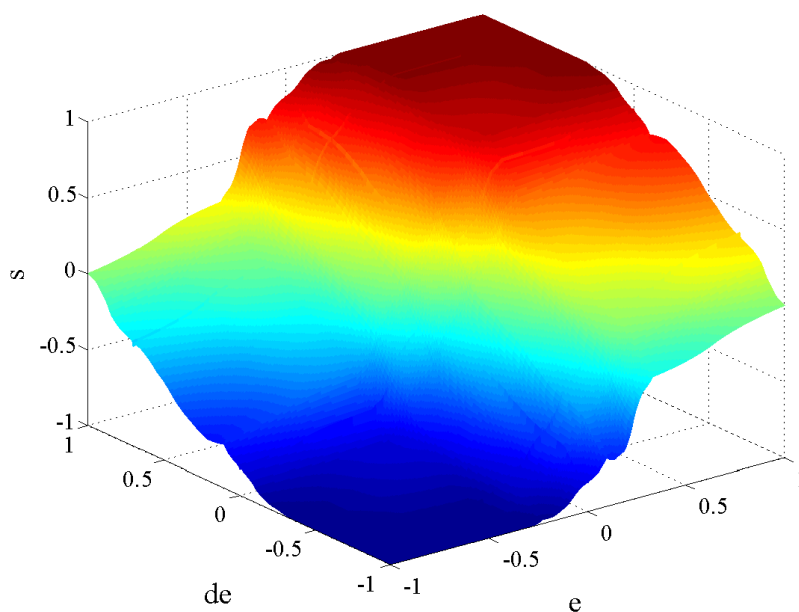


Figure 4.15: Fuzzy surface with a 301 points discretized grid and 100 zslices

### 4.1.3 Experimental results

The structure of the experimental DC/DC converter test bench described in the first part of the section is given on figure 4.18. The converter runs at a switching frequency of  $100kHz$  and the sampling frequency is set to  $10kHz$ .

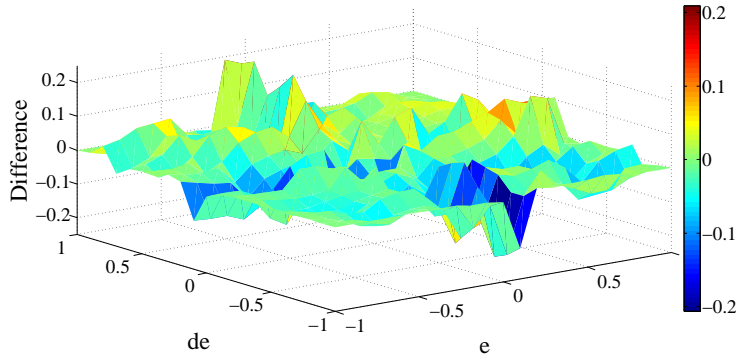


Figure 4.16: Interval Type-2 and General Type-2 fuzzy surfaces differences with a 21 points discretized grid

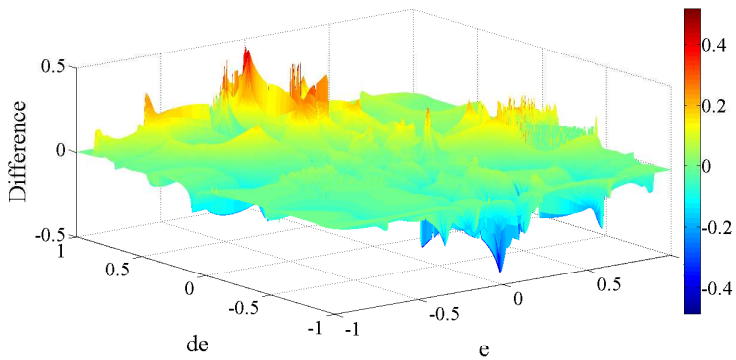


Figure 4.17: Interval Type-2 and General Type-2 fuzzy surfaces differences with a 301 points discretized grid

The control problem consists in the control of the duty cycle so that the output voltage remains controlled and constant. The experimental case consists in changing firstly the reference voltage from  $6V$  to  $60V$ . During the  $60V$  control phase, load resistance variation with step change was tested from  $47\Omega$  to  $140\Omega$ . Firstly, figure 4.19 permits confirming the good operation of the control.

The error in a control loop is usually defined as the deviation from set-point. There are a variety of ways of quantifying the cumulative error such as Integral Error (IE), Integral Absolute Error (IAE), Integral Squared Error (ISE), Integral Time Weighted Absolute Error (ITAE) and Integral Time Squared Error (ITSE). The IAE (equation 4.17) is used because all errors are penalized equally regardless of direction.

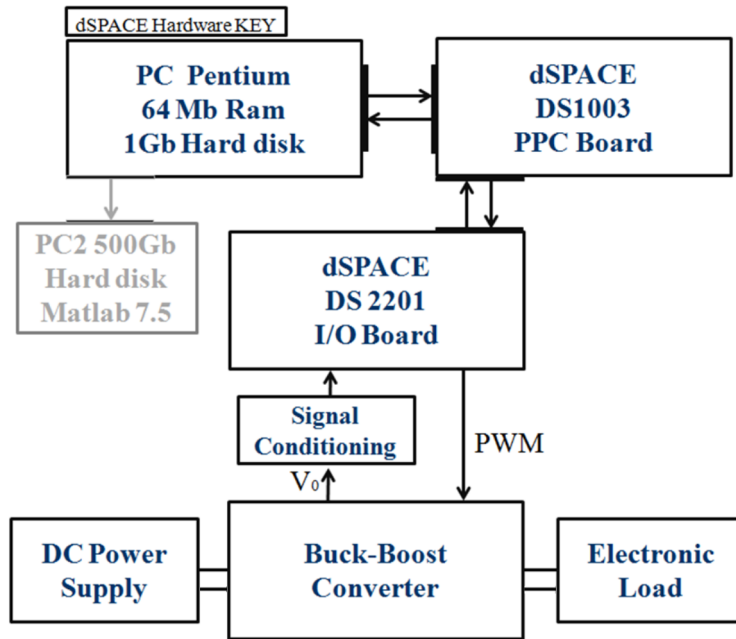


Figure 4.18: Direct Current test bench structure

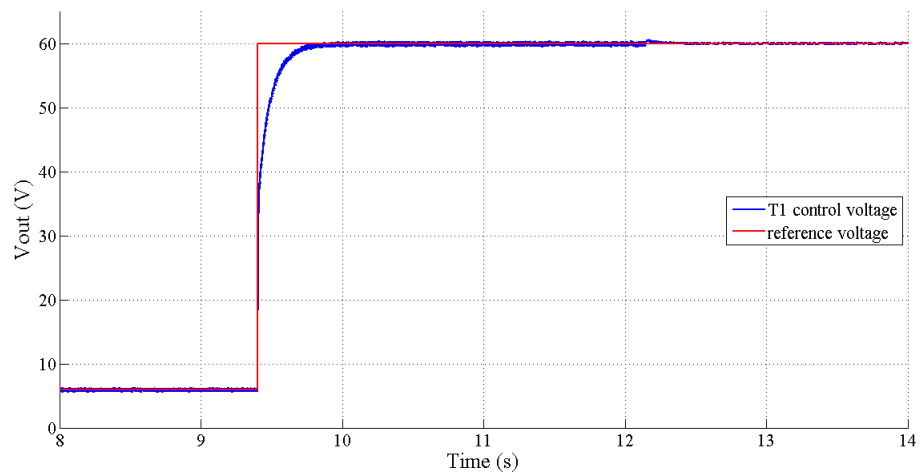


Figure 4.19: T1 only

$$IAE = \int_0^t |V_{out_{ref}} - V_{out_{meas}}(t)| dt \quad (4.17)$$

The table 4.2 presents the evolution of the IAE criteria according to uncertainty. Five uncertainties, from 0% (T1-FL) to 100% (IT2-FL) for two

different mesh grid discretization values (21 and 301) were tested. In both cases, IT2-FLCs have a lower IAE value than T1-FLCs. The best results are obtained for the highest uncertainty values (100%). Indeed, using an additional degree of freedom in the definition of MFs gives better performance in the face of highly uncertain conditions. Moreover, the table 4.2 permits to compare the influence of the precision of the implemented maps. A very thin map ( $grid = 301$ ) doesn't provide better results than the rougher one ( $grid = 21$ ).

<b>Grid = 21</b>		<b>Grid = 301</b>	
<b>Uncertainty (%)</b>	<b>IAE (V.s)</b>	<b>Uncertainty (%)</b>	<b>IAE (V.s)</b>
0	2.6698	0	2.6868
25	2.6531	25	2.6691
50	2.6108	50	2.6166
75	2.5914	75	2.6068
100	<b>2,5783</b>	100	<b>2,5863</b>

Table 4.2: T1 and IT2 comparison for two different grids

The next two tables (4.3 and 4.4) permit to compare improvements provided by the GT2-FL. In this aim, IT2-FL ( $zslice = 1$ ) was compared to GT2-FL (from 2 to 1000 zslices) with the same uncertainties (50% and 100%).

<b>Grid = 21</b>	
<b>Uncertainty = 50%</b>	
<b>zslice</b>	<b>IAE (V.s)</b>
1	2.568
2	2.5645
5	2.5689
100	<b>2.5629</b>
1000	2.5683

Table 4.3: IT2 and GT2 comparison for a 50% uncertainty

<b>Grid = 21</b>	
<b>Uncertainty = 100%</b>	
<b>zslice</b>	<b>IAE (V.s)</b>
1	2.5957
2	2.56
5	2.5558
100	2.5648
1000	2.5551

Table 4.4: IT2 and GT2 comparison for a 100% uncertainty

IAE results show that a high number of z-slices (100 and 1000) seems to improve the efficiency of the control. However, the evolution of the IAE results is more "uncertain". For instance, table 4.4 shows that the "100-zslices GT2-FLC" is less efficient than the "5-zslices GT2-FLC". IAE values were all calculated considering the evolution of the output load voltage represented on figure 4.20.

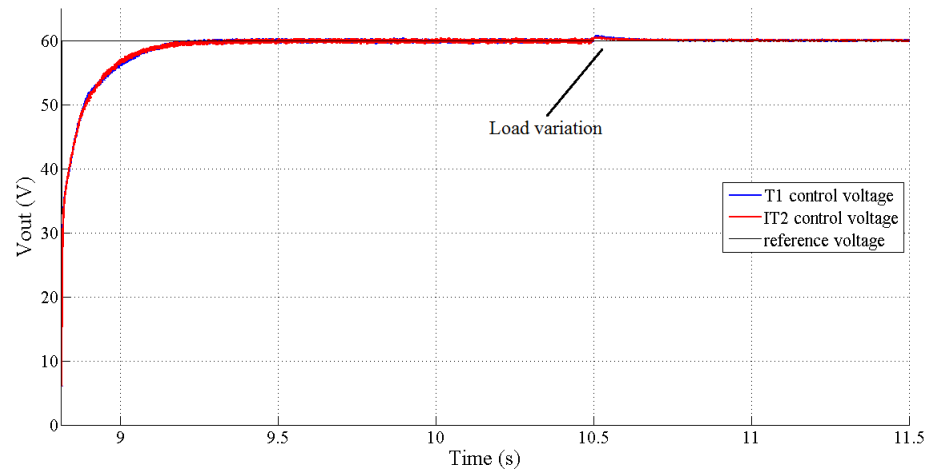


Figure 4.20: Experimental T1 and IT2 control results

To observe the contribution of the IT2-FLC compared to the T1-FLC, a zoom around the step change load resistance instant is depicted on figure 4.21.

The IT2-FLC permits to reduce significantly the over shoot of the controlled voltage during the step change of the load resistance value. The performances of such a fuzzy logic controller in real time conditions have been tested. Even if the controllers effectively compensate the over shoot,

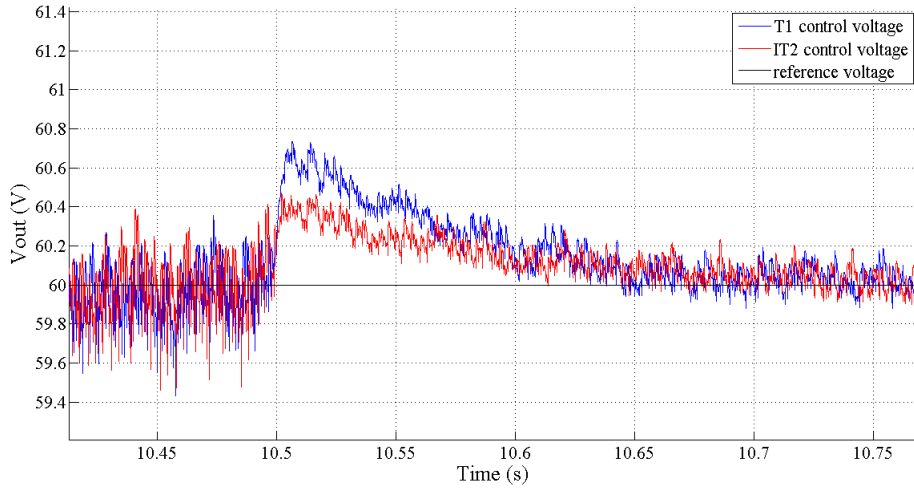


Figure 4.21: T1 and IT2 control zoom

the integral gain slows down the system and requires further study. Moreover, according to [Wagn09], it would be interesting to specify the GT2 MFs based on data which is directly sampled from the device. It would follow from a more accurate representation of the uncertainty associated with the device.

The second application of the fuzzy logic control is dedicated to the energy management of the HEL. Fuzzy logic provides a way to compute human knowledge easily and accommodates the real-world human knowledge and logic. It provides both an intuitive method for describing systems in human terms and automates the conversion of those system specifications into effective models.

## 4.2 Energy Management Strategies

The establishment of the EMS of the HEL is now tackled. It consists in determining the power references of the diesel driven generator set, the batteries and the UCs banks to provide the power required by the driving cycle and the control of the bus voltage.

### 4.2.1 Frequency Energy Management Strategy

To validate the good implementation of the previous presented models, a first EMS based on a frequency approach [Baer12b], is used. The driving cycle

power (figure 4.22) is filtered thanks to a low pass filter (cut-off frequency: 8 mHz). From this filter, low and high frequencies of the power mission are obtained. High frequencies define the UCs power request (or reference) and low frequencies, the batteries and the diesel driven generator set powers requests. The use of a low pass filter is an easy and effective way to solicited all the on-board sources without considering a possible recharge of the batteries. On the contrary, their full discharge permits to test the model under degraded conditions and to check the good implementation of the SOCs' limitations. Then, in a second step the optimal fuzzy logic EMS is an improvement of the frequency EMS by adding a fuzzy logic controller to deal with the batteries' recharge for instance.

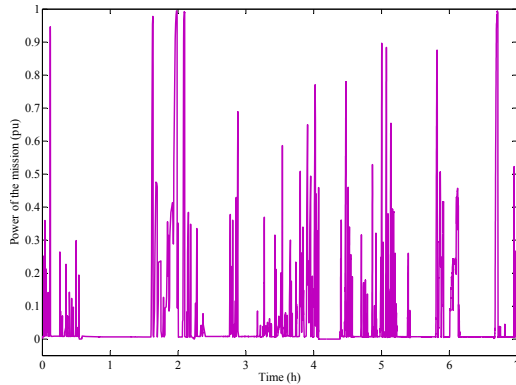


Figure 4.22: Power of the mission according to time

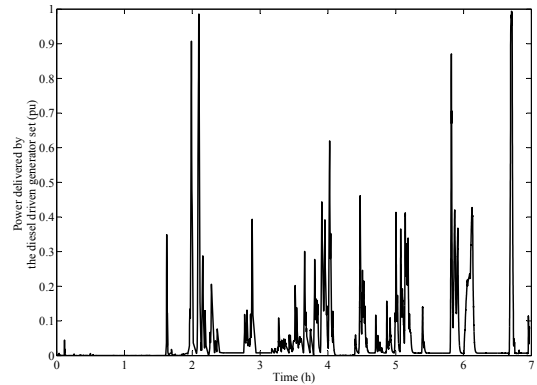


Figure 4.23: Power delivered by the diesel engine set according to time

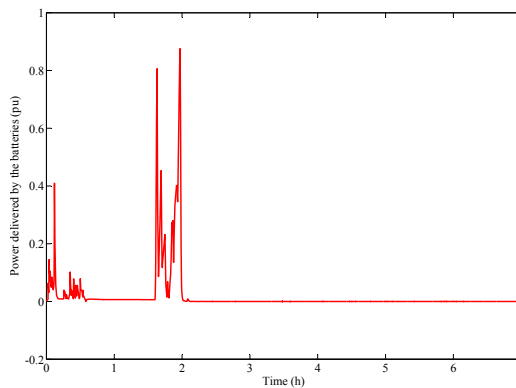


Figure 4.24: Power delivered by the batteries according to time

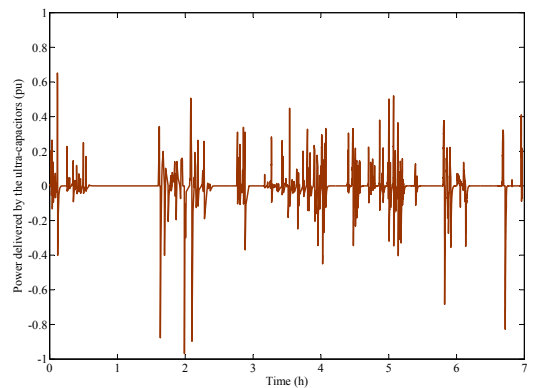


Figure 4.25: Power delivered by the UCs according to time

This EMS does not take into account a possible re-charge of the batteries. Thus, when batteries are totally discharged (figure 4.28), the elements are

no more solicited and the diesel driven generator set (figure 4.23) fulfils the power demand (figure 4.22).

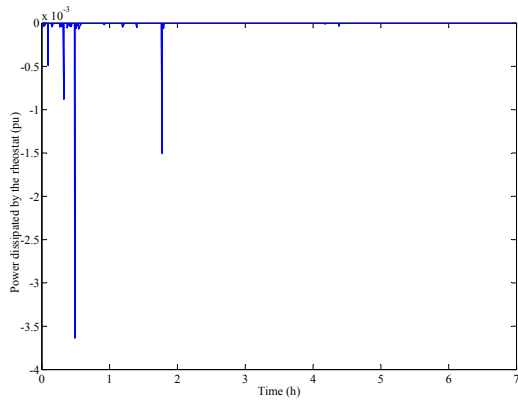


Figure 4.26: Power dissipated by the rheostat according to time

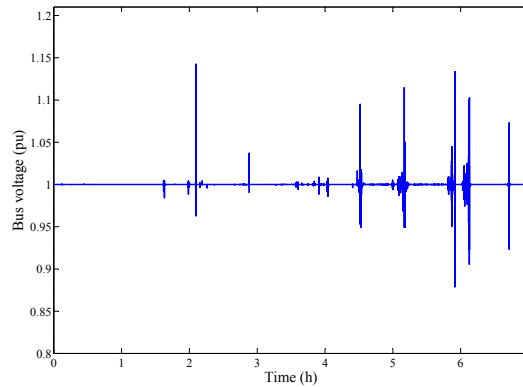


Figure 4.27: Evolution of the bus voltage according to time

Figure 4.27 also shows that the bus voltage remains stable. These simulation results also prove that in the case of a degraded mode (batteries and/or UCs totally discharged), the presented PCS insures the control of the bus voltage only by using the diesel driven generator set.

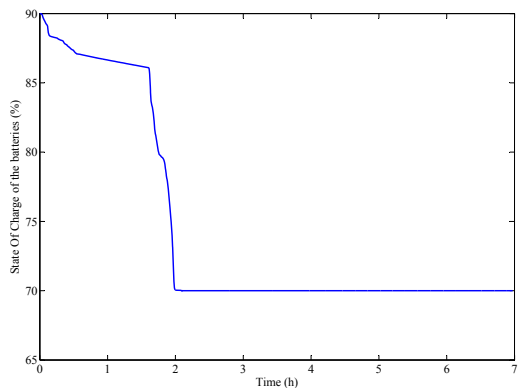


Figure 4.28: Evolution of the batteries estimated SOC according to time

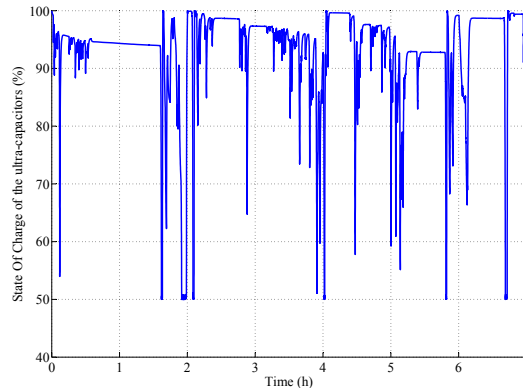


Figure 4.29: Evolution of the UCs estimated SOC according to time

Batteries and UCs' SOC are respectively limited between 70%-90% (figure 4.28) and 50%-100% (figure 4.29). It avoids over-charging and deep discharging of the elements.

## 4.2.2 Optimal Fuzzy Logic Energy Management Strategy

All the on-board sources (batteries, UCs and diesel driven generator set) participate in providing the necessary power to respond to the power requested by the HEL (powers requested by the driving cycle and the auxiliaries). Equation 4.18 is the mathematical relationship of the electrical energy balance of the HEL. The power of the mission ( $P_{mission}$ ) includes the power required by the driving cycle ( $P_{driving-cycle}$ ) and by the auxiliaries ( $P_{auxiliaries}$ ).

$$\begin{cases} P_{mission} = P_{driving-cycle} = P_{auxiliaries} + P_{traction} \\ P_{mission} = P_{batteries} + P_{ultra-capacitors} + P_{ICE} + P_{rheostat} \end{cases} \quad (4.18)$$

with:

- $P_{batteries}$ , the power delivered or recovered by the batteries' bank,
- $P_{ultra-capacitors}$ , the power delivered or recovered by the UCs' bank,
- $P_{ICE}$ , the power delivered by the ICE,
- $P_{rheostat}$ , the power dissipated by the rheostat.

### Ultra-Capacitors' Sub Energy Management Strategy

UCs have a high dynamic response, a high power density and a high lifespan (typically million of charge-discharge cycles can be considered). Generally, they last for their entire lifetime which makes them an "environmentally friendly" device. In order to reduce the stress on the batteries, UCs are dedicated for providing the high frequencies of the power required by the HEL. The power of the mission ( $P_{mission}$ ) is filtered thanks to a low pass filter characterized by its cut-off frequency ( $f_{filter}$ ). The principle has already been presented in the manuscript previously on figure 2.21.

$f_{filter}$  is defined according to a linear function (figure 4.30) linking the estimated SOC of the UCs ( $SOC_{uc_{est}}$ ) and the vehicle speed ( $v_{veh}$ ). The  $SOC_{uc_{est}}$  is expressed through the equation 4.19 and the variable  $e_{SOC_{uc}}^*$ .

$$e_{SOC_{uc}}^* = \frac{1}{DOD_{uc}} (SOC_{uc_{ref}} - SOC_{uc_{est}}) \quad (4.19)$$

with  $DOD_{uc}$ , the Depth Of Discharge (DOD) of the UCs. The DOD is normally stated as a percentage of the nominal capacity and can be seen as

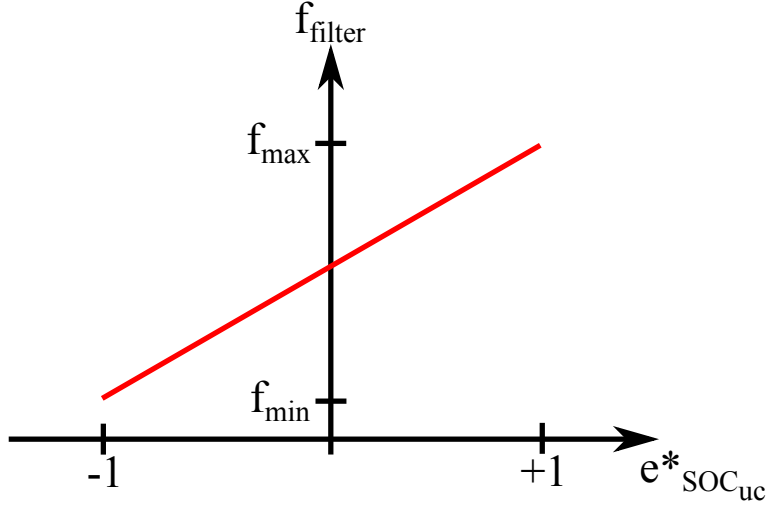


Figure 4.30: Evolution of the cut-off frequency of the filter

the usable capacity of an UC or a battery. 0% DOD means no discharge for instance.  $SOC_{uc_{ref}}$  is defined thanks to the equation 4.20 and represents the UCs' SOC reference according to their maximum ( $SOC_{uc_{max}}$ ), minimum ( $SOC_{uc_{min}}$ ) SOC and the vehicle speed ( $v_{veh}$ ).

$$SOC_{uc_{ref}} = SOC_{uc_{max}} - \frac{v_{veh}}{v_{max}} (SOC_{uc_{max}} - SOC_{uc_{min}}) \quad (4.20)$$

This relationship takes into account the possibility of recovering energy from braking of the HEL. Indeed, when the HEL is not in motion, in theory, the UCs should be fully charged to be used during the next acceleration. On the contrary, if the HEL reaches its maximum speed ( $v_{max}$ ), the UCs should be discharged to recover energy from future braking. To limit their SOC between their maximum ( $SOC_{uc_{max}}$ ) and minimum ( $SOC_{uc_{min}}$ ), a limitation factor (figure 4.31 - equation 4.21), is considered [Sola12b].

$$\alpha_{SOC_{uc}} = \begin{cases} \min \left( 1, \max \left( 0, \frac{SOC_{uc_{max}} - SOC_{uc_{est}}}{SOC_{uc_{max}} - SOC_{uc_{high}}} \right) \right) & \text{if } P_{uc_{ref}} > 0 \\ \min \left( 1, \max \left( 0, \frac{SOC_{uc_{est}} - SOC_{uc_{min}}}{SOC_{uc_{low}} - SOC_{uc_{min}}} \right) \right) & \text{if } P_{uc_{ref}} < 0 \end{cases} \quad (4.21)$$

with  $SOC_{uc_{low}}$ , the UCs' discharge limitation threshold and  $SOC_{uc_{high}}$ , the UCs' charge limitation threshold.

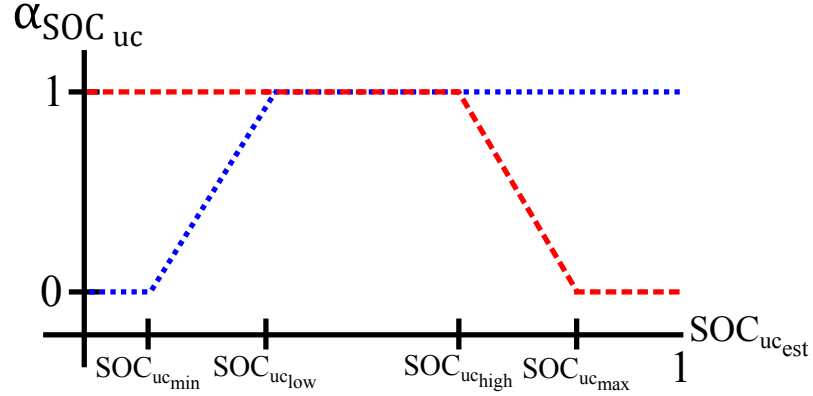


Figure 4.31: Evolution of the limitation factor according to the estimated UCs' SOC

### Batteries' Sub Energy Management Strategy

The power to be delivered or recovered by the batteries ( $P_{batt_{ref}}$ ) is calculated using the presented low frequency filtering of the power profile mission. The batteries' EMS is also made up of a limitation factor ( $\alpha_{SOC_{batt}}$ ) to limit their SOC. However, the reference of the batteries' SOC is not calculated using the speed but the acceleration of the locomotive (equation 4.22).

$$SOC_{batt_{ref}} = SOC_{batt_{max}} - \left| \frac{\dot{v}_{veh}}{\dot{v}_{max}} \right| (SOC_{batt_{max}} - SOC_{batt_{min}}) \quad (4.22)$$

Indeed, the calculation of the batteries' SOC reference ( $SOC_{batt_{ref}}$ ) using the speed of the locomotive is not a good choice. Let's take the example of a HEV such as a car running on a motorway at a relatively constant and high speed. By controlling the batteries' SOC using the speed of the vehicle, they would firstly be used until fully discharging them. Then, the ICE would take over. However, when leaving the motorway (city entrance for example), it wouldn't be possible to use the batteries before recharging them. The choice of maintaining the batteries' SOC as high as possible has been made possible by the use of the acceleration. This case can also be met when the locomotive is running at a cruise rhythm or constant speed. Thus, instead of using the speed, the  $SOC_{batt_{ref}}$  variable is defined according to the acceleration ( $\dot{v}_{veh}$ ) of the HEL.

## Diesel driven generator set and Rheostat Sub Energy Management Strategies

The EMS of the diesel driven generator set is based on a fuzzy logic controller. The developed controller has two inputs, one output and has the same structure as in [Sola12b]. The first input ( $dP$ ) is the difference between the reference load power ( $P_{bus}$ ) and the actual power delivered by the diesel driven generator set ( $P_{ICE_{meas}}$ ) (equation 4.23). This input aims at providing the whole amount of energy to drive the HEL. The second input is the error between the batteries' SOC and their dynamic reference ( $SOC_{batt_{ref}}$ ). This input aims at controlling the batteries' SOC.

$$dP = \frac{P_{bus_{ref}} - P_{ICE_{meas}}}{P_{bus_{max}}} \quad (4.23)$$

The output of the FLC ( $dP_{ICE}$ ) is the relative power change of the diesel driven generator set. The figure 4.32 represents the implemented controller.

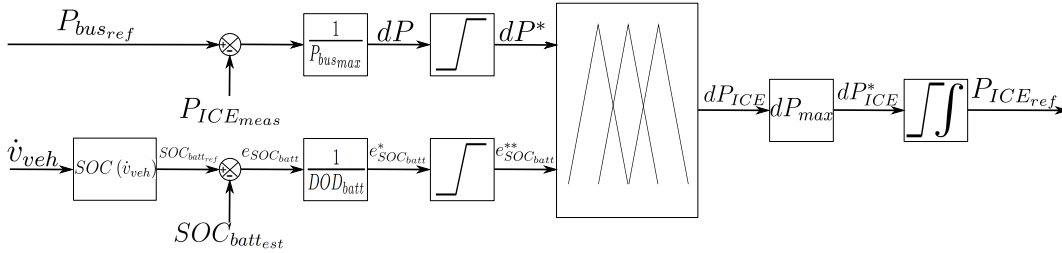


Figure 4.32: Sub-Energy Management Strategy of the diesel driven generator set

The rheostat EMS is coupled with the diesel driven generator set one. All sources supply energy to maintain the bus voltage level. However, the EMS is a theoretical calculation of the powers to be provided by each on-board source. If equation 4.18 is not verified or in other words, if the sum of the power references generated by the EMS is less than the actual power mission, the bus voltage is collapsing and the system stops. Thus, the theoretical sum of power sources must be at least equal or higher than the real required power mission. Thus, a "security" is implemented into the EMS. This security aims at adding the different power references generated by the EMS ( $P_{batt_{ref}}$ ,  $P_{uc_{ref}}$  and  $P_{ICE_{ref}}$ ) and then at comparing the sum result with the actual required power mission ( $P_{bus_{ref}}$ ).

$$\begin{aligned}
P_{batt_{ref}} + P_{uc_{ref}} + P_{ICE_{ref}} - P_{bus_{ref}} &\leq 0 \\
&\iff e_{ref} \leq 0 \\
&\implies P_{rheostat_{ref}} = e_{ref}
\end{aligned} \tag{4.24}$$

$$\begin{aligned}
P_{batt_{ref}} + P_{uc_{ref}} + P_{ICE_{ref}} - P_{bus_{ref}} &> 0 \\
&\iff e_{ref} > 0 \\
&\implies P'_{ICE_{ref}} = e_{ref} + P_{ICE_{ref}}
\end{aligned} \tag{4.25}$$

If the sum of the calculated powers is higher than the power requested by the mission, the power difference is dissipated into the rheostat (equation 4.24), in order to avoid a sharp increase of the bus voltage level. If the sum is lower than the power mission, the difference is completed by the diesel driven generator set (equation 4.25). Figure 4.33 gives the representation of the whole implemented EMS which has been described previously (equations 4.18 to 4.25).

## Fuzzy Logic Controller design

**Fuzzy sets and rule base design** For generalization purposes, all inputs and the output of the FLC (errors or rate changing variables) are normalized between  $[-1; +1]$ . Each linguistic value is designated by a MF. Seven trapezoidal and triangles-type MFs are used for each input over the universe of discourse. For the output, singletons and/or intervals are used. Inputs and output of the FLC are labelled as "NH - negative high", "NM - negative medium", "NL - negative low", "Z - zero", "PL - positive low", "PM - positive medium", and "PH - positive high". The inference system is composed of 49 rules. Each rule presents a condition introduced by an IF expression and an action expression introduced by the THEN expression. The considered rule base is proposed in table 4.5.

		$e^{*SOC_{batt}}$						
		NH	NM	NL	Z	PL	PM	PH
$dP$	NH	NH	NH	NH	NH	NM	NL	Z
	NM	NH	NH	NH	NM	NL	Z	PL
	NS	NH	NH	NM	NL	Z	PL	PM
	Z	NH	NM	NL	Z	PL	PM	PH
	PS	NM	NL	Z	PL	PM	PH	PH
	PM	NL	Z	PL	PM	PH	PH	PH
	PH	Z	PL	PM	PH	PH	PH	PH

Table 4.5: Rule base used in the Fuzzy Energy Management Strategy

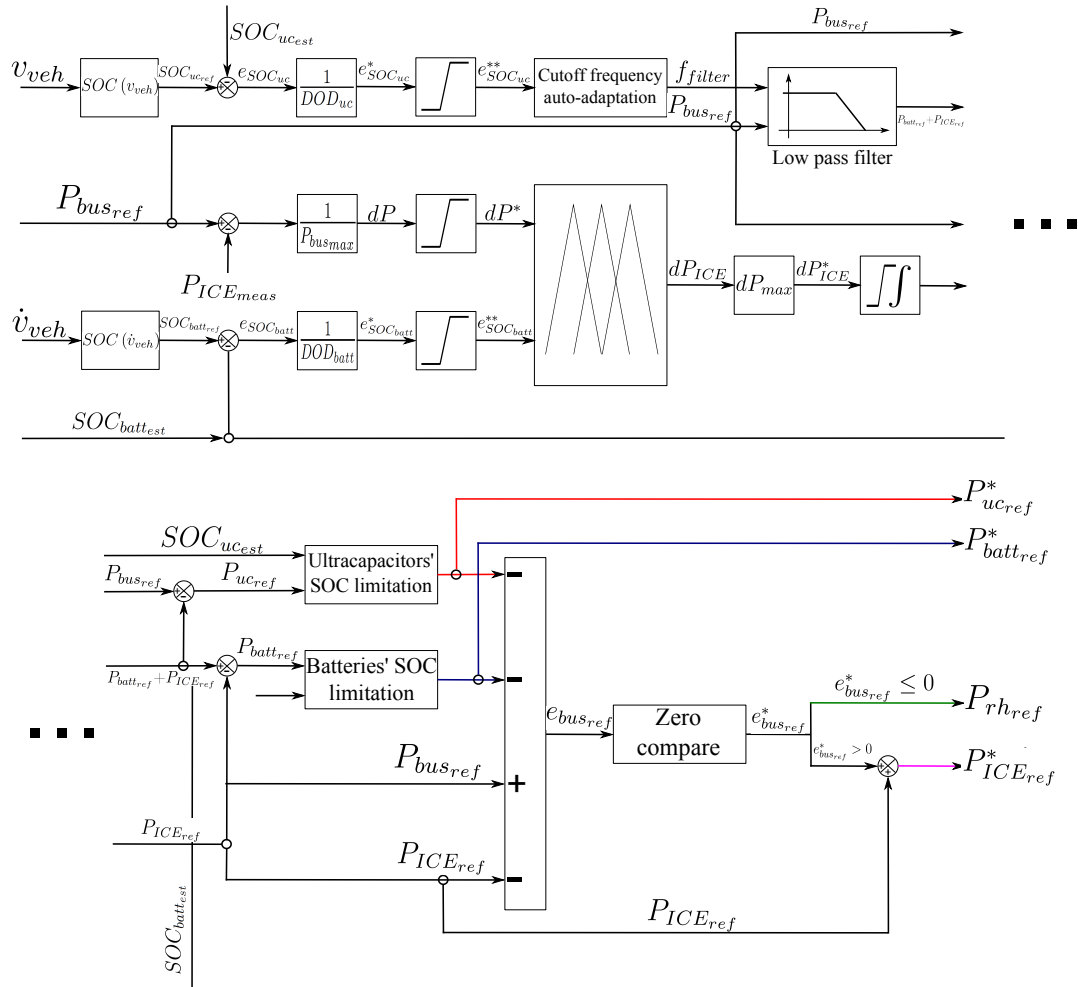


Figure 4.33: Global Energy Management Strategy

An example of the system rule is IF  $dP$  is NH AND  $e_{SOC_{batt}}^*$  is NH THEN  $dP_{ICE}$  is NH. IF the power delivered by the diesel driven generator set is higher than the power required by the mission AND if the batteries must be discharged THEN the power delivered by the diesel driven generator set is reduced.

**Membership functions parameters optimization using a Genetic Algorithm** The GA optimization method ([Wagn07], [Gref86], [Kris88]) consists in selecting the best individuals of a population regarding a given fitness function and applying them the crossover and mutation operators. The new individuals are also evaluated regarding their fitness function in

order to keep the best chromosomes. When the stop criterion is reached, the GA stops. Here, the selected stop criterion is a given fixed number of generations.

**Interval Type-2 FLC synthesis using a Genetic Algorithm** A chromosome is composed of a set of parameters of the Type-2 FLC MFs. The chromosome includes the Interval Type-2 MFs parameters of the inputs, the output of the Type-2 FLC and the frequencies ( $f_{min}$  and  $f_{max}$ ) defined previously. To define the inputs' interval Type-2 triangle MFs, 5 parameters are needed (figure 4.34). An interval MF for the output of the FLC is defined using 2 parameters (figure 4.35).

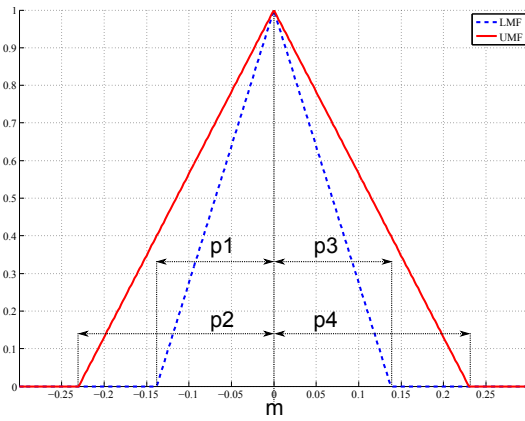


Figure 4.34: Interval Type-2 MF definition

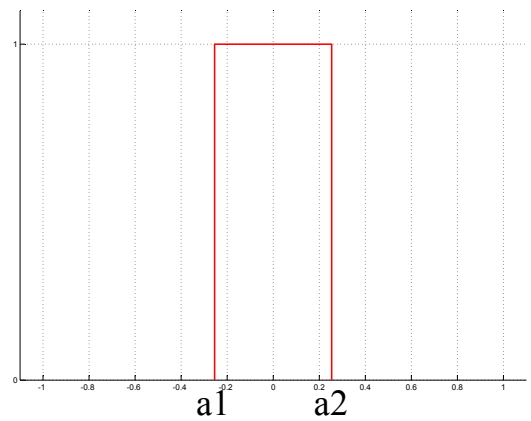


Figure 4.35: Output MF definition

Thus, the chromosome is made up of  $7 \times 5 + 7 \times 5 + 7 \times 2 + 2 = 86$  genes (figure 4.36).

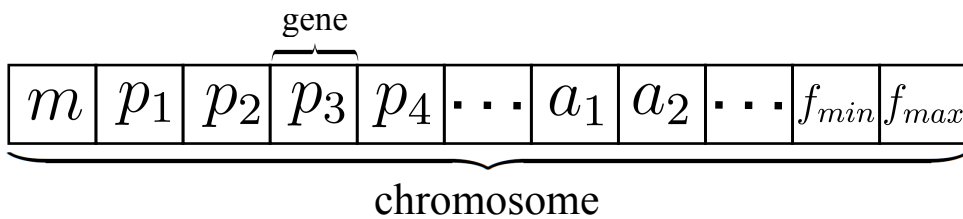


Figure 4.36: Structure of the IT2 FLC chromosome used for optimization

Each GA population consists of 86 chromosomes. The GA uses a tournament selection strategy [Alva04]. The GA based system procedure can be summarized as follows:

1. 88 chromosomes are generated randomly. In this step, the values of the generated parameters must be compared and checked. Indeed, a lot of special wrong cases are possible and must be treated. For instance, an order relation exists like:

$$\begin{aligned}
p_1 &\leq p_2 \\
p_3 &\leq p_4 \\
a_1 &\leq a_2 \\
f_{min} &\leq f_{max}
\end{aligned} \tag{4.26}$$

These special cases are crippling. Thus, chromosomes presenting at least one of those characteristics are deleted and replaced by a new chromosome also generated randomly and respecting the equation 4.26.

2. The FLC is synthesized using the parameters of the considered chromosome and the fitness function is evaluated. The evaluation is performed in loading the FLC in the EMR Simulink model of the HEL. The fitness function value is calculated for each chromosome and permits evaluating its performance. In this study, the fitness function is directly linked to the minimization of the global fuel consumption of the HEL. According to the considered power supply system, minimizing the use of the diesel driven generator set leads reducing the primary energy consumption, increasing autonomy, and reducing pollutant emissions. Thus, the fitness function aims at maximizing the total amount of energy delivered and recovered by the batteries, the UCs and minimizing the energy provided by the diesel driven generator set (equation 4.27).

$$\begin{aligned}
max \left( \int_0^{t_{mission}} |P_{batt}(t)| dt \right) + max \left( \int_0^{t_{mission}} |P_{uc}(t)| dt \right) + \\
min \left( \int_0^{t_{mission}} P_{ICE}(t) dt \right)
\end{aligned} \tag{4.27}$$

It was observed that the only use of the term relating to the energy provided by the diesel driven generator set to define the fitness function was not a good solution. Indeed, the optimal solution would be a full solicitation of the batteries until they reach their minimum acceptable SOC and then, the primary source would deliver the necessary power to cover the rest of the mission without recharging the batteries. The

integration of the batteries and UCs' terms into the fitness function permits using them during all the mission.

3. While the value of the chromosome counter is less than 88, proceed the previous step, otherwise proceed the next step.
4. Some methods such as the roulette wheel [Chan07], elite selection or stochastic universal selection [Shar11] exist. Here, the selection step is based on a biased tournament selection method. It consists in selecting randomly the individuals or chromosomes of the initial population two by two. Their respective fitness function values are compared. The one having the highest fitness value is selected and the other one is eliminated. A random variable is generated to bias the selection process and to maintain the diversity of the individuals within the population. Thus, 44 tournaments are performed and the selected population is made up of the half of the population.
5. The crossover rule consists in recombining the genetic characteristics of the selected population. Thanks to the crossover step the population, which size is half reduced because of the selection step, is doubled to complete the generation. The crossover step uses an arithmetic mathematical relationship. For continuous problems, the crossover is applied to a couple of chromosomes and is a weighted average of the genes of the parents (selected population). If  $[a_i, b_i, c_i]$  and  $[a_j, b_j, c_j]$  are two parents (randomly chosen to make a couple too) and  $p$  a random weight in  $[0,1]$ , 2 chromosomes or children are created (equation 4.28).

$$\begin{cases} chromosome_1 = p \times [a_i, b_i, c_i] + (1 - p) \times [a_j, b_j, c_j] \\ chromosome_2 = p \times [a_j, b_j, c_j] + (1 - p) \times [a_i, b_i, c_i] \end{cases} \quad (4.28)$$

6. The mutation step consists in randomly changing the value of a gene with a very low probability (between 0.001 and 0.01). Thus, it randomly modifies the solutions' characteristics. It permits to introduce diversity or noise in the population and also to provide a global solution.
7. This last population is saved like a new generation. The generation counter is incremented and the algorithm starts a new generation with the FLC creation step.

The figure 4.37 sums up the described steps. In the study, the efficiency of the implemented FLCs is compared using the total amount of energy provided

by the diesel driven generator set. Indeed, the main aim of the optimisation step is to minimise the diesel driven generator use which is quantified thanks to the energy term.

**General Type-2 FLC synthesis using a Genetic Algorithm** Interval Type-2 (IT2) FLCs deal very well with the high levels of uncertainties present in the studied application. However, General Type-2 (GT2) FLCs are expected to further extend this capability in modelling the uncertainty in the third dimension of the MFs. In theory, GT2 sets have the ability to model uncertainties more accurately than IT2 sets. A superior control performance in comparison to T1 and IT2 FLCs is expected. Even if the converter experimental results have proven the effectiveness of the fuzzy logic control, it remains difficult to conclude on a superior control performance of the Type-2 fuzzy logic compared to the Type-1. This new application is another opportunity to study and discuss it. In a GT2 sets, the uncertainty can be modelled for example by a triangular secondary MF as proposed in [Wagn10]. The GT2 fuzzy logic theory has already been presented and applied in the previous study dedicated to the DC/DC converter. As described in [Wagn09], even if a triangular MF is not the best shape to model the system uncertainties (changing drivers, fluctuating environmental conditions, vehicle speed, driving cycle, ageing of the on-board power sources and storage units), it remains to be a first good approximation. Instead of using isoscele triangular MFs, a new improved chromosome is implemented to optimize the parameters of the triangular MFs of the third dimension of the FLC based on zSlices (figure 4.38). The same GA is used and the 86 parameters of the previous described chromosome are kept. To model the triangular MFs of the third dimension of the GT2-FLC, 21 parameters are added to the existing 86 ones.

The only available degree of freedom is the position of the summit of the triangles. Thus, the 21 new parameters ( $2 \text{ inputs} \times 7 \text{ MFs} + 1 \text{ output} \times 7 \text{ MFs} = 21 \text{ MFs} = 21 \text{ triangular MFs}$  in the third dimension), represented on figure 4.39, are added.

It would have been possible to use a chromosome based on only 21 genes and determine the GT2-FLC according to the results of the IT2-FLC best individuals. However, such a solution doesn't guarantee a global optimum result but a local optimum one. The use of 107 genes aims at determining the global optimum for the GT2-FLC. Moreover, the size of the populations is changed to 108 individuals instead of 88. The number of individuals or the size of a population is chosen in order to have as many genes as individuals.

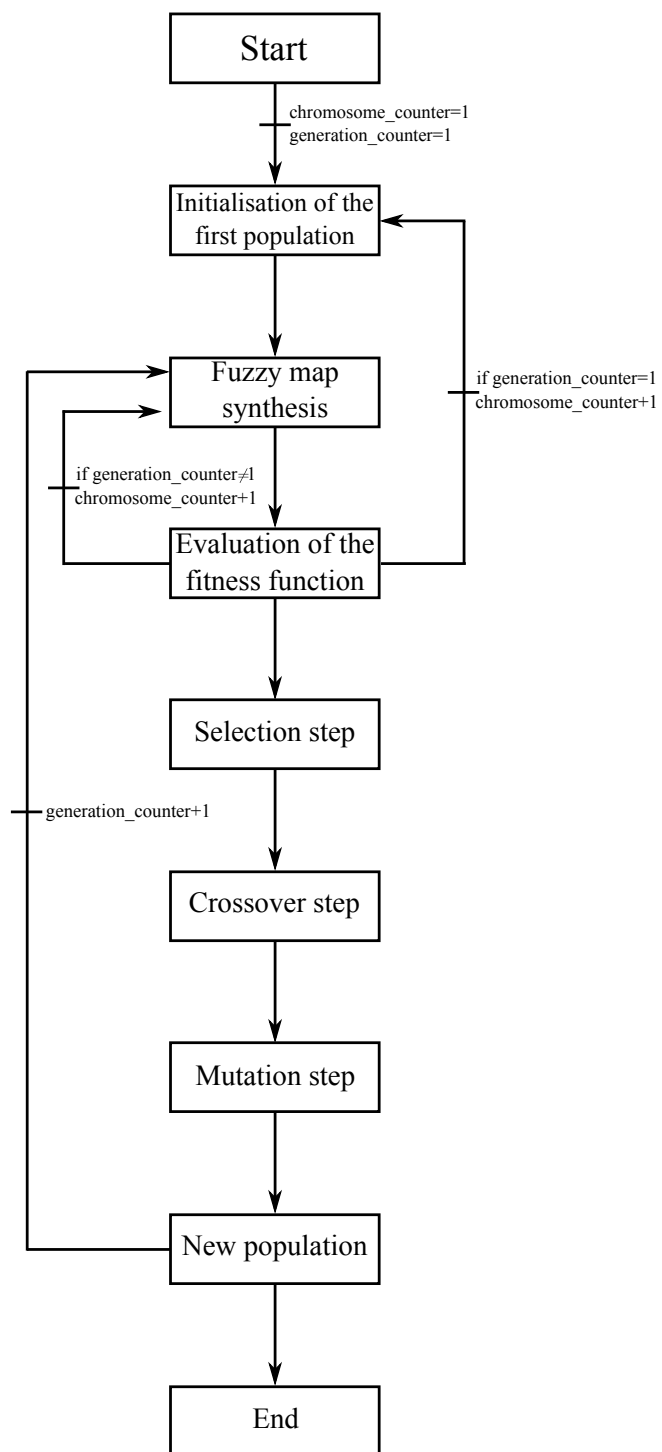


Figure 4.37: Implemented Genetic Algorithm

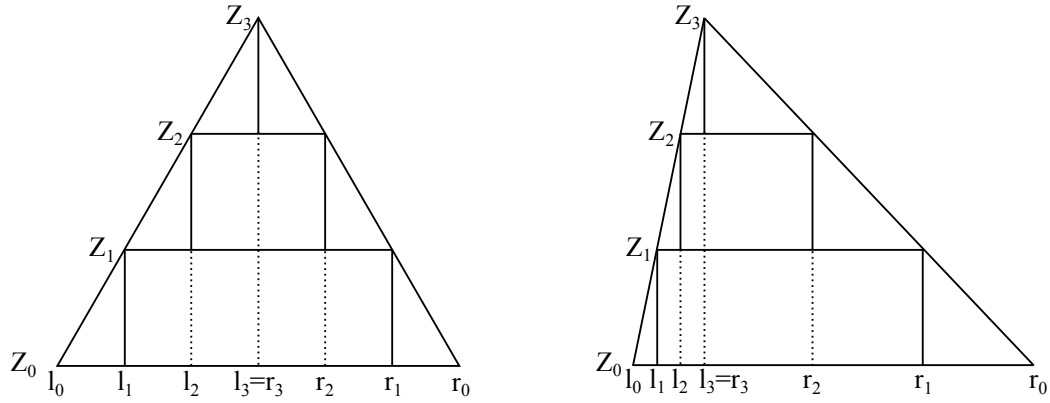


Figure 4.38: Third dimension isoscele triangular Membership Functions

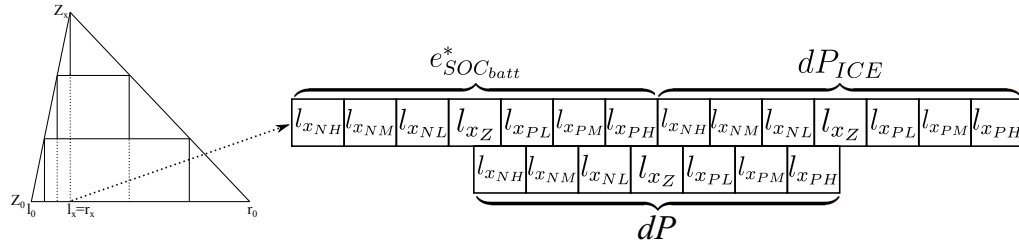


Figure 4.39: Modeling of the third dimension using a chromosome of 21 genes.

### Simulation results

Four different FLCs with the same structure (figure 4.32) are simulated. Now, their efficiency is compared. The comparison criterion is the total amount of energy delivered by the diesel driven generator set for the 30 different driving cycles. The four FLCs are based on:

- a survey-based type-2 fuzzy logic system for energy management in HEV [Sola12b],
- an optimized Type-1 FLC using a GA,
- an optimized Interval Type-2 FLC using a GA,
- an optimized General Type-2 FLC based on 10 zSlices using a GA.

In this study, the GA is performed on only one driving cycle (the most difficult one determined in the chapter 2). In theory, each driving cycle has its own set of optimized parameters. Thus, it would be necessary to create

a macro controller able to recognize in real time the type of driving cycle. However, this kind of work is the problematic of another study. For each studied FLCs, corresponding figures present the obtained and used MFs for the inputs and the output, the corresponding fuzzy control map and results of simulation. The evolution of the batteries and UCs' SOCs according to time are also depicted. SOCs' figures are superimposed to the evolution of the vehicle speed/acceleration versus time. The evolution of the powers delivered or consumed by the elements for the considered driving cycle are given. A zoom is then realized on a part of the powers' figure to study a more accurate representation of the evolution of those powers. A last figure represents the evolution of the bus voltage according to time. Power values, the bus voltage, the vehicle speed and acceleration are normalized on the figures.

### Comparison of the fuzzy maps

**Survey based Type-2 Fuzzy Logic Controller** This FLC has been designed in [Sola12b] using human expertise. As a first approach, the optimization of the FLC's parameters had not been considered. The survey using linguistic labels was conducted among ten experts on HEVs. Figures 4.40 to 4.43 present the obtained MFs and fuzzy map using the human expertise method. IT2 MFs were implemented for the FLC inputs and centroids for the output.

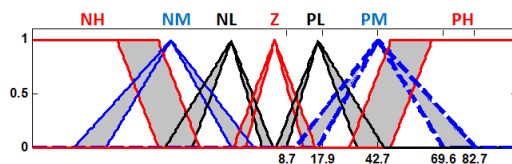


Figure 4.40:  $dP$  Membership Functions implemented in [Sola12b]

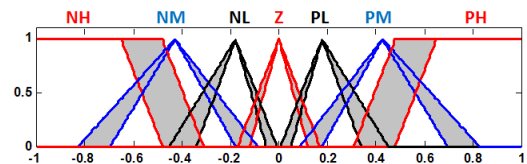


Figure 4.41:  $e_{SOC_{batt}}^*$  Membership Functions implemented in [Sola12b]

The figure 4.43 is a representation of the evolution of the output of the FLC ( $dP_{ICE}$ ) according to the two inputs ( $dP$  and  $e_{SOC_{batt}}^*$ ).

**Optimized Type-1 Fuzzy Logic Controller using a Genetic Algorithm** The MFs' parameters of the optimized T1-FLC are determined using the presented GA (the chromosome is made up of 51 genes or parameters). Triangular and trapezoid MFs are also used for inputs (figures 4.44 and 4.45) and singletons for the output (figure 4.46). The obtained fuzzy map is represented on figure 4.47.

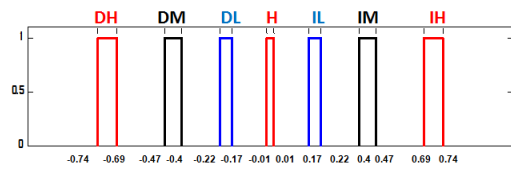


Figure 4.42:  $dP_{ICE}$  Membership Functions implemented in [Sola12b]

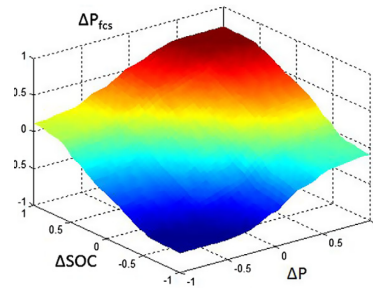


Figure 4.43: Fuzzy map controller implemented in [Sola12b]

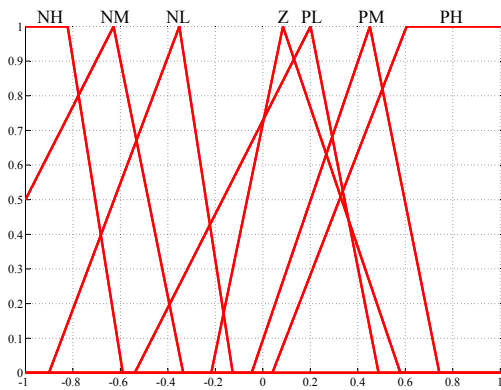


Figure 4.44:  $dP$  Membership Functions implemented for optimized T1-Fuzzy Logic Controller

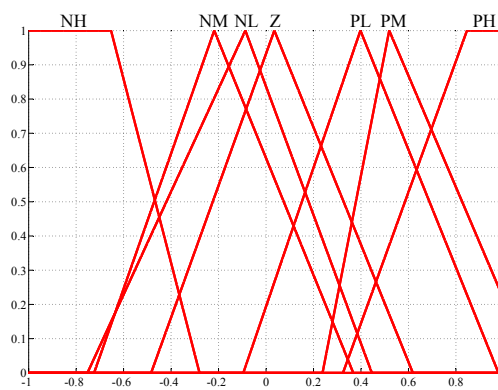


Figure 4.45:  $e^*_{SOC_{batt}}$  Membership Functions implemented for optimized T1-Fuzzy Logic Controller

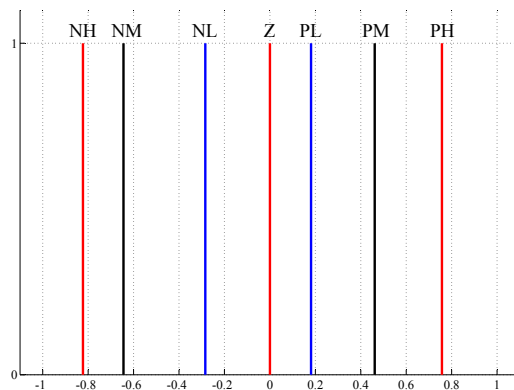


Figure 4.46:  $dP_{ICE}$  Membership Functions implemented for optimized T1-Fuzzy Logic Controller

**Optimized Interval Type-2-Fuzzy Logic Controller using a Genetic Algorithm** The optimized IT2-FLC has its MFs' parameters deter-

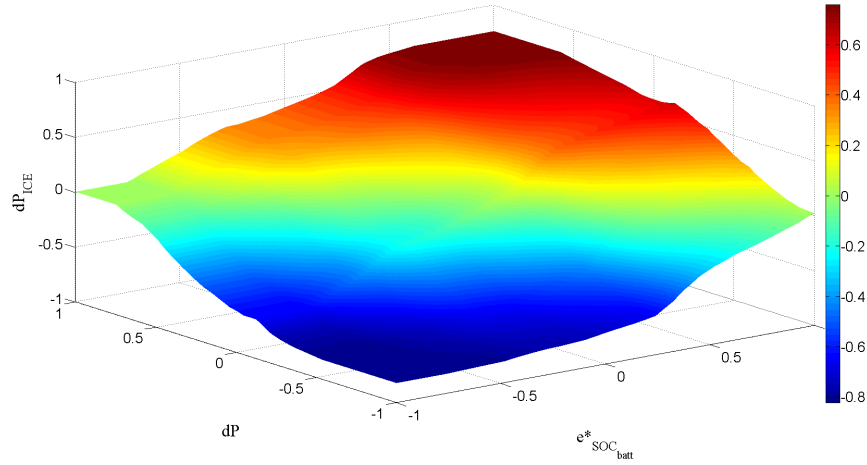


Figure 4.47: Fuzzy map controller implemented for optimized T1-Fuzzy Logic Controller

mined using the presented GA with 86 genes to represent one individual. Triangular MFs are used for inputs (figures 4.48 and 4.49) and interval MFs for the output (figure 4.50). The obtained fuzzy map is represented on figure 4.51. The Footprint Of Uncertainty (FOU) is the shaded area on figures 4.48 and 4.49.

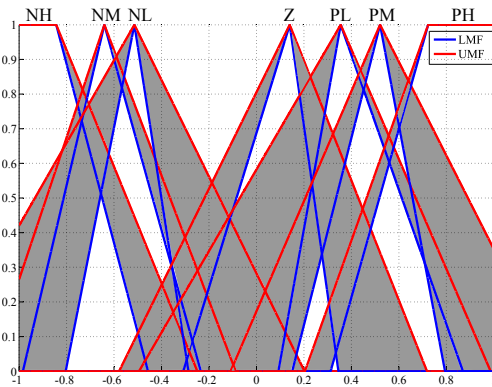


Figure 4.48:  $dP$  Membership Functions implemented for optimized IT2-Fuzzy Logic Controller

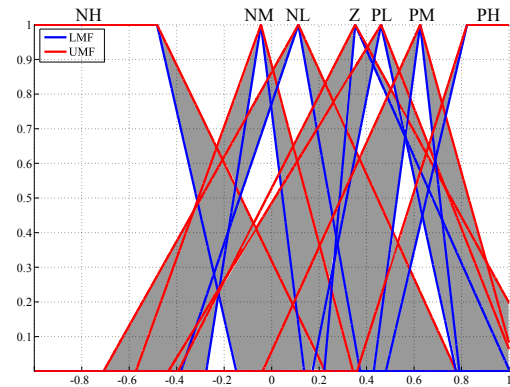


Figure 4.49:  $e^*_{SOC_{batt}}$  Membership Functions implemented for optimized IT2-Fuzzy Logic Controller

Figure 4.52 presents the differences between the two fuzzy maps describing the optimized T1 and IT2-FLCs.

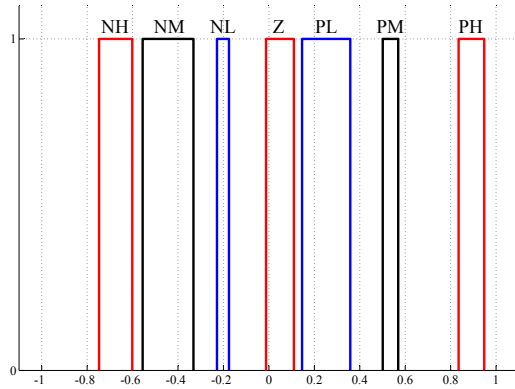


Figure 4.50:  $dP_{ICE}$  Membership Functions implemented for optimized IT2-Fuzzy Logic Controller

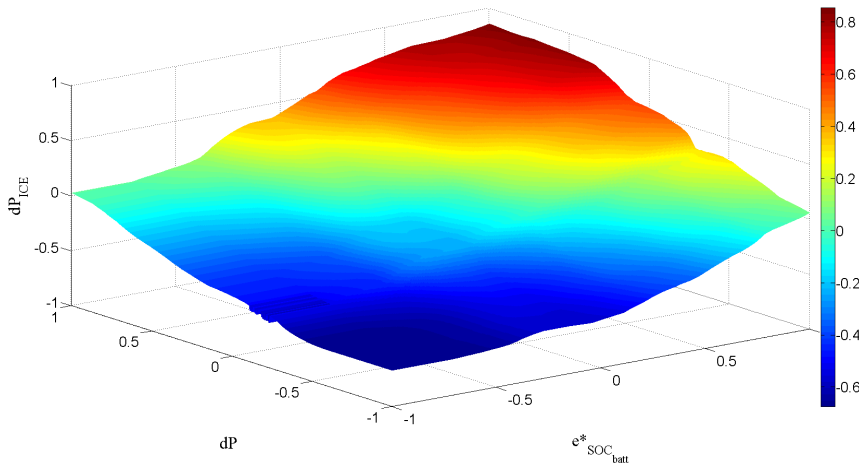


Figure 4.51: Fuzzy map controller implemented for optimized IT2-Fuzzy Logic Controller

**Optimized General Type-2 Fuzzy Logic Controller using a Genetic Algorithm** A possible way to improve the GT2-FLC efficiency based on triangular MFs is to use the same GA but with a different chromosome. Thus, a new optimized set of parameters describing the summits of the triangular MFs (figure 4.38) is obtained. The figure 4.56 represents the new fuzzy map of this optimized GT2-FLC generated by the new MFs for inputs (figures 4.53 and 4.54) and the output (figure 4.55) and the figure 4.57 presents the differences between this optimized GT2-FLC and the previous optimized IT2-FLC.

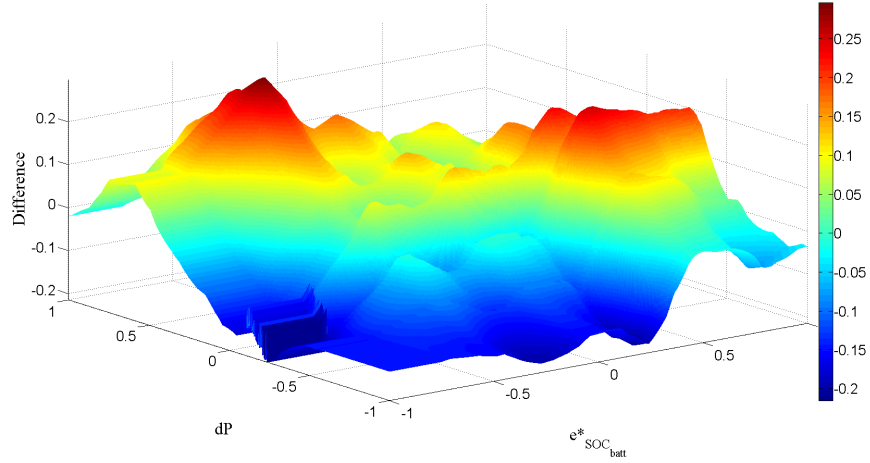


Figure 4.52: Differences between the optimized T1 (figure 4.47) and optimized IT2 (figure 4.51) fuzzy map controllers

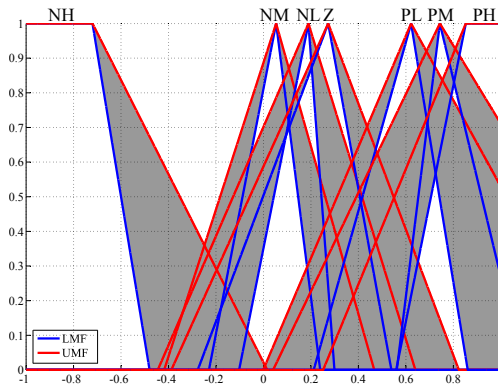


Figure 4.53:  $dP$  Membership Functions implemented for optimized GT2-Fuzzy Logic Controller

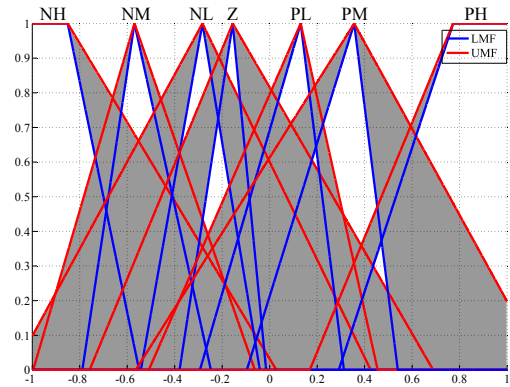


Figure 4.54:  $e^*_{SOC_{batt}}$  Membership Functions implemented for optimized GT2-Fuzzy Logic Controller

**Comparison of the efficiency of the implemented Fuzzy Logic Controllers** To check if the presented differences between the 4 implemented FLCs have a significant impact on the studied system, different simulation results are now presented. Simulation results are based on:

- the evolution of the power delivered by the sources and dissipated by the rheostat,
- the evolution of the batteries and UCs' SOC<sub>s</sub> according to the vehicle's speed and acceleration,

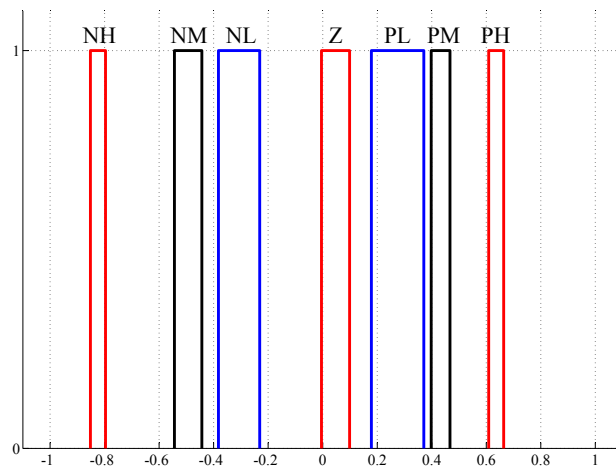


Figure 4.55:  $dP_{ICE}$  Membership Functions implemented for optimized GT2-Fuzzy Logic Controller

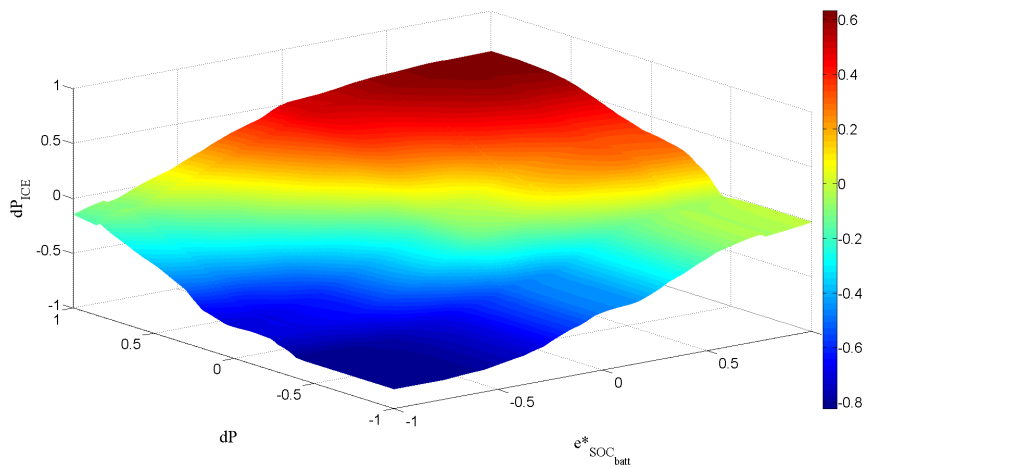


Figure 4.56: Fuzzy map controller implemented for optimized GT2-Fuzzy Logic Controller

- the bus voltage control to guarantee the system stability,
- the total amount of energy delivered by the diesel driven generator set according to the considered synthesized FLC and to the driving cycle.

**Power distribution** The figure 4.58 aims at proving the good working of the implemented intelligent EMS in terms of powers' repartition between the different on-board sources. Indeed, the total power required by the mis-

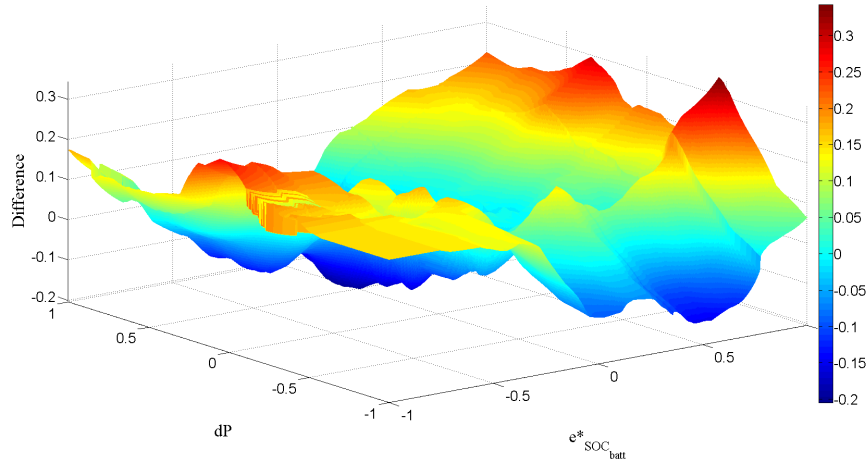


Figure 4.57: Differences between the optimized IT2 (figure 4.51) and optimized GT2 (figure 4.56) fuzzy map controllers

sion is provided by the sum of all the power sources (equation 4.18). In the case of a conventional diesel-electric vehicle, the primary source (diesel driven generator set) had to ensure the totality of the mission by itself. In other words, according to figure 4.58, it had to ensure 100% of the power peaks of the mission (1 on the ordinate axis of the graph). Now, the hybridization of the system and the implemented intelligent EMS permits to reduce by 40% the use of the diesel driven generator set thanks to the batteries and UCs (at time = 2h). This power peak reduction makes it possible to downsize also the primary source of about 40%.

The figure 4.59 is a zoom of the figure 4.58. This figure confirms the good working of the sub-EMSs. Indeed, UCs (respectively batteries) provide the high frequencies (respectively the low frequencies) of the power mission thanks to the implemented low pass filter and batteries are recharged when necessary.

**Batteries and Ultra-Capacitors' States Of Charge** The figure 4.60 represents the evolution of the batteries' SOC and the acceleration of the vehicle according to time. In accordance to equation 4.20, batteries are solicited (for charging and discharging) during acceleration phases of the vehicle. Moreover, the implemented EMS limits their SOC between 70% and 90%. The batteries are fully charged (90%) when starting and finishing the driving cycle. Indeed, it permits considering the start of the locomotive in good conditions without wasting time by recharging them if necessary for

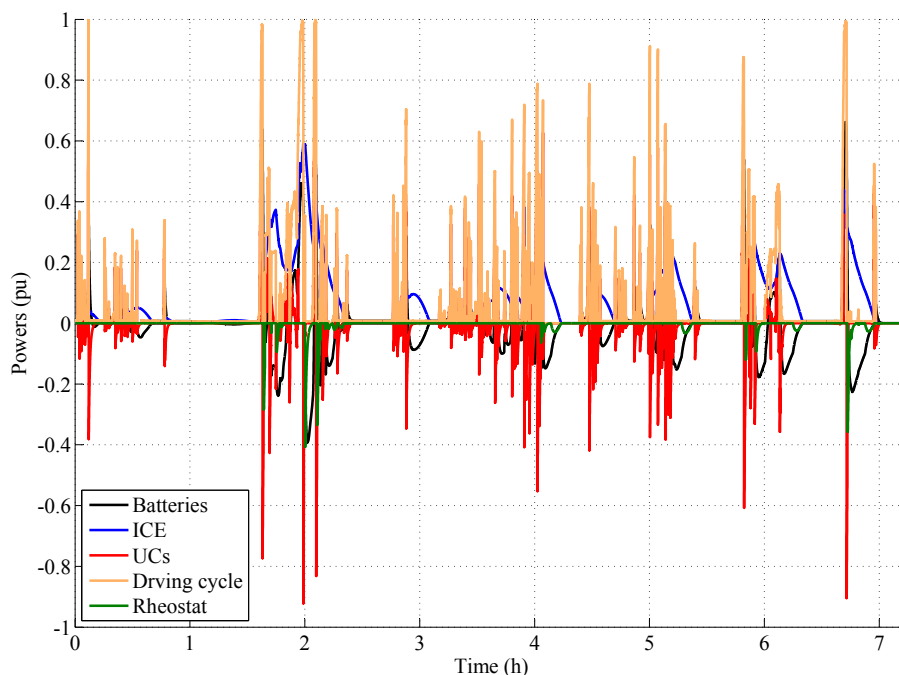


Figure 4.58: Evolution of the different powers (driving cycle, batteries, Internal Combustion Engine, UCs and rheostat) according to time

the next freight activity.

Figure 4.61 represents the evolution of the UCs' SOC and the speed of the vehicle according to time. In accordance with the equation 4.22, UCs are used when the vehicle is in motion and are charged when it is stopped. Their SOC is also limited between 50% and 100% (equation 4.21).

**Bus voltage control** It is important to verify the good control of the bus voltage in order to have a stability of the whole system. Figure 4.62 confirms that the implemented EMS also permits controlling it during all the driving cycle (around 7h in this case).

**Comparison of the 4 Fuzzy Logic Controllers for the 30 driving cycles of the vehicle** The previous remarks and results show the effectiveness of the intelligent EMS which has been implemented. Some considerations about powers were also underlined. Thus, energetic comparisons are now realized. Comparisons aim at determining the efficiencies of the 4 different FLCs in reducing the use of the diesel engine.

The table 4.6 presents the total amount of energy delivered by the primary source for the 30 different driving cycles and the 4 FLCs. According to the

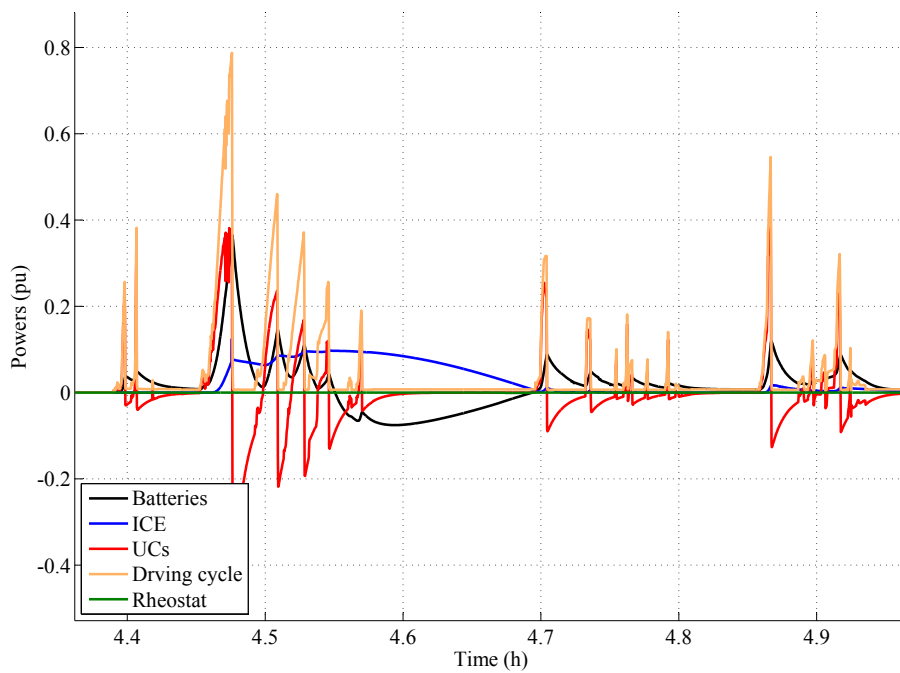


Figure 4.59: Zoom on the evolution of the different powers (driving cycle, batteries, Internal Combustion Engine, UCs and rheostat) according to time

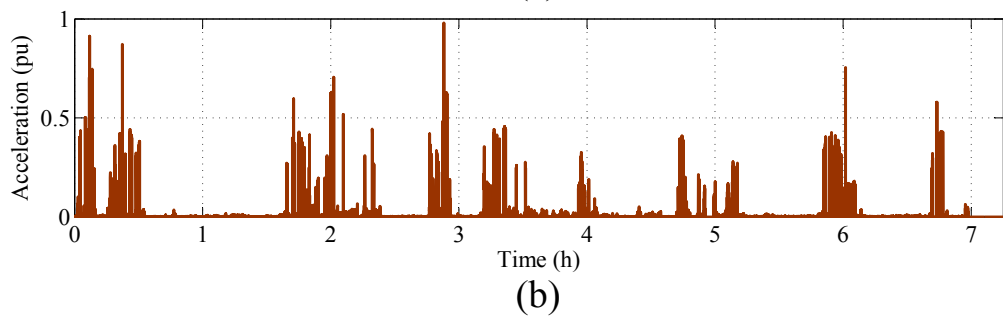
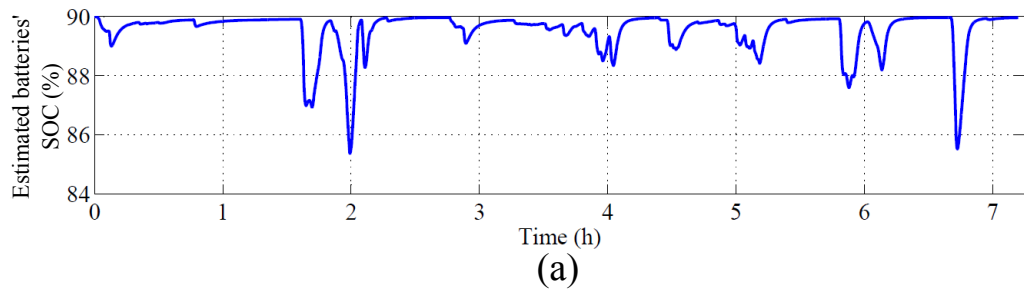


Figure 4.60: Evolution of the estimated batteries' SOC (a) and evolution of the acceleration of the vehicle (b) according to time

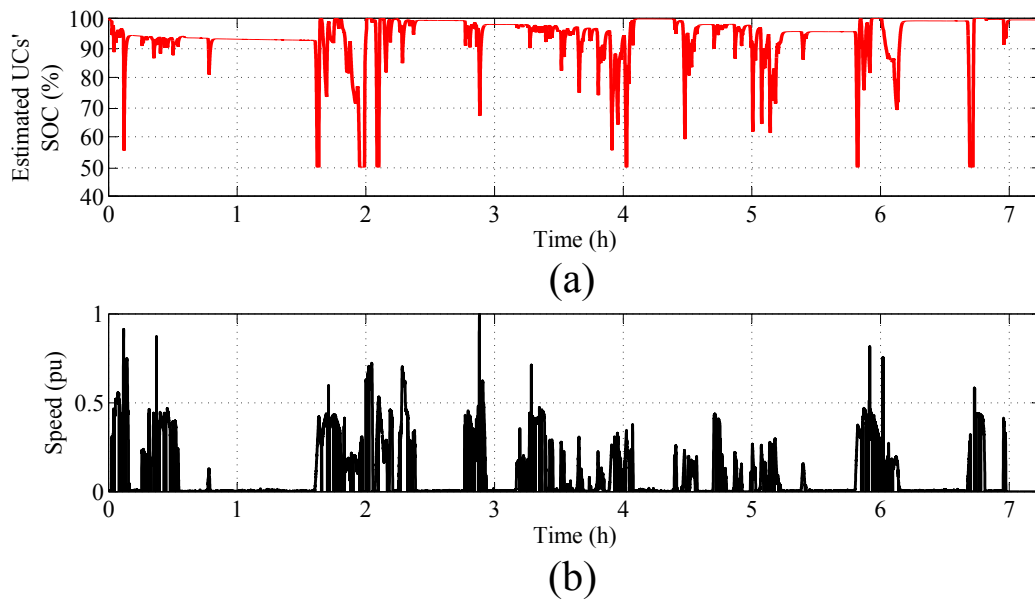


Figure 4.61: Evolution of the estimated UCs' SOC (a) and evolution of the speed of the vehicle (b) according to time

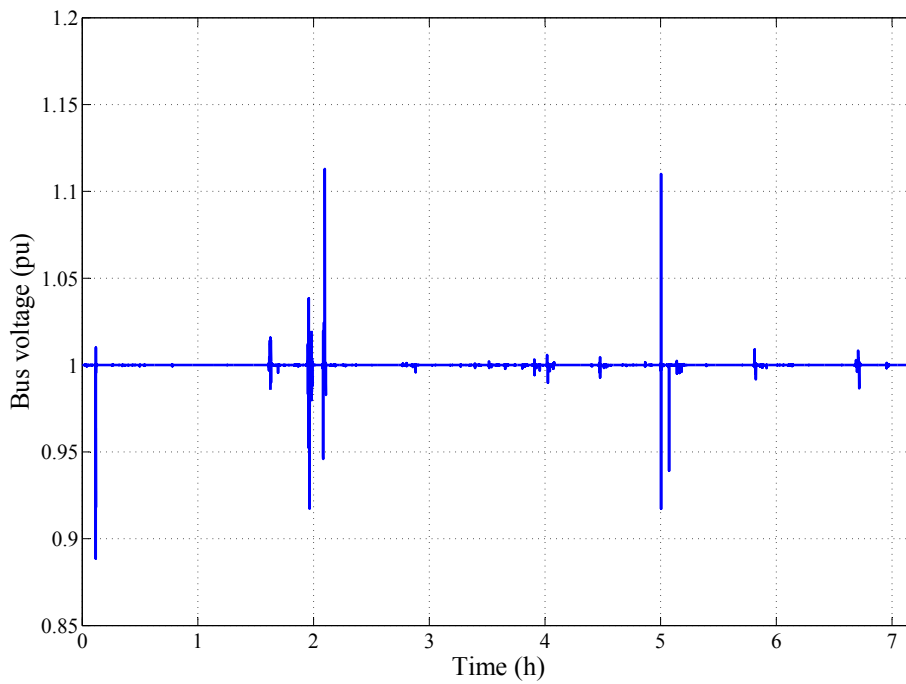


Figure 4.62: Evolution of the bus voltage according to time

	Controller	Energy (MJ)		Controller	Energy (MJ)		Controller	Energy (MJ)
Mission 1	IT2 (survey)	17,3	Mission 6	IT2 (survey)	989	Mission 11	IT2 (survey)	932,3
	T1 (GA)	16,77		T1 (GA)	779,904		T1 (GA)	744,164
	IT2 (GA)	16,029		IT2 (GA)	773,092		IT2 (GA)	733,375
	GT2 (GA)	15,701		GT2 (GA)	778,292		GT2 (GA)	741,069
Mission 2	IT2 (survey)	5,1	Mission 7	IT2 (survey)	1105,7	Mission 12	IT2 (survey)	911,9
	T1 (GA)	5,2805		T1 (GA)	917,883		T1 (GA)	677,404
	IT2 (GA)	5,3657		IT2 (GA)	894,858		IT2 (GA)	671,76
	GT2 (GA)	5,2805		GT2 (GA)	903,13		GT2 (GA)	675,607
Mission 3	IT2 (survey)	30,9	Mission 8	IT2 (survey)	92,2	Mission 13	IT2 (survey)	611,4
	T1 (GA)	32,86		T1 (GA)	86,829		T1 (GA)	504,564
	IT2 (GA)	32,944		IT2 (GA)	84,697		IT2 (GA)	501,874
	GT2 (GA)	32,668		GT2 (GA)	83,644		GT2 (GA)	504,197
Mission 4	IT2 (survey)	1042,6	Mission 9	IT2 (survey)	803,1	Mission 14	IT2 (survey)	96,8
	T1 (GA)	866,32		T1 (GA)	620,904		T1 (GA)	74,004
	IT2 (GA)	841,502		IT2 (GA)	621,886		IT2 (GA)	76,047
	GT2 (GA)	858,901		GT2 (GA)	620,428		GT2 (GA)	75,477
Mission 5	IT2 (survey)	882,6	Mission 10	IT2 (survey)	905,6	Mission 15	IT2 (survey)	751,6
	T1 (GA)	767,09		T1 (GA)	722,024		T1 (GA)	583,984
	IT2 (GA)	766,632		IT2 (GA)	712,955		IT2 (GA)	582,673
	GT2 (GA)	766,22		GT2 (GA)	718,304		GT2 (GA)	583,554
Mission 16	IT2 (survey)	501,1	Mission 21	IT2 (survey)	30,4	Mission 26	IT2 (survey)	1032,1
	T1 (GA)	407,704		T1 (GA)	27,944		T1 (GA)	867,1637
	IT2 (GA)	411,743		IT2 (GA)	29,52		IT2 (GA)	868,906
	GT2 (GA)	411,628		GT2 (GA)	28,25		GT2 (GA)	879,207
Mission 17	IT2 (survey)	781,2	Mission 22	IT2 (survey)	1722,4	Mission 27	IT2 (survey)	231,8
	T1 (GA)	674,504		T1 (GA)	1355,284		T1 (GA)	182,644
	IT2 (GA)	672,532		IT2 (GA)	1353,204		IT2 (GA)	184,056
	GT2 (GA)	674,693		GT2 (GA)	1327,808		GT2 (GA)	183,853
Mission 18	IT2 (survey)	740,7	Mission 23	IT2 (survey)	133,8	Mission 28	IT2 (survey)	1973,2
	T1 (GA)	638,984		T1 (GA)	108,873		T1 (GA)	1612,544
	IT2 (GA)	634,972		IT2 (GA)	105,284		IT2 (GA)	1566,332
	GT2 (GA)	640,912		GT2 (GA)	106,179		GT2 (GA)	1607,489
Mission 19	IT2 (survey)	703,2	Mission 24	IT2 (survey)	138,1	Mission 29	IT2 (survey)	982,9
	T1 (GA)	537,724		T1 (GA)	117,244		T1 (GA)	786,344
	IT2 (GA)	537,894		IT2 (GA)	119,093		IT2 (GA)	764,731
	GT2 (GA)	537,354		GT2 (GA)	118,594		GT2 (GA)	741,1899
Mission 20	IT2 (survey)	806,7	Mission 25	IT2 (survey)	1268,7	Mission 30	IT2 (survey)	459,5
	T1 (GA)	630,664		T1 (GA)	1002,284		T1 (GA)	394,104
	IT2 (GA)	618,2		IT2 (GA)	990,693		IT2 (GA)	395,699
	GT2 (GA)	630,703		GT2 (GA)	994,109		GT2 (GA)	397,882
	IT2 - survey							
	T1 - GA							
	IT2 - GA							
	GT2 - GA							

Table 4.6: Energy provided by the diesel driven generator set according to the 4 implemented FLCs

results:

- the survey based IT2 FLC gives better results for 2 driving cycles,
- the optimized T1-FLC gives better results for 7 driving cycles,
- the optimized IT2-FLC gives better results for 14 driving cycles,
- the optimized GT2-FLC gives better results for 7 driving cycles.

As a result, for 93.3% of the driving cycles, optimized controllers give better results than the FLC based on a survey. Among the optimized FLCs, Type-2 optimized FLCs present better results than the optimized T1 one for 75% of the considered driving cycles. Thus, the GA permits to reduce the use of the ICE (or increase the use of the batteries and UCs) and Type-2 Fuzzy Logic better takes into account the discussed uncertainties inherent to the system. However, among the optimized Type-2 FLCs, the optimized GT2-FLC only gives better results than the IT2-FLC for 50% of the considered driving cycles. The GT2-FLC best results only concern 23.3% of the 30 missions. Comparing the survey based on FLC and the optimized T1-FLC, the best improvement is obtained for the mission 14 with 131% ( $100 \times \frac{96.8}{74.004}$ ) improvement. In the same way, the mission 12 presents the best improvement between the optimized IT2 and survey based FLCs with 136% and 133% for the mission 29 between the optimized GT2 and the survey based FLCs.

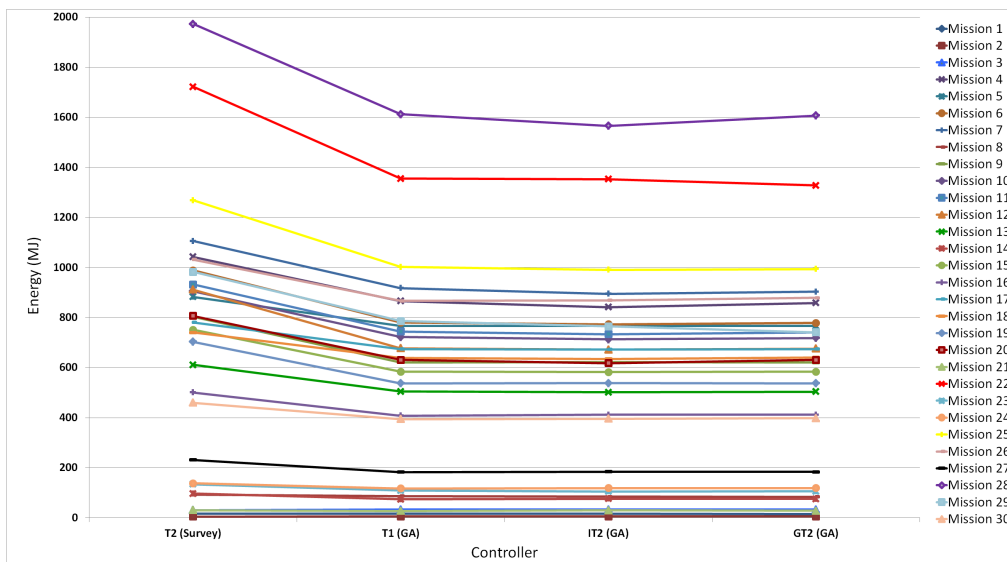


Figure 4.63: Evolution of the energy delivered by the diesel driven generator set according to the implemented controllers and the considered power mission

The figure 4.63 presents the results of the table in a different way. The total amount of energy provided by the ICE is represented according to the FLCs and the considered driving cycle. The limited improvement of the optimized GT2-FLS could be explained by the choice of the secondary membership function based on triangular MFs. Even if the summits of the triangles are parameters of the GA, this approximation seems to be insufficient to model this third dimension and obtain better results compared to

the other FLCs. Moreover, this limited improvement is also explained by the optimization process which is performed on a specific driving cycle which is characterized by important power peaks, fast power variations and important time duration. These characteristics are equally the same for most of the driving cycles presenting better results with the GT2-FLCs (mission number 22 for instance). However, the driving cycles presenting characteristics contrary to the previous ones (poor time duration, low power peaks and slow power variations), like the mission number 2, do not present improvement in the energy minimization.

### 4.3 Chapter conclusion

The first application presented the control of the output voltage of a DC/DC buck converter test bench using a fuzzy logic controller. It has the same structure as a Proportional-Integral-Derivative controller with a non-linear behaviour. The Proportional-Derivative part is represented by the implemented fuzzy map. The comparison between T1 and IT2-FLCs, based on the Integral Absolute Error (IAE) criteria, has proven that the IT2 approach gives better performance in the face of highly uncertain conditions. However, a thinner mesh grid is not more accurate than a "rougher" one. Even if, a high number of z-slices provides better results in favour of the GT2-FL approach compared to the IT2-FL approach, a high number of z-slices do not necessarily improve the control performances. A more accurate representation of the GT2-MFs based on data directly sampled from the device is another possible approach.

The second application dealt with the design of the HEL's EMS. A first EMS only based on the SOCs' limitation and the frequency repartition of the power permitted to validate the good implementation of the on-board sources' models and controls. Another EMS, based on Type-1 and Type-2 Fuzzy Logic control, was also implemented. Due to the complexity of the structure of the HEL, the dynamical behaviours and the characteristics of the on-board sources, the fuel consumption minimization problem get complicated. To address it, optimized T1, IT2 and GT2 FLSs were employed for fuel economy purpose. The simulation results have shown that:

- the 4 proposed FLSs are able to manage the energy distribution,
- the SOCs' limitations are respected,
- the dynamics of the power are shared between the ICE-batteries and the UCs,

- the bus voltage remains well controlled.

According to the aim of the GA, optimized T2-FLSs are more effective than the optimized T1-FLS which is also more effective than the survey based IT2-FLS. However, because of the results of the GT2-FLS, the future ongoing research would probably focus on a more accurate determination of the third dimension MFs. Moreover, the determination of a new hybrid driving cycle including the specificities of all the missions and the improvement of the GA are also of high interest. Moreover, to be fully independent from the filtering cutoff frequency, a wavelet transform algorithm can be implemented. Indeed, wavelets are recent tools in signal processing. They permit the analysis of local properties in a non stationary signal, and for different scales of time [Ibra11]. Moreover, the use of other real time methods such as a wavelet non linear autoregressive neural network permits both separating high and low frequency components from a real power demand signal and predicting future values of this power demand signal [Ibra13].



# Conclusion and outlooks

Nowadays, the ecological, environmental and economical contexts relative to the transport are important sociological issues. Even if the railway transport is more efficient than other transport means, the sector is also submitted to the same problems. The European freight activities are mainly performed thanks to shunting locomotives powered by diesel-electric propulsions. To save money, reduce pollution and noise, limit fuel consumption and meet the energetic needs, it is necessary to develop new solutions in order to efficiently generate, store, convert and deliver the electrical energy. Thus, these challenges to be faced by human societies in energy and transportation presented in chapter 1 can be resolved through hybrid electric vehicles and efficient energy management strategies. This thesis comes within this context. It takes part of the FEMTO-ST Laboratory and the Alstom Transport research works in electrical engineering. Here, the research work proposes new scientific contributions in the modelling of a hybrid electric locomotive using the EMR and the development of the system's energy management strategy partly based on the optimisation of a type-2 FLC.

Having discussed the topology of a conventional electric locomotive and the expected improvements toward a hybrid electric architecture and the secondary sources' sizing according to the most constraining driving cycle in the chapter 2, the modelling of the locomotive's on-board sources is presented in the chapter 3. The hybrid electric locomotive presents a series architecture and it is made up of a bank of batteries, UCs, a diesel driven generator set and a rheostat. A bus capacity ensures the electrical energy balance of the system. The diesel driven generator set supplies energy to the system and permits recharging the batteries and the ultra-capacitors. The rheostat dissipates energy if necessary. A first dynamical EMR of the diesel engine is developed, the modelling and the parameter identification of the ultra-capacitors was performed in previous researches in the laboratory and experimental characterization of the batteries contributed to the improvement of their modelling. The batteries' experimental characterizations aim

at improving the original model's insufficiencies and assumptions relative to the thermal behaviour. Complementary experimental results ( $C_3$  rate) are available appendix D. The MCS and then the PCS identifications (appendices A and C) emphasize the physical and virtual sensors to be set up and consider the technical and economical constraints of the locomotive. For instance, they estimate the batteries and ultra-capacitors SOCs.

These innovative solutions in the modelling, the design and the implementation of a hybrid electric locomotive get ahead of the implementation of a new energy management strategy. It remains to be a crucial research subject which is addressed in chapter 4. This chapter focuses on the application of the fuzzy logic control through two applications:

- the control of the output voltage of a converter using type-1 and type-2 FLCs. This first application aims at evaluating the performances of the type-1 and type-2 fuzzy logic controllers in real time conditions and at performing preliminary tests. The test bench is easy to implement, to use, relatively economical and the evaluation is performed under controlled conditions in Laboratory.
- the design, the implementation and the validation by simulation of the EMS partly based on the optimisation of the used FLC's parameters using a GA.

Strategies' designs (second application) are decisive in the global efficiency of the hybrid electric system. This design obviously depends on the architecture of the system but its efficiency greatly depends also on the "designer" who is above all human. Thus, as much energy management strategies exist as designers. The developed EMS takes into account the sources' specifications, dynamics and limitations using real-time information (SOCs, bus voltage, speed of the locomotive...). The batteries are used with the diesel engine to provide the power's low frequencies of the driving cycle and the UCs, the high frequencies. Previous knowledge of the driving cycle is not known. Thus, the fuzzy logic which belongs to the on-line techniques has been identified to manage the global control of the diesel driven generator set. However, contrary to the off-line techniques, the on-line methods do not necessarily reach an optimal solution. Thus, the discussed efficiency of the EMS greatly depends on the parameters of the FLC. A previous work of the FEMTO-ST laboratory proposed a human expertise to design the FLC. This approach which was based on the "designer"'s knowledge was not optimal. Even if the use of the type-2 fuzzy logic permitted better considering

the uncertainty in the answers of the experts, it still remained to be a non-optimal solution. Here, to fulfil the requirements, the EMS is implemented in Matlab Simulink. The control surface is based on fuzzy logic controllers which parameters have been optimised using a GA in order to minimise the fuel consumption of the locomotive.

Finally, the simulation results of the EMS confirm the respect of the specifications and the reduction of the fuel consumption of the system thanks to the optimisation of the FLC using a GA. However, the solutions do not present enough evidence to affirm that optimised type-2 FLCs are always better performing than the optimised type-1 FLC. Indeed, performing the optimisation process on a specific driving cycle remains to be a limitation when applying it to the overall driving cycles.

## Research outlooks

The presented research works open up interesting perspectives:

- the improvement of the modelling of the ICE. The exhaust manifold dynamics, the integration of an exhaust gas recirculation valve, the temperature variation in the system are interesting points to be developed. They are also necessary in order to improve the dynamical behaviour of the model compared to static models like cartographies.
- The improvement of the modelling of the batteries. Indeed, the EMS is built in order to limit the batteries' stress (limitation of their SOC and use of a low pass filter) and avoid premature degradation. Long time experimental tests will be interesting to better take into account the batteries ageing according to their DOD, the operating temperature...
- The improvement of the optimisation process. Instead of performing it on the most constraining driving cycle, using a generic driving cycle regrouping all their characteristics may permit to improve the fuzzy logic controller performances [Jaaf12a, Jaaf12b].
- The extension of the optimisation problem to the sizing problem. Indeed, a very precise EMS improves the efficiency of the studied hybrid electric system and in consequence, the number of secondary sources' cells to be used on-board can be limited or reduced. However, a more basic EMS driving to a least efficiency would impose an over-sizing of the secondary sources. In other words, the sizing depends of the EMS and the EMS depends of the sizing too. This global problem may be solved by introducing into the existing GA both the FLC and sizing problem parameters.

- The replacement of the low pass filter by a wavelet transform. The cut-off frequency of the low pass filter is an important parameter to share the batteries and ultra-capacitors powers. Nevertheless, it induces a phase difference. The wavelet transform is able to perform the signal decomposition into high and low frequencies without introducing a phase difference.
- In real world applications physical devices such as sensors and actuators are susceptible to a wide range of uncertainties (environmental conditions, signal noise...). The improvement of the general type-2 FLC membership functions with experimental tests to determine the system sensibility to the noise and environmental conditions is necessary.





# Appendix A

## The Energetic Macroscopic Representation

### A.1 Energetic Macroscopic Representation

The EMR is a synthetic representation for complex systems. The formalism aims at modelling interactions between systems and sub-systems. The representation is based on the integral causality and graphically shows the action and reaction phenomena between a system and its environment [Lhom08]. The different used pictograms and colors permit a quick identification of the different elements of a system. The formalism is made up of four categories of elements:

- The sources. They are characterised by a light green oval and a dark green outline. Energy receiver or generator, they present only one input and output.
- The conversion elements. They are represented by an orange square or circle with a red outline. They realize an energetic conversion between two sources with no accumulation of energy. They present action and reaction inputs/outputs. If necessary a third input called adjustment input is available.
- The coupling elements. They are characterised by an orange square or circle superposition with red outlines. It explicitly traduces a power flow sharing out. An upstream coupling element distributes energy whereas a downstream coupling element collects it.
- The accumulation elements are represented by a rectangle with an orange oblique line and a red outline. They represent the energy accumu-

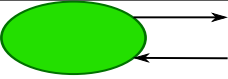
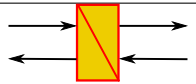
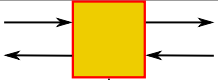
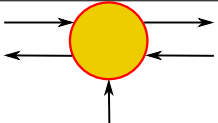
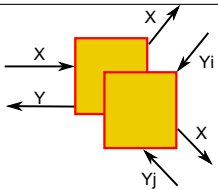
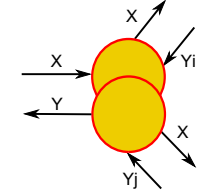
	Source
	Accumulation
	Mono-physical converter
	Multi-physical converter
	Mono-physical coupling
	Multi-physical coupling

Table A.1: Energetic Macroscopic Representation blocks [Boul10b]

lation between two energy sources. They respect the integral causality principle.

The table A.1 presents the four categories of elements [Chen09].

All elements intervene in different physical fields (electrical, thermal, mechanical, chemical...). The product of the action and reaction variables is always homogeneous to a power [Bous05]. The table A.2 presents the kinetic and corresponding potential variables for different physical fields.

## A.2 Maximum Control Structure

The MCS is deduced from the EMR and it is based on the mathematical reversal principle supposing all variables are measurable [Bous03]. The MCS design is performed in:

	Effort (e)	Flow (f)
Electric	Voltage (V)	Current (A)
Mechanics	Strength (N)	Speed ( $m/s$ )
Rotation	Torque ( $N.m$ )	Radial speed (rad/s)
Hydraulics	Pressure ( $N/m^2$ )	Flow ( $m^3/s$ )
Thermal	Temperature (K)	Entropy flow ( $W/K$ )
Chemical	Gibbs energy ( $J/mol$ )	Molar flow ( $mol/s$ )

Table A.2: Kinetic and potential variables [Lhom06]

- determining the EMR of the studied system. The MCS quality depends on the choices and the formulated hypothesis for the system's modelling,
- determining the setting chain which depends on the system and the specifications (from the control variable to the global output to be controlled),
- reversing each element in accordance with the setting chain. The obtained chain corresponds to the control path.

The energetic transfer doesn't intervene in the MCS design.

The output of an element of accumulation is a state variable. The intern relationship is causal (integral) and can't directly be reversed. In accordance with the reversal principle, the output is controlled thanks to an indirect reversal. In the MCS version of the element, a controller is used. To highlight the causal characteristic of the controller, a blue parallelogram with a reversed oblique stroke is also used (figure A.1).

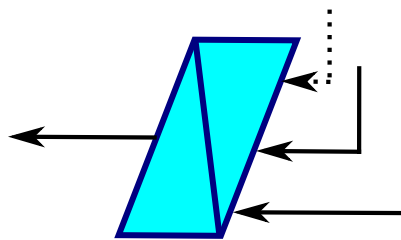


Figure A.1: Maximum Control Structure of an element of accumulation

The inversion of the equations doesn't rise problem for the conversion and the coupling elements if the considered equations and relationships are well known, stationary and linear or bilinear (figures A.2 and A.3).

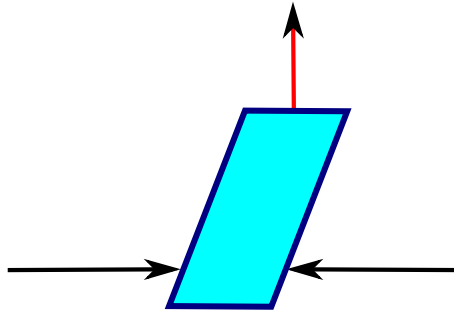


Figure A.2: Maximum Control Structure of an element of conversion

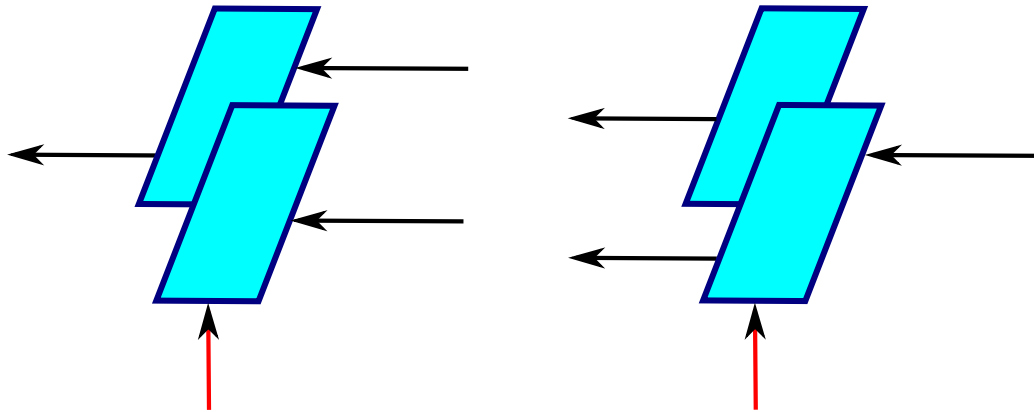


Figure A.3: Maximum Control Structure of a coupling element (upstream - left and downstream - right)

### A.3 Practical Control Structure

The MCS is a theoretical structure which maximises the system's operations and measures [Lhom11]. Simplifications are possible. They can deteriorate the control's performances in aid of a lower cost or easiness implementation. The PCS's deduction from the MCS is a compromise. Moreover, the control design is based on the following hypothesis: all variables are measurable. Thus, the control design approach aims at simplifying the control structure. In general, the method consists in making more complex the control structure as problems occur. The simplification benefit resides in the justification of all the performed simplifications. The PCS design is performed in simplifying the MCS (cost, calculating time, specifications...) and in estimating the non-measurable variables. For instance, electromotive forces are information required by the MCS of a machine. They are non measurable variables. Even if torque sensors exist, they remain to be expensive. Thus, the preferred

solution is not to measure it neither. The blocks have the same form like for the MCS ones (figures A.1, A.2 and A.3) but with a purple color.



# Appendix B

## The salient pole synchronous machine modelling

### B.1 The d-q synchronous reference frame

Equations that govern a three phase alternative machine depend on resistances, inductances and mutual inductances of its rotor and its stator. Those mutual inductances are linked to the relative position of the rotor with the stator. Thus, to simplify differential equations, it is easier to work in the d-q frame than in the three phase one.

Considering voltages, currents and flux three phase components as  $X_a$ ,  $X_b$ ,  $X_c$  and as  $X_d$ ,  $X_q$  in the dq frame, Park (equation B.1) and Concordia transformations permit to pass from one frame to the other one.

$$\begin{bmatrix} X_d \\ X_q \end{bmatrix} = \sqrt{\frac{2}{3}} \times \begin{bmatrix} \cos(\theta) & \cos\left(\theta - \frac{2\pi}{3}\right) & \cos\left(\theta + \frac{2\pi}{3}\right) \\ -\sin(\theta) & -\sin\left(\theta - \frac{2\pi}{3}\right) & -\sin\left(\theta + \frac{2\pi}{3}\right) \end{bmatrix} \begin{bmatrix} X_a \\ X_b \\ X_c \end{bmatrix} \quad (\text{B.1})$$

This operation can be done using Concordia transformation too (equations B.2, B.3).

$$\begin{bmatrix} X_\alpha \\ X_\beta \end{bmatrix} = \sqrt{\frac{2}{3}} \times \begin{bmatrix} 1 & -\frac{1}{2} & -\frac{1}{2} \\ 0 & \frac{\sqrt{3}}{2} & -\frac{\sqrt{3}}{2} \end{bmatrix} \begin{bmatrix} X_a \\ X_b \\ X_c \end{bmatrix} \quad (\text{B.2})$$

$$\begin{bmatrix} X_d \\ X_q \end{bmatrix} = \sqrt{\frac{2}{3}} \times \begin{bmatrix} \cos(\theta) & \sin(\theta) \\ -\sin(\theta) & \cos(\theta) \end{bmatrix} \begin{bmatrix} X_\alpha \\ X_\beta \end{bmatrix} \quad (\text{B.3})$$

with  $\theta$  the angle between the rotor and the stator.

## B.2 The salient pole synchronous machine model

The mathematical model of the salient pole synchronous machine is presented here. The machine corresponds to the figure B.1 in the three phase frame and figure B.2 in the Park frame.

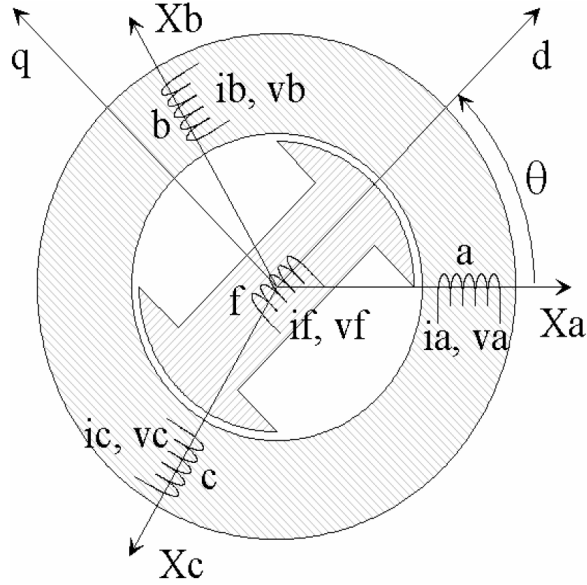


Figure B.1: Model of the synchronous machine in the three phase frame

The following convention is adopted:

- $L_d$ : equivalent inductance of the armature along d axis (H).
- $L_q$ : equivalent inductance of the armature along q axis (H).
- $R_s$ : equivalent resistance of the stator windings ( $\Omega$ ).
- $L_f$ : inductance of the inductor (H).
- $M_{sf}$ : mutual inductance between the stator and the rotor (H).
- $R_f$ : resistance of the inductor ( $\Omega$ ).
- $p$ : pole pair number,
- $f$ : friction coefficient,
- $J$ : rotor inertia.

To simplify equations, parameter M is defined as  $M = \sqrt{\frac{3}{2}}M_{sf}$ .

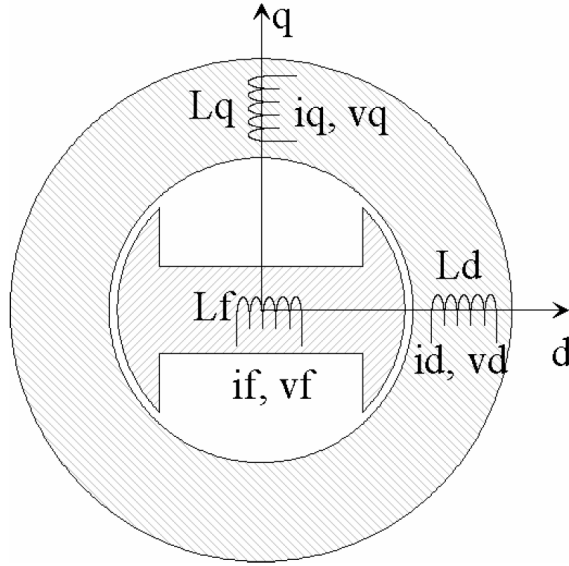


Figure B.2: Model of the synchronous machine in the three phase frame

## B.2.1 Parks' equations of the machine

### Voltages

$$V_d = R_s I_d + \frac{d\phi_d}{dt} - \omega_r \phi_q \quad (\text{B.4})$$

$$V_q = R_s I_q + \frac{d\phi_q}{dt} + \omega_r \phi_d \quad (\text{B.5})$$

$$V_f = R_f I_f + \frac{d\phi_f}{dt} \quad (\text{B.6})$$

### Flux

$$\phi_d = L_d I_d + M I_f \quad (\text{B.7})$$

$$\phi_q = L_q I_q \quad (\text{B.8})$$

$$\phi_f = L_f I_f + M I_d \quad (\text{B.9})$$

### Electromechanical torque

$$\Gamma_{load} = p(\phi_d I_q - \phi_q I_d) \quad (\text{B.10})$$

## B.2.2 dq currents decoupling

Differential equations (B.4 to B.6) are developed thanks to equations B.7 to B.9.

$$V_d = R_s I_d + L_d \frac{dI_d}{dt} - \omega_r \phi_q + M \frac{dI_f}{dt} \quad (\text{B.11})$$

$$V_q = R_s I_q + L_q \frac{dI_q}{dt} + \omega_r (L_d I_d + M I_f) \quad (\text{B.12})$$

$$V_f = R_f I_f + L_f \frac{dI_f}{dt} + M \frac{dI_d}{dt} \quad (\text{B.13})$$

An interdependence between d and q axis variables clearly appears. To express transfer functions between  $V_d$ ,  $V_q$  and  $I_d$ ,  $I_q$ , from equation B.11,  $\frac{dI_f}{dt}$  is replaced thanks to equation B.9.

$$V_d = R_s I_d + \frac{dI_d}{dt} \left( L_d - \frac{M^2}{L_f} \right) - \omega_r \phi_q + \frac{M}{L_f} \frac{d\phi_f}{dt} \quad (\text{B.14})$$

To solve the equation B.14 interdependence, the voltages  $V'_d$ - $V'_q$  (equation B.15) and electromotive forces  $e_d$ - $e_q$  (equation B.16) are defined.

$$\begin{cases} V'_d = R_s I_d + L_d \frac{dI_d}{dt} \\ V'_q = R_s I_q + L_q \frac{dI_q}{dt} \end{cases} \quad (\text{B.15})$$

$$\begin{cases} e_d = -\omega_r \phi_q + M \frac{dI_f}{dt} \\ e_q = \omega_r \phi_d \end{cases} \quad (\text{B.16})$$

Thus, equations B.11, B.12 can be simplified as:

$$\begin{cases} V_d = V'_d + e_d \\ V_q = V'_q + e_q \end{cases} \quad (\text{B.17})$$

and transfer functions modelling currents' dynamics are deduced:

$$\begin{cases} \boxed{\frac{I_d(s)}{V'_d(s)} = \frac{1}{R_s} \frac{1}{1 + \frac{L_d}{R_s} s}} \\ \boxed{\frac{I_q(s)}{V'_q(s)} = \frac{1}{R_s} \frac{1}{1 + \frac{L_q}{R_s} s}} \end{cases} \quad (\text{B.18})$$

### B.2.3 Inductor current decoupling

Because of equation B.13, it appears that another coupling with dq voltages exists.

$$\left\{ \begin{array}{l} \frac{dI_f}{dt} = \frac{1}{L_f} (L_f - R_f I_f) - \frac{M}{L_f} \frac{dI_d}{dt} \\ \Leftrightarrow \frac{dI_f}{dt} = \frac{1}{L_f} V_f - \frac{R_f}{L_f} I_f - \frac{M}{L_f} \frac{dI_d}{dt} \end{array} \right. \quad (\text{B.19})$$

Transfer function appears to be:

$$\left\{ \begin{array}{l} I_f(s) = \frac{\frac{1}{R_f}}{1 + \frac{L_f}{R_f}s} V_f(s) - \frac{\frac{M}{R_f}s}{1 + \frac{L_f}{R_f}s} I_d(s) \\ \Leftrightarrow I_f(s) = \frac{\frac{1}{R_f}}{1 + \frac{L_f}{R_f}s} (V_f'(s) + MsI_d(s)) - \frac{\frac{M}{R_f}}{1 + \frac{L_f}{R_f}s} I_d(s) \\ \Leftrightarrow \boxed{I_f(s) = \frac{\frac{1}{R_f}}{1 + \frac{L_f}{R_f}s} V_f'(s)} \end{array} \right. \quad (\text{B.20})$$



# Appendix C

## PI and IP controllers synthesis

### C.1 PI controller synthesis

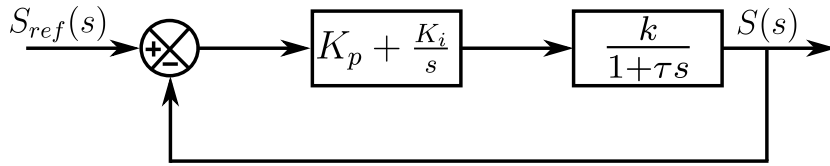


Figure C.1: PI controller structure

$$S(s) = \left( \frac{k}{1 + \tau s} \right) \left( K_p + \frac{K_i}{s} \right) (S_{ref}(s) - S(s))$$

$$\Leftrightarrow \frac{S(s)}{S_{ref}(s)} \left[ 1 + \left( \frac{k}{1 + \tau s} \right) \left( K_p + \frac{K_i}{s} \right) \right] = \left( \frac{k}{1 + \tau s} \right) \left( K_p + \frac{K_i}{s} \right)$$

$$\Leftrightarrow \frac{S(s)}{S_{ref}(s)} = \frac{\left( \frac{k}{1+\tau s} \right) \left( K_p + \frac{K_i}{s} \right)}{1 + \left( \frac{k}{1+\tau s} \right) \left( K_p + \frac{K_i}{s} \right)}$$

$$\Leftrightarrow \frac{S(s)}{S_{ref}(s)} = \frac{k \left( K_p + \frac{K_i}{s} \right)}{1 + \tau s + k \left( K_p + \frac{K_i}{s} \right)}$$

$$\Leftrightarrow \frac{S(s)}{S_{ref}(s)} = \frac{k K_p s + k K_i}{s + \tau s^2 + k K_p s + k K_i}$$

$$\Leftrightarrow \frac{S(s)}{S_{ref}(s)} = \frac{k K_i + k K_p s}{k K_i + s(1 + k K_p) + \tau s^2}$$

$$\Leftrightarrow \frac{S(s)}{S_{ref}(s)} = \frac{1 + \frac{K_p}{K_i} s}{1 + \left( \frac{K_p}{K_i} + \frac{1}{kK_i} \right) s + \frac{\tau}{kK_i} s^2}$$

Identification with a second order transfer function.

$$\begin{cases} \frac{2\epsilon}{\omega_n} = \frac{1}{K_i} \left( \frac{1}{k} + K_p \right) \\ \frac{1}{\omega_n^2} = \frac{\tau}{kK_i} \end{cases} \quad (C.1)$$

$$\Leftrightarrow \begin{cases} \frac{2\epsilon}{\omega_n} = \frac{k}{\tau\omega_n^2} \left( K_p + \frac{1}{k} \right) \\ K_i = \frac{\tau\omega_n^2}{k} \end{cases} \quad (C.2)$$

$$\Leftrightarrow \begin{cases} K_p = \left( \frac{2\epsilon}{\omega_n} \frac{\tau\omega_n^2}{k} \right) - \frac{1}{k} \\ K_i = \frac{\tau\omega_n^2}{k} \end{cases} \quad (C.3)$$

$$\Leftrightarrow \begin{cases} K_p = \frac{1}{k} (2\epsilon\tau\omega_n - 1) \\ K_i = \frac{\tau\omega_n^2}{k} \end{cases} \quad (C.4)$$

$$\Leftrightarrow \begin{cases} K_i = \frac{\tau\omega_n^2}{k} \\ K_p = \frac{2\epsilon K_i}{\omega_n} - \frac{1}{k} \end{cases} \quad (C.5)$$

## C.2 IP controller synthesis

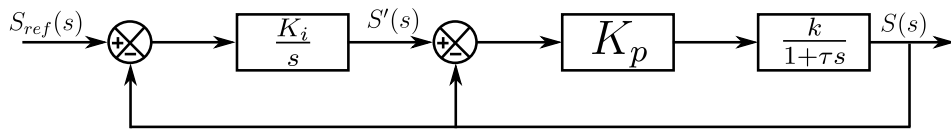


Figure C.2: IP controller structure

$$S(s) = \left( \frac{kK_p}{1 + \tau s} \right) [S'(s) - S(s)]$$

$$\begin{aligned}
&\Leftrightarrow S(s) = \left( \frac{kK_p}{1 + \tau s} \right) \left[ \frac{K_i}{s} (S_{ref}(s) - S(s)) - S(s) \right] \\
&\Leftrightarrow S(s) = \left( \frac{kK_p}{1 + \tau s} \right) \left[ \frac{K_i}{s} S_{ref}(s) - \frac{K_i}{s} S(s) - S(s) \right] \\
&\Leftrightarrow S(s) = \frac{kK_i K_p}{(1 + \tau s)s} S_{ref}(s) - S(s) \left[ \frac{kK_i K_p}{(1 + \tau s)s} + \frac{kK_p}{1 + \tau s} \right] \\
&\Leftrightarrow S(s) \left[ 1 + \frac{kK_i K_p}{(1 + \tau s)s} + \frac{kK_p}{1 + \tau s} \right] = \frac{kK_i K_p}{(1 + \tau s)s} \\
&\Leftrightarrow \frac{S(s)}{S_{ref}(s)} \left[ \frac{(1 + \tau s)s + kK_i K_p + kK_p s}{s(1 + \tau s)} \right] = \frac{kK_i K_p}{s(1 + \tau s)} \\
&\Leftrightarrow \frac{S(s)}{S_{ref}(s)} = \frac{kK_i K_p}{kK_i K_p + s(1 + kK_p) + \tau s^2} \\
&\Leftrightarrow \frac{S(s)}{S_{ref}(s)} = \frac{1}{1 + s \left( \frac{1}{K_i} + \frac{1}{kK_i K_p} \right) + s^2 \left( \frac{\tau}{kK_i K_p} \right)}
\end{aligned}$$

Identification with a second order transfer function.

$$\begin{cases} \frac{2\epsilon}{\omega_n} = \frac{1}{K_i} \left( 1 + \frac{1}{kK_p} \right) \\ \frac{1}{\omega_n^2} = \frac{\tau}{kK_i K_p} \end{cases} \quad (C.6)$$

$$\Leftrightarrow \begin{cases} K_i = \frac{\tau \omega_n^2}{kK_p} \\ K_p = \frac{2\epsilon \tau \omega_n - 1}{k} \end{cases} \quad (C.7)$$



## Appendix D

# Experimental characterization of the NiCd cell at $C_3$ rate

Tests are performed using a  $57A$  ( $C_3$ ) discharging current. The figure D.1 represents the evolution of the value of a single cell internal resistance according to its SOC and the working temperature at  $C_3$ .

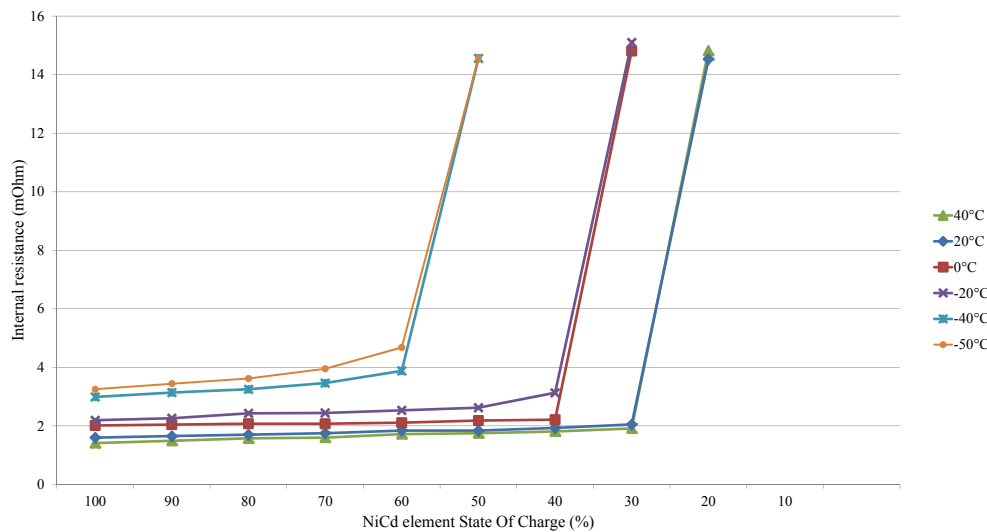


Figure D.1: Evolution of the internal resistance value of the cell according to its State Of Charge and the temperature ( $C_3$ )

Figures D.2 to D.7 also represent the evolution of the voltage of a NiCd single cell for different temperatures (from  $-50^{\circ}C$  to  $40^{\circ}C$ ), considering this  $C_3$  discharging current.

The table D.1 presents the maximum and the average errors of the Simulink model with the experimental data for the six temperatures.

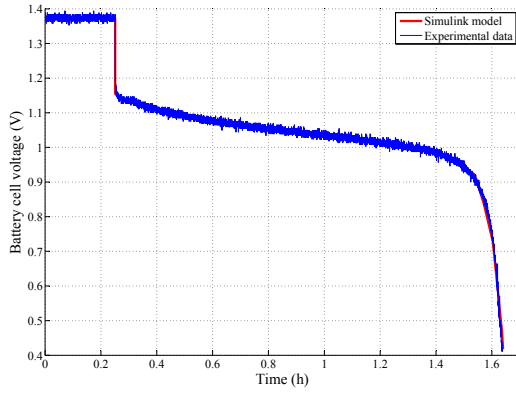


Figure D.2: NiCd's cell model validation for  $-50^{\circ}\text{C}$  ( $C_3$ )

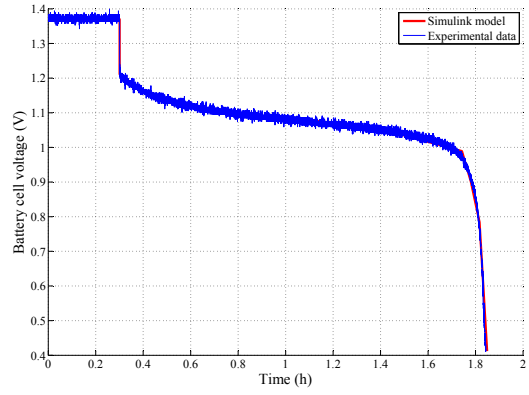


Figure D.3: NiCd's cell model validation for  $-40^{\circ}\text{C}$  ( $C_3$ )

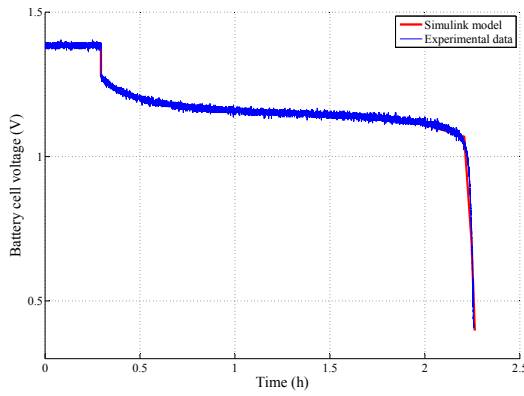


Figure D.4: NiCd's cell model validation for  $-20^{\circ}\text{C}$  ( $C_3$ )

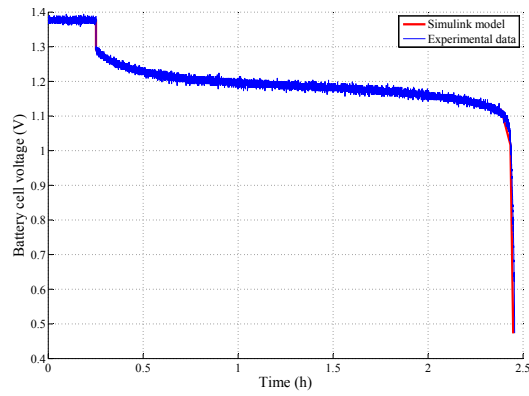


Figure D.5: NiCd's cell model validation for  $0^{\circ}\text{C}$  ( $C_3$ )

Temperature	Maximum error (%)	Average error (%)
$-50^{\circ}\text{C}$	31,4785	3,6235
$-40^{\circ}\text{C}$	11,7556	3,3504
$-20^{\circ}\text{C}$	28,5586	2,9219
$0^{\circ}\text{C}$	7,2812	2,4279
$20^{\circ}\text{C}$	25,5802	2,6638
$40^{\circ}\text{C}$	5,2387	1,9556

Table D.1: Maximum and average errors between the experimental data and the Simulink model at  $C_3$  rate.

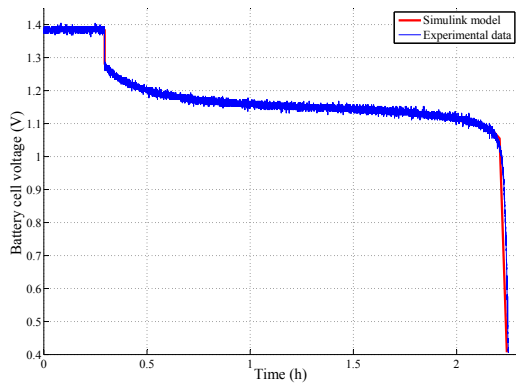


Figure D.6: NiCd's cell model validation for  $20^{\circ}\text{C}$  ( $C_3$ )

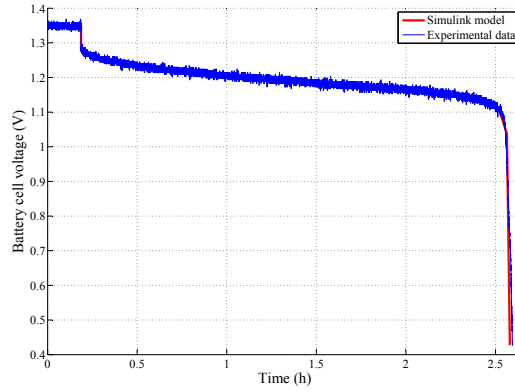


Figure D.7: NiCd's cell model validation for  $40^{\circ}\text{C}$  ( $C_3$ )



## Appendix E

### Batteries' characterization test bench specifications



## GENERAL SPECIFICATIONS

### OPERATION

**Constant Current:** 0 to selected full scale current

Prog. Accuracy

(Range): (high/med) ranges:  $\pm 0.25\%$   
(low) range:  $\pm 0.5\%$

Regulation:  $\pm 0.1\%$  of selected full scale

**Constant Resistance:** Constant Resistance mode operates in Amps/Volt, IEEE units entered in ohms or A/V

Prog. Accuracy:  $\pm 3\%$  of selected full scale

Regulation:  $\pm 3\%$  of selected full scale

**Constant Voltage:** 0 to selected full scale

Prog. Accuracy

(Range):

(high/med) ranges:  $\pm 0.25\%$

(low):  $\pm 0.5\%$

Regulation:  $\pm 0.15\%$  of selected full scale

**Constant Power:** 0 to full scale power

Prog. Accuracy:  $\pm 3\%$  of full scale

Regulation:  $\pm 3\%$  of full scale

### ANALOG MODE

**Ext. Prog:** 0 to 10 Volts input yields 0 to selected full scale loading in all operating modes.

Input Impedance: 330k Ohms

Prog. Response: Limited by internal adjustable slew rate limiter

### PULSE MODE

Frequency: 0.06Hz to 20kHz

Accuracy: 0.1%

Duty Cycle: 10 - 90%(Analog)

Accuracy: 0.1%

### Adjustable Slew Rate:

Max: 0 to full scale in 10 $\mu$ S

Min: 0 to full scale in 10mS

### OUTPUT SIGNALS

#### Current Sample Output:

Scaling: 10 Volts = selected full scale

Accuracy:  $\pm 0.5\%$  of selected full scale

#### Sync Output:

Timing: Synchronous with pulse generator.

Output: Sink with 10k pull up to +15V

### PROTECTION

#### Current Limit:

Analog Models: Approximately 105% of selected full scale current

#### Voltage Limit:

Analog Models: Load disconnect at 105% of selected full scale voltage

#### Power Limit:

Analog Models: Approximately 4250 Watts

**Thermal:** Load disconnect at internal temperature of 105°C

**Undervoltage:** Load inhibited at less than 1 Volt, when enabled

### MISCELLANEOUS

**AC Input:** User Selectable 100VAC, 120VAC, 200VAC, 240VAC,  $\pm 10\%$ , 48 - 62 Hz @ 350W

**Ambient Temp:** 0°C to 40°C

# SAFE OPERATING AREA & SPECIFICATIONS

Like the 2000W analog model, the RBL 800 watt analog programmable series has no compromise on performance, while adding a simple analog interface. Sleek and compact, the 800W model is ready to address all low-to-mid power load and test requirements. The analog programmable RBL 800W series provides all modes of operation, all functions, full scale range switching and master/slave paralleling standard. The 800W RBL model allows the customer the ultimate in flexibility when it comes to decision time! Stand alone or 19 inch rack mountable (see accessories page 33) unit will meet or exceed all your performance, reliability and quality expectations.

- High Speed Adjustable Slew Rate
- Pulse Load Shaping
- Front Panel or Remote Control
- Full Range Switching

## RBL 100-120-800

### OPERATING RANGES (FULL SCALES)

**Voltage:** 10 Volts, 50 Volts, 100 Volts  
**Current:** 2 Amps, 20 Amps, 120 Amps  
**Power:** 800 Watts

**Short Circuit:** 0.007 Ohms max.

### CONSTANT RESISTANCE RANGES

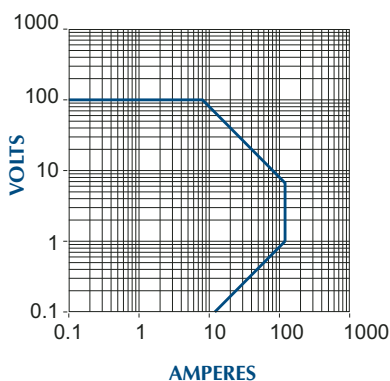
#### High Ohms Mode

Range	2A	20A	120A
10V	0-.1 A/V	0-1 A/V	0-6 A/V
50V	0-.02 A/V	0-.2 A/V	0-1.2 A/V
100V	0-.01 A/V	0-.1 A/V	0-.6 A/V

#### Low Ohms Mode

Range	2A	20A	120A
10V	0-1 A/V	0-10 A/V	0-60 A/V
50V	0-.2 A/V	0-2 A/V	0-12 A/V
100V	0-.1 A/V	0-1 A/V	0-6 A/V

### INPUT CHARACTERISTICS:



## RBL 400-120-800

### OPERATING RANGES (FULL SCALES)

**Voltage:** 20 Volts, 200 Volts, 400 Volts  
**Current:** 2 Amps, 20 Amps, 120 Amps  
**Power:** 800 Watts

**Short Circuit:** 0.03 Ohms max.

### CONSTANT RESISTANCE RANGES

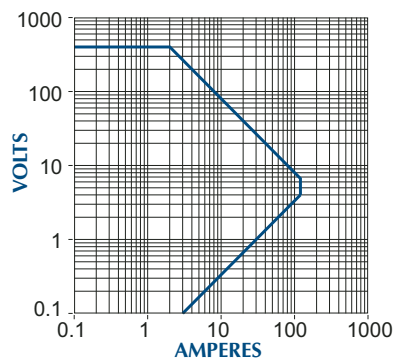
#### High Ohms Mode

Range	2A	20A	120A
20V	0-.05 A/V	0-.5 A/V	0-3 A/V
200V	0-.005 A/V	0-.05 A/V	0-.3 A/V
400V	0-.0025 A/V	0-.025 A/V	0-.15 A/V

#### Low Ohms Mode

Range	2A	20A	120A
20V	0-.5 A/V	0-5 A/V	0-30 A/V
200V	0-.05 A/V	0-.5 A/V	0-3 A/V
400V	0-.025 A/V	0-.25 A/V	0-1.5 A/V

### INPUT CHARACTERISTICS:



## RBL 600-40-800

### OPERATING RANGES (FULL SCALES)

**Voltage:** 20 Volts, 200 Volts, 600 Volts  
**Current:** 2 Amps, 20 Amps, 40 Amps  
**Power:** 800 Watts

**Short Circuit:** 0.035 Ohms max.

### CONSTANT RESISTANCE RANGES

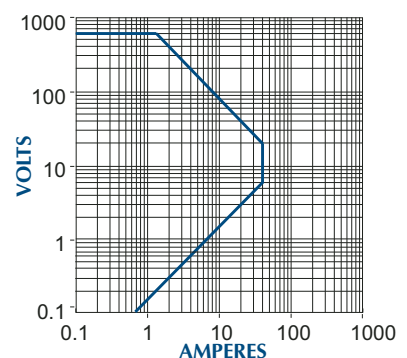
#### High Ohms Mode

Range	2A	20A	40A
20V	0-.05 A/V	0-.5 A/V	0-1 A/V
200V	0-.005 A/V	0-.05 A/V	0-.1 A/V
400V	0-.0025 A/V	0-.025 A/V	0-.05 A/V

#### Low Ohms Mode

Range	2A	20A	40A
20V	0-.5 A/V	0-5 A/V	0-10 A/V
200V	0-.05 A/V	0-.5 A/V	0-1 A/V
400V	0-.025 A/V	0-.25 A/V	0-.5 A/V

### INPUT CHARACTERISTICS:



# Sorensen SG Series

4–150 kW

## Programmable Precision High Power DC Power Supply

10–800 V

- High Power Density: up to 15 kW in 3U, 30 kW in a 6U chassis
- Wide Voltage Range: 0-10V up to 0-800V, in increments of 5 kW from 5 to 30 kW
- Fast Load Transient Response: Protection from undesired voltage excursions
- Low Ripple and Noise
- Hardware Trigger (Ethernet Option)
- Parallelable up to 150 kW
- Sequencing: Free system controller & speed up test
- Low audible noise: Temperature controlled variable speed fans



6–6000 A



208

400

480

ETHERNET



LXI

RS232

The Sorensen SG series (hereafter SG Series) represents the next generation of high power programmable DC power supplies. The SG Series is designed for exceptional load transient response, low noise and the highest power density in the industry. With a full 15 kW available down to 20VDC output in a 3U package the SG leads the industry in power density. The power density is enhanced by a stylish front air intake allowing supplies to be stacked without any required clearance between units.

At the heart of the SG series is a 5 kW power module. Depending on the output voltage, one to six modules can be configured in a single chassis to deliver 5 kW to 30 kW of power. Combinations of these chassis can then be easily paralleled to achieve power levels up to 150 kW. Paralleled units operate like one single supply providing total system current. Available in two control versions, the SGA has basic analog controls, while the SGI provides intelligent control features.

### SGI: Advanced Intelligent Control

(Sorensen General purpose Intelligent) The SGI combines onboard intelligent controls with the outstanding power electronics common to all SG family supplies. These controls enable sophisticated sequencing, constant power mode and save/recall of instrument settings. Looping of sequences makes the SGI ideal for repetitive testing. An impressive vacuum fluorescent graphical display in eight languages, context sensitive “soft” keys and front panel keyboard simplify programming of the SGI.

### SGA: Outstanding Value - Analog Control

(Sorensen General purpose Analog) The SGA, with its industry leading price performance, is available for customers requiring simple front panel analog controls or external control. With the same high performance power electronics as the SGI, the SGA provides essential features like 10- turn potentiometers for setting voltage and current, 3 ½ digit LED readout plus front panel over-voltage protection (OVP) preview/adjustment and reset.

**AMETEK**  
**Programmable Power**  
 9250 Brown Deer Road  
 San Diego, CA 92121-2267  
 USA

**AMETEK**<sup>®</sup>  
 PROGRAMMABLE POWER

# SG Series : Product Specifications

Common	
Remote Sense	Terminals are provided to sense output voltage at point of load. Maximum line drop 5% of rated voltage per line for 40-100V models, line drop 1V of rated voltage per line for 10-20V models, 1.5V for 30V models, 2% of rated voltage per line for models 160V and greater. (Greater line drop is allowed, but output regulation specifications no longer apply).
Parallel Operation	Up to 5 units may be paralleled for additional current within the power supply single-unit specifications, with exception of the DC output current set accuracy. Additional paralleled SG units will add 0.3% inaccuracy per unit. To parallel more than 5 units, contact factory.
Series Operation	Up to 2 units (see Output Float Voltage)

Input	
Nominal Voltage 3 phase, 3 wire + ground	208/220 VAC (operating range 187 - 242 VAC) 380/400 VAC (operating range 342 - 440 VAC) 440/480 VAC (operating range 396 - 528 VAC)
Frequency	47 – 63Hz , 400Hz ( 400Hz @ 208VAC, for 6U units is optional modification and does not carry CE, UL or CSA markings )
Power Factor	>0.9 typical for 208/220 VAC input (10V - 800V) >0.78 typical for 380/400 VAC input (40V, 60V - 800V, 0.9 available with modification "pf") >0.9 typical for 380/480 VAC input (10V - 30V, 50V) >0.7 typical for 440/480 VAC input (40V, 60V - 800V, 0.9 available with modification "pf") >0.9 typical for 440/480 VAC input (10V - 30V, 50V)
Protection ( typical )	½ cycle ride-through on all three phases, 3 cycle ride through on single phase; missing phase shutdown ( 800V model 6.4 msec on all 3 phases )

## Programming & Read-back Specifications ( with sense wires used )

	Programming		Read-Back / Monitoring		
	Accuracy	Resolution	Accuracy	Resolution	
Front panel Display	SGA: +/- (0.5%fs + 1 digit) SGI (40-800V) +/- 0.1% of voltage at full scale SGI (40-800V) +/- 0.4% of current at full scale  SGI (10-30V) 0.1% of set point +0.1% of voltage rating SGI (10-30V) 0.1% of set point +0.4% of current rating	SGA: 3.5 digits SGI: 4.0 digits	SGA: +/- (0.5%fs + 1 digit) SGI, Voltage: +/- 0.1% of full scale SGI, Current: +/- 0.4% of full scale  SGI (10-30V) 0.1% of actual +0.15% voltage rating	SGA: 3.5 digits SGI: 4.0 digits	Knob control & Display read-back
Remote Analog Interface	Voltage +/-0.25% of full scale Current (40-800V) 0.8% of full scale , (10-30V) 1.0% of full scale	NA	(40-800V) +/-1.0% of full scale  (10-30V) +/-0.5% of full scale	NA	25-pin D-sub connector (0~5 V or 0~10 V)
Remote Digital Interface	Voltage: +/- 0.1% of full scale, Current: +/- 0.4% of full scale	+/-0.002% of full scale	Voltage: +/- 0.1% of full scale Current: +/- 0.4% of full scale	+/-0.002% of full scale	RS-232C (Standard on SGI), Optional IEEE-488.2 and Optional LXI Compliant 10/100 base-T Ethernet (see Options)
OVP	+/- 1% of full scale	+/-0.002% of full scale			Programming range: 5-110% Configured from front panel, remote analog or via optional digital inputs
User I/O	Disconnect & Polarity-reversal relay control ( Only available with Ethernet Option )				Digital 10-pin Molex type connector See <a href="http://www.programmablepower.com">www.programmablepower.com</a>
Software	IVI & CVI drivers available under SUPPORT at: <a href="http://www.ProgrammablePower.com">www.ProgrammablePower.com</a>				

Physical	3U Models (10V-30V)	3U Models (40V-800V)	6U Models (40V-600V)
Width	19.00 in (48.3 cm)	19.00 in (48.3 cm)	19.00 in (48.3 cm)
Depth	28.09 in (71.4 cm)	26.4 in (67.1 cm)	27.06 in (68.8 cm)
Height	5.25 in (13.3 cm)	5.25 in (13.3 cm)	10.5 in (26.7 cm)
Weight	(4kW, 10V 15V) ≈<65 lbs (29 kg) (5kW, 20V 30V) ≈<65 lbs (29 kg) (8kW, 10V 15V) ≈<85 lbs (39 kg) (10kW, 20V 30V) ≈<85 lbs (39 kg) (12kW, 10V 15V) ≈<110 lbs (50 kg) (15kW, 20V 30V) ≈<110 lbs (50 kg)	(5kW) ≈ 40 lbs (18 kg) (10kW) ≈ 60 lbs (27 kg) (15kW) ≈ 80 lbs (36 kg)	(20kW) ≈ 120 lbs (54 kg) (25kW) ≈ 140 lbs (64 kg) (30kW) ≈ 160 lbs (73 kg)
Shipping Weight	Contact factory for more product & shipping weights		

# SG Series : Product Specifications

## 4-150 kW

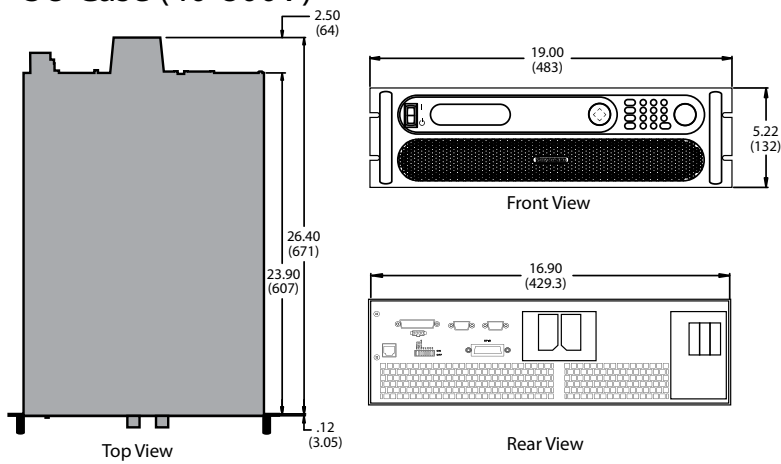
Output			
Ripple & Noise (Voltage Mode, Typical)	See Output: Voltage & Current Ranges Chart below. Ripple and noise specified at full load, nominal AC input. Noise measured with 6 ft. cable, 1µf at load		
Ripple (Current Mode)	<+/- 0.04% of full scale rms current		
DC Voltage Slew Rate (40-800V)	≈< 100 ms 5-95% of full scale typical - resistive load (Contact factory for model specific slew rates)		
Output Voltage Rise Time (10-30V)	Rise Time, ms, max	Condition	
	10	Measured from 10% to 90% of the output voltage change - resistive load, typical	
Output Voltage Fall Time (10-30V)	Fall Time, ms max	Condition	
	No Load 1	100% CC Load	100% CR Load
	50	10	10
Output Current Rise Time (10-30V)	Rise Time, ms max	Condition	
	20	Measured from 10% to 90% of the output current change - resistive load, typical	
Output Current Fall Time (10-30V)	Fall Time, ms max	Condition	
	10	Measured from 90% to 10% of the output current change - resistive load, typical	
DC Current Slew Rate	45A / ms typical - resistive load		
Line Regulation ( with sense wires used )	(±10% of nominal AC input, constant load) Voltage Mode: +/- 0.01% of full scale (40-800V) Current Mode: +/- 0.05% of full scale (40-800V) Voltage Mode and Current Mode: +/- 0.05% of full scale (10-30V)		
Load Regulation (with sense wires used)	(no load to full load, nominal AC input) Voltage Mode: +/- 0.02% of full scale (40-800V) Current Mode: +/- 0.1% of full scale Voltage Mode: +/- 0.05% of full scale (10-30V)		
Load Transient Response	Recovers within 1ms to +/-0.75% of full-scale of steadystate output for a 50% to 100% or 100% to 50% load change		
Efficiency	87% typical at nominal line and max load		
Stability	±0.05% of set point after 30 minute warm-up and over 8 hours at fixed line, load and temperature, typical		
Temperature Coefficient	0.02%/ C of maximum output voltage rating for voltage set point, typical 0.03%/ C of maximum output current rating for current set point, typical		
Output Float Voltage	Negative terminal within +/- 300 V of chassis potential. ( We recommend the use of optional isolated analog Interface (IAI). ) Supplies in "series" should be the same output voltage/current, in not system current is limited to lower of the two supplies.		

Output: Voltage and Current Ranges								
Power	3U			6U			Ripple & Noise	
	4/5 kW	8/10 kW	12/15 kW	16/20 kW	20/25 kW	24/30 kW	rms (20 Hz-300 kHz)	p-p (20 Hz-20 MHz)
Voltage	Current							
10	400	800	1200	1600*	2000*	2400*	20 mV	50 mV
15	267	534	801	1068*	1335*	1602*	20 mV	50 mV
20	250	500	750	1000*	1250*	1500*	20 mV	60 mV
30	167	334	501	668*	835*	1002*	20 mV	60 mV
40	125	250	375	500*	625*	750*	20 mV	75 mV
50	100	200	300	400*	500*	600*	20 mV	75 mV
60	83	167	250	333	417	500	20 mV	75 mV
80	63	125	188	250	313	375	20 mV	100 mV
100	50	100	150	200	250	300	20 mV	100 mV
160	31	63	94	125	156	188	25 mV	150 mV
200	25	50	75	100	125	150	25 mV	175 mV
250	20	40	60	80	100	120	30 mV	200 mV
330	15	30	45	61	76	91	30 mV	200 mV
400	12	25	38	50	63	75	40 mV	300 mV
600	8	17	25	33	42	50	60 mV	350 mV
800	6.2	12.5	18.7	25*	31.2*	37.5*	80 mV	500 mV

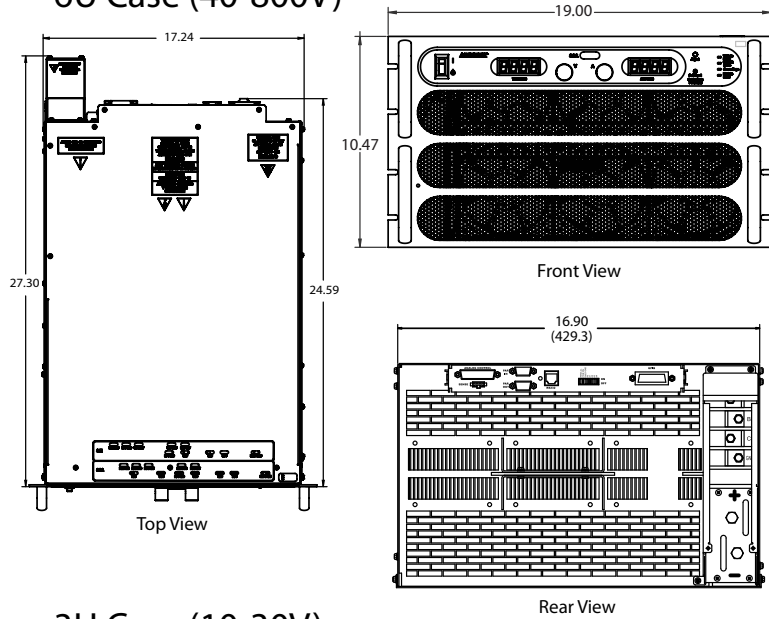
\* By way of paralleling 3U supplies

# SG Series : Product Diagram

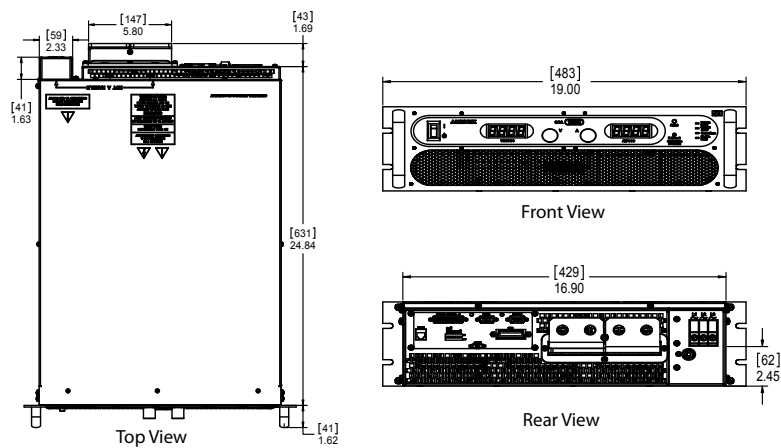
## 3U Case (40-800V)



## 6U Case (40-800V)

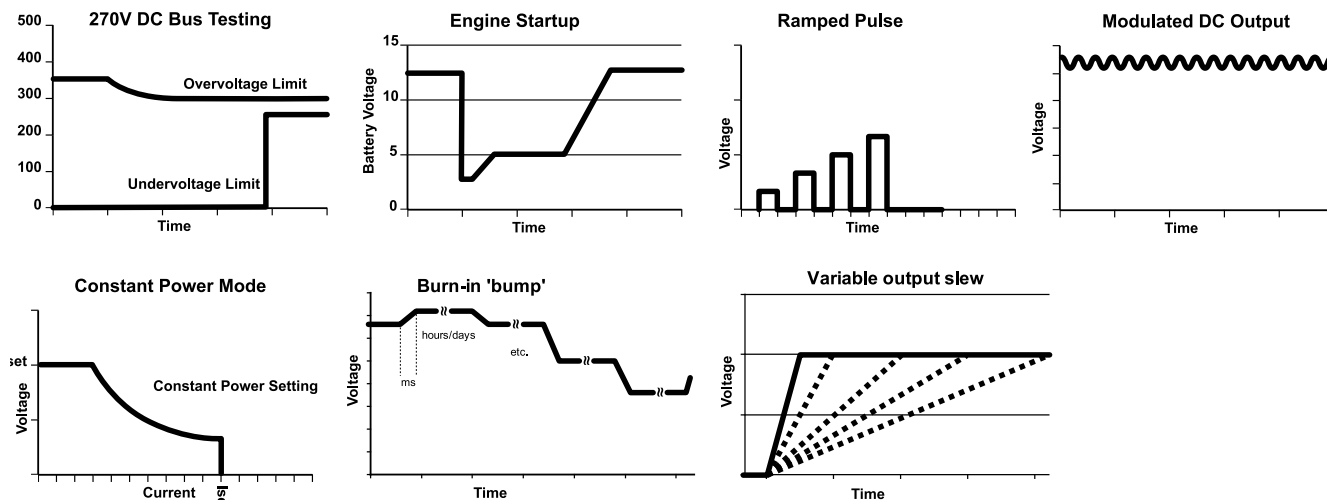


## 3U Case (10-30V)



Dimensions in inches (millimeters)

## Advanced Power Simulation



SGI model provides constant power mode allowing independent setting of the max voltage, current and power

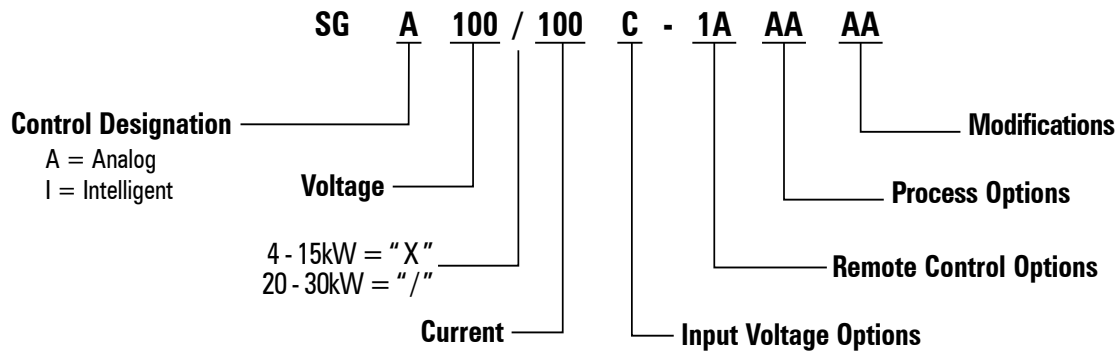
## SGI / SGA Comparison Chart

Feature	SGA	SGI
Modular Design	•	•
Fast Load Transient	•	•
Parallelable	•	•
Analog & Digital Summing	Optional	•
Direct Front Panel V/I Control	•	•
3½ Digit LED Readout	•	
Graphics Display		•
Sequencing		•
Save/Recall Setups		•
System Power Readouts		•
Constant Power Mode		•
IEEE-488.2/RS-232C	Optional	RS-232C Std, IEEE-488.2 Optional
LXI Class C Ethernet/ RS-232	Optional	RS-232C Std, Ethernet Optional
Front Panel Dust Filter	Optional (3U unit only)	Optional (3U unit only)

## Environmental

Operating Temperature	0 to 50° C
Storage Temperature	-25° C to 65° C
Humidity Range	Relative humidity up to 95% non-condensing, 0° C – 50° C
Altitude	Operating full power available up to 5,000 ft. (~1,500 m), derate 10% of full power for every 1,000 feet higher; non-operating to 40,000 ft. (~12,000 m)
Cooling	Front and side air inlet, rear exhaust. Temperature controlled, variable speed fans. Units may be stacked without spacing.
Regulatory	Certified to UL/CSA 61010 and IEC/EN 61010-1 by a NRTL, CE Compliant, Semi-F47 Compliant. LVD Categories: Installation Category II: Pollution Degree 2; Class II Equipment: for Indoor Use Only. EMC Directive, EN 61326:1998
Front Panel Dust Filter	30 PPI (Pores Per Inch) - must ensure adequate airflow and / or derate max. temperature. 3U unit only.

# SG Series



(For units up to 999A, Current is represented in numeric format (rounded to whole Amp), e.g., above "100" represents 100A. For units at 1000A and above, the current is represented by the format "XKX", e.g, 1K2 represents 1200A)

## Options and Accessories

Control Options	A: Analog I: Intelligent
Input Options	C: Input Voltage 187 / 242VAC, 3 Phase D: Input Voltage 342 / 440VAC, 3 Phase E: Input Voltage 396 / 528VAC, 3 Phase
Remote Control Options	0A: No Option 1A: IEEE-488.2 + RS-232C (Note: SGI comes standard with RS-232C) 1C: Ethernet + RS-232C 1D: Isolated Analog Control 1E: Shaft Locks (SGA series only)
Process Options	AA: No option AB: Certificate of Calibration (includes Test Data)
Modifications	AJ: Front panel dust filter - factory installed - 3U unit only CV: 400Hz AC input @ 208 VAC ( does not carry CE, CSA or UL marks ) ( 6U only ) STD on 3U PF: Passive power factor correction to 0.9 (Only applicable to 40V, 60V to 800V. Included in 10V-30V and 50V.)
Accessories	890-453-03: Paralleling Cable (for up to 5 units, requires one cable per unit placed in parallel) K550212-01: 3U Rack Slides (for 5kW, 10kW and 15kW models) K550213-01: 6U Rack Slides (for 20kW, 25kW and 30kW models) 5550568-01: Front panel dust filter - field installation kit - 3U unit only 5551082-01: Optional AC input cover kit - 3U unit only
Contact factory for other combinations	

### 3.3.6 ANALOG CONTROL CONNECTOR (J1)

The ANALOG CONTROL connector on the rear panel allows the unit to be configured for different operating configurations: local and remote current programming, local and remote voltage programming, current and voltage output monitoring, output enable/disable, etc. The setup and operating requirements of each configuration are provided in Sections 3.4 through 3.9.

#### ISOLATED ANALOG CONTROL (OPTION)

The Isolated Analog Control uses the same Analog Control connector (J1). This option fully isolates remote control signals and allows control of units not connected to a common ground. Control ground is isolated from power ground, which protects against potential damage from systems with high electrical noise or large ground loop currents.

**Note:** Some standard analog programming signals may not be available with this option. See Table 1.2.2 for details.



#### CAUTION!

This option is not intended to allow operation of the power supply at excessive voltages. Refer to Section 2 INSTALLATION for maximum terminal voltages.

Following are Figure 3-8 with the connector's pin-out diagram, and Table 3-1 with ANALOG CONTROL connector designations and functions:

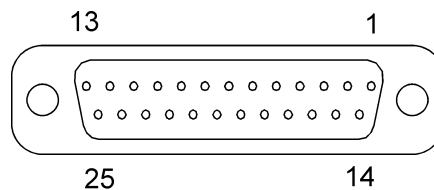


**Figure 3-8. ANALOG CONTROL Connector (J1) Pin-out**

Designator	Schematic Symbol	Electrical Chars.	Functional Description
1	ISO ON/OFF	$Z_{in} \sim 6 \text{ k}\Omega$	Isolated remote output on/off. Externally supplied AC/DC voltage source for on/off control. A positive (+) 12 to 240 VAC or 6 to 120 VDC voltage will enable the output, i.e., turn on the output of the supply. This input control is optically isolated from the power supply circuit up to 500 VDC. Circuit return Pin 2 (ISO RTN). See Section 3.7.
2	ISO RTN	—	Isolated circuit return used with isolated on/off control J1-1 and J1-14.
3	REM OV SET	$Z_{in} \sim 20 \text{ k}\Omega$	Remote overvoltage set. A remote signal sets the overvoltage trip level. 0.25-5.5 VDC = 5-110%. Apply a 10.5 VDC to 13.3 VDC signal for 7 seconds to reset an OVP condition. Circuit return Pin 6 (COM). See Section 3.8.
4	VP RTN	$Z_{in} \sim 10 \text{ k}\Omega$	Voltage programming return. Used with J1-9, J1-15 or J1-21 and must be referenced to Pin 6 (COM) circuit common.
5	ON/OFF	Must sink $\sim 1\text{mA}$ to enable	Remote output on/off. Switch/relay contacts or a direct short between this terminal and Pin 6 (COM) circuit common, enables the output, i.e., turns on the output of the supply. See Section 3.7.
6	COM <sup>†</sup>	-	Circuit common. Electrically equal to Pin 24. Same potential as the negative output terminal.
7	I MON	$Z_{out} \sim 100\Omega$	Output current monitor. 0-10 VDC equals 0-100% rated current. Minimum load resistance 10k $\Omega$ . Circuit return Pin 6 (COM).
8	V SET *	$Z_{out} \sim 100\Omega$	0-5 VDC (0-100%) front panel voltage potentiometer set point monitor output. Minimum load resistance 10k $\Omega$ . Circuit return Pin 6 (COM).
9	VP 5V	$Z_{in} \sim 10\text{k}\Omega$	Remote voltage programming using a 0-5 VDC source. Do not exceed 13.3 VDC. Circuit return Pin 4 or Pin 20 (VP RTN). See Section 3.5.
10	IP 5V	$Z_{in} \sim 10\text{k}\Omega$	Remote current programming using a 0-5 VDC source. Do not exceed 13.3 VDC. Circuit return Pin 23 or Pin 25 (IP RTN). See Section 3.4.

Designator	Schematic Symbol	Electrical Chars.	Functional Description
11	ISET *	$Z_{out} \sim 100\Omega$	0-5 VDC (0-100%) front panel current potentiometer set point monitor output. Minimum load resistance 10k $\Omega$ . Circuit return Pin 6 (COM).
12	Not Used		
13			
14	ISO TTL/CMOS	$Z_{in} \sim 2.2k\Omega$	Isolated TTL/CMOS on/off control. A high state TTL/CMOS voltage enables the output, i.e., turns on the output of the supply, and a low state or open connection disables the output, i.e., turns off the output of the supply.. Circuit return Pin 2 (ISO RTN). See Section 3.7.
15	VP 10V	$Z_{in} \sim 20k\Omega$	Remote voltage programming using a 0-10 VDC source. Do not exceed 25 VDC. Circuit return Pin 4 or Pin 20 (VP RTN). See Section 3.5.
16	IP 10V	$Z_{in} \sim 20k\Omega$	Remote current programming using a 0-10 VDC source. Do not exceed 25 VDC. Circuit return Pin 23 or Pin 25 (IP RTN). See Section 3.4.
17	FAULT	$Z_{out} \sim 100\Omega$	Fault state output. A high state (approximately +10 VDC) indicates a converter, temperature or bias supply fault, and the LED on the front panel will illuminate. Circuit return Pin 6 (COM).
18	S/D FAULT	$Z_{out} \sim 100\Omega$	Shutdown fault. This terminal goes to high state in the event of converter, temperature, overvoltage or bias supply fault. A 7 VDC to 13.3 VDC signal can be applied to this pin to shutdown the output of the unit. An 8 VDC minimum output signal is provided into a 10 k $\Omega$ minimum load, in the event of an internally generated shutdown. Circuit return Pin 6 (COM). See Section 3.9.
19	V MON	$Z_{out} \sim 100\Omega$	Output voltage monitor. 0-10 VDC equals to 0-100% rated voltage. Minimum load resistance 10k $\Omega$ . Circuit return Pin 6 (COM).
20	VP RTN	$Z_{in} \sim 10\Omega$	Voltage programming return. Used with J1-9, J1-15 or J1-21 and must be referenced to Pin 6 (COM) circuit common.
21	VP RES *	$\sim 10.8V$ compliance	1 milliamp current source for remote voltage programming using resistance. 0-5k ohm resistor referenced to Pin 4 or Pin 20 (VP RTN) will program the output voltage from 0-100%. See Section 3.5.

Designator	Schematic Symbol	Electrical Chars.	Functional Description
22	IP RES *	~ 10.8V compliance	1 milliamp current source for remote current programming using resistance. 0-5k ohm resistor referenced to Circuit return Pin 23 or Pin 25 (IP RTN) will program the output current from 0-100%. See Section 3.4.
23	IP RTN	Z <sub>in</sub> ~ 10kΩ	Current programming return. Used with J1-10, J1-16 or J1-22 and must be referenced to Pin 6 (COM) circuit common.
24	COM †	-	Circuit common. Electrically equal to Pin 6. Same potential as the negative output terminal.
25	IP RTN	Z <sub>in</sub> ~ 10kΩ	Current programming return. Used with J1-10, J1-16 or J1-22 and must be referenced to Pin 6 (COM) circuit common.

**Table 3–1. ANALOG CONTROL Connector (J1), Designations and Functions**

† Control ground is isolated from power ground with the isolated analog control (option). See Section 3.3.1

\* Signals not available with isolated analog control (option).



**CAUTION!**  
 If standard analog programming is used, note the programming return (J1-6 & J1-24) is at the same potential as the negative output terminal of the power supply. Observance of return connections should be made with respect to input programming signal equipment. Improper connection may result in ground loops and as a result internal power supply damage may occur. (Output current then flows to chassis by means of external connection to the J1 common (J1-6 & J1-24)).



# Bibliography

- [Affa03] A. Affanni, A. Bellini, C. Concari, G. Franceschini, E. Lorenzani, and C. Tassoni. “EV battery state of charge: neural network based estimation”. In: *Electric Machines and Drives Conference, 2003. IEMDC'03. IEEE International*, pp. 684–688 vol.2, 2003.
- [Akli07] C. Akli, X. Roboam, B. Sareni, and A. Jeunesse. “Energy management and sizing of a hybrid locomotive”. In: *European Conference on Power Electronics and Applications*, pp. 1–10, sept. 2007.
- [Akli08] C. Akli. *Conception systémique d'une locomotive hybride autonome. Application à la locomotive hybride de démonstration et d'investigations en énergétique LHyDIE développée par la SNCF*. PhD thesis, Université de Toulouse, juin 2008.
- [Alle10] A. L. Allegre, A. Bouscayrol, P. Delarue, P. Barrade, E. Chattot, and S. El-Fassi. “Energy Storage System With Supercapacitor for an Innovative Subway”. *IEEE Transactions on Industrial Electronics*, Vol. 57, No. 12, pp. 4001–4012, 2010.
- [Alle13] A.-L. Allegre, A. Bouscayrol, and R. Trigui. “Flexible real-time control of a hybrid energy storage system for electric vehicles”. *Electrical Systems in Transportation, IET*, Vol. 3, No. 3, pp. –, 2013.
- [Alva04] G. Alvarenga and G. Mateus. “Hierarchical tournament selection genetic algorithm for the vehicle routing problem with time windows”. In: *Hybrid Intelligent Systems, 2004. HIS '04. Fourth International Conference on*, pp. 410 – 415, dec. 2004.
- [Arce09] A. Arce, A. del Real, and C. Bordons. “MPC for battery/fuel cell hybrid vehicles including fuel cell dynamics and battery performance improvement”. *Journal of Process Control*, Vol. 19, No. 8,

pp. 1289 – 1304, 2009. Special Section on Hybrid Systems: Modeling, Simulation and Optimization.

- [Asae07] B. Asaei and M. Amiri. “High Efficient Intelligent Motor Control for a Hybrid Shunting Locomotive”. In: *Vehicle Power and Propulsion Conference, 2007. VPPC 2007. IEEE*, pp. 405 –411, 2007.
- [Aso07] S. Aso, M. Kizaki, and Y. Nonobe. “Development of Fuel Cell Hybrid Vehicles in TOYOTA”. In: *Power Conversion Conference - Nagoya, 2007. PCC '07*, pp. 1606 –1611, 2007.
- [Ates10] Y. Ates, O. Erdinc, M. Uzunoglu, and B. Vural. “Energy management of an FC/UC hybrid vehicular power system using a combined neural network-wavelet transform based strategy”. *International Journal of Hydrogen Energy*, Vol. 35, No. 2, pp. 774 – 783, 2010.
- [Ayad07] M. Ayad, M. Becherif, A. Djerdir, and A. Miraoui. “Sliding Mode Control for Energy Management of DC Hybrid Power Sources Using Fuel Cell, Batteries and Supercapacitors”. In: *International Conference on Clean Electrical Power, 2007. ICCEP '07*, pp. 500 –505, May 2007.
- [Ayad10] M. Ayad, M. Becherif, A. Henni, A. Aboubou, M. Wack, and S. Laghrouche. “Passivity-Based Control applied to DC hybrid power source using fuel cell and supercapacitors”. *Energy Conversion and Management*, Vol. 51, No. 7, pp. 1468 – 1475, 2010.
- [Baer11a] J. Baert, S. Jemei, D. Chamagne, D. Hissel, S. Hibon, and D. Hegy. “Sizing of a hybrid locomotive”. In: *Vehicle Power and Propulsion Conference (VPPC), 2011 IEEE*, pp. 1–6, 2011.
- [Baer11b] J. Baert, J. Pouget, D. Hissel, and M.-C. Pera. “Energetic Macroscopic Representation of a hybrid railway powertrain”. In: *Vehicle Power and Propulsion Conference (VPPC), 2011 IEEE*, pp. 1–6, sept. 2011.
- [Baer12a] J. Baert, S. Jemei, D. Chamagne, D. Hissel, D. Hegy, and S. Hibon. “Energetic macroscopic representation of a naturally-aspirated engine coupled to a salient pole synchronous machine”. In: *2012 IFAC Power Plants and Power Systems Control*, pp. 435–440, 2012.

- [Baer12b] J. Baert, S. Jemei, D. Chamagne, D. Hissel, S. Hibon, and D. Hegy. “Modeling and Energy Management Strategies of a Hybrid Electric Locomotive”. In: *Vehicle Power and Propulsion Conference (VPPC), 2012 IEEE*, pp. 990–995, 2012.
- [Baum00] B. Baumann, G. Washington, B. Glenn, and G. Rizzoni. “Mechatronic design and control of hybrid electric vehicles”. *Mechatronics, IEEE/ASME Transactions on*, Vol. 5, No. 1, pp. 58 –72, March 2000.
- [Bech07] M. Becherif, D. Paire, and A. Miraoui. “Energy management of solar panel and battery system with passive control”. In: *International Conference on Clean Electrical Power, 2007. ICCEP '07*, pp. 14 –19, May 2007.
- [Bech12a] M. Becherif, M. C. Pera, D. Hissel, and S. Jemei. “Estimation of the lead-acid battery initial state of charge with experimental validation”. In: *2012 IFAC Power Plants and Power Systems Control*, pp. 621–626, 2012.
- [Bech12b] M. Becherif, M. Pera, D. Hissel, and S. Jemei. “Estimation of the lead-acid battery initial state of charge with experimental validation”. In: *2012 IEEE Vehicle Power and Propulsion Conference (VPPC)*, pp. 469–473, 2012.
- [Beck05] R. Beck, F. Richert, A. Bollig, D. Abel, S. Saenger, K. Neil, T. Scholt, and K.-E. Noreikat. “Model Predictive Control of a Parallel Hybrid Vehicle Drivetrain”. In: *44th IEEE Conference on Decision and Control, 2005 and 2005 European Control Conference. CDC-ECC '05*, pp. 2670 – 2675, 2005.
- [Bezi02] H. Bezine, N. Derbel, and A. M. Alimi. “Fuzzy control of robot manipulators:: some issues on design and rule base size reduction”. *Engineering Applications of Artificial Intelligence*, Vol. 15, No. 5, pp. 401 – 416, 2002.
- [Bien11] D. Bienaime, N. Devillers, M.-C. Pera, F. Gustin, A. Berthon, and M. L. Hopdjanian. “Energetic macroscopic representation of an electric network embedded in a helicopter”. In: *Vehicle Power and Propulsion Conference (VPPC), 2011 IEEE*, pp. 1–6, 2011.
- [Bomb13] Bombardier. “Bombardier website”. <http://www.bombardier.fr/fr/transport/produits-et->

services/propulsion-et-contrôles/produits/gestion-de-l-energie?docID=0901260d801f0d24, 2013.

- [Bont05] S. Bontour, D. Hissel, H. Gualous, F. Harel, and J. M. Kauffmann. “Design of a parallel fuel cell-supercapacitor auxiliary power unit (APU)”. In: *Proceedings of the Eighth International Conference on Electrical Machines and Systems, 2005. ICEMS 2005*, pp. 911–915 Vol. 2, 2005.
- [Bont06] D. Bonta, V. Tulbure, and C. Festila. “Diesel-Engine Intelligent Control in Railway Traction”. In: *IEEE International Conference on Automation, Quality and Testing, Robotics, 2006*, pp. 318 – 320, May 2006.
- [Bord10] C. Bordons, M. Ridao, A. Perez, A. Arce, and D. Marcos. “Model Predictive Control for power management in hybrid fuel cell vehicles”. In: *Vehicle Power and Propulsion Conference (VPPC), 2010 IEEE*, pp. 1 –6, sept. 2010.
- [Bouc05] C. Bouchat. “Les voitures hybrides dans l’histoire”. <http://www.automania.be/fr/auto/automobilia/automobilia-historiques/les-voitures-hybrides-dans-l-histoire.html>, 2005.
- [Boul08] L. Boulon, D. Hissel, A. Bouscayrol, M.-C. Pera, and P. Delarue. “Multi physics modelling and representation of power and energy sources for Hybrid Electric Vehicles”. In: *Vehicle Power and Propulsion Conference, 2008. VPPC '08. IEEE*, pp. 1–6, 2008.
- [Boul09] L. Boulon. *Modélisation multiphysique des éléments de stockage et de conversion d’énergie pour les véhicules électriques hybrides. Approche systémique pour la gestion d’énergie*. PhD thesis, Université de Franche-Comté, juillet 2009.
- [Boul10a] L. Boulon, D. Hissel, A. Bouscayrol, O. Pape, and M.-C. Pera. “Simulation Model of a Military HEV With a Highly Redundant Architecture”. *IEEE Transactions on Vehicular Technology*, Vol. 59, No. 6, pp. 2654–2663, 2010.
- [Boul10b] L. Boulon, D. Hissel, A. Bouscayrol, and M.-C. Pera. “From Modeling to Control of a PEM Fuel Cell Using Energetic Macroscopic Representation”. *IEEE Transactions on Industrial Electronics*, Vol. 57, No. 6, pp. 1882 –1891, 2010.

- [Bous03] A. Bouscayrol, B. Davat, B. de Fornel, B. François, J. P. Hautier, F. Meibody-Tabar, E. Monmasson, M. Pietrzak-David, H. Razik, E. Semail, and F. Benkhoris. “Control structures for multi-machine multi-converter systems with upstream coupling”. *Mathematics and Computers in Simulation*, Vol. 63, No. 3-5, pp. 261 – 270, 2003. Modelling and Simulation of Electric Machines, Converters and Systems.
- [Bous05] A. Bouscayrol, P. Delarue, and X. Guillaud. “Power strategies for maximum control structure of a wind energy conversion system with a synchronous machine”. *Renewable Energy*, Vol. 30, No. 15, pp. 2273 – 2288, 2005.
- [Bubn10] P. Bubna, D. Brunner, S. Advani, and A. Prasad. “Prediction-based optimal power management in a fuel cell/battery plug-in hybrid vehicle”. *Journal of Power Sources*, Vol. 195, No. 19, pp. 6699 – 6708, 2010.
- [Caux10a] S. Caux, W. Hankache, M. Fadel, and D. Hissel. “On-line fuzzy energy management for hybrid fuel cell systems”. *International Journal of Hydrogen Energy*, Vol. 35, No. 5, pp. 2134 – 2143, 2010.
- [Caux10b] S. Caux, D. Wanderley-Honda, D. Hissel, and M. Fadel. “On-line Energy Management for HEV based on Particle Swarm Optimization”. pp. 1 – 6, sept. 2010.
- [Caza12] N. R. Cazarez-Castro, L. T. Aguilar, and O. Castillo. “Designing Type-1 and Type-2 Fuzzy Logic Controllers via Fuzzy Lyapunov Synthesis for nonsmooth mechanical systems”. *Engineering Applications of Artificial Intelligence*, Vol. 25, No. 5, pp. 971 – 979, 2012.
- [Cerr94] E. Cerruto, A. Consoli, A. Raciti, and A. Testa. “Energy flows management in hybrid vehicles by fuzzy logic controller”. In: *7th Mediterranean Electrotechnical Conference, 1994. Proceedings*, pp. 1314 –1317 vol.3, Apr. 1994.
- [Chan07] P.-C. Chang, S.-S. Chen, Q.-H. Ko, and C.-Y. Fan. “A Genetic Algorithm with Injecting Artificial Chromosomes for Single Machine Scheduling Problems”. In: *IEEE Symposium on Computational Intelligence in Scheduling, 2007. SCIS '07*, pp. 1 –6, april 2007.

- [Chen09] B. Chen, Y. Gao, M. Ehsani, and J. Miller. “Design and control of a ultracapacitor boosted hybrid fuel cell vehicle”. In: *Vehicle Power and Propulsion Conference, 2009. VPPC '09. IEEE*, pp. 696–703, 2009.
- [Chen10] K. Chen, P. Delarue, A. Bouscayrol, P. Vidal, and M. Pietrzak-David. “Minimum Copper Loss and Power Distribution Control Strategies of Double-Inverter-Fed Wound-Rotor Induction Machines Using Energetic Macroscopic Representation”. *IEEE Transactions on Energy Conversion*, Vol. 25, No. 3, pp. 642–651, 2010.
- [Chen11] Y. Cheng, R. Trigui, C. Espanet, A. Bouscayrol, and S. Cui. “Specifications and Design of a PM Electric Variable Transmission for Toyota Prius II”. *IEEE Transactions on Vehicular Technology*, Vol. 60, No. 9, pp. 4106–4114, 2011.
- [Chia03] J. Chiasson and B. Vairamohan. “Estimating the state of charge of a battery”. In: *Proceedings of the 2003 American Control Conference, 2003.*, pp. 2863 – 2868 vol.4, june 2003.
- [Chre08] D. Chrenko. *Energetic Macroscopic Representation Modeling and Control of a Low Temperature Fuel Cell System Fed by Hydrocarbons*. PhD thesis, december 2008.
- [Cord01] O. Cordon, F. Herrera, F. Gomide, F. Hoffmann, and L. Magdalena. “Ten years of genetic fuzzy systems: current framework and new trends”. In: *Joint 9th IFSA World Congress and 20th NAFIPS International Conference, 2001*, pp. 1241 –1246, 2001.
- [Cous06] R. Cousineau. “Development of a hybrid switcher locomotive the Railpower Green Goat”. *Instrumentation Measurement Magazine, IEEE*, Vol. 9, No. 1, pp. 25–29, 2006.
- [Devi11] N. Devillers, S. Jemei, D. Bienaime, M.-C. Pera, and F. Gustin. “Characterization for supercapacitor modelling”. *Submitted to IEEE Transactions on Industrial Electronics*, Vol. x, No. x, p. xx, 2011.
- [Devi12] N. Devillers. *Caractérisation et modélisation de composants de stockage électrochimique et électrostatique*. PhD thesis, Université de Franche-Comté, Octobre 2012.

- [Dush63] G. J. Dusheck, T. C. Hilinski, and F. L. Putzrath. “A Flexible Neural Logic Network”. *IEEE Transactions on Military Electronics*, Vol. 7, No. 2-3, pp. 208–213, 1963.
- [Erdi09] O. Erdinc, B. Vural, and M. Uzunoglu. “A wavelet-fuzzy logic based energy management strategy for a fuel cell/battery/ultra-capacitor hybrid vehicular power system”. *Journal of Power Sources*, Vol. 194, No. 1, pp. 369 – 380, 2009. XIth Polish Conference on Fast Ionic Conductors 2008.
- [Erik07] L. Eriksson. “Modeling and Control of Turbocharged SI and DI Engines”. *Oil Gas Science and Technology - Rev. IFP*, Vol. 62, No. 4, pp. 523–538, 2007.
- [Fang12] L. Fang, G. Xu, T. Li, and K. Zhu. “Optimal control of parallel hybrid electric vehicles”. In: *7th IEEE Conference on Industrial Electronics and Applications (ICIEA)*, pp. 423–427, 2012.
- [Farr93] S. Farrall, A. Cherry, and R. Jones. “Fuzzy control applied to automotive vehicles”. In: *IEE Colloquium on Two Decades of Fuzzy Control - Part 1*, pp. 5/1 –5/4, May 1993.
- [Feld09] L. Feldkamp, M. Abou-Nasr, and I. Kolmanovsky. “Recurrent neural network training for energy management of a mild Hybrid Electric Vehicle with an ultra-capacitor”. In: *IEEE Workshop on Computational Intelligence in Vehicles and Vehicular Systems, 2009. CIVVS '09.*, pp. 29 –36, 2009.
- [Fern11] L. M. Fernandez, P. Garcia, C. A. Garcia, and F. Jurado. “Hybrid electric system based on fuel cell and battery and integrating a single dc/dc converter for a tramway”. *Energy Conversion and Management*, Vol. 52, No. 5, pp. 2183 – 2192, 2011.
- [Gao11] M. Gao, Y. Liu, and Z. He. “Battery state of charge online estimation based on particle filter”. In: *Image and Signal Processing (CISP), 2011 4th International Congress on*, pp. 2233–2236, 2011.
- [Gong08] Q. Gong, Y. Li, and Z.-R. Peng. “Trip based optimal power management of plug-in hybrid electric vehicles using gas-kinetic traffic flow model”. In: *American Control Conference*, pp. 3225 –3230, 2008.

- [Gref86] J. Grefenstette. “Optimization of Control Parameters for Genetic Algorithms”. *IEEE Transactions on Systems, Man and Cybernetics*, Vol. 16, No. 1, pp. 122 –128, jan. 1986.
- [Gual05] H. Gualous, D. Hissel, S. Bontour, F. Harel, and J.-M. Kauffmann. “Power management of an embedded fuel cell - supercapacitor APU”. In: *2005 European Conference on Power Electronics and Applications*, pp. 8 pp.–P.8, 2005.
- [Guo11] L. Guo, K. Yedavalli, and D. Zinger. “Design and modeling of power system for a fuel cell hybrid switcher locomotive”. *Energy Conversion and Management*, Vol. 52, No. 2, pp. 1406 – 1413, 2011.
- [Gutf11] O. Gutfleisch, M. A. Willard, E. Brück, C. H. Chen, S. G. Sankar, and J. P. Liu. “Magnetic Materials and Devices for the 21st Century: Stronger, Lighter, and More Energy Efficient”. *Advanced Materials*, Vol. 23, No. 7, pp. 821–842, 2011.
- [Hadd03] W. Haddad, S. Nersesov, and V. Chellaboina. “Energy-based control for hybrid port-controlled Hamiltonian systems”. *Automatica*, Vol. 39, No. 8, pp. 1425 – 1435, 2003.
- [Haji06] M. Hajimiri and F. Salmasi. “A Fuzzy Energy Management Strategy for Series Hybrid Electric Vehicle with Predictive Control and Durability Extension of the Battery”. In: *IEEE Conference on Electric and Hybrid Vehicles, 2006. ICEHV '06*, pp. 1 –5, 2006.
- [Hank08] W. Hankache. *Gestion Optimisée de l’énergie électrique d’un Groupe électrogène Hybride à Pile à Combustible*. PhD thesis, Institut National Polytechnique, 2008.
- [Hans99] M. Hanss. “Identification of enhanced fuzzy models with special membership functions and fuzzy rule bases”. *Engineering Applications of Artificial Intelligence*, Vol. 12, No. 3, pp. 309 – 319, 1999.
- [Heyw88] J. Heywood. *Internal combustion engine fundamentals*. McGraw-Hill series in mechanical engineering, 1988.
- [Hija06] A. Hijazi. *Modélisation électrothermique, commande et dimensionnement d’un système de stockage d’énergie par supercondensateurs avec prise en compte de son vieillissement : application*

à la récupération de l'énergie de freinage d'un trolleybus. PhD thesis, Université Claude Bernard Lyon 1, 2006.

- [Hiss01] D. Hissel, P. Maussion, and J. Faucher. “Fuzzy logic controllers for electrotechnical devices - On-site tuning approach”. *The European Physical Journal - Applied Physics*, Vol. 16, No. 03, pp. 195–208, 2001.
- [Hiss98] D. Hissel. *Contribution à la commande de dispositifs électrotechniques par logique floue*. PhD thesis, Institut National Polytechnique de Toulouse, 1998.
- [Hoim10] H. Hoimoja, I. Roasto, and A. Keskula. “Design concepts for a hybrid diesel electric shunting locomotive powertrain”. In: *Electronics Conference (BEC), 2010 12th Biennial Baltic*, pp. 293–296, oct. 2010.
- [Ibra11] M. Ibrahim, S. Jemei, J. Wimmer, and D. Hissel. “On board energy management for a hybrid vehicle: wavelets based approach”. In: *International Scientific Conference on hybrid and electric vehicles, RHEVE 2011*, p. , december 2011.
- [Ibra13] M. Ibrahim, S. Jemei, J. Wimmer, and D. Hissel. “Wavelet-Neural Network Approach for On-line Prediction of Time Series: Application on Power Demand Signal in a Fuel Cell Hybrid Vehicle (FCHV)”. In: *5th International Conference on Fundamentals and Development of Fuel Cells, FDFC 2013*, p. , april 2013.
- [Iwan98] L. Iwan and R. Stengel. “The application of neural networks to fuel processors for fuel cell vehicles”. In: *Proceedings of the 37th IEEE Conference on Decision and Control, 1998*, pp. 1585–1590, Dec. 1998.
- [Jaaf09] A. Jaafar, C. Akli, B. Sareni, X. Roboam, and A. Jeunesse. “Sizing and Energy Management of a Hybrid Locomotive Based on Flywheel and Accumulators”. *IEEE Transactions on Vehicular Technology*, Vol. 58, No. 8, pp. 3947–3958, oct. 2009.
- [Jaaf10] A. Jaafar, B. Sareni, X. Roboam, and M. Thiounn-Guermeur. “Sizing of a hybrid locomotive based on accumulators and ultracapacitors”. In: *Vehicle Power and Propulsion Conference (VPPC), 2010 IEEE*, pp. 1–6, sept. 2010.

- [Jaaf12a] A. Jaafar, B. Sareni, and X. Roboam. “Signal synthesis by means of evolutionary algorithms”. *Inverse Problems in Science and Engineering*, Vol. 20, No. 1, pp. 93–104, 2012.
- [Jaaf12b] A. Jaafar, B. Sareni, and X. Roboam. “Clustering analysis of railway driving missions with niching”. *COMPEL: The International Journal for Computation and Mathematics in Electrical and Electronic Engineering*, Vol. vol. 31, pp. 920–931, 2012.
- [Jama09] J. Jamaludin, N. Rahim, and W. Hew. “Development of a self-tuning fuzzy logic controller for intelligent control of elevator systems”. *Engineering Applications of Artificial Intelligence*, Vol. 22, No. 8, pp. 1167 – 1178, 2009.
- [Jamm09] E. Jammeh, M. Fleury, C. Wagner, H. Hagra, and M. Ghanbari. “Interval Type-2 Fuzzy Logic Congestion Control for Video Streaming Across IP Networks”. *IEEE Transactions on Fuzzy Systems*, Vol. 17, No. 5, pp. 1123 –1142, oct. 2009.
- [Jeff04] C. Jefferson and J. Marquez. “Hybrid powertrain for a light rail vehicle”. In: *39th International Universities Power Engineering Conference, 2004. UPEC 2004.*, pp. 1267–1273, 2004.
- [Jeme04] S. Jemei, D. Hissel, M.-C. Pera, and J.-M. Kauffmann. “Dynamical recurrent neural network towards modeling of on-board fuel cell power supply”. In: *2004 IEEE International Symposium on Industrial Electronics*, pp. 471 – 476, May 2004.
- [Jian10] Z.-L. Jiang, W.-R. Chen, C.-H. Dai, and Z.-L. Cheng. “Optimal energy management for a fuel cell hybrid locomotive”. In: *2010 Seventh International Conference on Fuzzy Systems and Knowledge Discovery (FSKD)*, pp. 1320 –1323, 2010.
- [Joha07] L. Johannesson, M. Asbogard, and B. Egardt. “Assessing the Potential of Predictive Control for Hybrid Vehicle Powertrains Using Stochastic Dynamic Programming”. *IEEE Transactions on Intelligent Transportation Systems*, Vol. 8, No. 1, pp. 71 –83, 2007.
- [Kara03] E. Karakas. “The control of highway tunnel ventilation using fuzzy logic”. *Engineering Applications of Artificial Intelligence*, Vol. 16, No. 7, pp. 717 – 721, 2003.

- [Karn01] N. N. Karnik and J. M. Mendel. “Operations on type-2 fuzzy sets”. *Fuzzy Sets and Systems*, Vol. 122, No. 2, pp. 327 – 348, 2001.
- [Kerm09a] S. Kermani. *Gestion énergétique des véhicules hybrides : de la simulation à la commande temps réel*. PhD thesis, Université de Valenciennes et du Hainaut Cambrésis, 2009.
- [Kerm09b] S. Kermani, S. Delprat, T. Guerra, and R. Trigui. “Predictive control for HEV energy management: experimental results”. In: *Vehicle Power and Propulsion Conference, 2009. VPPC '09. IEEE*, pp. 364 –369, sept. 2009.
- [Kerm11] S. Kermani, R. Trigui, S. Delprat, B. Jeanneret, and T. Guerra. “PHIL Implementation of Energy Management Optimization for a Parallel HEV on a Predefined Route”. *IEEE Transactions on Vehicular Technology*, Vol. 60, No. 3, pp. 782–792, 2011.
- [Kess07] J. Kessels, M. Koot, B. de Jager, P. van den Bosch, N. Aneke, and D. Kok. “Energy Management for the Electric Powernet in Vehicles With a Conventional Drivetrain”. *IEEE Transactions on Control Systems Technology*, Vol. 15, No. 3, pp. 494 –505, may 2007.
- [Kris88] K. Kristinsson and G. Dumont. “Genetic algorithms in system identification”. In: *IEEE International Symposium on Intelligent Control, 1988. Proceedings*, pp. 597 –602, aug 1988.
- [Kutt10] S. Kutter and B. Bäker. “Predictive Online Control for Hybrids - Resolving the conflict between global optimality, robustness and real-time capability”. *IEEE*, Vol. 978-1-4244-8218-4/10/, pp. 1 – 6, 2010.
- [Lee90] C. Lee. “Fuzzy logic in control systems: fuzzy logic controller. II”. *IEEE Transactions on Systems, Man and Cybernetics*, Vol. 20, No. 2, pp. 419 –435, 1990.
- [Lesc10] J. Lescot, A. Sciarretta, Y. Chamailard, and A. Charlet. “On the integration of optimal energy management and thermal management of hybrid electric vehicles”. In: *Vehicle Power and Propulsion Conference (VPPC), 2010 IEEE*, pp. 1 –6, sept. 2010.
- [Letr12] T. Letrouve, A. Bouscayrol, W. Lhomme, N. Dollinger, and F. Calvairac. “Reduced-scale hardware-in-the-loop simulation of

- a Peugeot 3008 Hybrid4 vehicle”. In: *Vehicle Power and Propulsion Conference (VPPC), 2012 IEEE*, pp. 920–925, 2012.
- [Lhom04] W. Lhomme, A. Bouscayrol, and P. Barrade. “Simulation of a Series Hybrid Electric Vehicle based on Energetic Macroscopic Representation”. In: *IEEE International Symposium on Industrial Electronics, 2004. Ajaccio, France*, pp. 1 – 6, May 2004.
- [Lhom06] W. Lhomme, R. Trigui, P. Delarue, B. Jeanneret, A. Bouscayrol, and F. Badin. “Switched Causal Modeling of Transmission with Clutch in Hybrid Electric Vehicles”. In: *Vehicle Power and Propulsion Conference, 2006. VPPC '06. IEEE*, pp. 1 –6, 2006.
- [Lhom08] W. Lhomme, R. Trigui, P. Delarue, B. Jeanneret, A. Bouscayrol, and F. Badin. “Switched Causal Modeling of Transmission With Clutch in Hybrid Electric Vehicles”. *IEEE Transactions on Vehicular Technology*, Vol. 57, No. 4, pp. 2081–2088, 2008.
- [Lhom11] W. Lhomme, R. Trigui, A. Bouscayrol, P. Delarue, B. Jeanneret, and F. Badin. “Inversion-based control of a vehicle with a clutch using a switched causal modelling”. *Intern. J. Syst. Sci.*, Vol. 42, No. 2, pp. 319–334, Feb. 2011.
- [Li12] H. Li, H. Liu, H. Gao, and P. Shi. “Reliable Fuzzy Control for Active Suspension Systems With Actuator Delay and Fault”. *IEEE Transactions on Fuzzy Systems*, Vol. 20, No. 2, pp. 342 –357, april 2012.
- [Liao08] R. Liao, C. Chan, J. Hromek, G. Huang, and L. He. “Fuzzy logic control for a petroleum separation process”. *Engineering Applications of Artificial Intelligence*, Vol. 21, No. 6, pp. 835 – 845, 2008.
- [Lin03] C.-C. Lin, H. Peng, J. Grizzle, and J.-M. Kang. “Power management strategy for a parallel hybrid electric truck”. *IEEE Transactions on Control Systems Technology*, Vol. 11, No. 6, pp. 839 – 849, 2003.
- [Lin05] J. Lin. “An active vibration absorber of smart panel by using a decomposed parallel fuzzy control structure”. *Engineering Applications of Artificial Intelligence*, Vol. 18, No. 8, pp. 985 – 998, 2005.

- [Liu08] J. Liu and H. Peng. “Modeling and Control of a Power-Split Hybrid Vehicle”. *IEEE Transactions on Control Systems Technology*, Vol. 16, No. 6, pp. 1242–1251, 2008.
- [Lou12] C. W. Lou and M. C. Dong. “Modeling data uncertainty on electric load forecasting based on Type-2 fuzzy logic set theory”. *Engineering Applications of Artificial Intelligence*, Vol. , No. 0, pp. –, 2012.
- [Louk10] D. Loukakou, H. Gualous, Y. Cheng, C. Espanet, and F. Dubas. “Sizing and experimental characterization of ultra-capacitors for small urban hybrid electric vehicle”. In: *Vehicle Power and Propulsion Conference (VPPC), 2010 IEEE*, pp. 1–7, 2010.
- [Mai10] H. C. M. Mai, R. Bernard, P. Bigot, F. Dubas, D. Chamagne, and C. Espanet. “Consideration of radial magnetic forces in brushless DC motors”. In: *International Conference on Electrical Machines and Systems (ICEMS)*, pp. 1–6, 2010.
- [Mamd99] E. Mamdani and S. Assilian. “An experiment in linguistic synthesis with a fuzzy logic controller”. *Int. J. Hum.-Comput. Stud.*, Vol. 51, pp. 135–147, August 1999.
- [Mark03] T. Markel, M. Zolot, B. Keith, and A. Pesaran. “Energy Storage System Requirements for Hybrid Fuel Cell Vehicles”. *Advanced Automotive Battery Conference*, Vol. 1, pp. 1–12, 2003.
- [Maye12] C. Mayet, M. Mejri, A. Bouscayrol, J. Pouget, and Y. Riffonneau. “Energetic Macroscopic Representation and inversion-based control of the traction system of a hybrid locomotive”. In: *Vehicle Power and Propulsion Conference (VPPC), 2012 IEEE*, pp. 491–496, 2012.
- [McIn06] M. McIntyre, T. Burg, D. Dawson, and B. Xian. “Adaptive state of charge (SOC) estimator for a battery”. In: *American Control Conference, 2006*, p. 5 pp., june 2006.
- [Mend09] J. Mendel, F. Liu, and D. Zhai. “ $\alpha$ -Plane Representation for Type-2 Fuzzy Sets: Theory and Applications”. *IEEE Transactions on Fuzzy Systems*, Vol. 17, No. 5, pp. 1189–1207, oct. 2009.
- [Mill07] A. Miller, K. Hess, D. Barnes, and T. Erickson. “System design of a large fuel cell hybrid locomotive”. *Journal of Power Sources*,

- Vol. 173, No. 2, pp. 935 – 942, 2007. X Polish Conference on Systems with Fast Ionic Transport.
- [Mogh03] H. Moghbelli, Y. Gao, R. Langari, and M. Ehsani. “Investigation of hybrid fuel cell (HFC) technology applications on the future passenger railroad transportation”. In: *Rail Conference, 2003. Proceedings of the 2003 IEEE/ASME Joint*, pp. 39 – 53, 2003.
- [Mulo10] J. Mulot, F. Harel, S. Begot, D. Hissel, I. Rodel, S. Boblet, and M. Amiet. “Fuel cell system integration into a heavy-duty hybrid vehicle: preliminary experimental results”. In: *Vehicle Power and Propulsion Conference (VPPC), 2010 IEEE*, pp. 1–5, 2010.
- [Narj08] A. Narjiss. *Diagnostic Non-Intrusif d’une Pile à Combustible PEMFC Grâce au Convertisseur Statique*. PhD thesis, Université de Franche-Comté, september 2008.
- [Ocde11] *Ocde - Mondialisation, transport et environnement*. Editions OCDE, 2011.
- [Orte02] R. Ortega, A. van der Schaft, B. Maschke, and G. Escobar. “Interconnection and damping assignment passivity-based control of port-controlled Hamiltonian systems”. *Automatica*, Vol. 38, No. 4, pp. 585 – 596, 2002.
- [Pei06] F. Pei, K. Zhao, Y. Luo, and X. Huang. “Battery Variable Current-discharge Resistance Characteristics and State of Charge Estimation of Electric Vehicle”. In: *The Sixth World Congress on Intelligent Control and Automation, 2006. WCICA 2006.*, pp. 8314 –8318, 0-0 2006.
- [Phil96] C. Phillips, C. L. Karr, and G. Walker. “Helicopter flight control with fuzzy logic and genetic algorithms”. *Engineering Applications of Artificial Intelligence*, Vol. 9, No. 2, pp. 175 – 184, 1996.
- [Pill01] S. Piller, M. Perrin, and A. Jossen. “Methods for state-of-charge determination and their applications”. *Journal of Power Sources*, Vol. 96, No. 1, pp. 113 – 120, 2001. Proceedings of the 22nd International Power Sources Symposium.
- [Prei07] Z. Preitl, P. Bauer, B. Kulcsar, G. Rizzo, and J. Bokor. “Control Solutions for Hybrid Solar Vehicle Fuel Consumption Minimization”. In: *Intelligent Vehicles Symposium, 2007 IEEE*, pp. 767 –772, 2007.

- [Prok08] D. Prokhorov. “Toyota Prius HEV neurocontrol and diagnostics”. *Neural Networks*, Vol. 21, No. 2-3, pp. 458 – 465, 2008.
- [Rous08] G. Rousseau. *Véhicule hybride et commande optimale*. PhD thesis, Ecole des mines de Paris, 2008.
- [Salm00] M. Salman, N. Schouten, and N. Kheir. “Control strategies for parallel hybrid vehicles”. In: *proceedings of the 2000 American Control Conference*, pp. 524 –528, Sep. 2000.
- [Salm07] F. Salmasi. “Control Strategies for Hybrid Electric Vehicles: Evolution, Classification, Comparison, and Future Trends”. *IEEE Transactions on Vehicular Technology*, Vol. 56, No. 5, pp. 2393 –2404, 2007.
- [Schm12] K. Schmidt and Y. Boutalis. “Fuzzy Discrete Event Systems for Multi-objective Control: Framework and Application to Mobile Robot Navigation”. *IEEE Transactions on Fuzzy Systems*, Vol. PP, No. 99, p. 1, 2012.
- [Scor04] J. Scordia. *Approche systématique de l’optimisation du dimensionnement et de l’élaboration de lois de gestion d’énergie de véhicules hybrides*. PhD thesis, Université Henri Poincaré, 2004.
- [Shar11] S. Sharma and K. Gupta. “Solving the traveling salesmen problem through genetic algorithm with new variation order crossover”. In: *International Conference on Emerging Trends in Networks and Computer Communications (ETNCC)*, pp. 274 –276, april 2011.
- [Shep65] C. M. Shepherd. “Design of Primary and Secondary Cells: II . An Equation Describing Battery Discharge”. *Journal of The Electrochemical Society*, Vol. 112, No. 7, pp. 657–664, 1965.
- [Si09] J. Si, L. Yang, C. Lu, J. Sun, and S. Mei. “Approximate dynamic programming for continuous state and control problems”. In: *17th Mediterranean Conference on Control and Automation, 2009. MED ’09.*, pp. 1415–1420, 2009.
- [Sola09] J. Solano-Martinez, L. Boulon, D. Hissel, M.-C. Pera, and M. Amiet. “Energetic macroscopic representation of a multiple architecture heavy duty hybrid vehicle”. In: *Vehicle Power and Propulsion Conference, 2009. VPPC ’09. IEEE*, pp. 1322 –1329, 2009.

- [Sola11] J. Solano, D. Hissel, M.-C. Pera, and M. Amiet. “Practical Control Structure and Energy Management of a Testbed Hybrid Electric Vehicle”. *IEEE Transactions on Vehicular Technology*, Vol. 60, No. 9, pp. 4139–4152, nov. 2011.
- [Sola12a] J. Solano. *Energy management of a hybrid electric vehicle: an approach based on type-2 fuzzy logic*. PhD thesis, Franche Comte University, February 2012.
- [Sola12b] J. Solano, R. I. John, D. Hissel, and M.-C. Pera. “A survey-based type-2 fuzzy logic system for energy management in hybrid electrical vehicles”. *Information Sciences*, Vol. 190, No. 0, pp. 192–207, 2012.
- [Stew04] P. Stewart, D. Stone, and P. Fleming. “Design of robust fuzzy-logic control systems by multi-objective evolutionary methods with hardware in the loop”. *Engineering Applications of Artificial Intelligence*, Vol. 17, No. 3, pp. 275–284, 2004.
- [Suge84] M. Sugeno and K. Murakami. “Fuzzy parking control of model car”. In: *The 23rd IEEE Conference on Decision and Control, 1984*, pp. 902–903, 1984.
- [Suge95] M. Sugeno, I. Hirano, S. Nakamura, and S. Kotsu. “Development of an intelligent unmanned helicopter”. In: *Proceedings of 1995 IEEE International Conference on Fuzzy Systems, 1995. International Joint Conference of the Fourth IEEE International Conference on Fuzzy Systems and The Second International Fuzzy Engineering Symposium*, pp. 33–34, March 1995.
- [Syed11] S. A. Syed, W. Lhomme, A. Bouscayrol, B. Vulturescu, S. Butterbach, O. Pape, and B. Petitdidier. “Inversion-based control of series-parallel HEV for municipal trucks”. In: *Vehicle Power and Propulsion Conference (VPPC), 2011 IEEE*, pp. 1–6, 2011.
- [Teki04] M. Tekin, D. Hissel, M.-C. Pera, and J. M. Kauffmann. “Energy management strategy for embedded fuel cell system using fuzzy logic”. In: *2004 IEEE International Symposium on Industrial Electronics*, pp. 501–506 vol. 1, 2004.
- [Toyo13] Toyota. “Toyota global”. <http://www.toyota-global.com/innovation/environmental-technology/technology-file/>, 2013.

- [Trem07] O. Tremblay, L.-A. Dessaint, and A.-I. Dekkiche. “A Generic Battery Model for the Dynamic Simulation of Hybrid Electric Vehicles”. In: *Vehicle Power and Propulsion Conference, 2007. VPPC 2007. IEEE*, pp. 284–289, sept. 2007.
- [Trem09] O. Tremblay. “Experimental Validation of a Battery Dynamic Model for EV Applications”. *World Electric Vehicle Journal*, Vol. 3, 2009.
- [Uno11] M. Uno and K. Tanaka. “Accelerated ageing testing and cycle life prediction of supercapacitors for alternative battery applications”. In: *2011 IEEE 33rd International Telecommunications Energy Conference (INTELEC)*, pp. 1–6, 2011.
- [Urba07] M. Urbain, S. Rael, B. Davat, and P. Desprez. “State Estimation of a Lithium-Ion Battery Through Kalman Filter”. In: *Power Electronics Specialists Conference, 2007. PESC 2007. IEEE*, pp. 2804–2810, 2007.
- [Uzun08] M. Uzunoglu and M. Alam. “Modeling and Analysis of an FC/UC Hybrid Vehicular Power System Using a Novel-Wavelet-Based Load Sharing Algorithm”. *IEEE Transactions on Energy Conversion*, Vol. 23, No. 1, pp. 263–272, 2008.
- [Vena09] G. K. Venayagamoorthy, L. L. Grant, and S. Doctor. “Collective robotic search using hybrid techniques: Fuzzy logic and swarm intelligence inspired by nature”. *Engineering Applications of Artificial Intelligence*, Vol. 22, No. 3, pp. 431–441, 2009.
- [Verd10] N. Verdonck, A. Chasse, P. Pognant-Gros, and A. Sciarretta. “Automated Model Generation for Hybrid Vehicles Optimization and Control”. *Oil Gas Sci. Technol. - Rev. IFP*, Vol. 65, No. 1, pp. 115–132, 2010.
- [Vino07] E. Vinot, R. Trigui, B. Jeanneret, J. Scordia, and F. Badin. “HEVs Comparison and Components Sizing Using Dynamic Programming”. In: *Vehicle Power and Propulsion Conference, 2007. VPPC 2007. IEEE*, pp. 314–321, 2007.
- [Wagn07] C. Wagner and H. Hagnas. “A Genetic Algorithm Based Architecture for Evolving Type-2 Fuzzy Logic Controllers for Real World Autonomous Mobile Robots”. In: *IEEE International Conference on Fuzzy Systems, 2007. FUZZ-IEEE 2007.*, pp. 1–6, july 2007.

- [Wagn09] C. Wagner and H. Hagnas. “Novel Methods for the Design of General Type2 Fuzzy Sets based on Device Characteristics and Linguistic Labels Surveys”. In: *European Society for Fuzzy Logic and Technology*, pp. 537–543, 2009.
- [Wagn10] C. Wagner and H. Hagnas. “Toward General Type-2 Fuzzy Logic Systems Based on zSlices”. *IEEE Transactions on Fuzzy Systems*, Vol. 18, No. 4, pp. 637 –660, aug. 2010.
- [Walt07] L. Walter. *Gestion d’énergie de véhicules électriques hybrides basée sur la représentation énergétique macroscopique*. PhD thesis, Université des Sciences et Technologies de Lille, 2007.
- [Wang06a] A. Wang and W. Yang. “Design of Energy Management Strategy in Hybrid Electric Vehicles by Evolutionary Fuzzy System Part II: Tuning Fuzzy Controller by Genetic Algorithms”. In: *The Sixth World Congress on Intelligent Control and Automation, 2006. WCICA 2006*, pp. 8329 –8333, 2006.
- [Wang06b] A. Wang and W. Yang. “Design of Energy Management Strategy in Hybrid Vehicles by Evolutionary Fuzzy System Part I: Fuzzy Logic Controller Development”. In: *The Sixth World Congress on Intelligent Control and Automation, 2006. WCICA 2006.*, pp. 8324 –8328, 2006.
- [Wu07] D. Wu and J. Mendel. “Enhanced Karnik-Mendel Algorithms for Interval Type-2 Fuzzy Sets and Systems”. In: *Fuzzy Information Processing Society, 2007. NAFIPS ’07. Annual Meeting of the North American*, pp. 184 –189, june 2007.
- [Wu10] Z. Wu, D. Depernet, and C. Espanet. “Optimal design of electrical drive and power Converter for hybrid electric powertrain”. In: *Vehicle Power and Propulsion Conference (VPPC), 2010 IEEE*, pp. 1–8, 2010.
- [Wu12] D. Wu. “On the Fundamental Differences Between Type-1 and Interval Type-2 Fuzzy Logic Controllers”. *IEEE Transactions on Fuzzy Systems*, Vol. PP, No. 99, p. 1, 2012.
- [Xin11] Z. Xin and T. Yi. “Research of hybrid electric locomotive control strategy”. In: *2011 International Conference on System Science, Engineering Design and Manufacturing Informatization (ICSEM)*, pp. 118–122, 2011.

- [Xion13] R. Xiong, H. He, F. Sun, and K. Zhao. “Evaluation on State of Charge Estimation of Batteries With Adaptive Extended Kalman Filter by Experiment Approach”. *IEEE Transactions on Vehicular Technology*, Vol. 62, No. 1, pp. 108–117, 2013.
- [Zena10] A. Zenati, P. Desprez, H. Razik, and S. Rael. “Impedance measurements combined with the fuzzy logic methodology to assess the SOC and SOH of lithium-ion cells”. In: *Vehicle Power and Propulsion Conference (VPPC), 2010 IEEE*, pp. 1–6, 2010.
- [Zhan08] X. Zhang, C. C. Mi, A. Masrur, and D. Daniszewski. “Wavelet-transform-based power management of hybrid vehicles with multiple on-board energy sources including fuel cell, battery and ultracapacitor”. *Journal of Power Sources*, Vol. 185, No. 2, pp. 1533 – 1543, 2008.
- [Zieg93] J. G. Ziegler and N. B. Nichols. “Optimum Settings for Automatic Controllers”. *Journal of Dynamic Systems, Measurement, and Control*, Vol. 115, No. 2B, pp. 220–222, 1993.
- [Zubi00] L. Zubieta and R. Bonert. “Characterization of double-layer capacitors for power electronics applications”. *IEEE Transactions on Industry Applications*, Vol. 36, No. 1, pp. 199 –205, jan/feb 2000.





## Résumé :

Dans le cadre du transport de marchandises par voie ferroviaire, un certain nombre de verrous limitent les efforts consentis pour un fret plus "propre". Des améliorations doivent être faites afin de limiter le nombre de locotracteurs assurant les charges/décharges de marchandises en bout de ligne. Dans cette perspective, FEMTO-ST et Alstom Transport ont pour objectif de concevoir et développer un système de gestion d'énergie pour locomotive électrique hybride. Composée d'un groupe électrogène couplé à des accumulateurs électrochimiques et des super-condensateurs, la locomotive électrique hybride permet d'accroître la souplesse et l'efficacité du transport ferroviaire électrique, tout en réduisant encore son impact environnemental. Cette étude a consisté dans un premier temps à développer une modélisation macroscopique de la chaîne de traction électrique hybride et à proposer une structuration de la commande avec l'identification des capteurs matériels et logiciels nécessaires au contrôle optimal de la chaîne de traction. La caractérisation expérimentale des moyens de stockage a permis l'amélioration comportementale et dynamique des modèles correspondant. Dans un second temps, le contrôle de la tension de sortie d'un hacheur dévolteur a permis d'étudier l'application de la logique floue de type-2 (intervalle et générale) dans le cas d'applications industrielles (relativement simples). Enfin, une gestion innovante des flux d'énergie au sein d'un système plus complexe: locomotive électrique hybride, a été développée. Mettant en oeuvre la logique floue de type-2 et des algorithmes s'inspirant de la théorie de l'évolution, cette gestion d'énergie optimale opère en temps réel et sans connaissance a priori du cycle de conduite. La gestion fréquentielle ainsi que le contrôle des états de charge des sources secondaires du véhicule contribuent également à leur bon fonctionnement.

**Mots-clés :** Locomotives électriques hybrides, accumulateurs électrochimiques, super-condensateurs, caractérisation expérimentale, stratégie de gestion d'énergie, logique floue de type-2, algorithme génétique, représentation énergétique macroscopique, dimensionnement fréquentiel.

## Abstract:

To achieve a "greener" freight transport, efforts are still needed to overcome some technological barriers. New improvements must be carried out to limit the shunting locomotives' use intended for the goods' load/unload. Considering this aim, FEMTO-ST and Alstom Transport decided to conceive and develop an energy management strategy system for hybrid electric locomotives. Such locomotives include a diesel driven generator set which is coupled with batteries and ultra-capacitors. The architecture aims at improving the flexibility, the effectiveness of the electrical railway transport and at reducing the environmental impact of these activities again. Firstly, the study consists in implementing a macroscopic modelling of the hybrid electric powertrain. Then, the control is optimally designed by identifying the hardware and software sensors of the powertrain. The dynamics and the behaviour of the secondary sources' models are improved thanks to their experimental characterizations. Secondly, the use of Type-2 Fuzzy Logic (interval and general) controllers permits to study their efficiency in the control of a very simple industrial system: the output voltage of a buck converter. Lastly, based on the obtained results, an innovative management of the system's energy flows is developed in the case of the hybrid electrical locomotive. The use of the type-2 fuzzy logic and evolutionary algorithms permit to optimally perform a real time energy management strategy without a priori knowledge of the duty cycle. The frequency approach and the secondary sources' state of charge control contribute to their efficient use.

**Keywords:** Hybrid Electric Locomotives, batteries, ultra-capacitors, experimental characterization, energy management strategy, Type-2 fuzzy logic, genetic algorithm, Energetic Macroscopic Representation, frequency sizing.

The logo for SPIM (École doctorale SPIM) features a stylized white 'S' on a green horizontal bar, followed by the letters 'PIM' in a large, white, sans-serif font.